Weak Production of K and η Mesons off the Nucleon

Abstract of the thesis submitted for the award of the Degree of Doctor of Philosophy in Physics

By

MOHAMMAD RAFI ALAM

Department
Of
Physics

Aligarh Muslim University
Aligarh, India

Supervisor
Dr. Mohammad Sajjad Athar

Contents

Contents i

List of Publications iii

1 Introduction 1

2 Weak Production of K and $\bar{K}$ 5
2.1 Neutrino Induced Kaon Production 5
2.2 Antineutrino Induced $K^-/\bar{K}^0$ Production 9

3 Charged Lepton Induced One Kaon Production 11

4 η Production 15

5 Associated Kaon Production 19

6 Conclusions 23

Bibliography 25

Bibliography 25

List of Publications

International

1. M. Rafi Alam, S. Chauhan, M. Sajjad Athar and S. K. Singh,
"*$\bar{\nu}_l$ Induced Pion Production from Nuclei at $\sim$1 GeV*,"
Phys. Rev. D 88, 077301 (2013)

2. M. Rafi Alam, I. Ruiz Simo, M. Sajjad Athar and M. J. Vicente Vacas,
"*Charged Lepton Induced One Kaon Production off the Nucleon*,"
Phys. Rev. D 87, 053008 (2013)

3. M. Rafi Alam, I. Ruiz Simo, M. Sajjad Athar and M. J. Vicente Vacas,
"*Antineutrino Induced Antikaon Production off the Nucleon*,"
Phys. Rev. D 85, 013014 (2012)

4. M. Rafi Alam, I. Ruiz Simo, M. Sajjad Athar and M. J. Vicente Vacas,
"*Weak Kaon Production off the Nucleon*,"
Phys. Rev. D 82, 033001 (2010)

5. M. Rafi Alam, L. Alvarez-Ruso, I. Ruiz Simo, M. Sajjad Athar, M. J. Vicente Vacas and S. K. Singh,
"*Weak Strangeness and Eta Production*,"
To appear in the IOP Conference Proceedings (NuFact2013)

6. M. Rafi Alam, I. Ruiz Simo, M. Sajjad Athar, L. Alvarez-Ruso and M. J. Vicente Vacas,

"*Weak Production of Strange Particles off the Nucleon,*"
To appear in the American Institute of Physics Conference Proceedings (NuInt2012)
e-Print:arXiv:1303.5924 [hep-ph].

7. M. Rafi Alam, L. Alvarez-Ruso, M. Sajjad Athar and M. J. Vicente Vacas,
"*Weak η Production off the Nucleon,*"
To appear in the American Institute of Physics Conference Proceedings (NuInt2012)
e-Print:1303.5951 [hep-ph].

8. M. Rafi Alam, I. Ruiz Simo, M. Sajjad Athar and M. J. Vicente Vacas,
"*Neutrino(Antineutrino) Induced Single Kaon(Antikaon) Production,*"
Presented in XXV International Conference on Neutrino Physics and Astrophysics, (Neutrino 2012) Kyoto, Japan.

9. M. Rafi Alam, I. Ruiz Simo, M. Sajjad Athar and M. J. Vicente Vacas,
"*Kaon Production off the Nucleon,*"
AIP Conf. Proc. 1382, 173 (2011).

10. M. Rafi Alam, I. Ruiz Simo, M. Sajjad Athar and M. J. Vicente Vacas,
"*Strange Particle Production at Low and Intermediate Energies,*"
AIP Conf. Proc. 1405, 152 (2011)

National

1. M. Rafi Alam, I. Ruiz Simo, M. Sajjad Athar and M. J. Vicente Vacas,
"*ν-Induced Weak Kaon Production from Nucleons and Nuclei,*"
Department of Atomic Energy Symp. on Nucl. Phys. 55, 526 (2010).

2. M. Rafi Alam, I. Ruiz Simo, M. Sajjad Athar and M. J. Vicente Vacas,
"*$\bar{\nu}$-Induced Kaon Production,*"
Department of Atomic Energy Symp. on Nucl. Phys. 56, 762 (2011).

3. S. Chauhan, F. Zaidi, H. Haider, M. Rafi Alam, and M. Sajjad Athar
"*Monte Carlo Generators vs Nuclear Model,*"
Department of Atomic Energy Symp. on Nucl. Phys. 56, 1104 (2011).

4. M. Rafi Alam, I. Ruiz Simo, M. Sajjad Athar and M. J. Vicente Vacas,
"*$e^{\pm}$ Induced Single Kaon Production off the Neucleon.*"
Department of Atomic Energy Symp. on Nucl. Phys. 57, 662 (2012).

CHAPTER 1

Introduction

Neutrino oscillation physics has entered into an era of precision physics in which both theoretically and experimentally enormous efforts are going on for the better understanding of oscillation physics as well as for the understanding of hadron physics as these experiments are also providing cross section measurements for many quasielastic and inelastic processes induced by the neutrino and antineutrino on nuclear targets. The neutrino energy region of a few GeV is quite sensitive to the neutrino oscillation parameters. Therefore, most of the present experiments like MiniBooNE [1], K2K [2], T2K [3], NOνA [4], etc. have taken data or have been planned in this energy region. These recent cross section measurements are available mostly for $\Delta S = 0$ processes in nonstrange sector. In strange sector neutrino Monte-Carlo generators use the results of older work available in literature for $\Delta S = 0$ and $\Delta S = 1$ processes. On the theoretical side there are very few works available in literature. However, specific and precise knowledge about these processes would be very important for the analysis of ongoing and future neutrino oscillation experiments. These processes would also facilitate in the understanding of hadron structure and their properties. In the present thesis we have performed theoretical calculations for some of the channels which are not well studied like single kaon production, eta production and associated particle production processes. These studies are performed for neutrino/antineutrino induced reaction off free nucleon target. We have also performed calculation for the weak production of kaon from nucleon induced by electron/positron beam.

Neutrino/Antineutrino induced charged current(CC), $|\Delta S| = 1$ process is particularly appealing for several reasons. One of them is the important background that it could produce, due to atmospheric neutrino interactions in the proton decay searches [5]. There is a strong prediction from the super-symmetric grand unified theories(SUSY GUTs) [6] for the protons to have life time more than predicted by the minimal version of supersymmetric $SU(5)$ theories. There are other decay channels that open up, particularly s-quark production is favored, and final states involving kaons, for example, $p \to K\bar{\nu}$ would be a dominant decay mode of protons. Thus to see nucleon to decay, reliable estimate of kaons coming from the background, like from the interaction of atmospheric neutrinos, should be well estimated. For this theoretical understanding of kaon production from $\Delta S = 0$ as well as $\Delta S = 1$ processes are required. These processes are also useful in the understanding of the basic symmetries of the standard model, strange quark content of the nucleon, structure of weak hadronic form factors, etc. The study of single kaon production would also be important in the analysis of neutrino oscillation data to have the precise measurement of neutrino oscillation parameters.

Experimentally, the currently available data on strange particle production in the weak sector is restricted to a few events measured in bubble chamber experiments [7, 8, 9] with large systematic errors. However, the scenario is expected to change soon as MINERνA [10] at Fermilab has started taking data and they also plan to study strange particle production with large statistics. On the theoretical side, only limited efforts have been made to understand strange particle production in the weak sector. Due to the scarcity of theoretical work, the Monte Carlo generators used in the analysis of the experiments apply models that are not too well suited to describe the strangeness production at low energies. For instance, NEUT [11], used by K2K [2], T2K [3], Super-Kamiokande [12] and SciBooNE [13] only considers associated kaon production implemented by a model based on the excitation and later decay of resonances [11]. A similar model is used by other event generators like NEUGEN [14], NUANCE [15] (see also discussion in Ref. [16]) and GENIE [17]. However, it has been realized that this approach is not appropriate for low energy strange particle production. Furthermore, in the Monte Carlo generators, single kaon production is yet to be incorporated.

The other inelastic process that we have studied is the eta production induced by neutrinos/antineutrinos. Study of η production is interesting because of several reasons. For example, η is one of the important probe to search for the strange quark content of the nucleons [18]. Also a precise determination of η production cross section would help in subtracting the background in proton decay searches. In some supersymmetric grand unified theories, η mesons provide a prominent signal

for proton decay [19]. Therefore, its background contribution due to atmospheric neutrino interactions should be well estimated. Furthermore, η production channel is dominated by $S_{11}(1535)$ resonance excitation, therefore, it is expected that a precise measurement of the cross section will also allow to determine the axial properties of this resonance. In most of the Monte Carlo generators, eta contribution is obtained from Rein and Sehgal model [20] for the resonant pion production. We have not come across any theoretical/experimental study where using neutrino/antineutrino beam either the differential or total scattering cross section has been presented.

Recently, the importance of the study of kaon production induced by real and virtual photons on nucleons and nuclei, in an associated particle production process $\Delta S = 0$, has been emphasized with the development of accelerators like MAMI, TJNAF, LNS, ELSA, SPring-8, GRAAL, etc. [21, 22, 23, 24, 25] and dedicated detectors like KAOS [21] to measure kaon events. However, besides $\Delta S = 0$ associated particle production process, $\Delta S = 1$ single kaon production process may also give rise to some significant contribution to kaon events. Therefore, we have also studied weak interaction induced single kaon production in an electron/positron beam.

In Chapter-2, we have given a brief introduction of Chiral Perturbation Theory (χPT). After introducing χPT, we have presented and discussed the results for neutrino and antineutrino induced single kaon and antikaon production. In Chapter-3, we have presented the formalism of the electron/positron induced antikaon/kaon production. We have shown that kaon production through $\Delta S = 1$ process, may also contribute significantly in the beams of electron/positron in the experiments being performed at JLAB, Mainz, etc. We have presented and discussed the results for the differential and total scattering cross sections.

In Chapter-4, we have studied photo and neutrino/antineutrino induced eta particle production off the nucleons. We have obtained the results for the various distributions like eta momentum, lepton energy and Q^2 distributions as well as the results for the total scattering cross sections. We have used χPT approach to obtain the hadronic currents for the Born diagrams and the prescription of helicity amplitudes to obtain the contributions from the resonant $S_{11}(1535)$ and $S_{11}(1650)$ channels. In Chapter-5, we have studied associated particle production induced by neutrino and antineutrino. We have presently taken only the nonresonant diagrams and obtained the hadronic currents using χPT. The results for kaon momentum, Q^2 distributions and the results for the total scattering cross sections are presented. In Chapter-6, we summarize the results and conclude our findings.

CHAPTER 2

Weak Production of K and $\bar{K}$

In this chapter, we briefly discuss the formalism which has been used to describe the weak strangeness production. At low energies, it is possible to obtain model independent predictions using Chiral Perturbation Theory (χPT). We use the chiral Lagrangian obtained for the meson-meson and meson-baryon interactions and their interactions with external fields to write the hadronic currents for the various processes and using them we have obtained the differential and total scattering cross sections for $\nu-$induced K production and $\bar{\nu}-$induced $\bar{K}$ production. The basic parameters of the model are f_π, the pion decay constant, Cabibbo's angle, the proton and neutron magnetic moments and the axial vector coupling constants for the baryons octet. For antikaon production we have also included $\Sigma^*(1385)$ resonance.

2.1 Neutrino Induced Kaon Production

In neutrino induced reactions, the first inelastic reaction creating strange quark is the single kaon production. For single kaon production ($\Delta S = 1$), we have considered the following reactions:

$$\begin{aligned} \nu_\mu + p &\to \mu^- + K^+ + p \\ \nu_\mu + n &\to \mu^- + K^0 + p \\ \nu_\mu + n &\to \mu^- + K^+ + n \end{aligned} \tag{2.1}$$

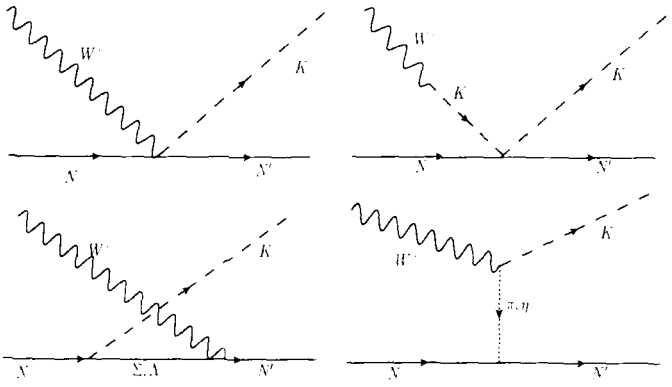

Figure 2.1: Feynman diagrams for the process $\nu N \rightarrow lN'K$. First row from left to right: contact term (labeled CT in the text), kaon pole term (KP); second row: u-channel diagram ($Cr\Sigma$, $Cr\Lambda$) and pion(eta) in flight (πP, (ηP).

The kaon production gets contribution from contact term, u-channel diagram, kaon pole term and pion/eta in flight term as shown in Fig.2.1. The hadronic currents are obtained using χPT and we have used a global dipole form factor with a mass of 1 GeV and multiplied it with the hadronic current. These currents are then contracted with the standard $V-A$ leptonic current to obtain the transition amplitude which is then used to get total(σ) and differential scattering cross sections like Q^2 distribution and kaon energy distribution.

We find that the contact term is dominant, followed by the u-channel diagram with a Λ intermediate state and the π exchange term. The kaon pole contributions are negligible. We must point out that the contact term coming from the chiral Lagrangian has not been taken into account in earlier works. Some of the results and our main observations have been presented here. For example, in Fig. 2.2, we have presented the total scattering cross sections for the processes mentioned in Eq. 2.1. In this figure, we have also shown the cross sections for the above processes, where we have tried to explore the validity of our calculation(particularly energy region) by comparing our results with the values for the associated production obtained by means of the GENIE Monte Carlo generator [17]. We observe that, due to the difference between the energy thresholds, single kaon production for $\nu_l + p \rightarrow l^- + K^+ + p$ is clearly dominant for neutrinos of energies below 1.5 GeV. For the other two channels associated production becomes comparable at lower energies. Still, single K^0 production off neutrons is larger than the associated production up to E_ν =1.3 GeV and even the much smaller K^+ production off neutrons is larger than

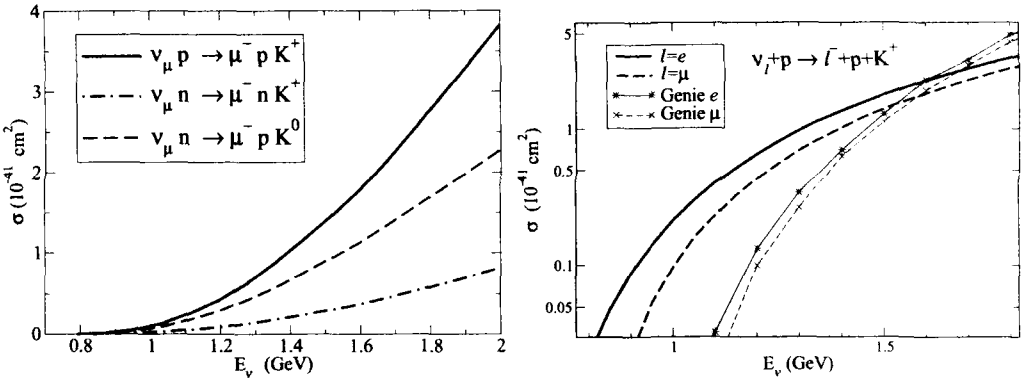

Figure 2.2: Cross sections(σ) as a function of the neutrino energy for single kaon production. In left panel: σ vs E_ν for the three $\Delta S = 1$ processes are shown and in the right panel: single kaon production vs. associated production obtained with GENIE [17] are shown.

Table 2.1: Cross sections averaged over the neutrino flux at different laboratories in units of 10^{-41} cm^2. Theoretical uncertainties correspond to a 10% variation of the form factor mass.

Process	ANL	MiniBooNE	T2K
$\nu_\mu n \to \mu^- K^+ n$	0.06(1)	0.07(1)	0.09(1)
$\nu_\mu p \to \mu^- K^+ p$	0.28(5)	0.32(5)	0.43(8)
$\nu_\mu n \to \mu^- K^0 p$	0.17(3)	0.20(3)	0.25(5)

the associated production up to E_ν =1.1 GeV. The consideration of these $\Delta S = 1$ channels is, therefore, important for the description of strangeness production for all low energy neutrino spectra and should be incorporated in the experimental analysis.

In Table 2.1, we show the total cross section results for the three channels averaged over the ANL [26], the MiniBooNE [27] and the off-axis (2.5 degrees) T2K [28] muon neutrino fluxes, all of them peaking at around 0.6 GeV.

We may get an idea of the magnitude of these channels by comparing their cross section with some recent results. For instance, the cross section for neutral current π^0 production per nucleon has been measured by the MiniBooNE collaboration [29] obtaining $\langle\sigma\rangle = (4.76 \pm 0.05 \pm 0.76) \times 10^{-40}$ cm^2 with a data set of some twenty

Table 2.2: Number of events calculated for single kaon production in water corresponding to the SuperK analysis for atmospheric neutrinos.

Process	Events e^-	Events μ^-
$\nu_l n \to l^- n K^+$	0.16	0.27
$\nu_l n \to l^- p K^0$	0.45	0.73
$\nu_l p \to l^- p K^+$	0.95	1.55
Total	1.56	2.55

thousand valid events. The cross sections predicted by our model with the same neutrino flux are around two orders of magnitude smaller, what means that a few hundreds of kaons should have been produced.

The atmospheric neutrino spectrum [30] also peaks at very low energies and our model should be very well suited to analyze the kaon production. In Table 2.2, we show the number of kaon events that has been obtained for the 22.5 kT of water target and for a period of 1489 days as in the SuperK analysis [31, 32] of proton decay. As in the Refs. [31, 32], we include cuts in the electron momentum ($p_e > 100$ MeV) and muon momentum ($p_\mu > 200$ MeV). We find that single kaon production is a very small source of background. In the SuperK analysis the kaon production was modeled following Ref. [20, 33] and only includes associated kaon production.

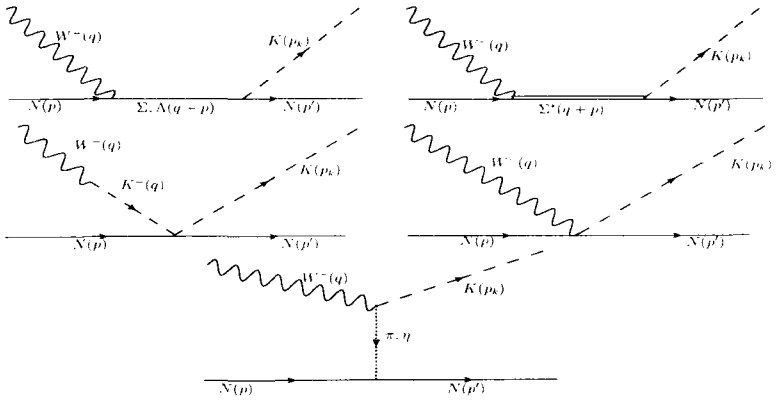

Figure 2.3: Feynman diagrams for the process $\bar{\nu}N \to lN'K$. First row from left to right: s-channel Σ, Λ propagator (labeled SC in the text), s-channel Σ^* resonance (SCR), second row: kaon pole term (KP); contact term (CT) and last row: pion(eta) in flight ($\pi P/\eta P$).

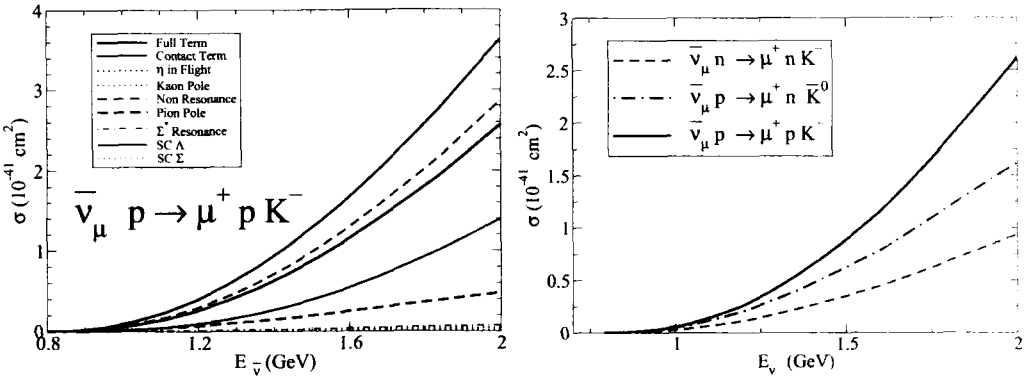

Figure 2.4: Left Panel: Contribution of the different terms to the total scattering cross sections σ vs E_ν. The labels are self explanatory. Right Panel: σ vs E_ν for the $\Delta S = 1$, $K^-/\bar{K}^0$ production.

2.2 Antineutrino Induced $K^-/\bar{K}^0$ Production

In the case of antineutrino induced process, we have considered the following reactions:

$$\begin{aligned} \bar{\nu}_\mu + p &\to \mu^+ + K^- + p \\ \bar{\nu}_\mu + p &\to \mu^+ + \bar{K}^0 + n \\ \bar{\nu}_\mu + n &\to \mu^+ + K^- + n \end{aligned} \tag{2.2}$$

In this case, besides the background terms, such as contact term, s-channel diagram, kaon pole and pion/eta in flight term, we have also included the contribution from lowest lying $\Sigma^*(1535)$ resonance as shown in Fig. 2.3.

The contribution from the different terms of the hadronic current to the transition amplitude while calculating total scattering cross section has been shown in the left panel of Fig. 2.4 for $\bar{\nu}_\mu p \to \mu^+ p K^-$ process. We may see that the contact term is the most dominating one while the contribution of the Σ^* resonance is very small. In the right panel of Fig. 2.4, we have presented the results for the total scattering cross section $K^-/\bar{K}^0$ production. We find that the cross section for the K^- production on proton target is largest, followed by the $\bar{K}^0$ production. While the K^- production on neutron target is smallest than the other channels.

The lowest energy antikaon associate production, ($K\bar{K}$, $|\Delta S| = 0$), has a quite high threshold ($\approx$ 1.75 GeV) and thus, it leads to even smaller cross sections in the range of energies we have explored. For instance, at 2 GeV, GENIE predicts

antikaon production cross sections at least two orders of magnitude smaller than our calculation.

In the next chapter we present the formalism and results for the $\Delta S = 1$ kaon production induced by electron/positron beam.

CHAPTER 3

Charged Lepton Induced One Kaon Production

The availability of very high luminosity beams has provided the opportunity to study the electromagnetic associated strangeness production of a strange and an anti-strange particle. The cross section for weak associated strangeness production is obviously much smaller than that of the electromagnetic ones. However, weak interaction allows the processes where only one strange/anti-strange($\Delta S = \pm 1$) particle is produced, and these reactions could have a substantially lower threshold. For instance, the threshold for electron induced weak K^- production on a proton is around 600 MeV whereas it is 1.5 GeV for electromagnetic production, as an additional kaon is required.

The study of weak kaon production induced by charged lepton beam could provide valuable information on the coupling constants D and F that govern the interaction of the $SU(3)$ lightest baryon octet with the pseudoscalar mesons and also their β decays. Also, one may investigate the Q^2 dependence of the weak axial form factors of nucleons and hyperons.

The processes considered here are the charged lepton induced weak $|\Delta S| = 1$ $K(\bar{K})$ production. The single antikaon(kaon) production channels induced by electrons(positrons) are the following

$$\begin{aligned} e^- + n &\to \nu_e + K^- + n & \qquad e^+ + n &\to \bar{\nu}_e + K^+ + n \\ e^- + p &\to \nu_e + \bar{K^0} + n & \qquad e^+ + n &\to \bar{\nu}_e + K^0 + p \\ e^- + p &\to \nu_e + K^- + p & \qquad e^+ + p &\to \bar{\nu}_e + K^+ + p \end{aligned} \tag{3.1}$$

Apart from the contributions from the lowest order chiral Lagrangian, we have also included the contribution of terms with $\Sigma^*(1385)$ resonance belonging to the SU(3) baryon decuplet, which is near the threshold of the NK system. This is suggested by the dominant role played by the $\Delta(1232)$ resonance in pion production reactions.

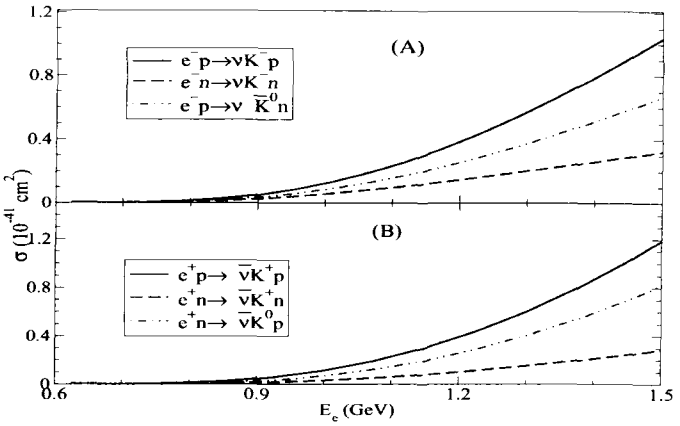

Figure 3.1: Cross section σ vs electron(positron) energy E_e for the $\bar{K}(K)$ production

In Fig. 3.1, we have shown the cross sections for the processes mentioned in Eq. 3.1. We find that $e^-(e^+) + p \to \nu_e(\bar{\nu}_e) + K^-(K^+) + p$ has the largest cross section followed by $e^-(e^+) + p(n) \to \nu_e(\bar{\nu}_e) + \bar{K}^0(K^0) + n(p)$ and $e^-(e^+) + n \to \nu_e(\bar{\nu}_e) + K^-(K^+) + n$. Furthermore, we find that the cross sections for the positron induced processes are larger than for the corresponding electron induced processes. This is basically due to the different interference between the s-channel and contact terms.

To estimate the number of events for single kaon production we have considered a luminosity of $5 \times 10^{37}\, s^{-1}$ cm^{-2} for MAMI, that corresponds to a 10 cm liquid hydrogen target at an electron beam current of 20 μA as described in Ref.[34]. For TJNAF, we take a luminosity of $5 \times 10^{38}\, s^{-1}$ cm^{-2} that corresponds to a current of 100 μA and a larger liquid hydrogen target [35] that has been used on the measurement of parity violating electron proton scattering. Under these conditions and for 1.5 GeV electrons, we would have some 480 events per day for the reaction $e^- + p \to \nu_e + K^- + p$ at TJNAF (48 at MAMI). For $e^- + p \to \nu_e + K^0 + n$ reaction. we would get 320 events per day at TJNAF (32 at MAMI). Certainly, the numbers could be changed by using different targets and/or current but equally important is the efficiency in the kaon detection, that depends on the kaon kinematics and the

detector.

In the next chapter we shall present the formalism for photon and neutrino induced η particle production process.

CHAPTER 4

η Production

We have studied the following charged current neutrino/antineutrino induced eta production process from nucleon

$$\nu_\mu + n \to \mu^- + \eta + p \qquad \bar{\nu}_\mu + p \to \mu^+ + \eta + n \tag{4.1}$$

In these processes from χPT symmetry only s- and u-channel nucleon pole terms contribute. Besides Born-terms, we have also considered $S_{11}(1535)$ and $S_{11}(1650)$ resonances. The Feynman diagrams corresponding to these processes are shown in Fig. 4.1.

However, before developing the formalism for the weak interaction induced eta production, we have obtained the cross section for the photon induced eta production off proton. This is to first fix the electromagnetic form factors by comparing it with the available results for scattering cross section from Crystal Ball experiment [36] and use them to obtain the isovector form factors for $\nu/\bar{\nu}$ induced processes off the nucleon. Born terms are calculated using a microscopical model based on the $SU(3)$ chiral Lagrangian. We consider $N^*(1535)$ as well as $N^*(1650)$ S_{11} resonant intermediate states. The vector form factors of the N-S_{11} transition have been obtained from the helicity amplitudes extracted in the analysis of world pion photo- and electroproduction data using the unitary isobar model [37]. The properties of the axial N-S_{11} transition current are basically unknown but assuming the pion-pole dominance of the pseudoscalar form factor, together with PCAC one may fix the axial coupling using the empirical $N^* \to N\pi$ partial decay width. We make an

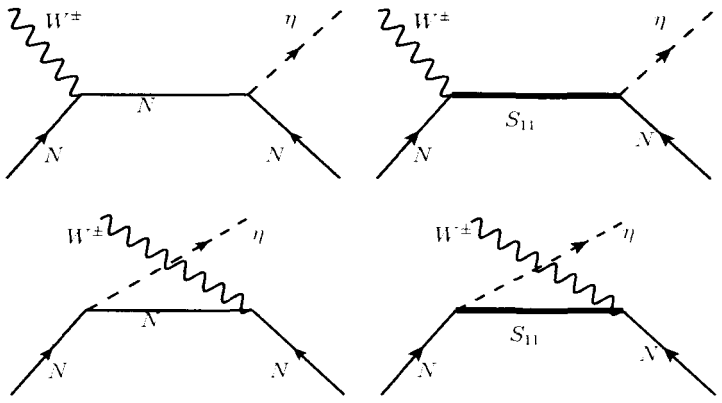

Figure 4.1: Feynman diagrams for the processes $\nu/\bar{\nu}(k)+N(p) \rightarrow \mu^{\mp}(k')+\eta(p_\eta)+N'(p')$. First row from left to right: s-channel nucleon pole(SC) and S_{11} resonance(SC N^*): second row: u-channel nucleon pole(UC) and S_{11} resonance (UC N^*).

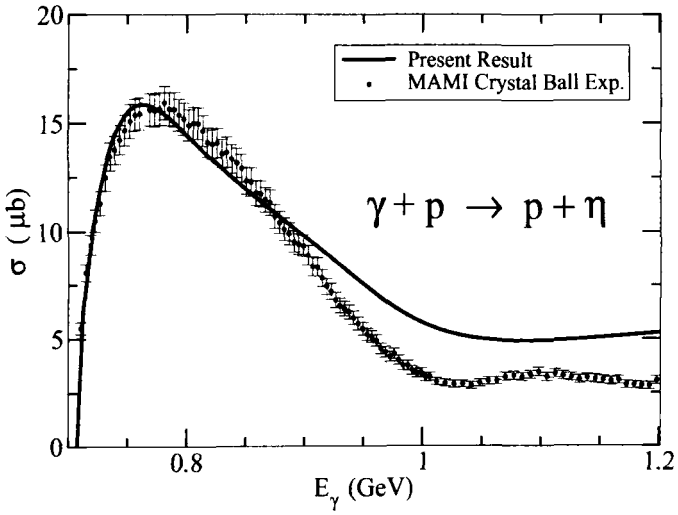

Figure 4.2: Cross section for $\gamma p \rightarrow \eta p$ process. The experimental points are obtained from MAMI crystal ball [36] and the results are shown upto the ΛK threshold.

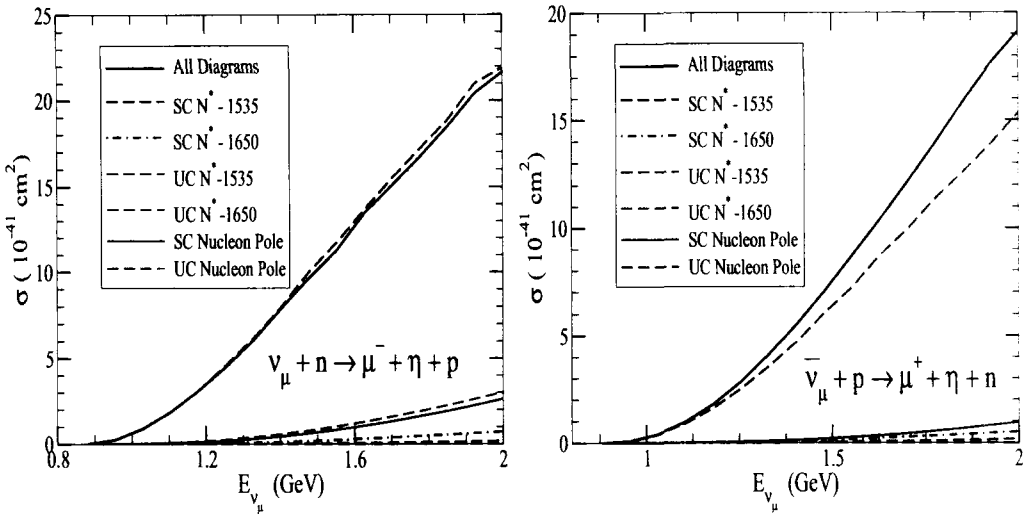

Figure 4.3: Contribution of the different Feynman diagrams to the total scattering cross section for the η production process, where SC and UC corresponds to the s-channel and u-channel nucleon pole and N^* resonances respectively.

educated guess for the dependence on the four-momentum square transferred by the neutrino, which ultimately remains to be determined experimentally. We find that the present results describe qualitatively well the experimental data represented by the MAMI Crystal Ball experiment [36] except at high photon energies as shown in Fig. 4.2.

In Fig. 4.3, the results for neutrino and antineutrino induced η production cross sections are presented both for the total as well as individual contributions of each diagram. We find that $S_{11}(1535)$ resonance is dominant while the contribution of $S_{11}(1650)$ to the total cross section is small. This can be understood easily because $S_{11}(1535)$ is lighter in mass and has a relatively larger branching ratio for $S_{11} \to N\eta$. We also find that the contribution of the nonresonant diagrams in the case of neutrino induced process is higher than the corresponding antineutrino induced processes. Also in neutrino mode the contribution of u-channel diagram is slightly larger than the corresponding s-channel diagram. We find that around 1-2 GeV the contribution of $S_{11}(1535)$ is very dominant for the neutrino induced process. In the case of antineutrino induced reaction up to $E_{\bar{\nu}}$ =1 GeV, $S_{11}(1535)$ is dominant, however at $E_{\bar{\nu}} = 1.5$ GeV its contribution is around 80% of the total η production cross section. The contribution of $S_{11}(1650)$ resonance is not more than 5% in the entire neutrino energy spectrum. Contributions from the s- and u-

channel diagrams of nucleon pole are around $10 - 15\%$ to the total cross section.

In the next chapter, we present the formalism for the associated particle production and present the results for the total scattering cross section as well as differential scattering cross section.

CHAPTER 5

Associated Kaon Production

The study of weak neutrino-nucleon/nucleus interactions involving associated particle production in the energy region of a few GeV has become one of the major theoretical and experimental area of interest due to its importance in the fields of astrophysics, cosmology, particle as well as nuclear physics. First of all a good understanding of these interactions would lead to a better insight into nucleon and nuclear structures. This will be an additional tool to complement the theories of particle and nuclear physics, the knowledge of which one obtains from electromagnetic reactions with real and virtual photons. Moreover, the study of neutrino induced ΔS=0 associated particle production processes provide an improved understanding of basic symmetries of the standard model, structure of the weak hadronic form factors, strange-quark content of the nucleon, coupling constants, etc. One may also get information on the medium modification of the elementary amplitudes. Furthermore, the efforts of proton decay searches at various laboratories like SuperK [38], HyperK [39], UNO [40], LAGUNA [41], etc., are going on where the atmospheric neutrinos while interacting with a nucleon target also produce kaons, either through $\Delta S = 0$ or $\Delta S = 1$ processes. This poses a background in the proton decay searches as the main source of proton decay in supersymmetric grand unified models has been proposed through $p \to K\bar{\nu}$. Therefore, the importance of thorough understanding and reliable estimate of the cross sections for neutrino induced kaon production contributing as background event has been emphasized as the proton decay experiments will be limited in statistics also [42, 43].

The experimental observations of the neutrino induced associated particle production processes are quite limited. These are limited both by statistics as well as by the large systematic errors. Earlier the experiments were performed at BNL[8], ANL [9] and CERN[44, 45, 46], however, to have neutrino oscillation parameters with high precision, many experiments are coming up in the energy range of a few GeV. For example, the MINERνA experiment at Fermi Lab [43], is a dedicated experiment to measure the cross sections, and their aim is also to study many associated particle production processes. This will allow physicists to gain considerable insight into the structure of the nucleon and the hadronic weak current via the (anti)neutrino induced weak production of strange particles. There are other planned experiment like LBNE [47] which would also be sensitive to the measurement of strange particles.

The basic reactions for $\nu(\bar{\nu})$ charged current induced associated particle production accompanied by a kaon from a nucleon(p or n) target are,

$$\begin{aligned} \nu_\mu n &\to \mu^- K^+ \Lambda & \bar{\nu}_\mu p &\to \mu^+ K^0 \Lambda \\ \nu_\mu p &\to \mu^- K^+ \Sigma^+ & \bar{\nu}_\mu p &\to \mu^+ K^0 \Sigma^0 \\ \nu_\mu n &\to \mu^- K^+ \Sigma^0 & \bar{\nu}_\mu p &\to \mu^+ K^+ \Sigma^- \\ \nu_\mu n &\to \mu^- K^0 \Sigma^+ & \bar{\nu}_\mu n &\to \mu^+ K^0 \Sigma^- \end{aligned}$$

The contribution to the hadronic current comes from the different pieces of the Lagrangian corresponding to the Feynman diagrams shown in Fig. 5.1.

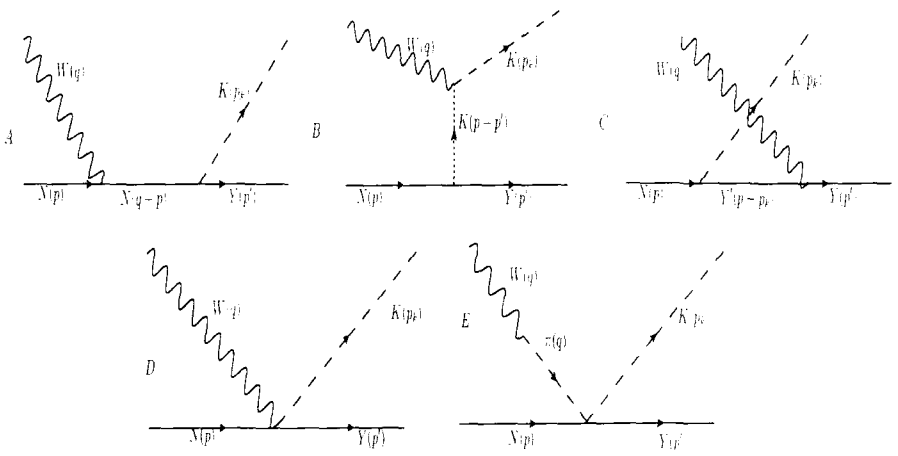

Figure 5.1: Feynman diagrams corresponding to the neutrino/antineutrino induced $\Delta S = 0$ kaon production process.

We generalize the nucleon and hyperon pole diagrams to incorporate form factors at the weak vertices following Refs. [48, 49].

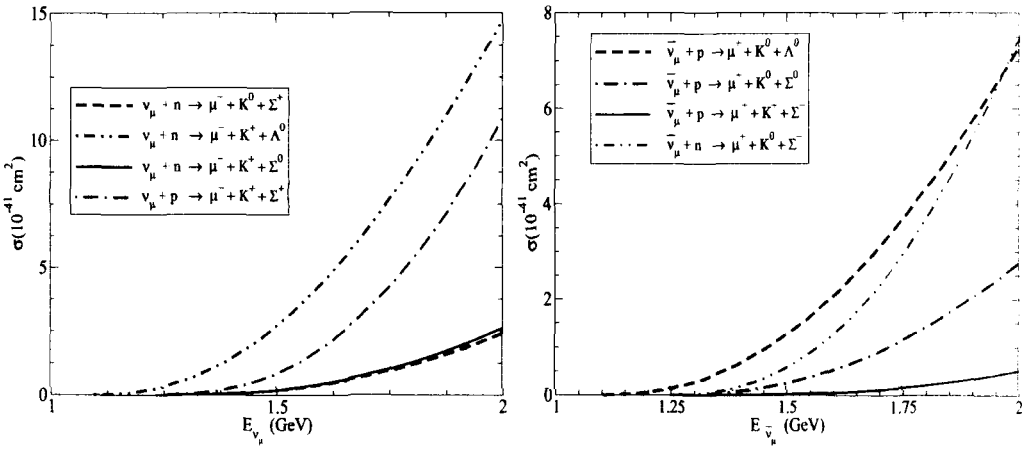

Figure 5.2: Cross section for neutrino and antineutrino induced $|\Delta S| = 0$ associated kaon production process.

In Fig. 5.2, we have presented the results for the neutrino(left panel) and antineutrino(right panel) induced $\Delta S = 0$ associated kaon production processes. In the case of neutrino induced reactions when we compare the results of the cross sections for the processes $\nu_\mu p \to \mu^- \Sigma^+ K^+$ and $\nu_\mu n \to \mu^- \Lambda K^+$, we find that the cross section for the $K^+\Sigma^+$ channel is around 70% smaller at $E_\nu = 1.5$ GeV and around 25% smaller at $E_\nu = 2$ GeV in comparison to the cross section for the $K^+\Lambda$ channel. While the cross sections for the other two channels namely $\nu_\mu n \to \mu^- \Sigma^+ K^0$ and $\mu^- \Sigma^0 K^+$ are much smaller than the $K^+\Lambda$ cross section.

While in the case of antineutrino induced production processes where one may notice that unlike the neutrino induced processes the channel with Λ in the final state is not very dominating. For example, we find that at low energies say $E_{\bar{\nu}_\mu} \sim 1.5$ GeV the cross section for $\bar{\nu}_\mu p \to \mu^+ K^0 \Lambda$ is around 55% larger than the cross section for $\bar{\nu}_\mu n \to \mu^+ K^0 \Sigma^-$, while around 2 GeV the production cross section for $\nu_\mu p \to \mu^+ K^0 \Lambda$ is comparable with that of $\bar{\nu}_\mu n \to \mu^+ K^0 \Sigma^-$. The cross section for the reaction $\bar{\nu}_\mu p \to \mu^+ K^0 \Sigma^0$ is around 40% smaller than the cross section for $K^0\Lambda$ channel at $E_{\bar{\nu}_\mu} = 2$ GeV, whereas $\bar{\nu}_\mu p \to \mu^+ K^+ \Sigma^-$ cross section is about 10% to the cross section of $K^0\Lambda$ channel.

In the next chapter, we finally conclude our findings and summarize the main results.

CHAPTER 6

Conclusions

In this thesis we study the weak production mechanism for the low lying meson having strange quark(s) like, $K^{\pm}, K^0, \bar{K}^0$ and η. A precise knowledge about these processes would be very important for the analysis of ongoing and future neutrino oscillation experiments as it would also facilitate in the understanding of hadron structure and their properties. The study of these processes are done using a microscopic model which is based on SU(3) Chiral Perturbation Theory(χPT). In particular, the parameters involved for the octet baryons are, Cabibbo angle, the pion decay constant, proton and neutron magnetic moments, and the axial-vector coupling constants D and F, are all known with a high precision. The predictions of the results should be more reliable at low and intermediate energies. In the case of $K^-/\bar{K}^0$ production we also incorporate the lowest lying strange resonance $\Sigma^*(1385)$. The weak couplings of the $\Sigma^*(1385)$ have been obtained from those of the $\Delta(1232)$ using SU(3) symmetry.

In the case of η production processes, the background terms are calculated using the chiral Lagrangian. However, from the photo- and electro- production of η mesons we know that the $S_{11}(1535)$ gives the dominant contribution to the scattering cross sections. Therefore, in our model we have included the $S_{11}(1535)$ resonance as well as $S_{11}(1650)$ resonance. The parameters involved in the resonance mechanism are obtained using the helicity amplitude. For the $\Delta S = 0$ associated kaon production, we generalized the hadronic currents that are obtained from the chiral Lagrangian to include the weak transition form factors for the baryon octet.

Our future plan is to include resonances in the associated particle production processes. We also plan to study these processes for nucleons bound inside the nuclear targets as all the neutrino/antineutrino experiments are using heavy nuclear targets to get significant number of events.

Bibliography

[1] A. Aguilar-Arevalo *et al.*, "First Measurement of the Muon Anti-Neutrino Double-Differential Charged Current Quasi-Elastic Cross Section," **Phys.Rev.**, **D88**, p. 032001, 2013. 1

[2] S. Ahn *et al.*, "Detection of accelerator produced neutrinos at a distance of 250-km," **Phys.Lett.**, **B511**, pp. 178–184, 2001. 1, 2

[3] K. Abe *et al.*, "The T2K Experiment," **Nucl.Instrum.Meth.**, **A659**, pp. 106–135, 2011. 1, 2

[4] M. Muether, "NOvA: Current Status and Future Reach," **Nucl. Phys. Proc. Suppl.**, **237-238**, p. 135, 2013. 1

[5] Y. Hayato *et al.*, "Search for proton decay through $p \to \bar{\nu} K^+$ in a large water Cherenkov detector," **Phys.Rev.Lett.**, **83**, pp. 1529–1533, 1999. 2

[6] G. Ross, **Grand Unified Theories**. Frontiers in physics, Westview Press, 1984. 2

[7] S. Barish, M. Derrick, T. Dombeck, L. Hyman, K. Jaeger, *et al.*, "Study of Neutrino Interactions in Hydrogen and Deuterium: Inelastic Charged Current Reactions," **Phys.Rev.**, **D19**, p. 2521, 1979. 2

[8] N. Baker, P. Connolly, S. Kahn, H. Kirk, M. Murtagh, *et al.*, "Strange Particle Production from Neutrino Interactions in the BNL 7-Ft Bubble Chamber," **Phys.Rev.**, **D24**, pp. 2779–2786, 1981. 2, 20

[9] S. Barish, M. Derrick, L. Hyman, P. Schreiner, R. Singer, *et al.*, "Strange-Particle Production in Neutrino Interactions," **Phys.Rev.Lett.**, **33**, p. 1446, 1974. 2, 20

[10] D. W. Schmitz, "The MINERvA neutrino scattering experiment at Fermilab," **AIP Conf.Proc.**, **1405**, pp. 243–249, 2011. 2

[11] Y. Hayato, "A neutrino interaction simulation program library NEUT," **Acta Phys.Polon.**, **B40**, pp. 2477–2489, 2009. 2, 2

[12] Y. Fukuda *et al.*, "Evidence for oscillation of atmospheric neutrinos," **Phys.Rev.Lett.**, **81**, pp. 1562–1567, 1998. 2

[13] Y. Kurimoto *et al.*, "Improved measurement of neutral current coherent π^0 production on carbon in a few-GeV neutrino beam," **Phys.Rev.**, **D81**, p. 111102, 2010. 2

[14] H. Gallagher, "The NEUGEN neutrino event generator," **Nucl.Phys.Proc.Suppl.**, **112**, pp. 188–194, 2002. 2

[15] D. Casper, "The Nuance neutrino physics simulation, and the future," **Nucl.Phys.Proc.Suppl.**, **112**, pp. 161–170, 2002. 2

[16] G. Zeller, "Low-energy neutrino cross-sections: Comparison of various Monte Carlo predictions to experimental data," **arXiv:hep-ex/0312061**, 2003. 2

[17] C. Andreopoulos, A. Bell, D. Bhattacharya, F. Cavanna, J. Dobson, *et al.*, "The GENIE Neutrino Monte Carlo Generator," **Nucl.Instrum.Meth.**, **A614**, pp. 87–104, 2010. 2, 6, 7

[18] C. B. Dover and P. M. Fishbane, "Eta and eta-prime scattering: a probe of the strange quark (s anti-s) content of the nucleon," **Phys.Rev.Lett.**, **64**, pp. 3115–3118, 1990. 2

[19] D. Wall *et al.*, "Search for nucleon decay with final states $l^+\eta^0$, $\bar{\nu}\eta^0$, and $\bar{\nu}\pi^{+,0}$ using Soudan-2," **Phys.Rev.**, **D62**, p. 092003, 2000. 3

[20] D. Rein and L. M. Sehgal, "Neutrino Excitation of Baryon Resonances and Single Pion Production," **Annals Phys.**, **133**, pp. 79–153, 1981. 3, 8

[21] P. Achenbach, "Strangeness physics with Kaos at MAMI," **arXiv:1101.4394**, 2011. 3, 3

[22] M. Sumihama, "Experimental results of K^+ photoproduction at SPring-8/LEPS," **Nucl.Phys.**, **A754**, pp. 303–309, 2005. 3

[23] R. Lawall, J. Barth, C. Bennhold, K.-H. Glander, S. Goers, *et al.*, "Measurement of the reaction $\gamma p \to K^0\Sigma^+$ at photon energies up to 2.6-GeV," **Eur.Phys.J.**, **A24**, pp. 275–286, 2005. 3

[24] K. Glander, J. Barth, W. Braun, J. Hannappel, N. Jopen, *et al.*, "Measurement of $\gamma p \to K^+\Lambda$ and $\gamma p \to K^+\Sigma^0$ at photon energies up to 2.6-GeV," **Eur.Phys.J.**, **A19**, pp. 251–273, 2004. 3

[25] P. Ambrozewicz *et al.*, "Separated structure functions for the exclusive electroproduction of $K^+\Lambda$ and $K^+\Sigma^0$ final states," **Phys.Rev.**, **C75**, p. 045203, 2007. 3

[26] S. Barish, J. Campbell, G. Charlton, Y. Cho, M. Derrick, *et al.*, "Study of Neutrino Interactions in Hydrogen and Deuterium. 1. Description of the Experiment and Study of the Reaction $\nu d \to \mu^- pp_s$," **Phys.Rev.**, **D16**, p. 3103, 1977. 7

[27] A. Aguilar-Arevalo *et al.*, "First Measurement of the Muon Neutrino Charged Current Quasielastic Double Differential Cross Section," **Phys.Rev.**, **D81**, p. 092005, 2010. 7

[28] A. Ichikawa, "The T2K long-baseline neutrino experiment," **Lect.Notes Phys.**, **781**, pp. 17–43, 2009. 7

[29] A. A. Aguilar-Arevalo *et al.*, "Measurement of ν_μ and $\bar{\nu}_\mu$ induced neutral current single π^0 production cross sections on mineral oil at $E_\nu \sim O(1 - GeV)$," **Phys.Rev.. D81**. p. 013005. 2010. 7

[30] M. Honda, T. Kajita, K. Kasahara, S. Midorikawa, and T. Sanuki, "Calculation of atmospheric neutrino flux using the interaction model calibrated with atmospheric muon data," **Phys.Rev., D75**, p. 043006, 2007. 8

[31] K. Kobayashi *et al.*, "Search for nucleon decay via modes favored by supersymmetric grand unification models in Super-Kamiokande-I," **Phys.Rev., D72**, p. 052007. 2005. 8, 8

[32] Y. Ashie *et al.*, "A Measurement of atmospheric neutrino oscillation parameters by SUPER-KAMIOKANDE I," **Phys.Rev., D71**, p. 112005, 2005. 8, 8

[33] D. Rein, "Angular Distribution In Neutrino Induced Single Pion Production Processes," **Z.Phys., C35**, pp. 43–64, 1987. 8

[34] I. Altarev, E. Schilling, S. Baunack, L. Capozza, J. Diefenbach, *et al.*, "A High power liquid hydrogen target for the Mainz A4 parity violation experiment," **Nucl.Instrum.Meth., A564**, pp. 13–25, 2006. 12

[35] K. Aniol *et al.*, "Parity violating electroweak asymmetry in polarized-e p scattering," **Phys.Rev., C69**, p. 065501, 2004. 12

[36] E. McNicoll *et al.*, "Study of the $\gamma p \to \eta p$ reaction with the Crystal Ball detector at the Mainz Microtron(MAMI-C)," **Phys.Rev., C82**, p. 035208, 2010. 15, 16, 17

[37] D. Drechsel, S. Kamalov, and L. Tiator, "Unitary Isobar Model - MAID2007," **Eur.Phys.J., A34**, pp. 69–97, 2007. 15

[38] C. Regis *et al.*, "Search for Proton Decay via $p \to \mu^+ K^0$ in Super-Kamiokande I, II, and III," **Phys.Rev., D86**, p. 012006, 2012. 19

[39] K. Abe, T. Abe, H. Aihara, Y. Fukuda, Y. Hayato, *et al.*, "Letter of Intent: The Hyper-Kamiokande Experiment — Detector Design and Physics Potential —," **arXiv:1109.3262**, 2011. 19

[40] C. K. Jung, "Feasibility of a next generation underground water Cherenkov detector: UNO," **AIP Conf.Proc., 533**, pp. 29–34, 2000. 19

[41] J. Kisiel *et al.*, "The LAGUNA project: Towards the giant liquid based detectors for proton decay searches and for low energy neutrino astrophysics," **PoS. EPS-HEP2009**. p. 283. 2009. 19

[42] W. Mann, T. Kafka, M. Derrick, B. Musgrave, R. Ammar, *et al.*, "K Meson Production By Muon-Neutrino - Deuterium Reactions Near Threshold: Implications For Nucleon Decay Searches," **Phys.Rev., D34**, pp. 2545–2553, 1986. 19

[43] N. Solomey, "A proposed study of neutrino-induced strange-particle production reactions at Minerva," **Nucl.Phys.Proc.Suppl., 142**, pp. 74–78, 2005. 19, 20

[44] H. Deden, F. Hasert, W. Krenz, J. Von Krogh, D. Lanske, *et al.*, "Strange Particle Production and Charmed Particle Search in the Gargamelle Neutrino Experiment," **Phys.Lett., B58**, pp. 361–366, 1975. 20

[45] O. Erriquez, M. Fogli Muciaccia, S. Natali, S. Nuzzo, A. Halsteinslid, *et al.*, "Strange Particle Production by anti-neutrinos," **Phys.Lett.**, **B70**, pp. 383–386, 1977. 20

[46] O. Erriquez, M. Fogli-Muciaccia, S. Natali, S. Nuzzo, A. Halsteinslid, *et al.*, "Production of Strange Particles in anti-neutrino Interactions at the CERN PS," **Nucl.Phys.**, **B140**, pp. 123–140, 1978. 20

[47] B. Choudhary *et al.*, "Proposal of Indian Institutions and Fermilab Collaboration for Participation in the Long-Baseline Neutrino Experiment at Fermilab," **LBNE**, **6704-v1**, 2013. 20

[48] S. Singh and M. Vicente Vacas, "Weak quasi-elastic production of hyperons," **Phys.Rev.**, **D74**, p. 053009, 2006. 20

[49] N. Cabibbo, E. C. Swallow, and R. Winston, "Semileptonic hyperon decays," **Ann.Rev.Nucl.Part.Sci.**, **53**, pp. 39–75. 2003. 20

Weak Production of K and η Mesons off the Nucleon

THESIS

SUBMITTED FOR THE AWARD OF THE DEGREE OF

Doctor of Philosophy

IN

PHYSICS

BY

MOHAMMAD RAFI ALAM

Supervisor

Dr. Mohammad Sajjad Athar

DEPARTMENT OF PHYSICS
ALIGARH MUSLIM UNIVERSITY
ALIGARH-202 002 (INDIA)

2013

PHYSICS DEPARTMENT
ALIGARH MUSLIM UNIVERSITY
ALIGARH - 202002 (INDIA)

PH.: 91-571-2700984
PH. & FAX: 91-571-2701001

November 01,2013

CERTIFICATE

Certified that the work reported in this Thesis entitled, "Weak Production of K and η Mesons off the Nucleon" is the original work of Mr. Mohammad Rafi Alam, done under my supervision.

Md. Sajjad Athar

(Mohammad Sajjad Athar)

Associate Professor

Contents

Contents i

Acknowledgement iii

List of Figures v

List of Tables ix

List of Publications xi

1 Introduction 1

2 Weak Production of K and $\bar{K}$ 11
- 2.1 Effective Field Theory 11
  - 2.1.1 Chiral Perturbation Theory 12
- 2.2 Neutrino Induced Kaon Production 19
  - 2.2.1 Formalism 20
  - 2.2.2 Results and Discussion 24
- 2.3 Antineutrino Induced $K^-/\bar{K}^0$ Production 34
  - 2.3.1 Formalism 35
  - 2.3.2 Results and Discussion 39

3 Charged Lepton Induced One Kaon Production 49
- 3.1 Introduction 49
- 3.2 Formalism 50
- 3.3 Results and Discussion 55

4 η Production **63**
4.1 Introduction 63
4.2 Formalism 65
4.2.1 Photoproduction of η 65
4.2.2 Weak Production of η 70
4.3 Results and Discussion 80

5 Associated Kaon Production **85**
5.1 Introduction 85
5.2 Formalism 88
5.2.1 Vector Form Factor 91
5.2.2 Axial Form Factor 93
5.3 Results and Discussion 96

6 Conclusions **105**

Appendix **111**

A $\Delta(1232)$ Decay Width **111**
A.1 The Lagrangian N$\Delta\pi$ 111
A.2 Width from Chiral Lagrangian 114
A.3 Relation between $\mathcal{C}$ and $C_5^A(0)$ 114

B Weak Magnetism in Hadronic Current **117**

C Kinematics **121**
C.1 Total Cross Section in Lab Frame 121
C.2 Recoil Factor 122
C.2.1 Kaon Momentum Distribution p_l 122

Bibliography **127**

Bibliography **127**

Acknowledgments

First of all, I would like to express my deep gratitude to my supervisor Dr Mohammad Sajjad Athar. His guidance helped me in all the time of research. Long hours of lively discussion with him will always be my asset which I will cherish. I thank him for his patience, understanding, kindness, and among other things, not letting me quit and helping me in finalizing this work. I am thankful to him for his continuous support and encouragement since I joined this department.

My sincere thanks to Prof. S. K. Singh for his constant encouragement and useful advice. We have also started a research collaboration with him.

Professor M. J. Vicente Vacas, I Ruiz Simo, and Luis Alvarez-Ruso, deserve special thanks for creating welcoming atmosphere throughout my stay at the University of Valencia, Spain. I thank them for their research collaboration and valuable suggestions. I hope that our collaboration will grow by leaps and bounds.

I am thankful to the Chairman, Department of Physics, Prof. Rahimullah Khan for providing me the basic facilities in the department.

My thanks are due to Dr. Shikha Chauhan and Ms. Huma Haider, my lab colleague for bearing me over the past years as well as helping me in the finalization of this work. Specially, Dr. Shikha Chauhan has spent her valuable time in proof reading of this thesis. I also want to thank my fellow labmate Ms. Farhana Zaidi.

Thanks are due to seminar staff of the department, specially to Mr. Shakeel Kirmani for his support.

I thank, my close friends, Jazbul, Shahab, Gaus, Maaz, Ikram, Jane Alam, Shahid, Hashim, Sheeraj, for making my stay in A.M.U. pleasant and always celebrating week ends in a great way.

I thank my entire family for their love and support, and especially my parents who always stood by me and allowed me to pursuit higher studies. This thesis is dedicated to my loving parents.

My special thanks to Prof. Mohammad Ozair, Mrs. Talat Ozair and Ms. Fauzia Ahmed for their support, help and encouragement.

I also acknowledge DST, Government of India for the financial support under Grant No. SR/S2/HEP-0001/2008, Maulana Azad National fellowship (J.R.F.) and Council of Scientific & Industrial Research (S.R.F.) for providing me financial assistance to complete this work.

Thanks are due to all those friends and relatives who have always wished me the best for life.

Md. Rafi Alam

Mohammad Rafi Alam

List of Figures

1.1 Contribution to the total scattering cross section [30]. 3

2.1 Feynman diagrams for the process $\nu N \to lN'K$. First row from left to right: contact term (labeled CT in the text), kaon pole term (KP): second row: u-channel diagram ($Cr\Sigma$, $Cr\Lambda$) and pion(eta) in flight (πP, (ηP) 21

2.2 Contribution of the different terms to the total cross section for $\nu_\mu p \to \mu K^+ p$ reaction. 24

2.3 Contribution of the different terms to the total cross section for $\nu_\mu n \to \mu K^0 p$ reaction. 25

2.4 Contribution of the different terms to the total cross section for $\nu_\mu n \to \mu K^+ n$ reaction. 25

2.5 Cross sections as a function of the neutrino energy for single kaon production vs. associated production obtained with GENIE [57]. . . . 27

2.6 Contribution of the different terms to the kaon energy distribution ($\frac{d\sigma}{dE_k}$) at $E_\nu = 1.5GeV$ for $\nu_\mu p \to \mu^- K^+ p$ process. 28

2.7 Contribution of the different terms to the kaon energy distribution ($\frac{d\sigma}{dE_k}$) at $E_\nu = 1.5GeV$ for $\nu_\mu n \to \mu^- K^0 p$ process. 28

2.8 Contribution of the different terms to the kaon energy distribution ($\frac{d\sigma}{dE_k}$) at $E_\nu = 1.5GeV$ for $\nu_\mu n \to \mu^- K^+ n$ process. 29

2.9 Contribution of the different terms to the Q^2 distribution ($\frac{d\sigma}{dQ^2}$) at $E_\nu = 1.5GeV$ for $\nu_\mu p \to \mu^- K^+ p$ process. 30

2.10 Contribution of the different terms to the Q^2 distribution ($\frac{d\sigma}{dQ^2}$) at $E_\nu = 1.5GeV$ for $\nu_\mu n \to \mu^- K^0 p$ process. 31

2.11 Contribution of the different terms to the Q^2 distribution ($\frac{d\sigma}{dQ^2}$) at $E_\nu = 1.5GeV$ for $\nu_\mu n \to \mu^- K^+ n$ process. 31
2.12 Q^2 distribution ($\frac{d\sigma}{dQ^2}$) at $E_\nu = 1GeV$ for single kaon production induced by neutrinos. The curves are labeled according to the final state of the process. 33
2.13 Feynman diagrams for the process $\bar{\nu}N \to lN'\bar{K}$. First row from left to right: s-channel Σ, Λ propagator (labeled SC in the text), s-channel Σ^* resonance (SCR), second row: kaon pole term (KP); contact term (CT) and last row: pion(eta) in flight ($\pi P/\eta P$). 34
2.14 Cross-section for the processes $\bar{\nu}_\mu N \to \mu^+ N'\bar{K}$ and $\bar{\nu}_e N \to e^+ N'\bar{K}$ as a function of the antineutrino energy 39
2.15 Contribution of the different terms to the total cross section for the process $\bar{\nu}_\mu p \to \mu^+ p K^-$. 41
2.16 Contribution of the different terms to the total cross section for the process $\bar{\nu}_\mu n \to \mu^+ n K^-$. 42
2.17 Contribution of the different terms to the total cross section for the process $\bar{\nu}_\mu p \to \mu^+ n \bar{K}^0$. 42
2.18 Contribution of the different terms to the kaon energy distribution ($\frac{d\sigma}{dE_k}$) at $E_\nu = 1.5GeV$ for $\bar{\nu}_\mu n \to \mu^+ K^- n$ process. 43
2.19 Contribution of the different terms to the kaon energy distribution ($\frac{d\sigma}{dE_k}$) at $E_\nu = 1.5GeV$ for $\bar{\nu}_\mu p \to \mu^+ K^- p$ process. 44
2.20 Contribution of the different terms to the kaon energy distribution ($\frac{d\sigma}{dE_k}$) at $E_\nu = 1.5GeV$ for $\nu_\mu p \to \mu^+ \bar{K}^0 n$ process. 44
2.21 Contribution of the different terms to the Q^2 distribution ($\frac{d\sigma}{dQ^2}$) at $E_\nu = 1.5GeV$ for $\bar{\nu}_\mu n \to \mu^+ K^- n$ process. 45
2.22 Contribution of the different terms to the Q^2 distribution ($\frac{d\sigma}{dQ^2}$) at $E_\nu = 1.5GeV$ for $\bar{\nu}_\mu p \to \mu^+ K^- p$ process. 46
2.23 Contribution of the different terms to the Q^2 distribution ($\frac{d\sigma}{dQ^2}$) at $E_\nu = 1.5GeV$ for $\bar{\nu}_\mu p \to \mu^+ \bar{K}^0 n$ process. 46

3.1 Feynman diagrams for the processes $e^- N \to \nu_e N'\bar{K}$ and $e^+ N \to \bar{\nu}_e N' K$. Here $\bar{K}$ stands for a K^- or $\bar{K}^0$ obtained in an electron induced process and K stands for K^+ or K^0 obtained in a positron induced process. First row from left to right: s-channel Σ^* resonance term (labeled SCR in the text) , s-channel (SC) and u-channel (UC) Σ, Λ propagator; second row: Pion/Eta meson ($\pi P/\eta P$) exchange terms. Contact term (CT) and finally kaon pole term (KP). 51
3.2 Cross section σ vs electron(positron) energy E_e for the $\bar{K}(K)$ production 55

3.3 Contribution of the different terms to the total cross section σ vs electron(positron) energy E_e for the $\bar{K}(K)$ production 57
3.4 Kaon angle distributions at electron energy $E_e = 1.5$ GeV 58
3.5 Kaon momentum distributions at electron energy $E_e = 1.5$ GeV . . . 59
3.6 Q^2 distribution at electron energy $E_e = 1.5$ GeV 59
3.7 Kaon momentum distribution at electron energy $E_e = 1.5$ GeV for the $e^- + p \to \nu_e(\bar{\nu}_e) + K^- + p$ channel for a dipole mass $M_F = 1.25$ and $M_F = 0.85$ GeV. The second curve ($M_F = 0.85$ GeV) has been scaled to get the same area. 60

4.1 Feynman diagrams for the processes $\gamma(q) + p(p) \to \eta(p_\eta) + p(p')$ . . . 66
4.2 Cross section for $\gamma p \to \eta p$ process. The experimental points are obtained from MAMI crystal ball [136] and the results are shown upto the ΛK threshold. 71
4.3 Feynman diagrams for the processes $\nu/\bar{\nu}(k) + N(p) \to \mu^{\mp}(k') + \eta(p_\eta) + N'(p')$. First row from left to right: s-channel nucleon pole(SC) and S_{11} resonance(SC N^*); second row: u-channel nucleon pole(UC) and S_{11} resonance (UC N^*). 72
4.4 Form factors for S_{11} resonances. The fittings are obtained using data from the MAMI Crystal Ball experiment [136]. 75
4.6 Pion pole contribution to the axial current. 76
4.5 The isovector F_1^V and F_2^V form factors for the S_{11} resonances. 77
4.7 Cross section corresponding to Feynman diagrams as shown in Fig. 4.3 78
4.8 Q^2 distribution corresponding to Feynman diagrams as shown in Fig. 4.3 79
4.9 Lepton Energy distribution corresponding to Feynman diagrams as shown in Fig. 4.3 81
4.10 Eta Energy distribution corresponding to Feynman diagrams as shown in Fig. 4.3 82

5.1 Feynman diagrams corresponding to the neutrino/antineutrino induced $\Delta S = 0$ kaon production process. 89
5.2 Weak transition vertex. 89
5.3 Cross section for neutrino induced $|\Delta S| = 0$ associated kaon production process. 96
5.4 Cross section for antineutrino induced $|\Delta S| = 0$ associated kaon production process. 97
5.5 Cross section for the $\nu_\mu + n \to \mu^- + K^+ + \Lambda$ process explicitly showing the Feynman diagrams involved. 97

5.6 Cross section for the $\bar{\nu}_\mu + p \to \mu^+ + K^0 + \Lambda$ process explicitly showing the Feynman diagrams involved. 98
5.7 Q^2- distribution for the ν_μ induced $|\Delta S| = 0$ associated kaon production process. 99
5.8 Q^2-distribution for the $\bar{\nu}_\mu$ induced $|\Delta S| = 0$ associated kaon production process. 99
5.9 E_k- distribution for the ν_μ induced $|\Delta S| = 0$ associated kaon production process. 101
5.10 E_k- distribution for the $\bar{\nu}_\mu$ induced $|\Delta S| = 0$ associated kaon production process. 101
5.11 Lepton energy distribution for the ν_μ induced $|\Delta S| = 0$ associated kaon production process. 102
5.12 Lepton energy distribution for the $\bar{\nu}_\mu$ induced associated kaon production process. 102

A.1 Feynman diagram for the Δ^{++} decay 111
A.2 Weak $n - \Delta^+$ transition vertex 115

B.1 s-channel diagram for $\bar{\nu}n \to l^+K^-n$ process. 117
B.2 Kaon pole dominance at weak vertex 118
B.3 Semileptonic decays of hyperons 118
B.4 Weak hyperon production. The conjugate diagram of Fig. B.3 119

List of Tables

1.1 Neutrino oscillation parameters. The upper row corresponds to the normal mass hierarchy and lower row inverted mass hierarchy [24]. . .

2.1 Relation between cartesian components and pseudoscalar meson fields.
2.2 Relation between cartesian components and baryon octet fields. . . .
2.3 Values of the parameters appearing in the hadronic currents. 2
2.4 Cross sections averaged over the neutrino flux at different laboratories in units of 10^{-41} cm^2. Theoretical uncertainties correspond to a 10% variation of the form factor mass. 3
2.5 Number of events calculated for single kaon production in water corresponding to the SuperK analysis for atmospheric neutrinos. 3
2.6 Constant factors appearing in the hadronic current 3
2.7 $< \sigma > (10^{-41} cm^2)$ for $\bar{K}$ production with MiniBooNE $\bar{\nu}_\mu$ flux and neutral current π^0 production (per nucleon) measured at MiniBooNE [110] 4

3.1 Constant factors appearing in the hadronic current 5

4.1 Parameters fitted using the data from the MAMI Crystal Ball [136] experiment 7
4.2 The coefficients of the functional form fit for the $G_E^p(Q^2)$, $G_E^n(Q^2)$, $G_M^p(Q^2)$ and $G_M^n(Q^2)$ in BBBA-05 parameterization. 7
4.3 Parameters used for the helicity amplitude 7

5.1 The standard form factors for weak CC transitions of the SU(3) baryon octet. 9

5.2 Constant factors appearing in the hadronic current. The upper sign corresponds to the processes with antineutrino and lower with neutrino. 95
5.3 Comparison of total cross section for the CC $\nu_\mu/\bar{\nu}_\mu$ induced $K\Lambda$ channel with the results of Shrock et al. [45]. 100

List of Publications

International

1. M. Rafi Alam, S. Chauhan, M. Sajjad Athar and S. K. Singh,
"$\bar{\nu}_l$ *Induced Pion Production from Nuclei at* $\sim$*1 GeV*,"
Phys. Rev. D 88, 077301 (2013)

2. M. Rafi Alam, I. Ruiz Simo, M. Sajjad Athar and M. J. Vicente Vacas,
"*Charged Lepton Induced One Kaon Production off the Nucleon*,"
Phys. Rev. D 87, 053008 (2013)

3. M. Rafi Alam, I. Ruiz Simo, M. Sajjad Athar and M. J. Vicente Vacas,
"*Antineutrino Induced Antikaon Production off the Nucleon*,"
Phys. Rev. D 85, 013014 (2012)

4. M. Rafi Alam, I. Ruiz Simo, M. Sajjad Athar and M. J. Vicente Vacas,
"*Weak Kaon Production off the Nucleon*,"
Phys. Rev. D 82, 033001 (2010)

5. M. Rafi Alam, L. Alvarez-Ruso, I. Ruiz Simo, M. Sajjad Athar, M. J. Vicente Vacas and S. K. Singh,
"*Weak Strangeness and Eta Production*,"
To appear in the IOP Conference Proceedings (NuFact2013)

6. M. Rafi Alam, I. Ruiz Simo, M. Sajjad Athar, L. Alvarez-Ruso and M. J. Vicente Vacas,
"*Weak Production of Strange Particles off the Nucleon*,"
To appear in the American Institute of Physics Conference Proceedings (NuInt2012)
e-Print:arXiv:1303.5924 [hep-ph].

7. M. Rafi Alam, L. Alvarez-Ruso, M. Sajjad Athar and M. J. Vicente Vacas, "*Weak η Production off the Nucleon*," To appear in the American Institute of Physics Conference Proceedings (NuInt2012) **e-Print**:1303.5951 [hep-ph].

8. M. Rafi Alam, I. Ruiz Simo, M. Sajjad Athar and M. J. Vicente Vacas, "*Neutrino(Antineutrino) Induced Single Kaon(Antikaon) Production*," Presented in XXV International Conference on Neutrino Physics and Astrophysics, (Neutrino 2012) Kyoto, Japan.

9. M. Rafi Alam, I. Ruiz Simo, M. Sajjad Athar and M. J. Vicente Vacas, "*Kaon Production off the Nucleon*," **AIP Conf. Proc. 1382**, 173 (2011).

10. M. Rafi Alam, I. Ruiz Simo, M. Sajjad Athar and M. J. Vicente Vacas, "*Strange Particle Production at Low and Intermediate Energies*," **AIP Conf. Proc. 1405**, 152 (2011)

National

1. M. Rafi Alam, I. Ruiz Simo, M. Sajjad Athar and M. J. Vicente Vacas, "*ν-Induced Weak Kaon Production from Nucleons and Nuclei*," **Department of Atomic Energy Symp. on Nucl. Phys. 55**, 526 (2010).

2. M. Rafi Alam, I. Ruiz Simo, M. Sajjad Athar and M. J. Vicente Vacas, "*$\bar{\nu}$-Induced Kaon Production*," **Department of Atomic Energy Symp. on Nucl. Phys. 56**, 762 (2011).

3. S. Chauhan, F. Zaidi, H. Haider, M. Rafi Alam, and M. Sajjad Athar "*Monte Carlo Generators vs Nuclear Model*," **Department of Atomic Energy Symp. on Nucl. Phys. 56**, 1104 (2011).

4. M. Rafi Alam, I. Ruiz Simo, M. Sajjad Athar and M. J. Vicente Vacas, "*$e^{\pm}$ Induced Single Kaon Production off the Neucleon*," **Department of Atomic Energy Symp. on Nucl. Phys. 57**, 662 (2012).

Chapter 1

Introduction

With the observation of continuous nature of β- spectrum by Chadwick [1] in 1914 and many more experiments [2, 3] confirming this observation, physicists were posed with difficult problems and that were to theoretically understand these experimental observations. The problems were not only associated with the energy-momentum conservation law but also with the violation of angular momentum conservation law. It was Pauli [4] who in 1930 suggested that the missing energy in the β-decay spectrum might be caused by some unseen weakly interacting particle. He proposed that this particle should have a very small mass, spin $\frac{1}{2}$ and should be neutral and called this particle "neutron". Three years later in 1933, Fermi [5] rechristened Pauli's neutron to neutrino and gave the theory of neutrino interaction with matter which was constructed in analogy with the Dirac's formulation of quantum electrodynamics and the Hamiltonian for the interaction was written as a product of four spinor fields now called as four Fermi point interaction given by

$$\mathcal{H} = g\bar{\Psi}_p \Gamma \Psi_n \bar{\Psi}_e \Gamma \Psi_\nu + h.c.$$

Fermi took the interaction to be vector in nature in analogy with the second order perturbation of quantum electrodynamics. Fermi's formulation gave a solid foundation to the Pauli's conjecture. Later it turned out that the Fermi's vector interaction is too sensitive to explain many experimental observations of nuclear beta decay. Gamow and Teller [6] showed that an axial vector or tensor interaction may be able to explain several experimental data. In Fermi's theory the bilinear covariants(Γ_i) could be scalar(1), vector(γ^μ), axial vector($\gamma^\mu\gamma^5$), tensor($\sigma^{\mu\nu}$) or pseudoscalar(γ^5) in nature. The question was what one should opt for. The controversy settled down to V-A(vector -axial vector) interaction [7, 8], after the observation of parity violation

in β-decay by Wu et al. [9], the prediction for which was made by Lee and Yang [10] and the helicity measurement by Goldhaber et al. [11] where it was found that all the neutrinos are left-handed. By the early 1960s it was fully established that the weak interaction Hamiltonian in β-decay($n \rightarrow p + e^- + \bar{\nu}_e$) should have the form

$$\mathcal{H}_{int} = \frac{G_F}{\sqrt{2}}[\bar{\Psi}_p \gamma_\mu (1 - \gamma_5)\Psi_n]\ [\bar{\Psi}_e \gamma_\mu (1 - \gamma_5)\Psi_\nu]$$

where G_F is the universal Fermi coupling constant. Since then neutrinos have travelled a long distance both theoretically as well as experimentally and gigantic efforts have been made to understand this mysterious particle. This is also because neutrinos are not only a fundamental particle but along with photons are the two most abundant particles in the universe. So to know the mysteries of the universe, we must also understand the properties of neutrinos. Experimentally, the first neutrino(in fact $\bar{\nu}_e$) was discovered by Reines and Cowan [12] in 1956 at Savannah river nuclear reactor plant in South Carolina and later other flavors of neutrinos ν_μ and ν_τ were discovered by Danby et al. [13] in 1963 and by DONUT Collaboration [14] in 2000, respectively.

In the Standard Model(SM) of particle physics, there are six charged leptons ($e^\pm, \mu^\pm, \tau^\pm$) and six neutral leptons ($\nu_e, \bar{\nu}_e, \nu_\mu, \bar{\nu}_\mu, \nu_\tau, \bar{\nu}_\tau$). These leptons can further be arranged in three different families or generations and arranged according to their weak isospin doublets as,

$$\begin{array}{lccc} Gen. \rightarrow & 1 & 2 & 3 \\ L \downarrow & & & \\ +1 & \begin{pmatrix} \nu_e \\ e^- \end{pmatrix} & \begin{pmatrix} \nu_\mu \\ \mu^- \end{pmatrix} & \begin{pmatrix} \nu_\tau \\ \tau^- \end{pmatrix} \\ -1 & \begin{pmatrix} e^+ \\ \bar{\nu}_e \end{pmatrix} & \begin{pmatrix} \mu^+ \\ \bar{\nu}_\mu \end{pmatrix} & \begin{pmatrix} \tau^+ \\ \bar{\nu}_\tau \end{pmatrix} \end{array}, \tag{1.1}$$

where L is a quantum number assigned to the leptons and known as "Lepton Quantum Number", which is different for the different generations.

In 1957 Pontecorvo [15] suggested that like $K^0 - \bar{K}^0$ regeneration phenomena, a neutrino may also oscillate into its antiparticle in vacuum if lepton number gets violated. Their study further continued and in 1969, Gribov and Pontecorvo [16] reiterated the concept of neutrino oscillation between different flavors of neutrinos if neutrinos have finite mass. Around the same time the problem with the observation of solar neutrino puzzle by Davis et al. [17] were reported. This was related with the fact that the observed number of neutrinos(ν_es) were different from the predictions of the Standard Solar Model [18]. Then in 1980s came the atmospheric neutrino

anomaly reported by IMB [19] and Kamiokande [20] experiments and later by other experiments where it was found that the predictions for the ratio $\frac{\nu_e+\bar{\nu}_e}{\nu_\mu+\bar{\nu}_\mu}$ which should be theoretically $\frac{1}{2}$ is close to 1.

Theoretically in 1986, Mikheyev and Smirnov [21] wrote a paper demonstrating that electron type neutrino(ν_e) may be converted into a muon type neutrino(ν_μ) in matter via a resonance like mechanism even if the intrinsic mixing angle be very small. Now the phenomena of ν-oscillation is well established due to the dedicated experiments using solar, atmospheric, reactor as well as accelerator neutrinos. The neutrino flavor eigen states($\nu_i, i = e, \mu, \tau$) and the mass eigen states($\nu_j, j = 1, 2, 3$) are related by a mixing matrix(U) known as Pontecorvo-Maki-Nakagawa-Sakata(PMNS) [22, 23] matrix and is given by

$$\begin{bmatrix}\nu_e\\ \nu_\mu\\ \nu_\tau\end{bmatrix} = U \times \begin{bmatrix}\nu_1\\ \nu_2\\ \nu_3\end{bmatrix} \tag{1.2}$$

where U is given by

$$U = \begin{pmatrix} c_{12}c_{13} & s_{12}c_{13} & s_{13}e^{-i\delta} \\ -s_{12}c_{23} - c_{12}s_{23}s_{13}e^{i\delta} & c_{12}c_{23} - s_{12}s_{23}s_{13}e^{i\delta} & s_{23}c_{13} \\ s_{12}s_{23} - c_{12}c_{23}s_{13}e^{i\delta} & -c_{12}s_{23} - s_{12}c_{23}s_{13}e^{i\delta} & c_{23}c_{13} \end{pmatrix} \times \begin{pmatrix} e^{i\phi_1/2} & 0 & 0 \\ 0 & e^{i\phi_2/2} & 0 \\ 0 & 0 & 1 \end{pmatrix}$$

$$U = \underbrace{\begin{pmatrix} c_{12} & s_{12} & 0 \\ -s_{12} & c_{12} & 0 \\ 0 & 0 & 1 \end{pmatrix}}_{Solar, Reactor} \times \underbrace{\begin{pmatrix} 1 & 0 & 0 \\ 0 & c_{23} & s_{23} \\ 0 & -s_{23} & c_{23} \end{pmatrix}}_{Atm., Acc.} \times \underbrace{\begin{pmatrix} c_{13} & 0 & s_{13}e^{-i\delta} \\ 0 & 1 & 0 \\ -s_{13}e^{i\delta} & 0 & c_{13} \end{pmatrix}}_{Reactor\ \&\ Other}$$

$$\times \begin{pmatrix} e^{i\phi_1/2} & 0 & 0 \\ 0 & e^{i\phi_1/2} & 0 \\ 0 & 0 & 1 \end{pmatrix} \quad \text{where } c_{ij}, s_{ij} = \cos\theta_{ij} \ \&\ \sin\theta_{ij} \text{ respectively.}$$

The evidence of tiny neutrino masses represents one of the indications of physics beyond the Standard Model(SM). However, the various parameters involved in oscillation physics needs to be very precisely determined. For a three flavor neutrino, the oscillation parameters and CP violating phase δ are given in Table 1.1 [24].

The different neutrino oscillation experiments in the last one decade have revealed information about the solar mixing angle θ_{12}, atmospheric mixing angle θ_{23} and very recently some constrain on θ_{13} have been obtained, see for example Ref. [25]. Now the pursuit is to see CP violation in the leptonic sector, and precise measurements of the neutrino mixing parameters besides knowing the other properties associated with this particle like their absolute masses, magnetic moment, etc.

parameter	best fit	3σ range
$\Delta m^2_{21}\,[10^{-5}eV^2]$	7.62	7.12 - 8.20
$\lvert\Delta m^2_{31}\rvert\,[10^{-3}eV^2]$	2.55 2.43	2.31-2.74 2.21- 2.64
$\sin^2\theta_{12}$	0.320	0.27 - 0.37
$\sin^2\theta_{23}$	0.613 0.6	0.36-0.68 0.37 - 0.67
$\sin^2\theta_{13}$	0.0246 0.0250	0.017-0.033
δ	0.8π -0.03π	$0\text{-}2\pi$

Table 1.1: Neutrino oscillation parameters. The upper row corresponds to the normal mass hierarchy and lower row inverted mass hierarchy [24].

The neutrino energy region of a few GeV is quite sensitive to the neutrino oscillation parameters. Therefore, most of the present experiments like MiniBooNE [26], K2K [27], T2K [28], NOνA [29], etc. have taken data or have been planned in this energy region. Neutrino detection proceeds basically through various channels of interaction with hadronic targets like quasielastic scattering, meson production due to resonance excitations and its subsequent decay, deep inelastic scattering process, etc. These may be understood by looking at the famous Lipari [30] curve in Fig.-1.1, where the cross section is plotted as a function of neutrino energy. Here the sensitivity of the average neutrino energy spectrum of the different neutrino experiments is also shown. Looking at the Lipari curve and the experimental focus of the different experiments, one realizes that a reliable estimate of cross sections for these different processes is necessary. Although lots of efforts are being made both theoretically and experimentally to understand neutrino-nucleus reaction cross sections still there is uncertainty in the cross sections of about 20-30% [31] in the energy region relevant to these experiments. This is because the neutrino fluxes are not very precisely known and the other reason for it is that all these experiments are being done using nuclear targets. As nobody can see a neutrino and measure its energy and momentum in the incoming beam, the energy of incoming neutrino is evaluated based on the kinematics of particles obtained in the final state depending on the detector acceptance and measurement accuracy. Therefore, it has been

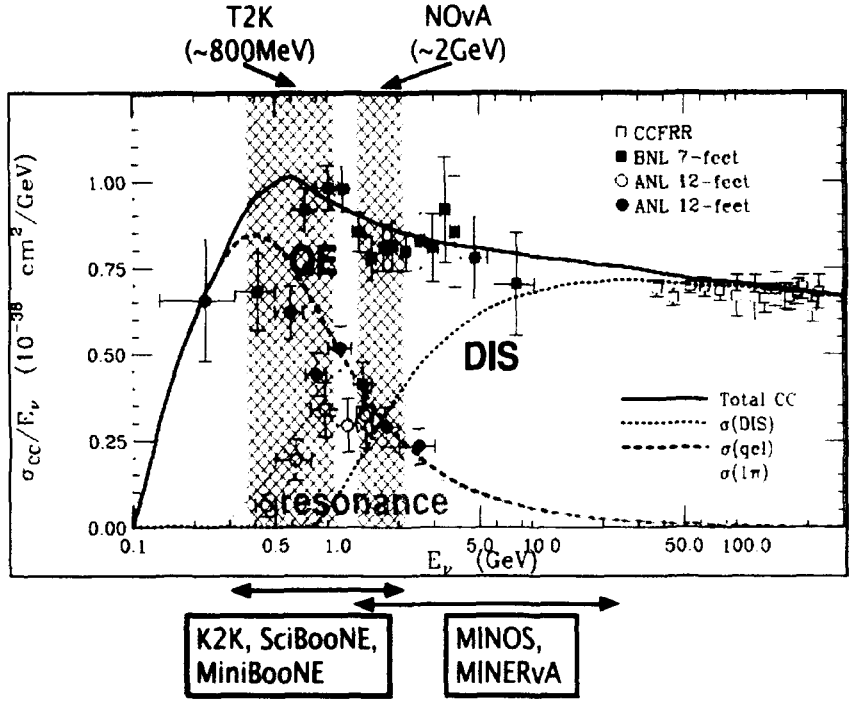

Figure 1.1: Contribution to the total scattering cross section [30].

pointed out that the reconstructed neutrino energy and the true neutrino energy may be different and true neutrino energy is really a difficult task to calculate as the nuclear medium effects make the calculation quite difficult. Furthermore, the nature of the neutrino-nucleus scattering cross section is also energy dependent, like at the low energies, it is the quasielastic scattering cross section which is dominant, whereas at high energies the contribution mainly comes from the deep inelastic scattering processes, while at ~1GeV the cross section may get contribution from all the possible inelastic channels besides these two. The inelastic channels include one pion production, multipion production, kaon production, η production, etc.

As the use of nuclear targets in neutrino experiments is unavoidable, therefore, it is very important to understand theoretically the nuclear medium effects in the ν-nucleus scattering cross section, and for this efforts have been made and on this topic various series of neutrino conferences like NnInt [32], NuFact [33] are continuously being organized. In the last one decade, the studies performed to understand the

nuclear medium effects in the neutrino nucleus cross sections were mainly confined to the quasielastic scattering and pion production processes [31]. However, in the few GeV energy region, other not so well known processes like kaon and hyperon production may also become important. In principle, their cross sections are smaller than for the pionic processes because of phase space and the Cabibbo suppression for $\Delta S = 1$ reactions. Nonetheless, in the coming years of precision neutrino physics, their knowledge could be relevant for the data analysis, apart from their own intrinsic interest related to the role played by the strange quarks in hadronic physics.

In neutrino(antineutrino) induced reactions, the first inelastic reaction creating charged current(CC) induced strange quarks is the single kaon production, with or without accompanying a pion, where the total strangeness change is by one unit (i.e. $\Delta S = 1$). The various possible reactions are

$$\begin{aligned}
\nu_l + p &\rightarrow l^- + K^+ + p & \bar{\nu}_l + p &\rightarrow l^+ + K^- + p \\
\nu_l + n &\rightarrow l^- + K^0 + p & \bar{\nu}_l + p &\rightarrow l^+ + \bar{K}^0 + n \\
\nu_l + n &\rightarrow l^- + K^+ + n & \bar{\nu}_l + n &\rightarrow l^+ + K^- + n, etc. \qquad (1.3)
\end{aligned}$$

where $l = e, \mu$.

The basic reactions for $\nu(\bar{\nu})$ induced charged current associated particle production ($\Delta S = 0$) from a nucleon(p or n) target are given by the following processes

$$\begin{aligned}
\nu_l + n &\rightarrow l^- + \Lambda^0 + K^+ & \bar{\nu}_l + p &\rightarrow l^+ + \Lambda^0 + K^0 \\
\nu_l + n &\rightarrow l^- + \Sigma^0 + K^+ & \bar{\nu}_l + p &\rightarrow l^+ + \Sigma^0 + K^0 \\
\nu_l + n &\rightarrow l^- + \Sigma^+ + K^0 & \bar{\nu}_l + p &\rightarrow l^+ + \Sigma^- + K^+ \\
\nu_l + p &\rightarrow l^- + \Sigma^+ + K^+ & \bar{\nu}_l + n &\rightarrow l^+ + \Sigma^- + K^0, etc. \qquad (1.4)
\end{aligned}$$

Besides the above mentioned CC $\Delta S = 0$ processes, single hyperon accompanied by a lepton may also be produced by $\Delta S = 1$ quasielastic processes induced by antineutrinos. The $\Delta S = 1$ charged current quasielastic (CCQE) process is not possible in neutrino mode because of $\Delta S \neq \Delta Q$ selection rule. The possible $\Delta S = 1$ CCQE single hyperon (1Y) production processes are,

$$\begin{aligned}
\bar{\nu}_l + p &\rightarrow l^+ + \Lambda^0 \\
\bar{\nu}_l + p &\rightarrow l^+ + \Sigma^0 \\
\bar{\nu}_l + n &\rightarrow l^+ + \Sigma^- \\
\bar{\nu}_l + n &\rightarrow l^+ + Y^* \qquad (1.5)
\end{aligned}$$

where Y^* is a hyperon resonance.

Apart from $\Delta S = 0$, charged current(CC) associated particle production of hyperons with kaons, strange particles may be produced in neutral current(NC), $\Delta S = 0$ processes through the following reaction:

$$\begin{aligned} \nu_l + p &\rightarrow \nu_l + \Lambda^0 + K^+ \\ \nu_l + n &\rightarrow \nu_l + \Lambda^0 + K^0 \\ \nu_l + p &\rightarrow \nu_l + \Sigma^+ + K^0 \\ \nu_l + p &\rightarrow \nu_l + \Sigma^0 + K^+ \\ \nu_l + n &\rightarrow \nu_l + \Sigma^0 + K^0, etc. \end{aligned} \tag{1.6}$$

Neutrino/Antineutrino induced charged current(CC) $|\Delta S| = 1$ process is particularly appealing for several reasons. One of them is the important background that it could produce, due to atmospheric neutrino interactions in the proton decay searches [34]. Proton decay predictions were made by the minimal version of supersymmetric SU(5) theories, where the predicted life time was about 10^{31} years and the decay was predicted through the observation of $p \rightarrow e^+ + \pi^0$. However, present experimental limits are more than 10^{33}years [35]. There is a strong prediction from the super-symmetric grand unified theories(SUSY GUTs) [36] for the protons to have life time more than this. Therefore, the nucleon decay studies have entered into a second generation phase, and more ambitious experiments like UNO [37], Hyper-K [38], ICARUS [39] etc. are planned for the future, using water-Cerenkov technique or liquid Argon Time Projection Chamber. There are other decay channels that open up where supersymmetric intermediate states are involved. Particularly s-quark production is favored, and final states involving kaons, for example, $p \rightarrow K\nu$ would be a dominant decay mode of protons. Thus to see nucleon to decay, reliable estimate of kaons coming from the background, like from the interaction of atmospheric neutrinos, should be well estimated. For this theoretical understanding of kaon production from $\Delta S = 0$ as well as $\Delta S = 1$ processes are required. These processes are also useful in the understanding of the basic symmetries of the standard model, strange quark content of the nucleon, structure of weak hadronic form factors, etc. The study of single kaon production would also be important in the analysis of neutrino oscillation data, specially from their own intrinsic interest related to the role played by the strange quarks in hadronic physics.

Experimentally, the currently available data is restricted to a few events measured in bubble chamber experiments [40, 41, 42] with large systematic errors. However, the scenario is expected to change soon as MINERνA [43] at Fermilab has started taking data and their main goal is to study nucleon dynamics in the nuclear medium.

MINERνA is using several nuclear targets like Carbon, Iron and Lead in the neutrino energy region of 1-20 GeV. It is also planned to study specifically the strange particle production and it is expected that thousands of events would be accumulated where a kaon is produced in the final state [44].

There are very few theoretical calculations which deal with strange particle production at low neutrino energies like the study by Shrock [45] and Mecklenburg [46] on the associated particle production induced by charged and neutral currents. Dewan [47] has studied strangeness changing (ΔS = 1) strange particle production and Amer et al. [48] have studied strange particle production assuming the dominance of s-channel resonant mechanism but the formalism is applicable at high neutrino energies. Singh et al. [49] and Mintz et al. [50] have studied antineutrino induced single hyperon production. Due to the scarcity of theoretical work, the MonteCarlo generators used in the analysis of the experiments apply models that are not too well suited to describe the strangeness production at low energies. For instance, NEUT [51], used by K2K [27], T2K [28], Super-Kamiokande [52] and SciBooNE [53] only considers associated kaon production implemented by a model based on the excitation and later decay of resonances [51]. A similar model is used by other event generators like NEUGEN [54], NUANCE [55] (see also discussion in Ref. [56]) and GENIE [57]. However, it has been realized that this approach is not appropriate for low energy strange particle production.

The other inelastic process that we have studied is the eta production induced by neutrinos/antineutrinos. Although eta production induced by electromagnetic process has been extensively studied both theoretically and experimentally but there is few literature on the η production induced by weak interaction. To the best of our knowledge there is absolutely no results for the differential as well as the total scattering cross section for neutrino and antineutrino induced η production off nucleon and nuclear targets. The basic reaction for the neutrino and antineutrino induced charged current eta production is

$$\begin{aligned} \nu_l + n &\longrightarrow l^- + p + \eta \\ \bar{\nu}_l + p &\longrightarrow l^+ + n + \eta \end{aligned} \tag{1.7}$$

where $l = e, \mu$. Study of η production is interesting because of several reasons. For example, η is one of the important probe to search for the strange quark content of the nucleons [58]. Also a precise determination of the η production cross section would help in subtracting the background in proton decay searches. In some supersymmetric grand unified theories, η mesons provide a prominent signal for proton decay [59]. Therefore, its background contribution due to atmospheric neutrino interactions should be well estimated. Furthermore, the η production channel

is likely to be dominated by $N^*(1535)$ resonance excitation. This state sits near the threshold of the $N\eta$ system and has large branching ratio for the $N\eta$ channel. Thus, a precise measurement of the cross section will also allow to determine the axial properties of this resonance. In addition to the above reasons, a second class (via pion pole) η production mechanism that could compete with resonance production in certain kinematic conditions has been singled out [60]. In most of the Monte Carlo generators, eta contribution is obtained from Rein and Sehgal model [61] for the resonant pion production. With the aim of reducing systematics in the neutrino oscillation experiments to measure precisely oscillation parameters a reasonable knowledge of these production cross section is required. We have not come across any theoretical/experimental study where using neutrino/antineutrino beam either the differential or total scattering cross section has been presented.

Recently, the importance of the study of kaon production induced by real and virtual photons on nucleons and nuclei has been emphasized due to the development of accelerators like MAMI, TJNAF, LNS, ELSA, SPring-8, GRAAL, etc. [62, 63, 64, 65, 66, 67, 68, 69, 70, 71, 72]. In particular, the availability of very high luminosity beams has given the opportunity to study the photo induced strange particle and antiparticle production [73, 74, 75, 76, 77, 78, 79, 80, 81, 82, 83]. This study is quite important keeping in mind the experimental efforts of studying kaon production using real or virtual photons obtained from the accelerators like MAMI, JLAB, LNS, ELSA, SPring-8, GRAAL, etc. [62, 63, 64, 65, 66, 67, 68, 69, 70, 71, 72] and using dedicated detectors for the kaon signal. However, at the energies of these experiments kaons coming from weak interaction may also contribute significantly.

In this work, we have performed studies for the single kaon production process induced by neutrino/antineutrino beams, eta production by these projectiles and electron/positron induced single kaon production process and neutrino/antineutrino induced associated particle production process. We develop a microscopical model based on the $SU(3)$ chiral Lagrangian. The basic parameters of the model are f_π, the pion decay constant, Cabibbo angle, the proton and neutron magnetic moments and the axial vector coupling constants for the baryons octet, D and F, that are obtained from the analysis of the semileptonic decays of neutron and hyperons.

In Chapter-2, we shall present in brief the basic ingredients those one require from Chiral Perturbation Theory (χPT) while writing hadronic current. We know that quantum chromodynamics is gauge theory of the strong interactions with color $SU(3)$ as the underlying gauge group. But at the same time we also understand that QCD can not be solved analytically. Therefore one uses an effective approach which is applicable in certain kinematical region. χPT is one such type of approach, an effective field theory, based on the symmetries of the underlying theory and general

principles of quantum field theory. One writes the most general possible Lagrangian based on the allowed symmetry principles. Then one obtains the matrix elements using this Lagrangian. After introducing χPT, we shall present and discuss the results for neutrino and antineutrino induced single kaon and antikaon production, respectively.

In Chapter-3, we have presented the formalism of the electron/positron induced antikaon/kaon production. We have shown that kaon production through $\Delta S = 1$ process may also contribute significantly in the beams of electron/positron in the experiments being performed at JLAB, Mainz, etc. We have presented and discussed the results for the differential and total scattering cross section.

In Chapter-4, we have studied photo and neutrino/antineutrino induced eta particle production off the nucleons. We have obtained the results for the various distributions like eta momentum, lepton energy and Q^2 distributions as well as the results for the total scattering cross sections by using χPT approach to obtain the hadronic currents for the Born diagrams and using the prescription of helicity amplitudes to obtain the contributions from the resonant $S_{11}(1535)$ and $S_{11}(1650)$ channels.

In Chapter-5, we have studied associated particle production induced by neutrino and antineutrino. We have presently taken only the nonresonant diagrams and obtained the hadronic currents using χPT. The results for kaon momentum, Q^2 distributions and the results for the total scattering cross sections are presented.

In Chapter-6 we summarize the results and conclude our findings.

Chapter 2

Weak Production of K and $\bar{K}$

In this chapter, we briefly discuss the model which has been used to describe the weak strangeness production. In Sec. 2.1, we present in brief the *Effective Field Theory* approach which is used to describe the dynamics of the reactions. In Secs. 2.2 and 2.3 we apply the formalism to obtain the results for neutrino and antineutrino induced $\Delta S = 1$ single kaon and antikaon production respectively.

2.1 Effective Field Theory

The ultimate goal of the physicists is to have a theory which should be able to explain and correlate all the known physical phenomena happening around us. This theory would be the "Theory of Everything". Using this theory one would be able to understand all the observed phenomena in terms of some fundamental dynamics among the basic constituents of nature. However, even if we are able to achieve this goal, a quantitative analysis at the most elementary level is going to be of little use for comprehensively describing nature at all physical scales. Therefore, to analyze a particular physical system, first the isolation of the system from the surrounding is required so that one would be able to understand that particular system without going into the details of the surrounding. To understand a particular system then one requires a smart choice of appropriate variables which should be able to describe the physical system which is more relevant for the problem at hand. Fortunately, many physical problems involve energy scales of wide energy range that gives an opportunity to study either low energy dynamics which is almost independent of the details of high energy scattering or vice versa. For example, by now it is well established that complete description of particle physics requires the powers of full

blown Quantum Field Theory(QFT). In the some large scheme of things we might resort to either some approximation or some limits of parameters involved. In this context for several decades we have come to the realization that for the description of some strongly interacting systems we might use a sort of reduced form of QFT called Effective Field Theory(EFT)[1]. In these theories some of the degrees of freedom are integrated out as their detailed inclusion is neither needed nor is manageable.

These effective field theories are basically tools to describe low energy physics where one defines low energy scale with respect to some reference energy scale Λ. In principle effective field theories contain infinite number of couplings which allow us to achieve order by order renormalization. Therefore, the use of effective field theory spares us the task of having to deal with the complications associated with the detailed dynamics of the underlying fundamental theory. For example, Quantum Chromodynamics(QCD) is a well established quantum field theory to describe strong interactions, with the quarks as building blocks for baryons and mesons, and the gluons as the mediators of the interaction. This has got unprecedented success at large momentum transfer. However, in the low energy domain, due to the growing of running QCD coupling and the associated confinement of quarks and gluons it becomes very difficult to perform a complete realistic analysis of the QCD dynamics in terms of these fundamental degrees of freedom. Therefore, at low energies we need an effective field theory and among the various effective field theories applicable at low energies, Chiral Perturbation Theory(χPT) is perhaps one of the most successful one [84, 85, 86], which has been found out to be very suitable at the energies below the typical hadron masses. It describes the dynamics of the lightest hadrons(mesons and baryons) as well as their interactions at low energies. The Lagrangian of χPT contains a set of coupling constants which are better known as low energy constants that not only describe the interactions of the lightest hadrons but also include the contributions of the resonances in some effective way. This theory has been successfully applied for understanding p–p scattering, π–N scattering, $\pi - \pi$ scattering, pion photoproduction data, etc.

2.1.1 Chiral Perturbation Theory

The gauge invariant QCD Lagrangian in the limit of vanishing quark masses is given by,

$$\mathcal{L}^0_{\rm QCD} = \overline{q} i\gamma^\mu \partial_\mu q - g\left(\overline{q}\,\gamma^\mu \frac{\lambda_\alpha}{2} q\right) G^\alpha_\mu - \frac{1}{4} G^\alpha_{\mu\nu} G^{\alpha\mu\nu} \tag{2.1}$$

[1]For details see Refs. [84, 85, 86, 87, 88, 89, 90, 91]

where q denotes the composite spinor for the color triplet quarks, G^{α}_{μ} is vector gluon field, $G^{\alpha}_{\mu\nu}$ is gluon field-strength tensor with α as a color index and g is the quark-gluon coupling strength. We have considered only light quarks viz. u, d and s. This Lagrangian has a global symmetry,

$$\mathcal{G} = \underbrace{SU(N_f)_L \otimes SU(N_f)_R}_{\text{chiral group } \mathcal{G}_\chi} \otimes U(1)_V \otimes U(1)_A \ ,$$

where N_f is the number of quark flavors and the subscripts denote the left(L) and right(R) handed quark fields. $\mathcal{G}_\chi$ is the chiral group for QCD, and for $N_f = 3$ quarks (u-, d- and s- quark), has a symmetry given by $\mathcal{G}_\chi = SU(3)_L \otimes SU(3)_R$. However, if such a symmetry exists, one would observe parity doublets of $SU(3)$ multiplets of particles. Although $SU(3)$ flavor symmetry has been observed but there is no evidence of parity doubling at least for the light hadrons like pions. Therefore, one of the $SU(3)$ groups has to be spontaneously broken. In the present case the breaking of chiral symmetry leads to appearance of Goldstone bosons. These Goldstone bosons in the case of $SU(3)$, are light pseudoscalar particles like pions, kaons and eta mesons.

In order to get the Lagrangian which describes the dynamics of these Goldstone bosons, we need continuous fields which should be described in terms of these Goldstone modes. The elements of $SU(3)$ are written in terms of a unitary matrix

$$U(\Theta) = \exp\left(-i\Theta_k \frac{\lambda_k}{2}\right) \ , \tag{2.2}$$

where Θ_k are the real set of parameters and λ_k are the Gell-Mann matrices given by

$$\lambda_1 = \begin{pmatrix} 0 & 1 & 0 \\ 1 & 0 & 0 \\ 0 & 0 & 0 \end{pmatrix}, \quad \lambda_2 = \begin{pmatrix} 0 & -i & 0 \\ i & 0 & 0 \\ 0 & 0 & 0 \end{pmatrix}, \quad \lambda_3 = \begin{pmatrix} 1 & 0 & 0 \\ 0 & -1 & 0 \\ 0 & 0 & 0 \end{pmatrix},$$
$$\lambda_4 = \begin{pmatrix} 0 & 0 & 1 \\ 0 & 0 & 0 \\ 1 & 0 & 0 \end{pmatrix}, \quad \lambda_5 = \begin{pmatrix} 0 & 0 & -i \\ 0 & 0 & 0 \\ i & 0 & 0 \end{pmatrix}, \quad \lambda_6 = \begin{pmatrix} 0 & 0 & 0 \\ 0 & 0 & 1 \\ 0 & 1 & 0 \end{pmatrix},$$
$$\lambda_7 = \begin{pmatrix} 0 & 0 & 0 \\ 0 & 0 & -i \\ 0 & i & 0 \end{pmatrix}, \quad \lambda_8 = \sqrt{\frac{1}{3}} \begin{pmatrix} 1 & 0 & 0 \\ 0 & 1 & 0 \\ 0 & 0 & -2 \end{pmatrix}. \tag{2.3}$$

Each Goldstone boson corresponds to the x-dependent cartesian component of the fields, $\phi_k(x)$. These cartesian components with Gell-Mann matrices λ_k gives a

parameterization of the Goldstone fields $\Phi(x)$ as

$$\Phi(x) = \sum_{k=1}^{8} \phi_k(x)\lambda_k = \begin{pmatrix} \phi_3 + \frac{\phi_8}{\sqrt{3}} & \phi_1 - i\phi_2 & \phi_4 - i\phi_5 \\ \phi_1 + i\phi_2 & \frac{\phi_8}{\sqrt{3}} - \phi_3 & \phi_6 - i\phi_7 \\ \phi_4 + i\phi_5 & \phi_6 + i\phi_7 & -2\frac{\phi_8}{\sqrt{3}} \end{pmatrix} \tag{2.4}$$

The component $\phi_k(x)$ are related to Goldstone field by the relation $\phi_k = \frac{1}{2}\mathrm{Tr}[\lambda_k \Phi(x)]$. Furthermore, these cartesian components are expressed in terms of the physical fields as given in Table 2.1

Table 2.1: Relation between cartesian components and pseudoscalar meson fields.

$\phi_1 + i\phi_2 \rightarrow$	$\sqrt{2}\pi^+$	$\phi_1 - i\phi_2 \rightarrow$	$\sqrt{2}\pi^-$	$\phi_3 \rightarrow$	π^0
$\phi_4 + i\phi_5 \rightarrow$	$\sqrt{2}K^+$	$\phi_4 - i\phi_5 \rightarrow$	$\sqrt{2}K^-$	$\phi_8 \rightarrow$	η
$\phi_6 + i\phi_7 \rightarrow$	$\sqrt{2}K^0$	$\phi_6 - i\phi_7 \rightarrow$	$\sqrt{2}\bar{K}^0$		

In the above table, the various entries like π^i, K^i & η stand for the pseudoscalar fields which depend on space time coordinates. However, for convenience we have dropped the x dependence from the fields. Using Table 2.1, Eq. 2.4 modifies to,

$$\Phi(x) = \sum_{k=1}^{8} \phi_k(x)\lambda_k = \begin{pmatrix} \pi^0 + \frac{1}{\sqrt{3}}\eta & \sqrt{2}\pi^+ & \sqrt{2}K^+ \\ \sqrt{2}\pi^- & -\pi^0 + \frac{1}{\sqrt{3}}\eta & \sqrt{2}K^0 \\ \sqrt{2}K^- & \sqrt{2}\bar{K}^0 & -\frac{2}{\sqrt{3}}\eta \end{pmatrix}. \tag{2.5}$$

For the baryons, we follow the same procedure as we did for the mesons. However, unlike the pseudoscalar mesons where the fields are real, in the case of B matrix each entry is a complex-field and the general representation is given by,

$$B(x) = \sum_{k=1}^{8} \frac{1}{\sqrt{2}} b_k(x)\lambda_k = \frac{1}{\sqrt{2}} \begin{pmatrix} b_3 + \frac{b_8}{\sqrt{3}} & b_1 - ib_2 & b_4 - ib_5 \\ b_1 + ib_2 & \frac{b_8}{\sqrt{3}} - b_3 & b_6 - ib_7 \\ b_4 + ib_5 & b_6 + ib_7 & -2\frac{b_8}{\sqrt{3}} \end{pmatrix}, \tag{2.6}$$

The component b_ks are related to Dirac fields and have been shown in Table 2.2,

Table 2.2: Relation between cartesian components and baryon octet fields.

$b_1 + ib_2 \rightarrow$	$\sqrt{2}\Sigma^+$	$b_1 - ib_2 \rightarrow$	$\sqrt{2}\Sigma^-$	$b_3 \rightarrow$	Σ^0
$b_4 + ib_5 \rightarrow$	$\sqrt{2}\Xi^0$	$b_4 - ib_5 \rightarrow$	$\sqrt{2}p$	$b_8 \rightarrow$	Λ
$b_6 + ib_7 \rightarrow$	$\sqrt{2}\Xi^-$	$b_6 - ib_7 \rightarrow$	$\sqrt{2}n$		

Using Table 2.2 the baryon matrix B may be given in terms of the four-component complex Dirac fields as

$$B(x) = \sum_{k=1}^{8} \frac{1}{\sqrt{2}} b_k(x)\lambda_k = \begin{pmatrix} \frac{1}{\sqrt{2}}\Sigma^0 + \frac{1}{\sqrt{6}}\Lambda & \Sigma^+ & p \\ \Sigma^- & -\frac{1}{\sqrt{2}}\Sigma^0 + \frac{1}{\sqrt{6}}\Lambda & n \\ \Xi^- & \Xi^0 & -\frac{2}{\sqrt{6}}\Lambda \end{pmatrix}. \quad (2.7)$$

After getting the parameterization of pseudoscalar meson octet $\Phi(x)$ in Eq. 2.5 and baryon octet $B(x)$ in Eq. 2.7, we now discuss the construction of Lagrangian for meson-meson, baryon-meson interactions and their interaction with external fields.

2.1.1.1 Meson - Meson Interaction

The simplest Lagrangian which should be chirally invariant may be constructed by using $SU(3)$ unitary matrix $U(x)$,

$$U(x) = \exp\left(i\frac{\Phi(x)}{f_\pi}\right), \quad (2.8)$$

where $\Phi(x)$ is given by Eq. 2.5 and f_π is a constant which can be obtained from weak decay of pions i.e. $\pi^+ \to \mu^+\nu_\mu$. The Lagrangian is written either in terms of increasing powers of momentum or equivalently in terms of increasing number of derivatives. The unitarity of $U(x)$ demands that, even to generate a non-trivial interaction, we need at least two derivatives to construct the Lagrangian, and this may be given as

$$\mathcal{L}^{(2)} = \frac{f_\pi^2}{4}\mathrm{Tr}\left[\partial_\mu \mathrm{U}^\dagger \partial^\mu \mathrm{U}\right]. \quad (2.9)$$

We must point out that the above Lagrangian represents the scattering among the members of the pseudoscalar mesons. However, if one introduces couplings to external fields, like

$$\begin{aligned} v^\mu &\to \text{vector} \\ a^\mu &\to \text{axialvector} \\ p &\to \text{pseudoscalar} \\ s &\to \text{scalar}, \end{aligned} \quad (2.10)$$

then this technique becomes more generalized. The QCD Lagrangian given by Eq. 2.1 in the presence of external fields now read as

$$\mathcal{L} = \mathcal{L}^0_{QCD} + \bar{q}\gamma_\mu(v^\mu + \gamma_5 a^\mu)q - \bar{q}(s - i\gamma_5 p)q. \quad (2.11)$$

It is more convenient to write the above Lagrangian in terms of the left(q_L) - handed and and right(q_R)- handed quark fields. For this we shall introduce left(l^μ) and right(r^μ) handed currents which are obtained from fields v^μ and a^μ as [87]:

$$r^\mu = \frac{1}{2}(v^\mu + a^\mu), \qquad l^\mu = \frac{1}{2}(v^\mu - a^\mu). \tag{2.12}$$

Inserting the above fields into the Eq. 2.11 and with some simplification, we get

$$\begin{aligned} \mathcal{L} &= \mathcal{L}^0_{QCD} + \bar{q}_L\gamma_\mu l^\mu q_L - \bar{\gamma}_\mu q_R r^\mu q_R - \bar{q}_R(s+ip)q_L - \bar{q}_L(s-ip)q_R \\ &\equiv \mathcal{L}^0_{QCD} + \mathcal{L}_{ext} \end{aligned} \tag{2.13}$$

Now we make the effective chiral Lagrangian invariant under the local transformations by replacing the partial derivatives by the covariant derivatives like

$$\begin{aligned} D^\mu U &\equiv \partial^\mu U - ir^\mu U + iUl^\mu, \\ D^\mu U^\dagger &\equiv \partial^\mu U^\dagger + iU^\dagger r^\mu - il^\mu U^\dagger. \end{aligned} \tag{2.14}$$

Thus the lowest-order $SU(3)$ chiral Lagrangian describing the pseudoscalar mesons in the presence of an external current is obtained as

$$\mathcal{L}^{(2)}_M = \frac{f_\pi^2}{4}\mathrm{Tr}[D_\mu U(D^\mu U)^\dagger] + \frac{f_\pi^2}{4}\mathrm{Tr}[\chi U^\dagger + U\chi^\dagger], \tag{2.15}$$

where the parameter $f_\pi(= 92.4MeV)$ is the pion decay constant. The second term appearing in the Lagrangian of Eq. 2.15 consists of scalar and pseudoscalar fields where the field χ is defined as

$$\chi = 2B_0(s+ip), \tag{2.16}$$

with B_0 as a constant. However, this term that incorporates the explicit breaking of chiral symmetry coming from the quark masses [86], is not relevant for our study.

For different interactions the left-(l^μ) and right-(r^μ) handed currents(for $SU(3)$ case only) are,

Interaction	r_μ	l_μ
EM	$-e\hat{Q}\mathcal{A}_\mu$	$-e\hat{Q}\mathcal{A}_\mu$
CC	0	$-\frac{g}{\sqrt{2}}(\mathcal{W}^+_\mu T_+ + \mathcal{W}^-_\mu T_-)$
NC	$g\ \tan\theta_W \sin\theta_W \hat{Q}\mathcal{Z}_\mu$	$-g\cos\theta_W\ \hat{Q}\mathcal{Z}_\mu$

(2.17)

where 'EM' stands for the electromagnetic, and 'CC' and 'NC' stands for the weak charge- and neutral-current interactions, respectively. $\mathcal{A}^{\mu}$ is the electromagnetic four-vector potential and '$\hat{Q}$' is the $SU(3)$ quark charge given by

$$\hat{Q} = \begin{pmatrix} \frac{2}{3} & 0 & 0 \\ 0 & -\frac{1}{3} & 0 \\ 0 & 0 & -\frac{1}{3} \end{pmatrix}, \text{ with EM coupling, } \alpha = \frac{e^2}{4\pi}.$$

$\mathcal{W}^{\pm}$ represents the W boson field and

$$T_{+} = \begin{pmatrix} 0 & V_{ud} & V_{us} \\ 0 & 0 & 0 \\ 0 & 0 & 0 \end{pmatrix} \quad \text{and} \quad \mathrm{T}_{-} = \begin{pmatrix} 0 & 0 & 0 \\ V_{ud} & 0 & 0 \\ V_{us} & 0 & 0 \end{pmatrix},$$

where V_{ij} are the elements of the Cabibbo-Kobayashi-Maskawa matrix [87]. $\mathcal{Z}_{l}$ is the weak Z-boson and the θ_W is the Weinberg angle given by [92],

$$\cos\theta_W = \frac{M_W}{M_Z} \cong 0.8815 \,.$$

In the next section, we briefly discuss the interaction of baryons with the pseudoscalar Goldstone bosons as well as with the external fields at low energies.

2.1.1.2 Baryon - Meson Interaction

Till now we have discussed the interaction of Goldstone bosons(pseudoscalar mesons) among themselves and with the external fields. To incorporate the baryons in the theory we have to take care of their masses which do not vanish in the chiral limit [90]. However, if we take nucleons as massive matter fields which couples to external currents and Goldstone fields(pions etc.), we have to then expand the Lagrangian according to their increasing number of momenta. Here we shall present in brief the extension of the formalism to incorporate the heavy matter fields. First we will discuss the interaction of mesons with $SU(3)$ baryon octet and then we extend our formalism to include the baryon decuplet fields.

To construct the meson-baryon Lagrangian, we first choose a suitable representation of baryons which transforms under the chiral group $\mathcal{G}_{\chi} = SU(N_f)_L \otimes SU(N_f)_R$, as we did while obtaining meson-meson Lagrangian in Sec. 2.1.1.1.

It is more convenient to define a new unitary matrix for the pseudoscalar field as

$$u = \sqrt{U} \equiv \exp\left(\mathrm{i}\frac{\Phi(\mathrm{x})}{2\mathrm{f}_{\pi}}\right).$$

Now we introduce a Lorentz vector u^μ which is known as *chiral vielbein* or simply as *vielbein* and is given by [87]:

$$u^\mu = i\left[u^\dagger(\partial^\mu - ir^\mu)u - u(\partial^\mu - il^\mu)u^\dagger\right]. \tag{2.18}$$

The vector u^μ is axial in nature as it changes sign under parity i.e. $u^\mu \overset{P}{\longmapsto} -u^\mu$. The lowest-order chiral Lagrangian for the baryon octet in the presence of an external current may be written in terms of the $SU(3)$ matrix B as,

$$\mathcal{L}^{(1)}_{MB} = \mathrm{Tr}\left[\bar{B}\left(i\not{D} - M\right)B\right] - \frac{D}{2}\mathrm{Tr}\left(\bar{B}\gamma^\mu\gamma_5\{u_\mu, B\}\right) - \frac{F}{2}\mathrm{Tr}\left(\bar{B}\gamma^\mu\gamma_5[u_\mu, B]\right), \tag{2.19}$$

where M denotes the mass of the baryon octet, and the parameters $D = 0.804$ and $F = 0.463$ are determined from the baryon semileptonic decays [93]. The covariant derivative of B is given by

$$D_\mu B = \partial_\mu B + [\Gamma_\mu, B], \tag{2.20}$$

where we use another vector known as *connection*, which is given by [87]:

$$\Gamma^\mu = \frac{1}{2}\left[u^\dagger(\partial^\mu - ir^\mu)u + u(\partial^\mu - il^\mu)u^\dagger\right]. \tag{2.21}$$

The next order meson baryon Lagrangian contains many new terms (see for instance Ref. [94]). Their importance for kaon production will be small at low energies and there are some uncertainties in the coupling constants. Nonetheless, for consistency with previous calculations, we will include the contribution to the weak magnetism coming from the pieces

$$\mathcal{L}^{(2)}_{MB} = d_5\mathrm{Tr}\left(\bar{B}[f^+_{\mu\nu}, \sigma^{\mu\nu}B]\right) + d_4\mathrm{Tr}\left(\bar{B}\{f^+_{\mu\nu}, \sigma^{\mu\nu}B\}\right) + \ldots, \tag{2.22}$$

where the tensor $f^+_{\mu\nu}$ can be reduced for our study to

$$f^+_{\mu\nu} = \partial_\mu l_\nu - \partial_\nu l_\mu - i[l_\mu, l_\nu]. \tag{2.23}$$

In this case, the coupling constants are fully determined by the proton and neutron anomalous magnetic moments. This same approximation has also been used in calculations of single pion production induced by neutrinos [95].

In our model for the $\Delta S = 1$, $K^-/\bar{K}^0$ production we have also considered the lowest lying resonance $\Sigma^*(1385)$, which is a member of the baryon decuplet. In the next section we present in brief the the treatment of (decuplet)resonance in our formalism.

2.1.1.3 Resonance in Chiral Perturbation Theory

The decuplet fields are represented by Rarita-Schwinger field with both vector and spinor indices. The spin-$\frac{3}{2}$ decuplet baryons form a fully-symmetric rank-3 tensor(T^{μ}_{ijk}), which in the present notation is given by a $3 \times 3 \times 3$ array of matrices

$$T_{ijk} = \begin{pmatrix} \Delta^{++} & \frac{1}{\sqrt{3}}\Delta^{+} & \frac{1}{\sqrt{3}}\Sigma^{*+} \\ \frac{1}{\sqrt{3}}\Delta^{+} & \frac{1}{\sqrt{3}}\Delta^{0} & \frac{1}{\sqrt{6}}\Sigma^{*0} \\ \frac{1}{\sqrt{3}}\Sigma^{*+} & \frac{1}{\sqrt{6}}\Sigma^{*0} & \frac{1}{\sqrt{3}}\Xi^{*0} \end{pmatrix} \begin{pmatrix} \frac{1}{\sqrt{3}}\Delta^{+} & \frac{1}{\sqrt{3}}\Delta^{0} & \frac{1}{\sqrt{6}}\Sigma^{*0} \\ \frac{1}{\sqrt{3}}\Delta^{0} & \Delta^{-} & \frac{1}{\sqrt{3}}\Sigma^{*-} \\ \frac{1}{\sqrt{6}}\Sigma^{*0} & \frac{1}{\sqrt{3}}\Sigma^{*-} & \frac{1}{\sqrt{3}}\Xi^{*-} \end{pmatrix}$$
$$\times \begin{pmatrix} \frac{1}{\sqrt{3}}\Sigma^{*+} & \frac{1}{\sqrt{6}}\Sigma^{*0} & \frac{1}{\sqrt{3}}\Xi^{*0} \\ \frac{1}{\sqrt{6}}\Sigma^{*0} & \frac{1}{\sqrt{3}}\Sigma^{*-} & \frac{1}{\sqrt{3}}\Xi^{*-} \\ \frac{1}{\sqrt{3}}\Xi^{*0} & \frac{1}{\sqrt{3}}\Xi^{*-} & \Omega^{-} \end{pmatrix}. \tag{2.24}$$

The interaction of the baryon decuplet with the octet meson and baryon and with the external weak field may be given as

$$\mathcal{L}_{dec} = \mathcal{C}\left(\epsilon^{abc}\bar{T}^{\mu}_{ade}u^{d}_{\mu,b}B^{e}_{c} + \text{h.c.}\right), \tag{2.25}$$

where $a - e$ are flavor indices. B corresponds to the baryon octet and u_{μ} is the $SU(3)$ representation of the pseudoscalar mesons interacting with weak left l_{μ} and right r_{μ} handed currents (See Eq. 2.17). $\mathcal{C}$ is a free parameter which is fitted to the $\Delta(1232)$ decay width and details of which is given in Appendix. A.

Using the Lagrangian for the meson-meson and meson-baryon interactions and their interactions with external fields, we now apply this formalism to write the hadronic currents for the various processes and using them we will obtain the differential and total scattering cross sections for ν–induced K production in Sec. 2.2 and $\bar{\nu}$–induced $\bar{K}$ production in Sec. 2.3. We must point out that in this thesis we have used the same formalism to write the hadronic currents for the various processes like e^{-}/e^{+} induced K-production, η production and associated K-production.

2.2 Neutrino Induced Kaon Production

In neutrino induced reactions, the first inelastic reaction creating strange quark is the single kaon production (without accompanying hyperons)[2]. This charged current(CC), $\Delta S = 1$ process is particularly appealing for several reasons. One of them is the important background that it could produce, due to atmospheric

[2]For antineutrinos the lowest threshold for $|\Delta S| = 1$ reactions is much lower and corresponds to hyperon production.

neutrino interactions, in the analysis of one of the main decay channels the proton has in many SUSY GUT models ($p \to \nu + K^+$) [96, 97, 98]. A second reason is its simplicity from a theoretical point of view. At low energies, it is possible to obtain model independent predictions using Chiral Perturbation Theory (χPT) and due to the absence of $S = 1$ baryonic resonances, the range of validity of the calculation could be extended to higher energies than for other channels. Furthermore, the kaon associated production (with accompanying hyperons) has a higher energy threshold (1.10 vs. 0.79 GeV) which implies that even when the associated production is not Cabibbo suppressed, for a wide energy region (such as the ANL, the MiniBooNE or the T2K neutrino spectrum), single kaon production could still be dominant [47].

2.2.1 Formalism

The basic reaction for the neutrino induced charged current kaon production is

$$\nu_l(k) + N(p) \to l^-(k') + N'(p') + K(p_k), \tag{2.26}$$

where $l = e, \mu$ and $N\&N'$=n,p. The expression for the differential cross section in the laboratory (lab) frame for the above process is given by,

$$d^9\sigma = \frac{1}{4ME(2\pi)^5} \frac{d\vec{k}'}{(2E_l)} \frac{d\vec{p}'}{(2E'_p)} \frac{d\vec{p}_k}{(2E_K)} \delta^4(k + p - k' - p' - p_k) \bar{\Sigma}\Sigma |\mathcal{M}|^2, \tag{2.27}$$

where $\vec{k}$ and $\vec{k}'$ are the 3-momenta of the incoming and outgoing leptons in the lab frame with energy E and E', respectively. The kaon lab momentum is $\vec{p}_k$ having energy E_K, M is the nucleon mass, $\bar{\Sigma}\Sigma|\mathcal{M}|^2$ is the square of the transition amplitude averaged(summed) over the spins of the initial(final) state. At low energies, this amplitude may be written as

$$\mathcal{M} = \frac{G_F}{\sqrt{2}} j_\mu^{(L)} J^{\mu(H)} = \frac{g}{2\sqrt{2}} j_\mu^{(L)} \frac{1}{M_W^2} \frac{g}{2\sqrt{2}} J^{\mu(H)}, \tag{2.28}$$

where $j_\mu^{(L)}$ and $J^{\mu(H)}$ are the leptonic and hadronic currents respectively, $G_F = \sqrt{2}\frac{g^2}{8M_W^2} = 1.16639(1) \times 10^{-5}\,\mathrm{GeV}^{-2}$ is the Fermi coupling constant and g is the gauge coupling. The leptonic current can be readily obtained from the standard model Lagrangian coupling the W bosons to the leptons

$$\begin{aligned} \mathcal{L} &= -\frac{g}{2\sqrt{2}} \left[W_\mu^+ \bar{\nu}_l \gamma^\mu (1 - \gamma_5) l + W_\mu^- \bar{l} \gamma^\mu (1 - \gamma_5) \nu_l \right] \\ &= -\frac{g}{2\sqrt{2}} \left[j_{(L)}^\mu W_\mu^+ + h.c. \right]. \end{aligned} \tag{2.29}$$

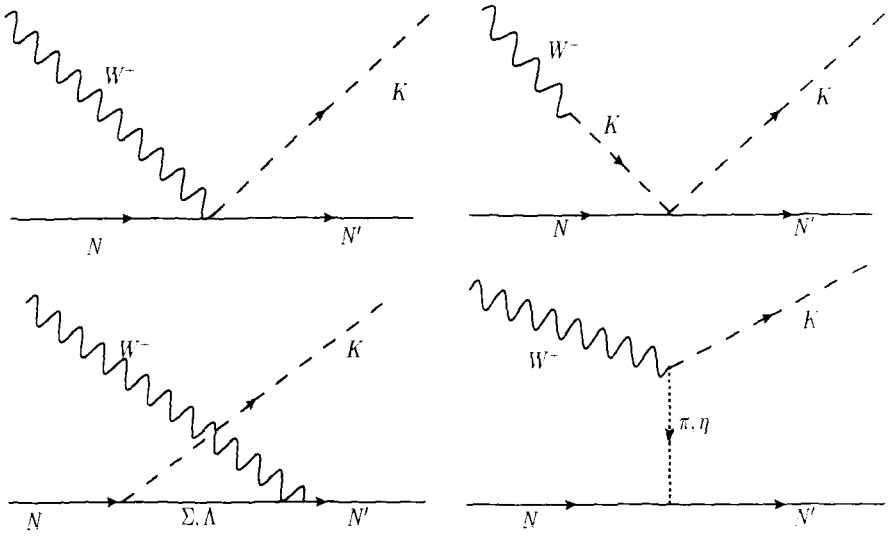

Figure 2.1: Feynman diagrams for the process $\nu N \to lN'K$. First row from left to right: contact term (labeled CT in the text), kaon pole term (KP); second row: u-channel diagram ($Cr\Sigma$, $Cr\Lambda$) and pion(eta) in flight (πP, (ηP)

For the evaluation of the hadronic current $J^{\mu(H)}$ we consider four different channels which are depicted in Fig. 2.1. There is a contact term (CT), a kaon pole (KP) term, a u-channel process with a Σ or Λ hyperon in the intermediate state and finally a meson (π, η) exchange term. The contribution of the different terms can be obtained in a systematic manner using χPT. This allows one to identify some terms that were missing in the approach of Ref. [47] which only included the u-channel diagrams in the calculation. For the specific reactions under consideration, there are not s-channel contributions given the absence of $S = 1$ baryonic resonances. The current of the KP term is proportional to q^μ. This implies, after contraction with the leptonic tensor, that the amplitude is proportional to the lepton mass and therefore very small.

Now, writing the amplitude for the coupling of the W boson to the hadrons for each of the terms in the form $\frac{g}{2\sqrt{2}}(J_H^\mu W_\mu^+ + \text{h.c.})$, for consistency with Eq. 2.28, we

Table 2.3: Values of the parameters appearing in the hadronic currents.

Process	A_{CT}	B_{CT}	$A_{Cr\Sigma}$	$A_{Cr\Lambda}$	A_{KP}	$A_{\pi P}$	$A_{\eta P}$
$\nu n \to lKn$	1	D-F	-(D-F)	0	1	1	1
$\nu p \to lKp$	2	-F	-(D-F)/2	(D+3F)	2	-1	1
$\nu n \to lKp$	1	-D-F	(D-F)/2	(D+3F)	1	-2	0

get the following contributions to the hadronic current

$$
\begin{aligned}
j^{\mu}\big|_{CT} &= -iA_{CT}V_{us}\frac{\sqrt{2}}{2f_{\pi}}\bar{N}(p')(\gamma^{\mu}+\gamma^{\mu}\gamma^{5}B_{CT})N(p),\\
j^{\mu}\big|_{Cr\Sigma} &= iA_{Cr\Sigma}V_{us}\frac{\sqrt{2}}{2f_{\pi}}N(p')\left(\gamma^{\mu}+i\frac{\mu_p+2\mu_n}{2M}\sigma^{\mu\nu}q_{\nu}+(D-F)(\gamma^{\mu}-\frac{q^{\mu}}{q^2-M_k^2}\not{q})\gamma^{5}\right)\\
&\quad\times\frac{\not{p}-\not{p}_k+M_{\Sigma}}{(p-p_k)^2-M_{\Sigma}^2}\not{p}_k\gamma^{5}N(p),\\
j^{\mu}\big|_{Cr\Lambda} &= iA_{Cr\Lambda}V_{us}\frac{\sqrt{2}}{4f_{\pi}}\bar{N}(p')\left(\gamma^{\mu}+i\frac{\mu_p}{2M}\sigma^{\mu\nu}q_{\nu}-\frac{D+3F}{3}(\gamma^{\mu}-\frac{q^{\mu}}{q^2-M_k^2}\not{q})\gamma^{5}\right)\\
&\quad\times\frac{\not{p}-\not{p}_k+M_{\Lambda}}{(p-p_k)^2-M_{\Lambda}^2}\not{p}_k\gamma^{5}N(p),\\
j^{\mu}\big|_{KP} &= iA_{KP}V_{us}\frac{\sqrt{2}}{4f_{\pi}}\bar{N}(p')(\not{q}+\not{p}_k)N(p)\frac{1}{q^2-M_k^2}q^{\mu},\\
j^{\mu}\big|_{\pi} &= iA_{\pi P}V_{us}(D+F)\frac{\sqrt{2}}{2f_{\pi}}\frac{M}{(q-p_k)^2-M_{\pi}^2}\bar{N}(p')\gamma^{5}.(q^{\mu}-2p_k{}^{\mu})N(p),\\
j^{\mu}\big|_{\eta} &= iA_{\eta P}V_{us}(D-3F)\frac{\sqrt{2}}{2f_{\pi}}\frac{M}{(q-p_k)^2-M_{\eta}^2}\bar{N}(p')\gamma^{5}.(q^{\mu}-2p_k{}^{\mu})N(p),
\end{aligned}
\tag{2.30}
$$

where, $q = k - k'$ is the four momentum transfer, $V_{us} = \sin\theta_C = 0.22$ where θ_C is the Cabibbo angle, $N(\cdot)$, $\bar{N}(\cdot)$ denote the nucleon spinors, $\mu_p = 1.7928\mu_N$ and $\mu_n = -1.9130\mu_N$[3] are the proton and neutron anomalous magnetic moments. The value of the various parameters in Eq. 2.30 are shown in Table 2.3. One may notice the induced pseudoscalar form factor in the $j^{\mu}\big|_{Cr\Sigma,Cr\Lambda}$ currents, which takes into account the coupling of the W boson to the baryon through a kaon. However, as for the KP term, its contribution is suppressed by a factor proportional to the final lepton mass and is negligible. Now, we discuss in some detail the terms that appear

[3] μ_N is nuclear magneton

in the coupling of the weak currents to the octet baryons for the u-channel diagram. With very general symmetry arguments, this coupling may be described in terms of three vector and three axial form factors. Following the notation of Ref. [93] we have

$$O_V^\mu = f_1\gamma^\mu + \frac{f_2}{M_B}\sigma^{\mu\nu}q_\nu + \frac{f_3}{M_B}q^\mu, \quad (2.31)$$

$$O_A^\mu = (g_1\gamma^\mu + \frac{g_2}{M_B}\sigma^{\mu\nu}q_\nu + \frac{g_3}{M_B}q^\mu)\gamma^5, \quad (2.32)$$

where M_B is the baryon mass. At the order considered, the chiral Lagrangian provides finite values for f_1, the weak magnetism form factor f_2, g_1 and a pole contribution to g_3. The scalar f_3 and a non-pole part of the pseudoscalar g_3 form factors would only appear at higher orders of the chiral expansion. Furthermore, their contributions to the amplitude is suppressed by a m_l (lepton mass) factor and they are usually neglected. The value of g_2 vanishes in the limit of exact $SU(3)$ symmetry and there is very little experimental information about it. In fact, it is also neglected in most analyses of hyperon phenomenology [99]. The values of f_1 and g_1 obtained from the lowest order chiral Lagrangian describe well the hyperon semileptonic decays [93, 99, 100]. The details of the inclusion of the weak magnetism form factor f_2 in our formalism is described in Appendix B.

Eventually, if the cross sections for the discussed processes were measured with more precision, one could use them to explore these form factors at several q^2 values. The current experimental information, based on the semileptonic decays, covers only a very reduced range for this magnitude.

Finally, we consider the q^2 dependence of the weak current couplings provided by the chiral Lagrangian discussed earlier. We must point out that, even at relatively low energies and low momenta of the hadrons involved in our study, q^2 reaches moderate values. The q^2 dependences of the needed form factors (e.g. $K\pi$, YN) are poorly known if at all. Several prescriptions have been used in the literature. For instance, for quasielastic scattering and single pion production, the vector form factors are usually related to the well known nucleon electromagnetic ones (see e.g. [95, 101, 102] and references therein). This procedure is well suited for these two cases because of isospin symmetry. However, in the $SU(3)$ sector we expect to have some symmetry breaking effects. Similarly, for the axial form factors, a q^2 dependence obtained from the nucleon-nucleon transition obtained in neutrino-nucleon quasielastic scattering is normally used. However, the axial mass is not well established and it runs from values around 1 GeV [103, 104] to 1.2 GeV recently obtained by the K2K [105] and MiniBooNE [106] collaborations. Again here, we expect a different behavior for the hyperon-nucleon vertices. One of the possible

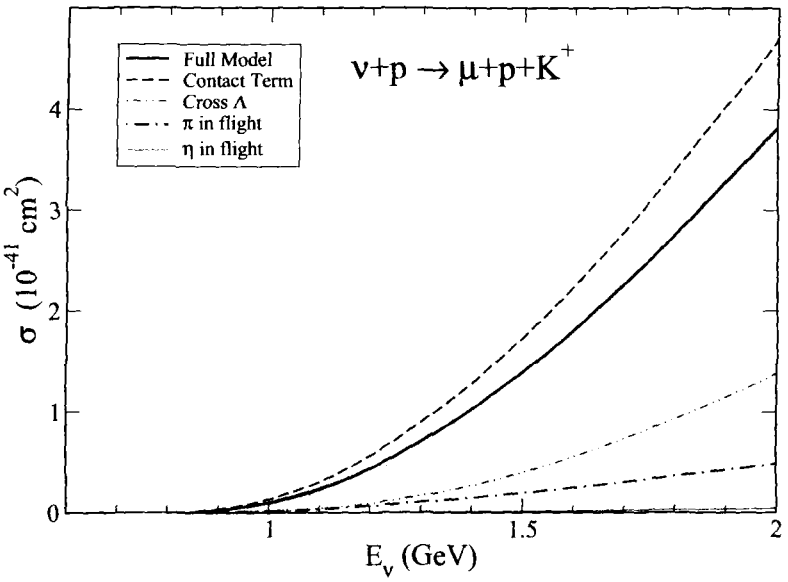

Figure 2.2: Contribution of the different terms to the total cross section for $\nu_\mu p \to \mu K^+ p$ reaction.

choices (e.g. [48]) is to use a dipole form with the mass of the vector(axial) meson that could couple the baryon to the current. In this work, in view of the present uncertainties, we adopt a global dipole form factor $F(q^2) = 1/(1 - q^2/M_F^2)^2$, with a mass $M_F \simeq 1$ GeV that multiplies the hadronic currents. Its effect, that should be small at low neutrino energies will give an idea of the uncertainties of the calculation and will be explored in the next section.

2.2.2 Results and Discussion

We consider the following reactions:

$$\begin{aligned} \nu_l + p &\to l^- + K^+ + p \\ \nu_l + n &\to l^- + K^0 + p \\ \nu_l + n &\to l^- + K^+ + n \quad (l = e,\ \mu) \end{aligned} \tag{2.33}$$

The total scattering cross section σ has been obtained by integrating over the kinematical variables[4] of Eq. 2.27 and using Eqs. 2.28-2.30. In Figs. 2.2-2.4, we

[4]The details are given in Appendix C.

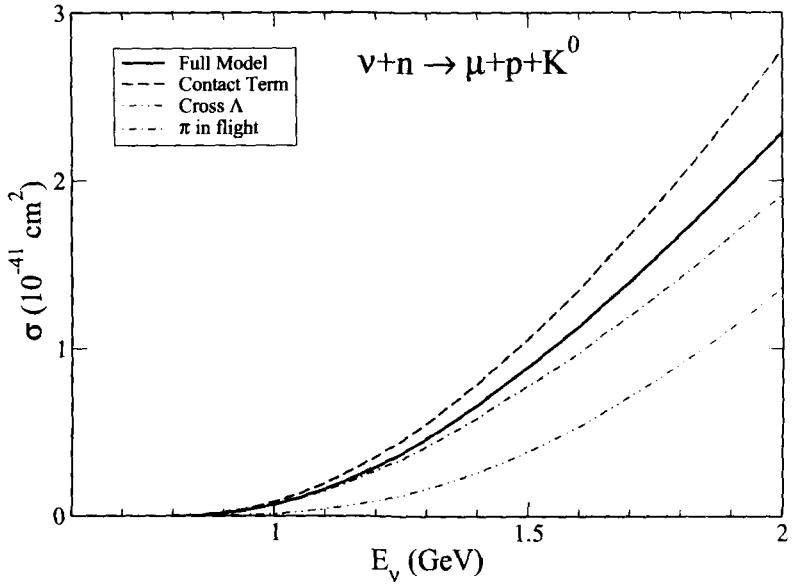

Figure 2.3: Contribution of the different terms to the total cross section for $\nu_\mu n \to \mu K^0 p$ reaction.

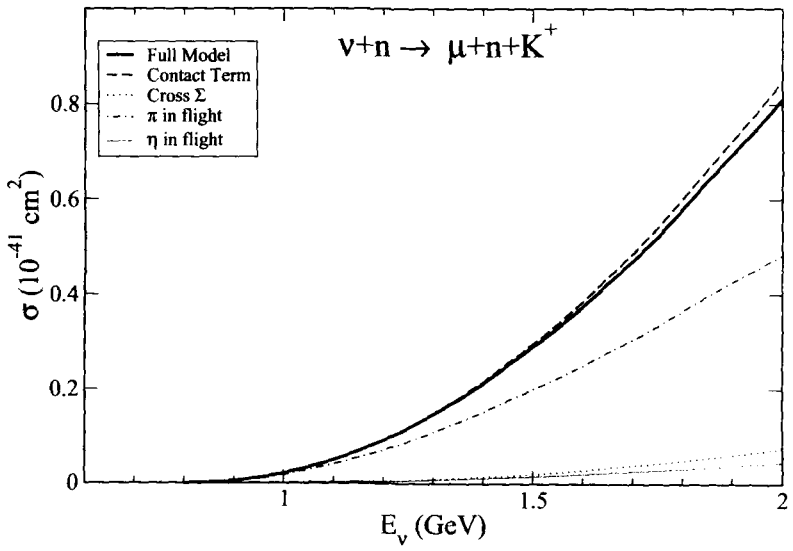

Figure 2.4: Contribution of the different terms to the total cross section for $\nu_\mu n \to \mu K^+ n$ reaction.

present the results of the contributions of the different diagrams to the total cross sections. The contribution coming from the kaon pole are negligible at the studied energies and are not shown in the figures although they are included in the full model curves. We observe the relevance of the contact term, not included in previous calculations.

Starting from $\nu_\mu + p \to \mu^- + K^+ + p$ channel as shown in Fig 2.2, we find that the contact term is in fact dominant. For example, in the neutrino energy range of $1.5 - 2.$ GeV the contact term is about $20 - 25\%$ higher than the net contribution to the total scattering cross section. The next major contribution comes from the u-channel diagram with a Λ in the intermediate state and the π exchange term where the fraction to the total cross sections are $\sim 35\%$ and $\sim 22\%$ respectively. As observed by Dewan [47] the u-channel Σ contribution is much less important, basically because of the larger coupling ($NK\Lambda \gg NK\Sigma$) of the strong vertex. The curve labeled as Full Model has been calculated with a dipole form factor with a mass of 1 GeV. The band in Fig. 2.2 corresponds to changing up and down this mass by a 10 percent. A similar effect is found in the other channels and we will only show the results for the central value of 1 GeV. These uncertainties, due to the vector/axial mass of the dipole form factor, would partially cancel in ratios of cross sections, such as $\sigma(K^0)/\sigma(K^+)$. Although the cancellation is not total, due to the different q^2 dependence of the channels, the uncertainty bands for the ratios, when the masses are changed by 10%, is less than 5%. We have also checked that the cross section obtained without the contact term and after correcting for the different values of the Cabibbo angle and the Yukawa strong coupling agree well with the result of Fig. 7 of Ref. [47] at its lowest energy. Higher energies are well beyond the scope of our model.

The process $\nu_\mu + n \to \mu^- + K^0 + p$ has a cross section of a similar size and the contact term is also the largest one with $\sim 20\%$ higher than the total cross section obtained by using full model, followed by the π exchange diagram and the u-channel (Λ) term. As for the previous channel, we observe a destructive interference between the different terms and the cross section obtained with the full model is smaller than that produced by the contact term alone.

Finally, the reaction $\nu_l n \to l^- K^+ n$ has a relatively smaller cross section probably because of the absence of Λ intermediate term which has significant contribution to the cross section in the other two diagrams. The contribution from the pion exchange term is substantially larger than the u-channel (Σ) term, as already noted in Ref. [47]. The contact term is also dominant for this channel and the total cross section calculated only with this term practically coincides with the full result. Therefore, we have found that the contact term, required by symmetry, play a major

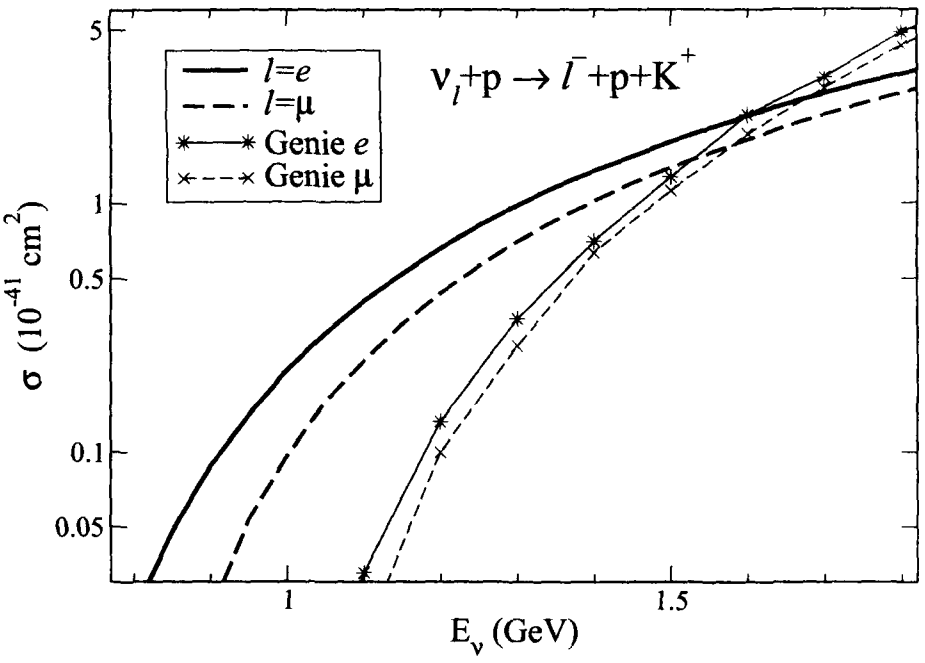

Figure 2.5: Cross sections as a function of the neutrino energy for single kaon production vs. associated production obtained with GENIE [57].

role in the description of the kaon production induced by neutrinos at low energies.

Above the energy threshold for the production of kaons accompanied by hyperons, this latter kind of processes could have larger cross sections due to the larger coupling for $\Delta S = 0$, (V_{ud} vs V_{us}). To explore this question and the range of energies where the processes we have studied are relevant we compare our results in Fig. 2.5, with the values for the associated production obtained by means of the GENIE Monte Carlo program [57]. We observe that, due to the difference between the energy thresholds, single kaon production for $\nu_l + p \to l^- + K^+ + p$ is clearly dominant for neutrinos of energies below 1.5 GeV. For the other two channels associated production becomes comparable at lower energies. Still, single K^0 production off neutrons is larger than the associated production up to 1.3 GeV and even the much smaller K^+ production off neutrons is larger than the associated production up to 1.1 GeV. The consideration of these $\Delta S = 1$ channels is therefore important for the description of strangeness production for all low energy neutrino spectra and should be incorporated in the experimental analysis.

After getting the considerable description of cross section at the energies below

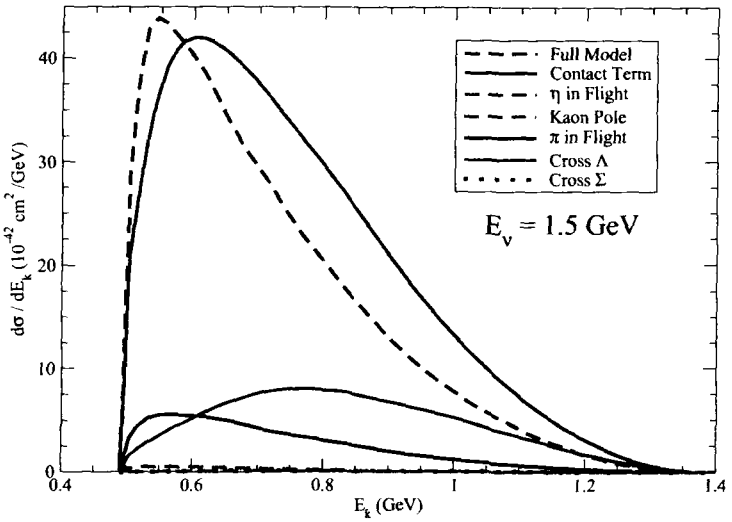

Figure 2.6: Contribution of the different terms to the kaon energy distribution ($\frac{d\sigma}{dE_k}$) at $E_\nu = 1.5GeV$ for $\nu_\mu p \rightarrow \mu^- K^+ p$ process.

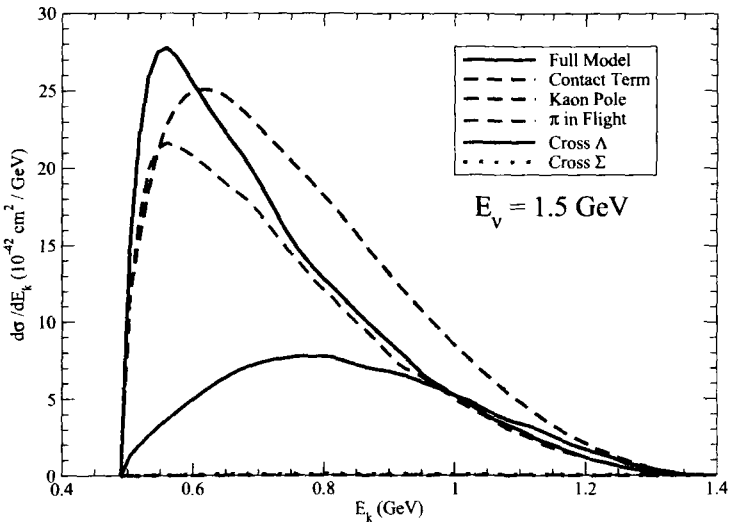

Figure 2.7: Contribution of the different terms to the kaon energy distribution ($\frac{d\sigma}{dE_k}$) at $E_\nu = 1.5GeV$ for $\nu_\mu n \rightarrow \mu^- K^0 p$ process.

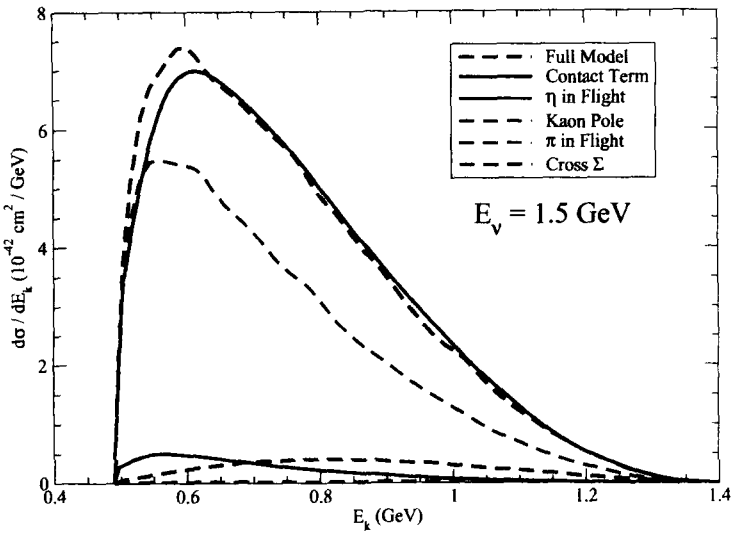

Figure 2.8: Contribution of the different terms to the kaon energy distribution ($\frac{d\sigma}{dE_k}$) at $E_\nu = 1.5GeV$ for $\nu_\mu n \to \mu^- K^+ n$ process.

2 GeV we obtain the differential cross section at $E_\nu = 1.5$ GeV i.e. near the $KN-$threshold. To explore the dynamics of the reactions we present the kaon energy distribution ($d\sigma/dE_k$) shown in Figs. 2.6-2.8 and the Q^2 distribution($d\sigma/dQ^2$) which are shown in Figs. 2.9-2.11.

In Figs. 2.6-2.8 we have presented the kaon energy distribution corresponding to the each Feynman diagram as shown in Fig. 2.1 for the neutrino lab energy of 1.5 GeV. As one may see that the results with full model in all the three cases peaks at low energies. It may also be observed from these curves that at low energies the main contribution comes from the contact term. For the $\nu_\mu n \to \mu^- K^+ n$, and $\mu^- K^0 p$ the contact term is followed by the pion exchange term and u-channel Λ diagram, whereas for the $\nu_\mu p \to \mu^- K^+ p$ we find that the pion exchange term and u-channel Λ diagram are approximately of same order. We may also notice that the u-channel mechanism is almost flat over the wide range of kaon energies as compared to the other diagrams.

The Q^2 distribution for the processes given in Eq. 2.33 are shown in Figs. 2.9-2.11 at neutrino energy 1.5 GeV. We find that the contact term is dominating for $\nu_\mu n \to \mu^- K^+ n$ and $\nu_\mu p \to \mu^- K^+ p$ processes, while in the peak region of Q^2 for the process $\nu_\mu n \to \mu^- K^0 p$ pion exchange term is dominating.

In Table 2.4, we show the total cross section results for the three channels averaged

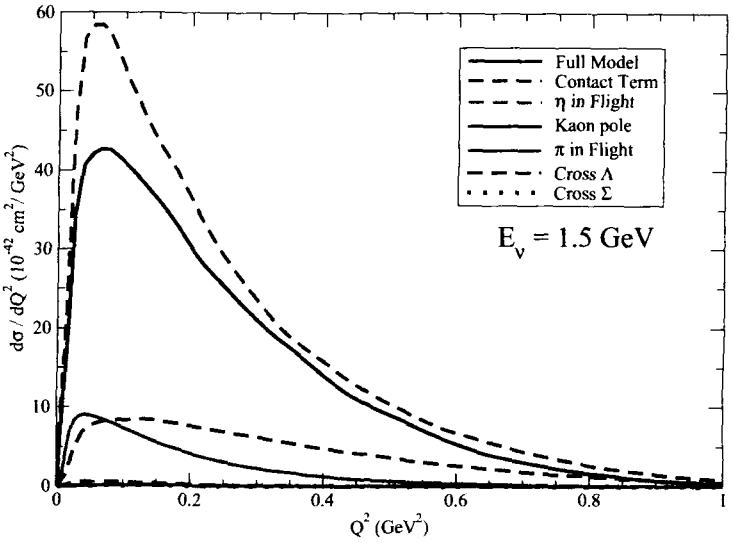

Figure 2.9: Contribution of the different terms to the Q^2 distribution ($\frac{d\sigma}{dQ^2}$) at $E_\nu = 1.5GeV$ for $\nu_\mu p \to \mu^- K^+ p$ process.

over the ANL [107], the MiniBooNE [108] and the off-axis (2.5 degrees) T2K [109] muon neutrino fluxes, all of them peaking at around 0.6 GeV. After normalization of the neutrino flux ϕ we have

$$\langle \sigma \rangle = \int_{E_{th}}^{E_{high}} dE\, \phi(E)\sigma(E), \tag{2.34}$$

where $E_{\rm th}$ is the threshold energy for each process and $E_{\rm high}$ is the maximum neutrino energy. As discussed previously, in these three cases, the neutrino energies are low enough for single kaon production to be relevant as compared to associated kaon

Table 2.4: Cross sections averaged over the neutrino flux at different laboratories in units of 10^{-41} cm^2. Theoretical uncertainties correspond to a 10% variation of the form factor mass.

Process	ANL	MiniBooNE	T2K
$\nu_\mu n \to \mu^- K^+ n$	0.06(1)	0.07(1)	0.09(1)
$\nu_\mu p \to \mu^- K^+ p$	0.28(5)	0.32(5)	0.43(8)
$\nu_\mu n \to \mu^- K^0 p$	0.17(3)	0.20(3)	0.25(5)

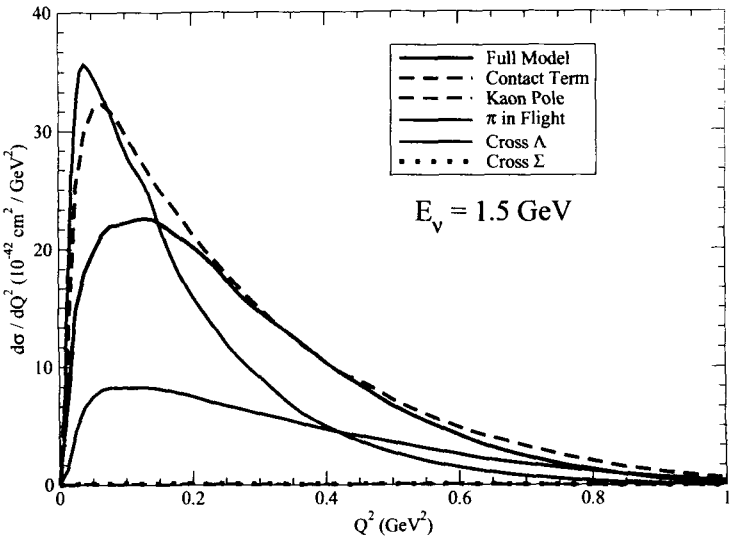

Figure 2.10: Contribution of the different terms to the Q^2 distribution ($\frac{d\sigma}{dQ^2}$) at $E_\nu = 1.5GeV$ for $\nu_\mu n \to \mu^- K^0 p$ process.

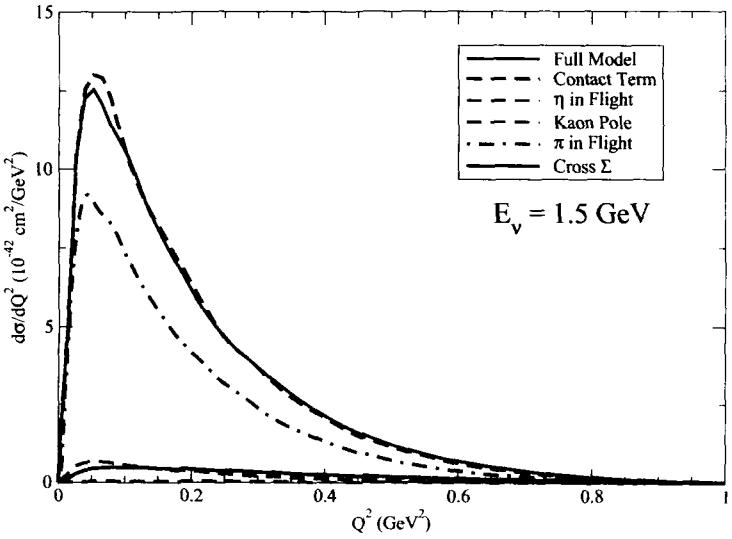

Figure 2.11: Contribution of the different terms to the Q^2 distribution ($\frac{d\sigma}{dQ^2}$) at $E_\nu = 1.5GeV$ for $\nu_\mu n \to \mu^- K^+ n$ process.

Table 2.5: Number of events calculated for single kaon production in water corresponding to the SuperK analysis for atmospheric neutrinos.

Process	Events e^-	Events μ^-
$\nu_l n \to l^- n K^+$	0.16	0.27
$\nu_l n \to l^- p K^0$	0.45	0.73
$\nu_l p \to l^- p K^+$	0.95	1.55
Total	1.56	2.55

production. Also the invariant mass of the hadronic system and the transferred momentum only reach the relatively small values where our model is more reliable.

We can get an idea of the magnitude of these channels by comparing their cross section with some recent results. For instance, the cross section for neutral current π^0 production per nucleon has been measured by the MiniBooNE collaboration [110] obtaining $\langle\sigma\rangle = (4.76 \pm 0.05 \pm 0.76) \times 10^{-40}$ cm^2 with a data set of some twenty thousand valid events. The cross sections predicted by our model with the same neutrino flux are around two orders of magnitude smaller, what means that a few hundreds of kaons should have been produced.

The atmospheric neutrino spectrum [111] also peaks at very low energies and our model should be very well suited to analyze the kaon production. In Table 2.5, we show the number of kaon events that has been obtained for the 22.5 kT of water target and for a period of 1489 days as in the SuperK analysis [98, 112] of proton decay. As in the Refs. [98, 112], we include cuts in the electron momentum ($p_e > 100$ MeV) and muon momentum ($p_\mu > 200$ MeV). We find that single kaon production is a very small source of background. In the SuperK analysis the kaon production was modeled following Ref. [61, 113] and only includes associated kaon production. Although some of the cuts applied in their analysis, such as looking for an accompanying hyperon, are useless for our case, we find that this source of background is negligible, given the smallness of our results and the totally different energy distribution of kaons and final leptons in the production and decay reactions.

Finally, in Fig. (2.12) we compare the Q^2 distribution for all the processes at relatively low value of neutrino energy $E_\nu = 1$ GeV. If high values of this magnitude are relevant, the results would be sensitive to higher orders of the chiral Lagrangian and/or a more precise description of the form factors. The reactions are always forward peaked (for the final lepton), even in the absence of any form factor ($F(q^2) = 1$), favoring relatively small values of the momentum transfer. In this figure, we also show the dependence of the cross section on the mass of the final lepton that

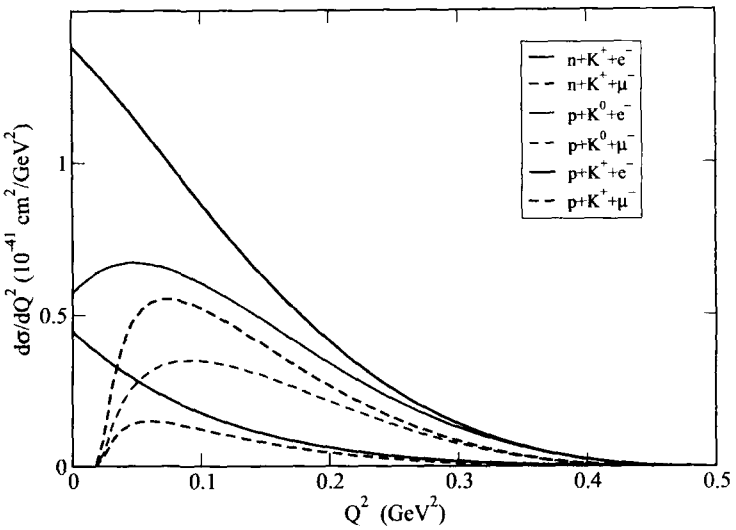

Figure 2.12: Q^2 distribution ($\frac{d\sigma}{dQ^2}$) at $E_\nu = 1GeV$ for single kaon production induced by neutrinos. The curves are labeled according to the final state of the process.

reduces the cross section at low Q^2 values. The process $\nu_e + n \rightarrow e^- + K^0 + p$ shows a slightly different behavior that reflects an important (and Q^2 dependent) interference between the pion exchange and the contact terms.

Till now we have discussed the kaon production off free nucleons. However, most of the experiments are carried out on detectors containing complex nuclei such as carbon, oxygen, iron etc. On the other hand, nuclear effects are known to be quite large for pion production induced by neutrinos [102, 114, 115, 116]. Fortunately, this question is much simpler for the kaons. Firstly, because there is no kaon absorption and the final state interaction is reduced to a repulsive potential, small when compared with the typical kaon energies, secondly, because of the absence of resonant channels in the production processes. We should remember here that some of the major nuclear effects for pion production are originated by the modification of the $\Delta(1232)$ properties on nuclei. Other nuclear effects, such as Fermi motion and Pauli blocking will only produce minor changes on the cross section and can easily be implemented in the Monte Carlo codes.

2.3 Antineutrino Induced $K^-/\bar{K}^0$ Production

Now we discuss single antikaon production off nucleons. The theoretical model is necessarily more complicated than for kaons because resonant mechanisms, absent in the kaon case, could be relevant. On the other hand, the threshold for associated antikaon production corresponds to the $K - \bar{K}$ channel and it is much higher than for the kaon case (KY). This implies that the process we study is the dominant source of antikaons for a wide range of antineutrino energies.

The study may be useful in the analysis of antineutrino experiments at MINERνA, NOνA, T2K and others. For instance, MINERνA has plans to investigate several strange particle production reactions with both neutrino and antineutrino beams [44] with high statistics. Furthermore, the T2K experiment [117] as well as beta beam experiments [118] will work at energies where the single kaon/antikaon production may be important.

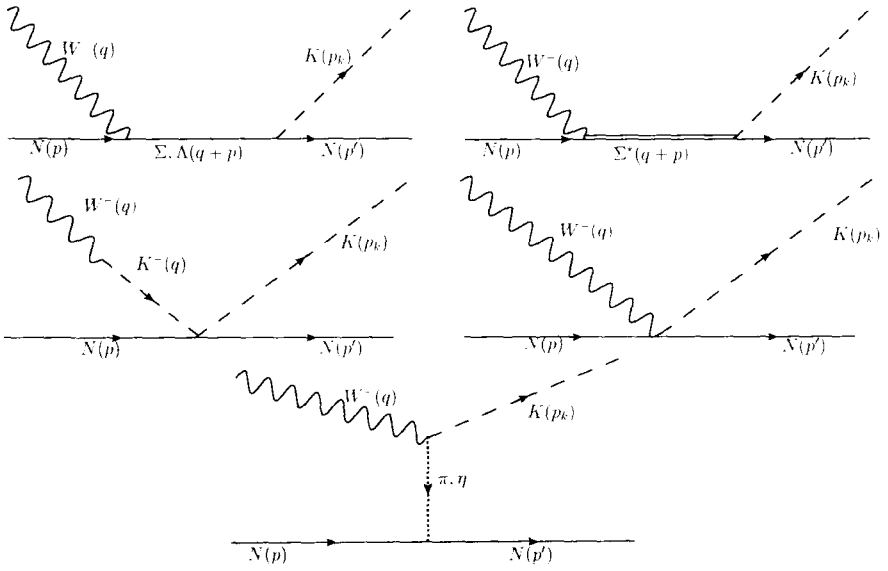

Figure 2.13: Feynman diagrams for the process $\bar{\nu}N \to lN'\bar{K}$. First row from left to right: s-channel Σ, Λ propagator (labeled SC in the text), s-channel Σ^* resonance (SCR), second row: kaon pole term (KP); contact term (CT) and last row: pion(eta) in flight ($\pi P/\eta P$).

2.3.1 Formalism

The basic reaction for antineutrino induced charged current antikaon production is

$$\bar{\nu}_l(k) + N(p) \rightarrow l(k') + N'(p') + \bar{K}(p_k), \tag{2.35}$$

where $l = e^+, \mu^+$ and $N\&N'$ are nucleons. The expression for the differential cross section in the laboratory frame for the above process is given by

$$d^9\sigma = \frac{1}{4ME(2\pi)^5} \frac{d\vec{k}'}{(2E_l)} \frac{d\vec{p}'}{(2E'_p)} \frac{d\vec{p}_k}{(2E_k)} \delta^4(k + p - k' - p' - p_k) \bar{\Sigma}\Sigma |\mathcal{M}|^2. \tag{2.36}$$

where $k(k')$ is the momentum of the incoming(outgoing) lepton with energy $E(E')$. $p(p')$ is the momentum of the incoming(outgoing) nucleon. The kaon 3-momentum is $\vec{p}_k$ having energy E_k, M is the nucleon mass, $\bar{\Sigma}\Sigma|\mathcal{M}|^2$ is the square of the transition amplitude averaged(summed) over the spins of the initial(final) state. It can be written as

$$\mathcal{M} = \frac{G_F}{\sqrt{2}} j_\mu J^\mu = \frac{g}{2\sqrt{2}} j_\mu \frac{1}{M_W^2} \frac{g}{2\sqrt{2}} J^\mu, \tag{2.37}$$

where j_μ and J^μ are the leptonic and hadronic currents respectively, $G_F = \sqrt{2}\frac{g^2}{8M_W^2}$ is the Fermi coupling constant, g is the gauge coupling and M_W is the mass of the W-boson. The leptonic current can be readily obtained from the standard model Lagrangian coupling the W bosons to the leptons

$$\mathcal{L} = -\frac{g}{2\sqrt{2}} \left[j^\mu W_\mu^- + h.c. \right]. \tag{2.38}$$

We construct a model including non-resonant terms and the decuplet resonances, that couple strongly to the pseudoscalar mesons. The same approach successfully describes the pion production case (see for example Ref. [95]). The channels that contribute to the hadronic current are depicted in Fig. 2.13. There are s-channels with Σ, Λ(SC) and Σ^*(SCR) as intermediate states, a kaon pole (KP) term, a contact term (CT), and finally a meson (πP,ηP) exchange term. For these specific reactions there is no u-channel process with hyperons in the intermediate state.

The contribution coming from different terms are obtained from the χPT La-

Process	B_{CT}	A_{CT}	A_Σ	A_Λ	A_{KP}	A_π	A_η	A_{Σ^*}
$\bar{\nu}n \to l^+K^-n$	D-F	1	-1	0	-1	1	1	2
$\bar{\nu}p \to l^+K^-p$	-F	2	$-\frac{1}{2}$	1	-2	-1	1	1
$\bar{\nu}p \to l^+\bar{K}^0n$	-D-F	1	$\frac{1}{2}$	1	-1	-2	0	-1

Table 2.6: Constant factors appearing in the hadronic current

grangian as discussed in Sec. 2.1.1. The contributions to the hadronic current are

$$
\begin{aligned}
J^\mu|_{CT} &= iA_{CT}V_{us}\frac{\sqrt{2}}{2f_\pi}\bar{N}(p')\,(\gamma^\mu + B_{CT}\,\gamma^\mu\gamma_5)\,N(p) \\
J^\mu|_\Sigma &= iA_\Sigma(D-F)V_{us}\frac{\sqrt{2}}{2f_\pi}\bar{N}(p')\not{p}_k\gamma_5\frac{\not{p}+\not{q}+M_\Sigma}{(p+q)^2-M_\Sigma^2}\left(\gamma^\mu + i\frac{(\mu_p+2\mu_n)}{2M}\sigma^{\mu\nu}q_\nu\right. \\
&+ \left.(D-F)\left\{\gamma^\mu - \frac{q^\mu}{{q^2-M_k}^2}\not{q}\right\}\gamma^5\right)N(p) \\
J^\mu|_\Lambda &= iA_\Lambda V_{us}(D+3F)\frac{1}{2\sqrt{2}f_\pi}\bar{N}(p')\not{p}_k\gamma^5\frac{\not{p}+\not{q}+M_\Lambda}{(p+q)^2-M_\Lambda^2}\left(\gamma^\mu + i\frac{\mu_p}{2M}\sigma^{\mu\nu}q_\nu\right. \\
&- \left.\frac{(D+3F)}{3}\left\{\gamma^\mu - \frac{q^\mu}{{q^2-M_k}^2}\not{q}\right\}\gamma^5\right)N(p) \\
J^\mu|_{KP} &= iA_{KP}V_{us}\frac{\sqrt{2}}{2f_\pi}\bar{N}(p')\not{q}\,N(p)\frac{q^\mu}{q^2-M_k^2} \\
J^\mu|_\pi &= iA_\pi\frac{M\sqrt{2}}{2f_\pi}V_{us}(D+F)\frac{2{p_k}^\mu - q^\mu}{{(q-p_k)^2-m_\pi}^2}\bar{N}(p')\gamma_5 N(p) \\
J^\mu|_\eta &= iA_\eta\frac{M\sqrt{2}}{2f_\pi}V_{us}(D-3F)\frac{2{p_k}^\mu - q^\mu}{{(q-p_k)^2-m_\eta}^2}\bar{N}(p')\gamma_5 N(p) \\
J^\mu|_{\Sigma^*} &= -iA_{\Sigma^*}\frac{C}{f_\pi}\frac{1}{\sqrt{6}}\,V_{us}\,\frac{p_k^\lambda}{P^2-M_{\Sigma^*}^2+i\Gamma_{\Sigma^*}M_{\Sigma^*}}\,\bar{N}(p') \\
&\times\; P_{RS_{\lambda\rho}}(\Gamma_V^{\rho\mu}+\Gamma_A^{\rho\mu})N(p)
\end{aligned}
\tag{2.39}
$$

In $\Gamma_V^{\rho\mu}+\Gamma_A^{\rho\mu}$, the same form of the transition form factors are taken as for the Δ^+ case. A_{CT}, B_{CT},etc. are the constant factors and have been tabulated in Table 2.6.

As it is the case for the $\Delta(1232)$ in pion production, we expect that the weak excitation of the $\Sigma^*(1385)$ resonance and its subsequent decay in NK may be important. The lowest order SU(3) Lagrangian coupling the pseudoscalar mesons with

decuplet-octet baryons in presence of external weak current is given by

$$\mathcal{L}_{dec} = \mathcal{C}\left(\epsilon^{abc}\bar{T}^{\mu}_{ade}u^{d}_{\mu,b}B^{e}_{c} + h.c.\right), \tag{2.40}$$

where T^{μ} is the SU(3) representation of the decuplet fields, $a-e$ are flavor indices[5]. B corresponds to the baryon octet and u_{μ} is the SU(3) representation of the pseudoscalar mesons interacting with weak left l_{μ} and right r_{μ} handed currents (See Eq. 2.17). The parameter $\mathcal{C} \simeq 1$ has been fitted to the $\Delta(1232)$ decay-width. The spin 3/2 propagator for Σ^* is given by

$$G^{\mu\nu}(P) = \frac{P^{\mu\nu}_{RS}(P)}{P^2 - M^2_{\Sigma^*} + iM_{\Sigma^*}\Gamma_{\Sigma^*}}, \tag{2.41}$$

where $P = p + q$ is the momentum carried by the resonance, $q = k - k'$ and $P^{\mu\nu}_{RS}$ is the projection operator

$$P^{\mu\nu}_{RS}(P) = \sum_{spins}\psi^{\mu}\bar{\psi}^{\nu} = -(\not{P} + M_{\Sigma^*})\left[g^{\mu\nu} - \frac{1}{3}\gamma^{\mu}\gamma^{\nu} - \frac{2}{3}\frac{P^{\mu}P^{\nu}}{M^2_{\Sigma^*}} + \frac{1}{3}\frac{P^{\mu}\gamma^{\nu} - P^{\nu}\gamma^{\mu}}{M_{\Sigma^*}}\right]. \tag{2.42}$$

with M_{Σ^*} the resonance mass and ψ^{μ} the Rarita-Schwinger spinor. The Σ^* width obtained using the Lagrangian of Eq. 2.40 may be written as

$$\Gamma_{\Sigma^*} = \Gamma_{\Sigma^*\to\Lambda\pi} + \Gamma_{\Sigma^*\to\Sigma\pi} + \Gamma_{\Sigma^*\to N\bar{K}}, \tag{2.43}$$

where

$$\Gamma_{\Sigma^*\to Y,meson} = \frac{C_Y}{192\pi}\left(\frac{\mathcal{C}}{f_{\pi}}\right)^2\frac{(W+M_Y)^2 - m^2}{W^5}\lambda^{3/2}(W^2, M^2_Y, m^2) \times \Theta(W - M_Y - m). \tag{2.44}$$

Here, m, M_Y are the masses of the emitted meson and baryon. $\lambda(x,y,z) = (x-y-z)^2 - 4yz$ and Θ is the step function. The factor C_Y is 1 for Λ and $\frac{2}{3}$ for N and Σ.

Using symmetry arguments, the most general $W^-N \to \Sigma^*$ vertex may be written in terms of a vector and an axial-vector part as,

$$\begin{aligned}\langle\Sigma^*; P = p+q\,|V^{\mu}|N;p\rangle &= V_{us}\bar{\psi}_{\alpha}(\vec{P})\Gamma^{\alpha\mu}_{V}(p,q)\,u(\vec{p}),\\ \langle\Sigma^*; P = p+q\,|A^{\mu}|N;p\rangle &= V_{us}\bar{\psi}_{\alpha}(\vec{p})\Gamma^{\alpha\mu}_{A}(p,q)\,u(\vec{p}),\end{aligned} \tag{2.45}$$

[5]The physical states of the decuplet are: $T_{111} = \Delta^{++}, T_{112} = \frac{\Delta^+}{\sqrt{3}}, T_{122} = \frac{\Delta^0}{\sqrt{3}}, T_{222} = \Delta^-, T_{113} = \frac{\Sigma^{*+}}{\sqrt{3}}, T_{123} = \frac{\Sigma^{*0}}{\sqrt{6}}, T_{223} = \frac{\Sigma^{*-}}{\sqrt{3}}, T_{113} = \frac{\Xi^+}{\sqrt{3}}, T_{133} = \frac{\Xi^0}{\sqrt{3}}, T_{333} = \Omega^-$.

where

$$\begin{aligned}
\Gamma_V^{\alpha\mu}(p,q) &= \left[\frac{C_3^V}{M}(g^{\alpha\mu}\not{q} - q^\alpha\gamma^\mu) + \frac{C_4^V}{M^2}(g^{\alpha\mu}q\cdot P - q^\alpha P^\mu)\right. \\
&\quad \left. + \frac{C_5^V}{M^2}(g^{\alpha\mu}q\cdot p - q^\alpha p^\mu) + C_6^V g^{\mu\alpha}\right]\gamma_5 \\
\Gamma_A^{\alpha\mu}(p,q) &= \left[\frac{C_3^A}{M}(g^{\alpha\mu}\not{q} - q^\alpha\gamma^\mu) + \frac{C_4^A}{M^2}(g^{\alpha\mu}q\cdot P - q^\alpha P^\mu)\right. \\
&\quad \left. + C_5^A g^{\alpha\mu} + \frac{C_6^A}{M^2}q^\mu q^\alpha\right]. \qquad (2.46)
\end{aligned}$$

Our knowledge of these form factors is quite limited. The Lagrangian of Eq. 2.40 gives us only $C_5^A(0) = -2\mathcal{C}/\sqrt{3}$ (for the $\Sigma^{*-}(1385)$ case). However, using SU(3) symmetry we can relate all other form factors to those of the $\Delta(1232)$ resonance, such that $C_i^{\Sigma^{*-}}/C_i^{\Delta^+} = -1$ and $C_i^{\Sigma^{*-}}/C_i^{\Sigma^{*0}} = \sqrt{2}$. See Refs. [95, 114, 119, 120, 121] for details of the $WN\Delta$ form-factors. In the Δ case, the vector form factors are relatively well known from electromagnetic processes and there is some information on the axial ones from the study of pion production. We will use the same set as in Ref. [95, 121], where pion production induced by neutrinos has been studied, except for $C_5^A(0)$, obtained directly from the Lagrangian and C_6^A. These latter two form factors are related by PCAC so that $C_6^A = C_5^A M^2/(m_K^2 - q^2)$.

Even from relatively low neutrino energies, other baryonic resonances, beyond the $\Sigma^*(1385)$, could contribute to the cross section, as they are close to the kaon nucleon threshold. However, their weak couplings are basically unknown. Also, the theoretical estimations of these couplings are still quite uncertain. Nonetheless, recent advances in the radiative decays of these resonances, both experimental and theoretical (see, e.g., Refs. [122, 123]), may help to develop a more complete model in the future.

Finally, we consider the q^2 dependence of the weak current couplings provided by the chiral Lagrangian. In this work, we follow the same procedure as in Ref. [124][6] and adopt a global dipole form factor $F(q^2) = 1/(1 - q^2/M_F^2)^2$, with a mass $M_F \simeq 1$ GeV that multiplies with all the hadronic currents, except the resonant one, that has been previously discussed. Its effect, that should be small at low neutrino energies will give an idea of the uncertainties of the calculation and will be explored in the next section.

[6] A more detailed discussion can be found there.

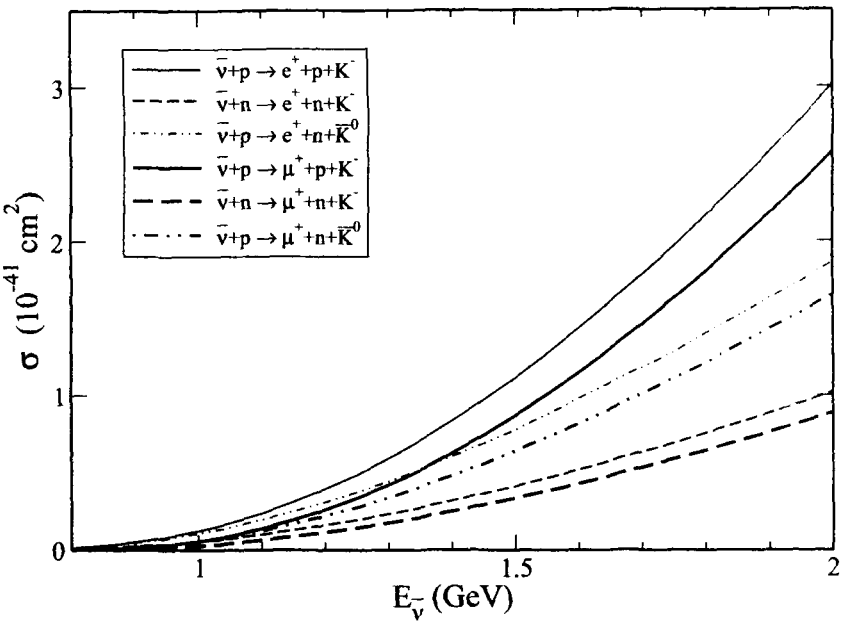

Figure 2.14: Cross-section for the processes $\bar{\nu}_\mu N \to \mu^+ N' \bar{K}$ and $\bar{\nu}_e N \to e^+ N' K$ as a function of the antineutrino energy

2.3.2 Results and Discussion

We consider the following strangeness changing ($|\Delta S| = 1$) charged-current reactions:

$$\begin{aligned} \bar{\nu}_l + p &\to l^+ + K^- + p \\ \bar{\nu}_l + p &\to l^+ + \bar{K}^0 + n \\ \bar{\nu}_l + n &\to l^+ + K^- + n\,. \end{aligned} \tag{2.47}$$

The total scattering cross section σ has been obtained by integrating over the kinematical variables[7] of Eq. 2.36 and using Eqs. 2.37-2.39. In Fig. 2.14, we show their total cross section for electronic($\bar{\nu}_e$) and muonic($\bar{\nu}_\mu$) antineutrinos as a function of neutrino energy. We obtain similar values to the cross sections of kaon production induced by neutrinos as obtained in Sec. 2.2.2, even when there are no resonant contributions. The electronic antineutrino cross sections are slightly larger, but they do not present any other distinguishing feature. For all channels, the cross

[7]The details are given in Appendix C.

Table 2.7: $< \sigma >$ $(10^{-41} cm^2)$ for $\bar{K}$ production with MiniBooNE $\bar{\nu}_\mu$ flux and neutral current π^0 production (per nucleon) measured at MiniBooNE [110]

Process	$< \sigma >$
$\bar{\nu}_\mu + p \rightarrow \mu^+ + K^- + p$	0.11
$\bar{\nu}_\mu + p \rightarrow \mu^+ + K^0 + n$	0.08
$\bar{\nu}_\mu + n \rightarrow \mu^+ + K^- + n$	0.04
$\bar{\nu}_\mu + N \rightarrow \bar{\nu}_\mu + N + \pi^0$	$14.8 \pm 0.5 \pm 2.3$

sections are very small, as compared to other processes induced by antineutrinos at these energies, like pion production, due to the Cabibbo suppression and to the smallness of the available phase space.

Before discussing in more detail each of the channels, we will make some comments. First, the lowest energy antikaon associate production, ($K\bar{K}$, $|\Delta S| = 0$), has a quite high threshold ($\approx$ 1.75 GeV) and thus, it leads to even smaller cross sections in the range of energies we have explored. For instance, at 2 GeV, GENIE predicts antikaon production cross sections at least two orders of magnitude smaller than our calculation.

As it was expected, our results would lead to a very minor signal in past experiments. For instance, we have evaluated the flux averaged cross-section $< \sigma >$ for the MiniBooNE antineutrino flux [125] in the sub GeV energy region. The results are given in Table 2.7 and compared with the recent measurement of the neutral current π^0 production per nucleon with the same flux [110]. We find that the antikaon production cross section is around two orders of magnitude smaller than the NC π^0 one at MiniBooNE. Given the number of neutral pions observed for the antineutrino beam we expect that only a few tens of antikaons were produced in this experiment. One should notice here that the average antineutrino energy at MiniBooNE is well below the kaon threshold. Thus, we are only sensitive to the high energy tail of the flux. One could expect a relatively larger signal for the atmospheric neutrino $\bar{\nu}_e$ and $\bar{\nu}_\mu$ induced events at SuperK, given the larger neutrino energies. But even there we find a very small background from antikaon events. Taking the antineutrino fluxes from Ref. [111] we have calculated the event rates for the 22.5kT water target and a period of 1489 days as in the SuperK analysis of Ref. [112]. We obtain 0.8 e^+ and 1.5 μ^+ events. Although the model has large uncertainties at high energies, the rapid fall of the neutrino spectrum implies that the high energy tail contributes very little to the background.

Our results correspond to relatively low antineutrino energies, where our model is

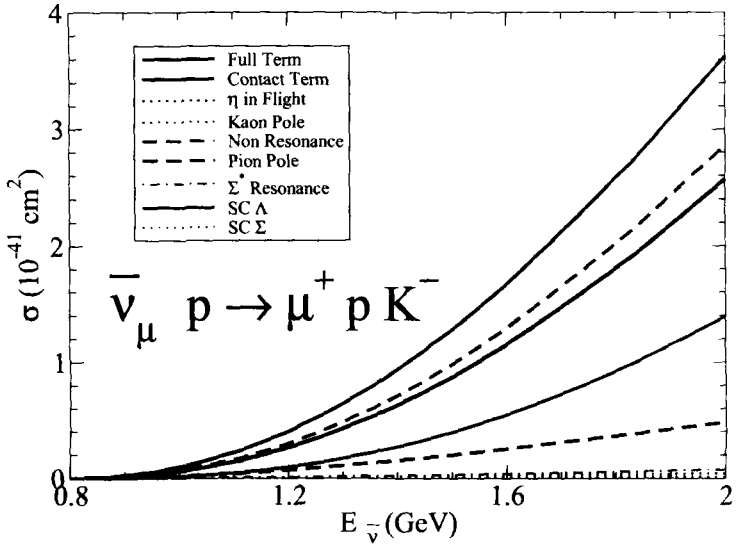

Figure 2.15: Contribution of the different terms to the total cross section for the process $\bar{\nu}_\mu p \to \mu^+ p K^-$.

more reliable. However, the model could also be used to compare with data obtained at much higher neutrino energies selecting events such that the invariant mass of hadronic part is close to antikaon-nucleon threshold and the transferred momentum q is small. This procedure has been used, for instance, in the analysis of two pion production induced by neutrinos [126, 127].

In Fig. 2.15, we show the size of the different contributions to the $\nu_\mu p \to \mu^+ p K^-$ reaction. The cross section is clearly dominated by the non-resonant terms, and more specifically the contact term has the largest contribution. We see the destructive interference that leads to a total cross section smaller than that predicted by the CT term alone. We could also remark the negligible contribution of the $\Sigma^*(1385)$ channel. In fact, the addition of the $\Sigma^*(1385)$ resonance leads to the further lowering of the cross section which is about 7% at 2 GeV. This fact is at variance with the strong Δ dominance for pion production and it can be easily understood because the Σ^* mass is below the kaon production threshold. We have also explored the uncertainties associated with the form factor. The curve labeled as "Full Model" has been calculated with a dipole form factor with a mass of 1 GeV. The band corresponds to a 10 percent variation of this parameter. The effect is similar in the other channels and we will only show the results for the central value of 1 GeV. Apart from the CT term the s-channel with Λ propagator and pion pole give a significant

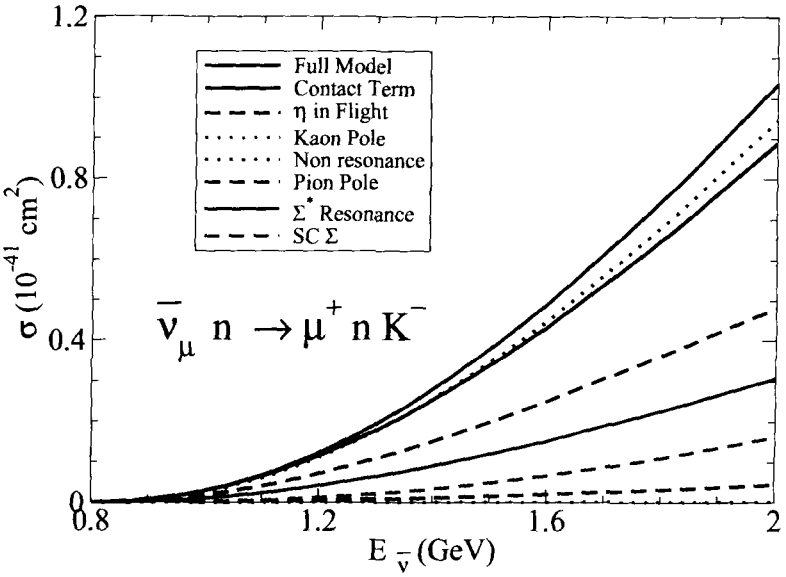

Figure 2.16: Contribution of the different terms to the total cross section for the process $\bar{\nu}_\mu n \to \mu^+ n K^-$.

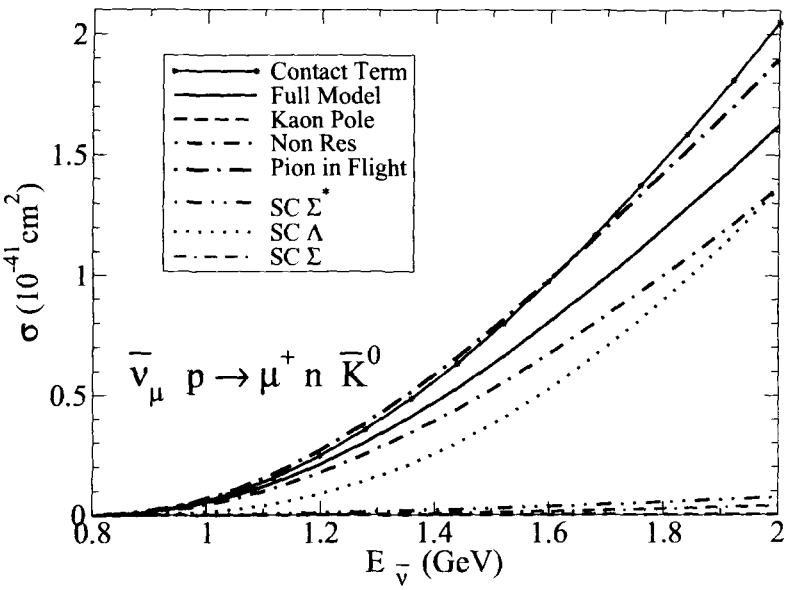

Figure 2.17: Contribution of the different terms to the total cross section for the process $\bar{\nu}_\mu p \to \mu^+ n \bar{K}^0$.

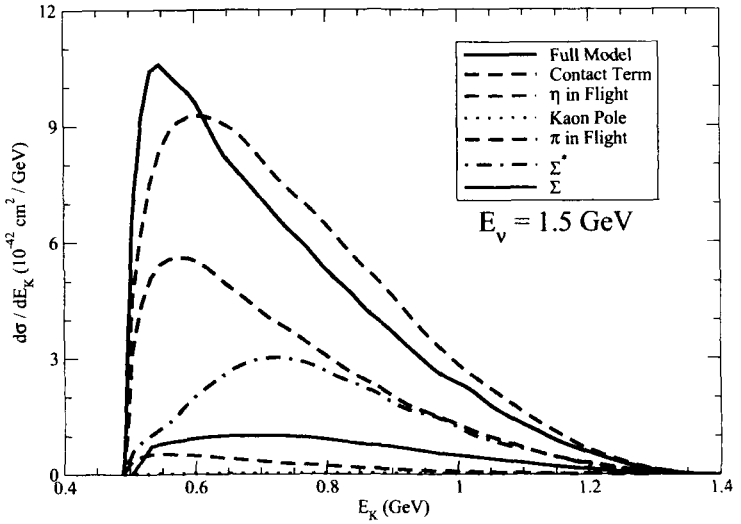

Figure 2.18: Contribution of the different terms to the kaon energy distribution $(\frac{d\sigma}{dE_k})$ at $E_\nu = 1.5GeV$ for $\bar{\nu}_\mu n \to \mu^+ K^- n$ process.

contribution to the cross sections. The contributions from other channels are very low and they are not visible at the said energies.

In Figs. 2.16 and 2.17, we show the other two channels. As in the previous case here also the CT term is very important. We observe, however, that the pion-pole term gives a contribution as large as the CT one for the $\bar{\nu}_\mu p \to \mu^+ n \bar{K}^0$ process. For the $\bar{\nu}_\mu n \to \mu^+ n K^-$ case, we find a substantial contribution of the Σ^* resonance, due to the larger value of the couplings (see Table 2.6). As in the first case, there is some destructive interference between the different mechanisms participating in these processes.

In Figs. 2.18-2.20, we present the kaon energy distribution $(d\sigma/dE_k)$ at E_ν = 1.5GeV as we did for the neutrino induced reactions in Sec. 2.2.2. For the $\nu_\mu n \to \mu^+ K^- n$ we find that here also CT term is dominant, followed by the π exchange term(πP) and the Σ^* resonance(SCR) term. In the peak energy region the CT term is slightly lower as compared to the full model. Here we would like to emphasize that the shape of the Σ^* resonance is relatively flat over the region of interest while all the other diagrams are peaked near the kaon rest mass. In Fig. 2.19, we present the results for the kaon energy distribution for $\bar{\nu}_\mu p \to \mu^+ K^- p$. Here we find that the peak of CT term and results obtained by using the full model coincide, however, CT term is wider in nature. The next contribution to the differential cross section

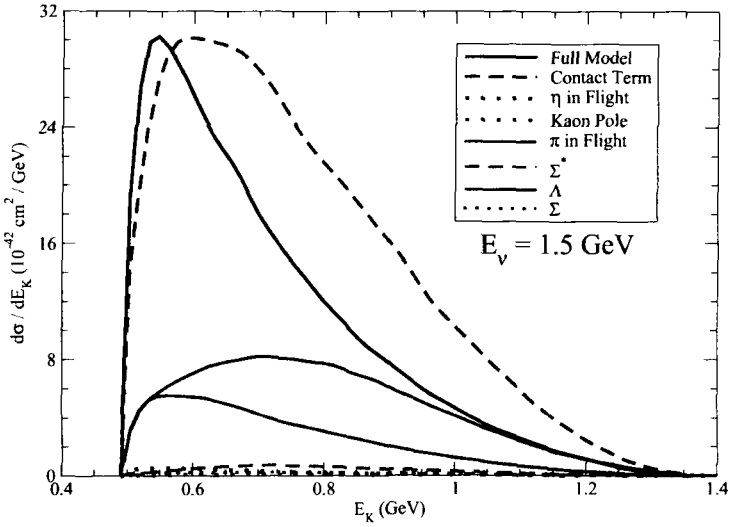

Figure 2.19: Contribution of the different terms to the kaon energy distribution $(\frac{d\sigma}{dE_k})$ at $E_\nu = 1.5GeV$ for $\bar{\nu}_\mu p \rightarrow \mu^+ K^- p$ process.

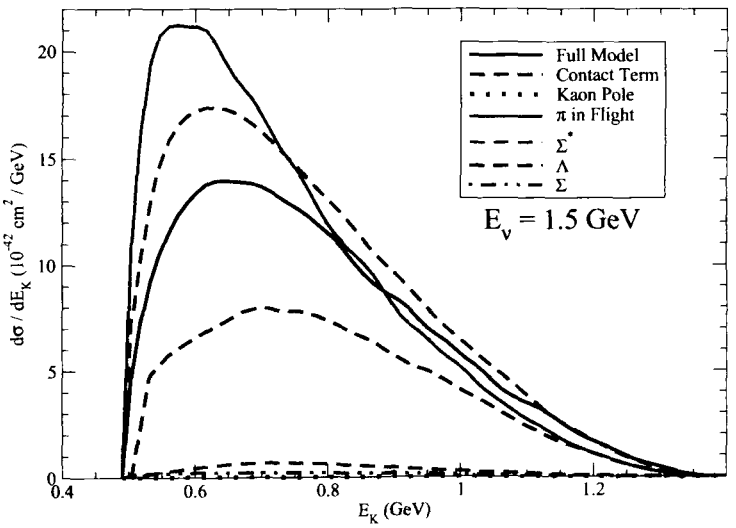

Figure 2.20: Contribution of the different terms to the kaon energy distribution $(\frac{d\sigma}{dE_k})$ at $E_\nu = 1.5GeV$ for $\bar{\nu}_\mu p \rightarrow \mu^+ \bar{K}^0 n$ process.

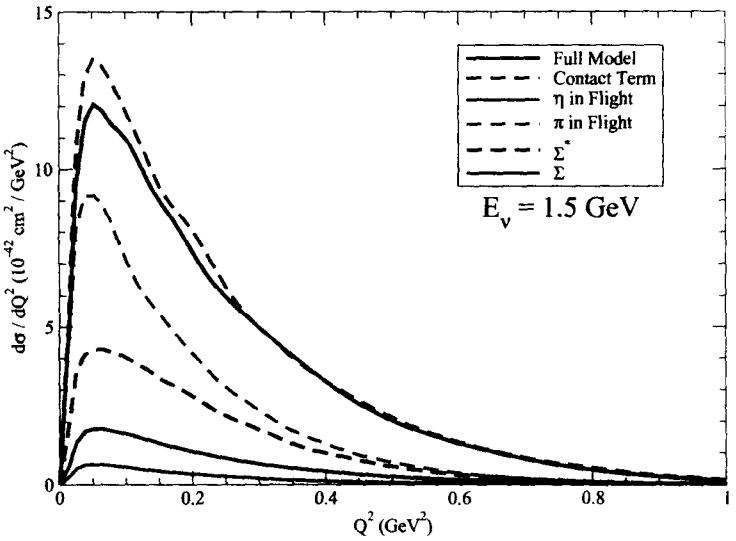

Figure 2.21: Contribution of the different terms to the Q^2 distribution ($\frac{d\sigma}{dQ^2}$ at $E_\nu = 1.5GeV$ for $\bar{\nu}_\mu n \to \mu^+ K^- n$ process.

comes from the s-channel Λ term, the distribution of which is flat in nature. We find that there is hardly any contribution from the resonant term. In the case of ν_μ induced reaction $\bar{\nu}_\mu p \to \mu^+ \bar{K}^0 n$ (Fig. 2.20) we find that the CT term peaks $\sim 25\%$ higher than the results obtained using the full model. While πP contribution in this case is even stronger. However, the s-channel mechanism with Λ as an intermediate state is smaller than the full model in the peak region of kaon energy. We may also notice that the shape of the distribution for $\bar{\nu}_\mu p \to \mu^+ \bar{K}^0 n$ process is relatively broader in nature as compared to the other two channels.

In Figs. 2.21-2.23, we have presented the results for Q^2 distribution i.e. $d\sigma/dQ^2$ vs Q^2 at $E_{\bar{\nu}} = 1.5$GeV. We find the Q^2 distribution to be sharply peaked at low Q^2. The contribution from the different terms of the hadronic current to the total Q^2 distribution is slightly of different nature as compared to these contributions in the case of kaon energy distribution. This difference is mainly driven by the CT term and s-channel mechanism. Both of which are sharply peaked unlike their E_k distributions. For example, in the case of $\bar{\nu}_\mu n \to \mu^+ K^- n$ the peak of CT term is about 12% higher than the full model, unlike in the case of $d\sigma/dE_k$ where it is slightly lower in the peak region. However, the shape of both the distributions are different which otherwise give the same cross section. The other important contributions come from πP and resonance mechanism. While in the case of $\bar{\nu}_\mu p \to \mu^+ K^- p$ the

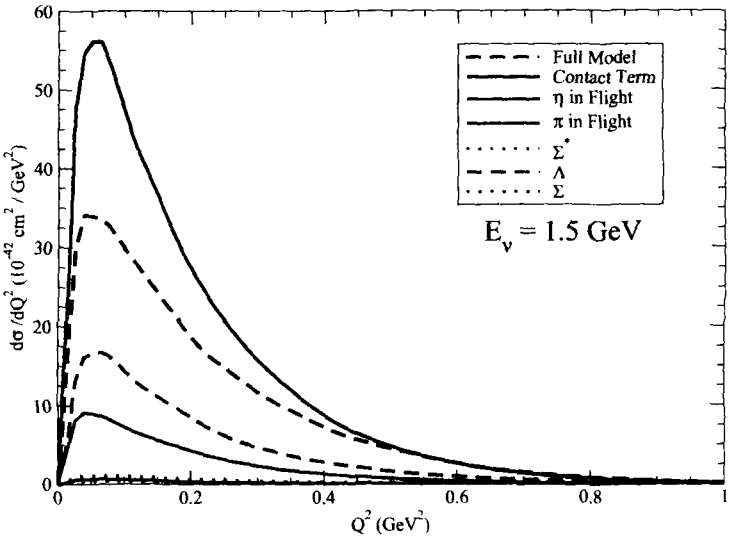

Figure 2.22: Contribution of the different terms to the Q^2 distribution ($\frac{d\sigma}{dQ^2}$) at $E_\nu = 1.5GeV$ for $\bar{\nu}_\mu p \to \mu^+ K^- p$ process.

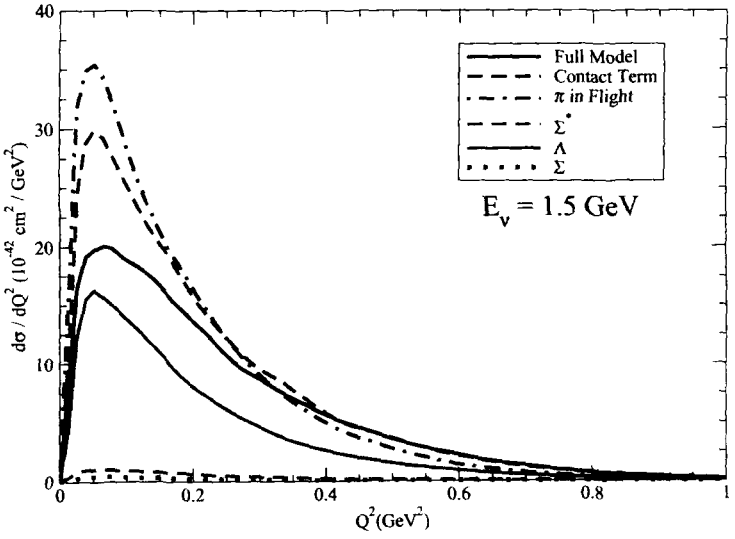

Figure 2.23: Contribution of the different terms to the Q^2 distribution ($\frac{d\sigma}{dQ^2}$) at $E_\nu = 1.5GeV$ for $\bar{\nu}_\mu p \to \mu^+ \bar{K}^0 n$ process.

CT term is about 55% higher in the peak region in compare to the full model. This also suggests that the contribution from other diagrams comes with opposite sign which tend to reduce the cross section. In Fig. 2.23, we have presented the Q^2 distribution for $\bar{\nu}_\mu p \to \mu^+ \bar{K}^0 n$ channel. We find that the pion exchange term comes out to be most dominant one followed by the CT term. While the s-channel Λ is very close to the full model and the shape of the distribution is largely determined by it.

Thus we find that the study of single kaon production induced by $\nu_\mu/\bar{\nu}_\mu$ is important in the energy region of $\sim$ 1 GeV. These studies would be relevant for the precise measurement of ν-oscillation parameters as well as to the background study of nucleon decay searches.

In the next chapter we shall present the formalism and results for the electron/positron induced single kaon production based on the formalism discussed in the present chapter.

Chapter 3

Charged Lepton Induced One Kaon Production

3.1 Introduction

With the development of accelerators like MAMI, JLAB, LNS, ELSA, SPring-8, GRAAL, etc. [62, 63, 64, 65, 66, 67, 68, 69, 70, 71, 72], the importance of the study of kaon production induced by real and virtual photons on nucleons and nuclei has been laid. In particular, the availability of very high luminosity beams has provided the opportunity to study the electromagnetic associated strangeness production [73, 74, 75, 76, 77, 78, 79, 80, 81, 82, 83] of a strange and an anti-strange particle.

The cross section for weak associated strangeness production is obviously much smaller than that of the electromagnetic ones. However, weak interaction allows for processes where only one strange/anti-strange particle is produced, ($\Delta S = \pm 1$) and these reactions could have a substantially lower threshold. For instance, the threshold for electron induced weak K^- production on a proton is around 600 MeV whereas it is 1.5 GeV for electromagnetic production, as an additional kaon is required.

The study of these reactions could provide valuable information on the coupling constants D and F that govern the interaction of the $SU(3)$ lightest baryon octet with the pseudoscalar mesons and also their β decays. More specifically, the $g_A(= D + F)$ combination, related to the neutron β decay, is very well known, but the knowledge of the D and F values are less precise [93]. Also, one may investigate the Q^2 dependence of the weak axial form factors of nucleons and hyperons. Here we explore the possibility of doing such experiments and present a quantitative anal-

ysis of the charged current reaction in which a kaon/antikaon is produced without conserving ΔS. This study is based on the formalism which we have discussed in Chapter-2 and here it has been extended for single kaon production off the nucleon obtained from electron as well as positron beams.

We proceed by introducing the formalism in brief in Sec. 3.2. Results and discussions are presented in Sec. 3.3.

3.2 Formalism

The processes considered here are the charged lepton induced weak $|\Delta S| = 1$, $K(\bar{K})$ production. The single antikaon production channels induced by electrons are

$$\begin{aligned} e^- + n &\rightarrow \nu_e + K^- + n \\ e^- + p &\rightarrow \nu_e + \bar{K^0} + n \\ e^- + p &\rightarrow \nu_e + K^- + p, \end{aligned} \tag{3.1}$$

and the corresponding positron induced channels are

$$\begin{aligned} e^+ + n &\rightarrow \bar{\nu}_e + K^+ + n \\ e^+ + n &\rightarrow \bar{\nu}_e + K^0 + p \\ e^+ + p &\rightarrow \bar{\nu}_e + K^+ + p \end{aligned} \tag{3.2}$$

The expression for the differential cross section in the laboratory frame for the above processes is given by

$$d^9\sigma = \frac{1}{4ME_e(2\pi)^5}\frac{d\vec{k'}}{(2E_\nu)}\frac{d\vec{p'}}{(2E'_p)}\frac{d\vec{p_k}}{(2E_k)}\delta^4(k+p-k'-p'-p_k)\bar{\Sigma}\Sigma|\mathcal{M}|^2, \tag{3.3}$$

where $k(k')$ is the momentum of the incoming(outgoing) lepton with energy $E_e(E_\nu)$, $p(p')$ is the momentum of the incoming(outgoing) nucleon with mass M. The kaon 3-momentum is $\vec{p_k}$ having energy E_k, $\bar{\Sigma}\Sigma|\mathcal{M}|^2$ is the square of the transition amplitude averaged(summed) over the spins of the initial(final) state. The transition amplitude may be written as

$$\mathcal{M} = \frac{G_F}{\sqrt{2}} j_\mu J^\mu = \frac{g}{2\sqrt{2}} j_\mu \frac{1}{M_W^2} \frac{g}{2\sqrt{2}} J^\mu, \tag{3.4}$$

where j_μ and J^μ are the leptonic and hadronic currents respectively, $G_F = \sqrt{2}\frac{g^2}{8M_W^2}$ is the Fermi coupling constant, g is the gauge coupling and M_W is the mass of the W-boson.

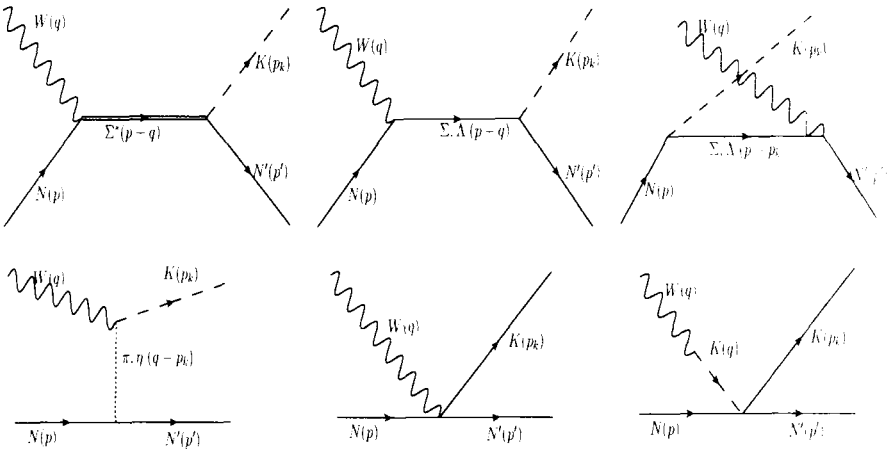

Figure 3.1: Feynman diagrams for the processes $e^- N \to \nu_e N' \bar{K}$ and $e^+ N \to \nu_e N' K$. Here $\bar{K}$ stands for a K^- or $\bar{K}^0$ obtained in an electron induced process and K stands for K^+ or K^0 obtained in a positron induced process. First row from left to right: s-channel Σ^* resonance term (labeled SCR in the text) , s-channel (SC) and u-channel (UC) Σ, Λ propagator; second row: Pion/Eta meson ($\pi P/\eta P$) exchange terms, Contact term (CT) and finally kaon pole term (KP).

First, we shall discuss the leptonic current, the hadronic current and the transition amplitude corresponding to the reactions shown in Eq. 3.1. The leptonic current is obtained from the Standard Model Lagrangian coupling of the W-boson to the leptons

$$\begin{aligned} \mathcal{L} &= -\frac{g}{2\sqrt{2}} \left[W_\mu^- \bar{l} \gamma^\mu (1-\gamma_5) \nu_l + W_\mu^+ \bar{\nu}_l \gamma^\mu (1-\gamma_5) l \right] \\ &= -\frac{g}{2\sqrt{2}} \left[j_{(L)}^\mu W_\mu^- + \text{h.c.} \right]. \end{aligned} \tag{3.5}$$

The Feynman diagrams that contribute to the hadronic current are depicted in Fig. 3.1. There is a meson (πP,ηP) exchange term, a contact term (CT) and a kaon pole (KP) term. For the electron induced reactions we also have the s-channel diagrams with Σ, Λ(SC) and Σ^*(SCR) as intermediate states. In the case of positron induced reactions the s-channel diagrams (SC and SCR) do not contribute, but we must include the u-channel (UC) one. The contributions to the hadronic current coming from different terms are written using the Lagrangian obtained from chiral perturbation theory(χPT).

We have also included the contribution of terms with $\Sigma^*(1385)$ resonance belonging to the SU(3) baryon decuplet, which is near the threshold of the NK system. This is suggested by the dominant role played by the $\Delta(1232)$ resonance in pion production reactions. For the weak excitation of the $\Sigma^*(1385)$ resonance and its subsequent decay in NK, the lowest order SU(3) Lagrangian coupling the pseudoscalar mesons with decuplet-octet baryons in presence of external weak current is given by:

$$\mathcal{L}_{dec} = \mathcal{C}\left(\epsilon^{abc}\bar{T}^{\mu}_{ade}u^{d}_{\mu,b}B^{e}_{c} + h.c.\right), \tag{3.6}$$

where T^{μ} is the SU(3) representation of the decuplet fields, $\mathcal{C}$ is a parameter which is fixed by fitting the $\Delta(1232)$ decay width and $a - e$ are flavor indices.

The spin 3/2 propagator for Σ^* is given by

$$G^{\mu\nu}(P) = \frac{P^{\mu\nu}_{RS}(P)}{P^2 - M^2_{\Sigma^*} + iM_{\Sigma^*}\Gamma_{\Sigma^*}}, \tag{3.7}$$

where $P = p + q$ is the momentum carried by the resonance, $q = k - k'$ and $P^{\mu\nu}_{RS}$ is the projection operator

$$\begin{aligned} P^{\mu\nu}_{RS}(P) &= \sum_{spins} \psi^{\mu}\bar{\psi}^{\nu} \\ &= -(\not{P} + M_{\Sigma^*})\left[g^{\mu\nu} - \frac{1}{3}\gamma^{\mu}\gamma^{\nu} - \frac{2}{3}\frac{P^{\mu}P^{\nu}}{M^2_{\Sigma^*}} + \frac{1}{3}\frac{P^{\mu}\gamma^{\nu} - P^{\nu}\gamma^{\mu}}{M_{\Sigma^*}}\right], \end{aligned} \tag{3.8}$$

with M_{Σ^*} the resonance mass and ψ^{μ} the Rarita-Schwinger spinor. The Σ^* width obtained using the Lagrangian of Eq. 3.6 may be written as

$$\Gamma_{\Sigma^*} = \Gamma_{\Sigma^*\to\Lambda\pi} + \Gamma_{\Sigma^*\to\Sigma\pi} + \Gamma_{\Sigma^*\to N\bar{K}}\ , \tag{3.9}$$

where

$$\begin{aligned} \Gamma_{\Sigma^*\to Y,\phi} &= \frac{C_Y}{192\pi}\left(\frac{\mathcal{C}}{f_{\pi}}\right)^2 \frac{(W + M_Y)^2 - m^2}{W^5}\lambda^{3/2}(W^2, M^2_Y, m^2) \\ &\quad \times \Theta(W - M_Y - m). \end{aligned} \tag{3.10}$$

Here, m, M_Y are the masses of the emitted meson(ϕ) and baryon. $\lambda(x, y, z) = (x - y - z)^2 - 4yz$ and Θ is the unit step function. The factor C_Y is 1 for Λ and $\frac{2}{3}$ for N and Σ.

Using symmetry arguments, the most general $W^- N \to \Sigma^*$ vertex may be written in terms of a vector and an axial-vector part as,

$$\begin{aligned} \langle \Sigma^*; P = p + q \,|V^\mu|N; p\rangle &= V_{us}\bar{\psi}_\alpha(\vec{P})\Gamma_V^{\alpha\mu}(p,q)\,u(\vec{p}), \\ \langle \Sigma^*; P = p + q \,|A^\mu|N; p\rangle &= V_{us}\bar{\psi}_\alpha(\vec{P})\Gamma_A^{\alpha\mu}(p,q)\,u(\vec{p}), \end{aligned} \tag{3.11}$$

where

$$\begin{aligned} \Gamma_V^{\alpha\mu}(p,q) &= \left[\frac{C_3^V}{M}(g^{\alpha\mu}\not{q} - q^\alpha\gamma^\mu) + \frac{C_4^V}{M^2}(g^{\alpha\mu}q\cdot P - q^\alpha P^\mu)\right. \\ &\quad \left. + \frac{C_5^V}{M^2}(g^{\alpha\mu}q\cdot p - q^\alpha p^\mu) + C_6^V g^{\mu\alpha}\right]\gamma_5 \\ \Gamma_A^{\alpha\mu}(p,q) &= \left[\frac{C_3^A}{M}(g^{\alpha\mu}\not{q} - q^\alpha\gamma^\mu) + \frac{C_4^A}{M^2}(g^{\alpha\mu}q\cdot P - q^\alpha P^\mu)\right. \\ &\quad \left. + C_5^A g^{\alpha\mu} + \frac{C_6^A}{M^2}q^\mu q^\alpha\right]. \end{aligned} \tag{3.12}$$

The details of the C_i N-Σ^* transition form factors are given in Ref. [121, 128]. For all background terms, we adopt a global dipole form factor $F(q^2) = 1/(1-q^2/M_F^2)^2$, with a mass $M_F \simeq 1.05$ GeV that multiplies the hadronic currents. Its effect for energies of electron presently available at the accelerators will be discussed.

Process	B_{CT}	A_{CT}	A_Σ	A_Λ	$A_{Cr\Sigma}$	$A_{Cr\Lambda}$	A_{KP}	A_π	A_η	$A_{\Sigma'}$
$e^- n \to \nu K^- n$	D-F	1	-1	0	0	0	-1	1	1	2
$e^- p \to \nu K^- p$	-F	2	$-\frac{1}{2}$	1	0	0	-2	-1	1	1
$e^- p \to \nu \bar{K}^0 n$	-D-F	1	$\frac{1}{2}$	1	0	0	-1	-2	0	-1
$e^+ n \to \bar{\nu} K^+ n$	D-F	-1	0	0	-1	0	-1	-1	-1	0
$e^+ p \to \bar{\nu} K^+ p$	-F	-2	0	0	$-\frac{1}{2}$	1	-2	1	-1	0
$e^+ n \to \bar{\nu} K^0 n$	-D-F	-1	0	0	$\frac{1}{2}$	1	-1	2	0	0

Table 3.1: Constant factors appearing in the hadronic current

The final expressions of the hadronic currents j^μ for the electron as well as

positron induced processes are obtained using the present formalism as

$$
\begin{aligned}
J^{\mu}|_{CT} &= iA_{CT}V_{us}\frac{\sqrt{2}}{2f_{\pi}}\bar{N}(p')\,(\gamma^{\mu}+B_{CT}\,\gamma^{\mu}\gamma_5)\,N(p)\\
j^{\mu}\big|_{Cr\Sigma} &= iA_{Cr\Sigma}V_{us}\frac{\sqrt{2}}{2f_{\pi}}\bar{N}(p')\left(\gamma^{\mu}+i\frac{\mu_p+2\mu_n}{2M}\sigma^{\mu\nu}q_{\nu}+(D-F)(\gamma^{\mu}-\frac{q^{\mu}}{q^2-M_k^2}\not{q})\gamma^5\right)\\
&\quad\times\frac{\not{p}-\not{p}_k+M_{\Sigma}}{(p-p_k)^2-M_{\Sigma}^2}\not{p}_k\gamma^5N(p),\\
j^{\mu}\big|_{Cr\Lambda} &= iA_{Cr\Lambda}V_{us}\frac{\sqrt{2}}{4f_{\pi}}\bar{N}(p')\left(\gamma^{\mu}+i\frac{\mu_p}{2M}\sigma^{\mu\nu}q_{\nu}-\frac{D+3F}{3}(\gamma^{\mu}-\frac{q^{\mu}}{q^2-M_k^2}\not{q})\gamma^5\right)\\
&\quad\times\frac{\not{p}-\not{p}_k+M_{\Lambda}}{(p-p_k)^2-M_{\Lambda}^2}\not{p}_k\gamma^5N(p),\\
J^{\mu}|_{\Sigma} &= iA_{\Sigma}(D-F)V_{us}\frac{\sqrt{2}}{2f_{\pi}}\bar{N}(p')\not{p}_k\gamma_5\frac{\not{p}+\not{q}+M_{\Sigma}}{(p+q)^2-M_{\Sigma}^2}\left(\gamma^{\mu}+i\frac{(\mu_p+2\mu_n)}{2M}\sigma^{\mu\nu}q_{\nu}\right.\\
&+\left.(D-F)\left\{\gamma^{\mu}-\frac{q^{\mu}}{q^2-{M_k}^2}\not{q}\right\}\gamma^5\right)N(p)\\
J^{\mu}|_{\Lambda} &= iA_{\Lambda}V_{us}(D+3F)\frac{1}{2\sqrt{2}f_{\pi}}\bar{N}(p')\not{p}_k\gamma^5\frac{\not{p}+\not{q}+M_{\Lambda}}{(p+q)^2-M_{\Lambda}^2}\left(\gamma^{\mu}+i\frac{\mu_p}{2M}\sigma^{\mu\nu}q_{\nu}\right.\\
&-\left.\frac{(D+3F)}{3}\left\{\gamma^{\mu}-\frac{q^{\mu}}{q^2-{M_k}^2}\not{q}\right\}\gamma^5\right)N(p)\\
J^{\mu}|_{KP} &= iA_{KP}V_{us}\frac{\sqrt{2}}{2f_{\pi}}\bar{N}(p')\not{q}\;N(p)\frac{q^{\mu}}{q^2-M_k^2}\\
J^{\mu}|_{\pi} &= iA_{\pi}\frac{M\sqrt{2}}{2f_{\pi}}V_{us}(D+F)\frac{2{p_k}^{\mu}-q^{\mu}}{(q-p_k)^2-{m_{\pi}}^2}\bar{N}(p')\gamma_5N(p)\\
J^{\mu}|_{\eta} &= iA_{\eta}\frac{M\sqrt{2}}{2f_{\pi}}V_{us}(D-3F)\frac{2{p_k}^{\mu}-q^{\mu}}{(q-p_k)^2-{m_{\eta}}^2}\bar{N}(p')\gamma_5N(p)\\
J^{\mu}|_{\Sigma^*} &= -iA_{\Sigma^*}\frac{\mathcal{C}}{f_{\pi}}\frac{1}{\sqrt{6}}\,V_{us}\,\frac{p_k^{\lambda}}{P^2-M_{\Sigma^*}^2+i\Gamma_{\Sigma^*}M_{\Sigma^*}}\\
&\quad\times\bar{N}(p')\,P_{RS_{\lambda\rho}}(\Gamma_V^{\rho\mu}+\Gamma_A^{\rho\mu})\,N(p)
\end{aligned}
\tag{3.13}
$$

In $\Gamma_V^{\rho\mu}+\Gamma_A^{\rho\mu}$, the form factors are taken as for the Δ^+. $A_i(i=CT,Cr\Sigma,etc.)$ are constants which are tabulated in Table 3.1.

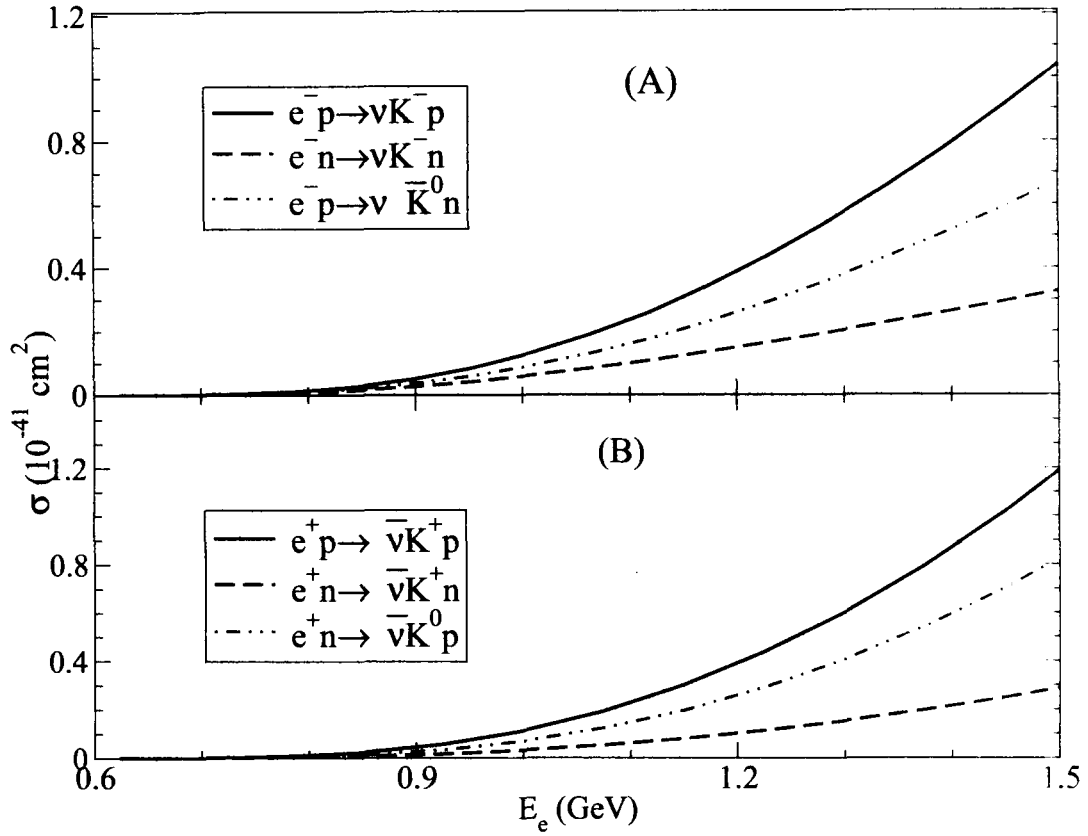

Figure 3.2: Cross section σ vs electron(positron) energy E_e for the $\bar{K}(K)$ production

3.3 Results and Discussion

The total scattering cross section σ has been obtained by integrating over the kinematical variables of Eq. 3.3 and using Eqs. 3.4-3.13. Firstly, we present in Fig. 3.2 the results for the total scattering cross section σ for the reactions given in Eqs. 3.1 and 3.2.

We find that $e^-(e^+) + p \to \nu_e(\bar{\nu}_e) + K^-(K^+) + p$ has the largest cross section followed by $e^-(e^+) + p(n) \to \nu_e(\bar{\nu}_e) + \bar{K}^0(K^0) + n(p)$ and $e^-(e^+) + n \to \nu_e(\bar{\nu}_e) + K^-(K^+) + n$. Furthermore, we find that the cross sections for the positron induced processes are larger than for the corresponding electron induced processes. This is basically due to the different interference between the s-channel and contact terms, as can be seen in Fig. 3.3, where we explicitly show the contribution of the individual

terms of the hadronic current for the two channels[1].

We find that the contribution of the contact term is the largest followed by the mechanism with a Λ in the intermediate state, the π pole term, etc. The contribution due to the Σ^* in cross section for the discussed energies is quite small, for example it is around 10% at E_e =1 GeV and 5% at E_e =1.5 GeV of the total cross section. Therefore, these reactions are not suitable to learn about the $\Sigma^*(1385)$ resonance properties. The contributions of Λ intermediate states both in UC and SC are larger than those corresponding to the Σ hyperon, which can be easily understood by the corresponding Clebsch-Gordan coefficients. Similar is the trend for the other channels not shown in the figure.

Given the smallness of the resulting cross sections, it is important to consider the feasibility of their experimental measurement. Here, we will only discuss electron processes. Let us remark that at energies below 1.5 GeV and in electron induced reactions, the presence of an antikaon in the final state fully defines the process, in the sense that it is necessarily a charge exchange weak production process and there is no other additional strange particle in the final state[2]. This is so because of the higher energy threshold of any other mechanism that could produce antikaons. Therefore, there is no need to measure other particles in coincidence.

To estimate the number of events for single kaon production we have considered a luminosity of $5 \times 10^{37} s^{-1}$ cm^{-2} for MAMI, that corresponds to a 10 cm liquid hydrogen target at an electron beam current of 20 μA as described in Ref.[129]. For TJNAF, we take a luminosity of $5 \times 10^{38} s^{-1}$ cm^{-2} that corresponds to a current of 100 μA and a larger liquid hydrogen target [130] that has been used on the measurement of parity violating electron proton scattering. Under these conditions and for 1.5 GeV electrons, we would have some 480 events per day for the reaction $e^- + p \to \nu_e + K^- + p$ at TJNAF (48 at MAMI). For $e^- + p \to \nu_e + \bar{K}^0 + n$ reaction, we would get 320 events per day at TJNAF (32 at MAMI). Certainly, the numbers could be changed by using different targets and/or current but equally important is the efficiency in the kaon detection, that depends on the kaon kinematics and the detector.

The kaon angle and momentum distributions for the electron induced processes are shown in Figs. 3.4 and 3.5 at an electron energy of E_e = 1.5 GeV, that could be appropriate for both the TJNAF and MAMI facilities. As shown in Fig. 3.4, the three channels under study are forward peaked, specially for the $\bar{K}^0$ production. The

[1]Certainly, these individual contributions are not observable and they are shown here to help explaining the sensitivity of the physical processes to the various parameters.

[2]Processes with additional particles, such as a pion, are also expected to be much smaller because of their phase space.

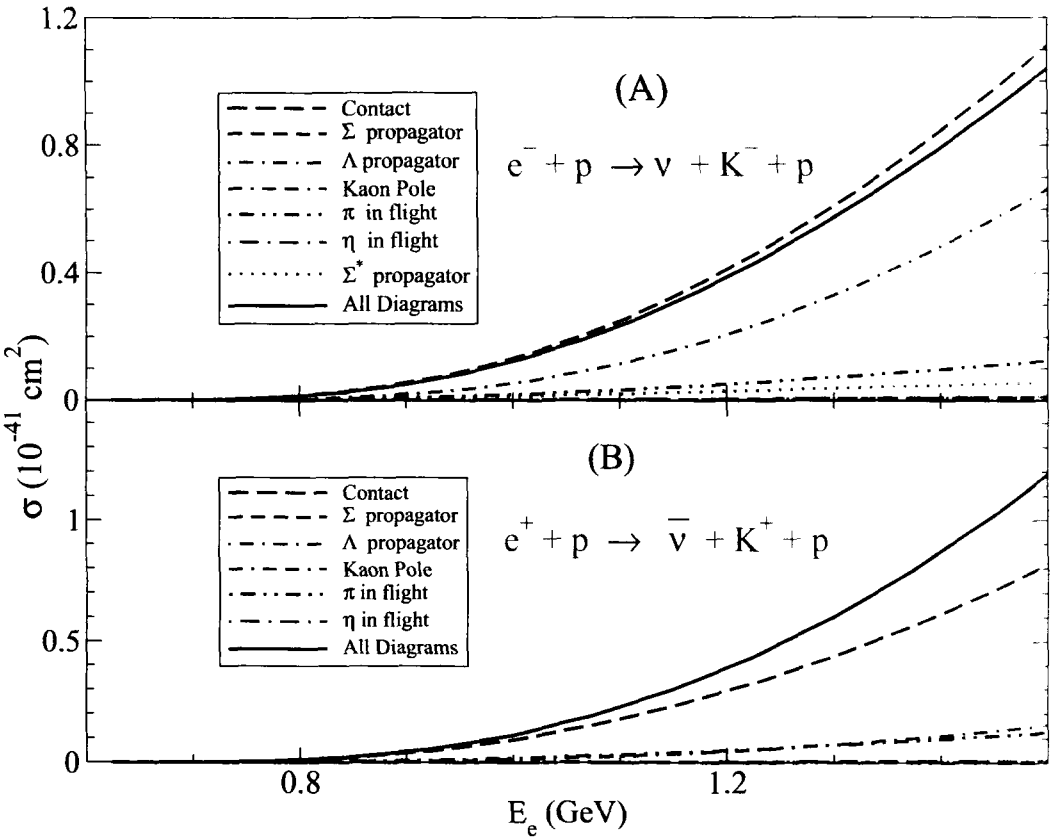

Figure 3.3: Contribution of the different terms to the total cross section σ vs electron(positron) energy E_e for the $\bar{K}(K)$ production

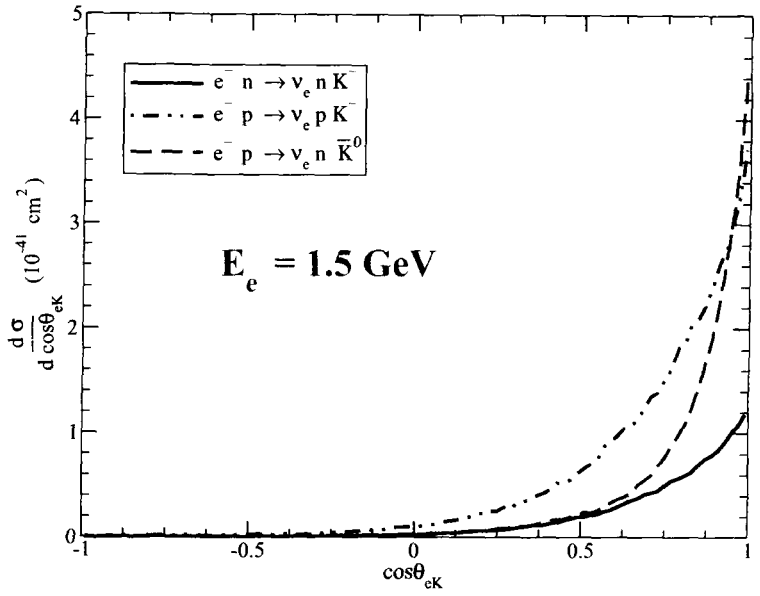

Figure 3.4: Kaon angle distributions at electron energy $E_e = 1.5$ GeV

momentum distributions peak around 0.3 GeV for $e^- n \to \nu_e K^- n$, and $e^- p \to \nu_e K^- p$ while for $e^- p \to \nu_e \bar{K}^0 n$ it peaks around 0.6 GeV. This is because the contact term, which has dominant contribution for K^- production channels, peaks at low p_k. For $\bar{K}^0$ production, there is a significant contribution from s-channel Λ term, which flattens for a wide range of p_k. Its interference with the contact term shifts the peak for the kaon momentum distribution.

As an example, we have applied in our calculation some cuts corresponding to the KAOS spectrometer at MAMI. Following Ref. [62], the kaon momentum has been restricted to the range $400 - 700\ MeV/c$ and the kaon angle to the range $21 - 43°$. For electron energies of 1.5 GeV, these cuts would reduce the signal by a factor ≈ 6. Moreover, taking into account the kaons survival probability in KAOS [63] would further reduce the number of events by a similar factor. Thus, the measurement of these cross section at currently existing facilities, with their luminosities and detectors would require quite long runs.

We have also investigated how the Q^2 dependence of the weak form factors would affect our predictions. As mentioned above, very little is known about this dependence given that the existing experimental information comes from beta decay that occurs for very low Q^2 values. In this calculation, we are assuming a simple dipole dependence and the same form factor for all background channels. Thus,

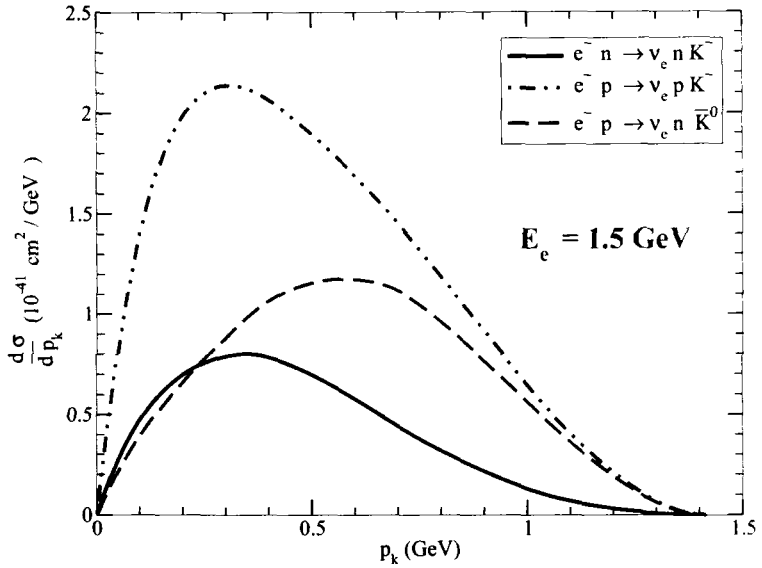

Figure 3.5: Kaon momentum distributions at electron energy $E_e = 1.5$ GeV

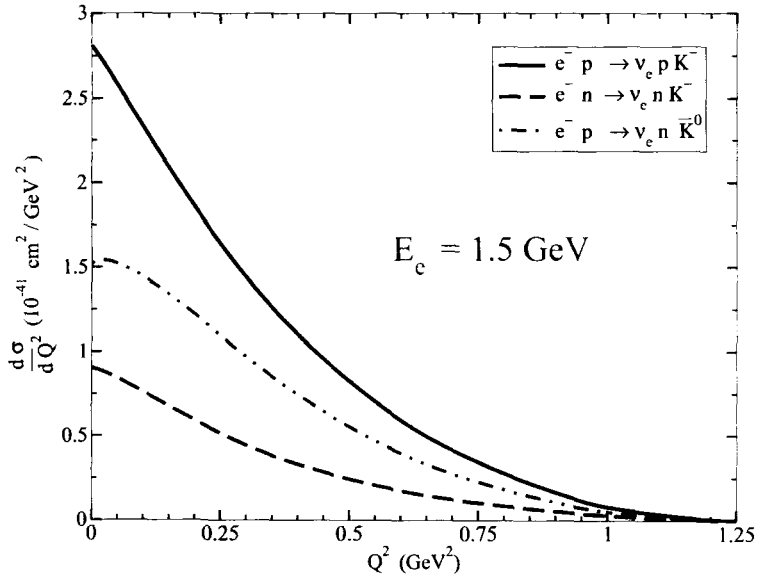

Figure 3.6: Q^2 distribution at electron energy $E_e = 1.5$ GeV

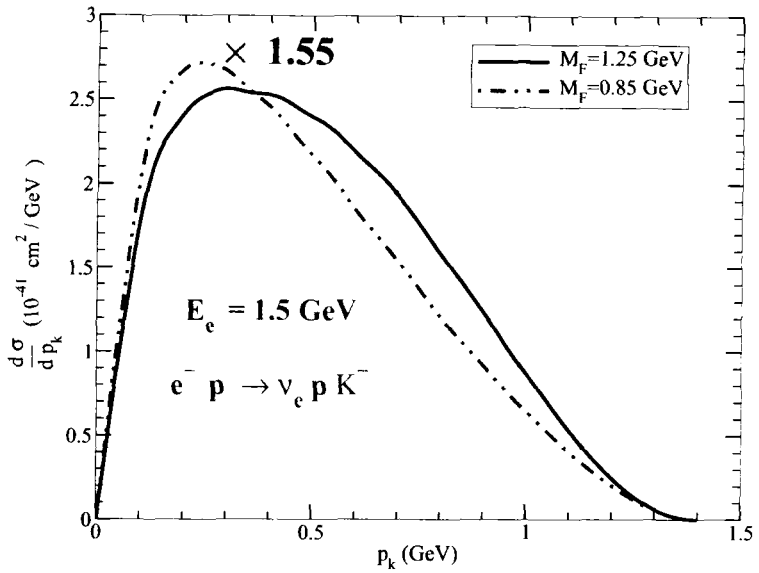

Figure 3.7: Kaon momentum distribution at electron energy $E_e = 1.5$ GeV for the $e^- + p \rightarrow \nu_e(\bar{\nu}_e) + K^- + p$ channel for a dipole mass $M_F = 1.25$ and $M_F = 0.85$ GeV. The second curve ($M_F = 0.85$ GeV) has been scaled to get the same area.

we can only obtain some idea on the uncertainty/sensitivity of our results to the form factors. As can be seen in Fig. 3.6, the processes have a small contribution from large Q^2 values. Thus the size of the cross section depends moderately on the form factors. For instance, by changing the dipole mass($M_F = 1.05$ GeV), a 20% up/down, one gets changes of about 10% for the neutron channel and about 28% for the two proton channels at $E_e = 1.5$ GeV. We have also studied the sensitivity of the electron induced cross sections to the D and F parameters, that govern the hyperon beta decays. For that, we have modified the D value by a 5% while keeping g_A(=D + F)=1.26 constant. Our results show cross sections that grow around 5% for the proton processes and decrease by a similar factor for the neutron case. This implies that some ratios, such as $\sigma_{\bar{K}^0}/\sigma_{K^-}$ on deuteron could be a sensitive probe for these parameters.

The measurement of the Q^2 dependence would require the detection of the final nucleon in addition to the kaon. However, also some purely kaonic observables show some sensitivity to the form factors. For instance, Fig. 3.7 shows how a larger dipole mass pushes the kaon momentum towards larger values.

Thus, the study performed here predict cross sections that, although small, could

be measured at current experimental facilities. Furthermore, our results could facilitate the study of the hyperon/nucleon weak coupling constants and their form factors.

In the next chapter, we present the formalism for photon and neutrino induced η particle production process.

Chapter 4

η Production

4.1 Introduction

Efforts are being made both theoretically as well as experimentally to study eta production induced by virtual as well as real photons from nucleons and nuclei [131, 132, 133]. For example the studies performed at ELSA in Bonn, MAMI in Mainz have revealed properties associated with eta meson [133, 134, 135]. Recently results have been reported from Mainz Microtron(MAMI-C) [136] using Crystal Ball and TAPS multiphoton spectrometer in the energy range of 707MeV to 1.4GeV for the differential as well as total scattering cross section. Photoproduction of eta meson off the nucleon, $\gamma+N \rightarrow \eta+N$, provides a useful and an alternative tool to study nucleon resonances besides the other processes through which one gets information like πN scattering and pion photoproduction processes. Since ηN couples only to nucleon resonances with isospin I = $\frac{1}{2}$, therefore, these processes are comparatively more cleaner and selective to distinguish other resonances in comparison to other sources those are being used. Due to this property, η production, provides an opportunity to access to less explored nucleon resonances, like the resonances of higher mass about which little information is available. Recently, eta photoproduction experiments have proven a useful tool in the search for narrow nucleon resonances like the $N^*(1685)$ resonance [137]. As the lifetime of η meson is very short, therefore, it can not be detected directly and is reconstructed from its decay products.

The neutrino/antineutrino-induced eta production is interesting because of several reasons, e.g. η is one of the important probes to search for the strange quark content of the nucleons [58], also a precise determination of η production cross section would help in subtracting the background in proton decay searches, etc. In

some supersymmetric grand unified theories, η mesons provide a prominent signal for proton decay [59]. Therefore, its background contribution due to atmospheric neutrino interactions should be well estimated. Furthermore, η production channel is expected to be dominated by $N^*(1535)$ resonance excitation like in the case of electromagnetic processes, and this state sits near the threshold of the $N\eta$ system and hence has large branching ratio and thus a precise measurements of the cross section will also allow to determine the axial properties of this resonance. Moreover, a second class (via pion pole) η production mechanism that could compete with resonance production in certain kinematic conditions has been singled out [60]. Finally, theoretical models like the present one allow to improve the Monte Carlo simulations which are being used to analyze neutrino oscillation experiments.

In spite of the efforts being made to understand ηN interaction little progress has been made in comparison to πN interaction. Unlike the case of pion scattering and pion photoproduction where πNN coupling is preferred to be pseudovector (PV), in the case of ηNN coupling one takes either a pseudoscalar(PS) coupling as preferred by Breitmoser et al. [138] or Kirchbach et al. [139], or a PV coupling. For a PS coupling, the coupling constant $g^2_{\eta NN}/4\pi$ varies between 0 and 7 with the large couplings arising from fits of one boson exchange potentials [140]. However, in our formalism which is based on chiral approach pseudovector coupling is preferred.

Like the Δ dominance in the pion production process, η production is dominated by $S_{11}(1535)$ resonance. In the numerical calculations we have considered $S_{11}(1535)$ and $S_{11}(1650)$ resonances as well as contribution from Born diagrams. We have not found in literature any (experimental or theoretical) study that gives the differential or total scattering cross sections for η production off the nucleon using neutrino or antineutrino beams. However, we must point out that Dombey [60] has studied weak η production but no numerical results are presented. Therefore, our present study would be quite useful in estimating the event rates coming from eta meson production in the neutrino oscillation experiments being performed to determine precisely the oscillation parameters.

We have studied photon induced eta production to first fix the electromagnetic form factors by comparing it with the available results for scattering cross section from Crystal Ball experiment [136] and use them to obtain the isovector form factors for $\nu/\bar{\nu}$ induced processes off the nucleon. Born terms are calculated using a microscopical model based on the $SU(3)$ chiral Lagrangian. The basic parameters of the model are f_π, the pion decay constant, Cabibbo angle, the proton and neutron magnetic moments and the axial vector coupling constants for the baryon octet, D and F, that are obtained from the analysis of the semileptonic decays of neutron and hyperons. We consider $N^*(1535)$ as well as $N^*(1650)$ S_{11} resonant intermediate

states. The vector form factors of the N-S_{11} transition have been obtained from the helicity amplitudes extracted in the analysis of world pion photo- and electroproduction data using the unitary isobar model [140]. The properties of the axial N-S_{11} transition current are basically unknown but assuming the pion-pole dominance of the pseudoscalar form factor, together with PCAC one can fix the axial coupling using the empirical $N^* \to N\pi$ partial decay width. We make an educated guess for the dependence on the 4-momentum square transferred by the neutrino, which ultimately remains to be determined experimentally.

In the Sec. 4.2, we briefly discuss the formalism for the photoproduction of eta meson and for the charged current neutrino/antineutrino induced η production off the nucleon. Finally, we present and discuss our results in Sec. 4.3.

4.2 Formalism

4.2.1 Photoproduction of η

The reaction for the η production induced by real photon is,

$$\gamma(q) + N(p) \to \eta(p_\eta) + N(p') \tag{4.1}$$

for which the differential scattering cross section in lab frame is given by,

$$d\sigma = (2\pi)^4 \delta^4(p_\eta + p' - q - p) \frac{1}{4q_0 M} \frac{d^3p_n}{(2\pi)^3 2E_\eta} \frac{d^3p'}{(2\pi)^3 2E'} \overline{\sum} |\mathcal{M}_r^{(s)}|^2, \tag{4.2}$$

where p & p' are four momenta for initial and final nucleon. The photon 4-momentum is denoted by q, while the 4-momentum for η meson is p_η. The transition amplitude is $\mathcal{M}_r^{(s)}$, the square of which may be written as:

$$|\mathcal{M}_r^{(s)}|^2 = e^2 \epsilon_\mu^{*(s)} \epsilon_\nu^{(s)} H^{\mu\nu} \tag{4.3}$$

where e is the electromagnetic gauge coupling(or simply the electric charge) and $\epsilon_\nu^{(s)}$ and its conjugate $\epsilon_\mu^{*(s)}$ are the photon polarization vectors with the superscript 's' representing its polarization state. If the photon polarization is unknown then the summation over all polarization states are performed, which results,

$$\overline{\sum}_{s=\pm 1} \epsilon_\mu^{*(s)} \epsilon_\nu^{(s)} \longrightarrow -g_{\mu\nu}. \tag{4.4}$$

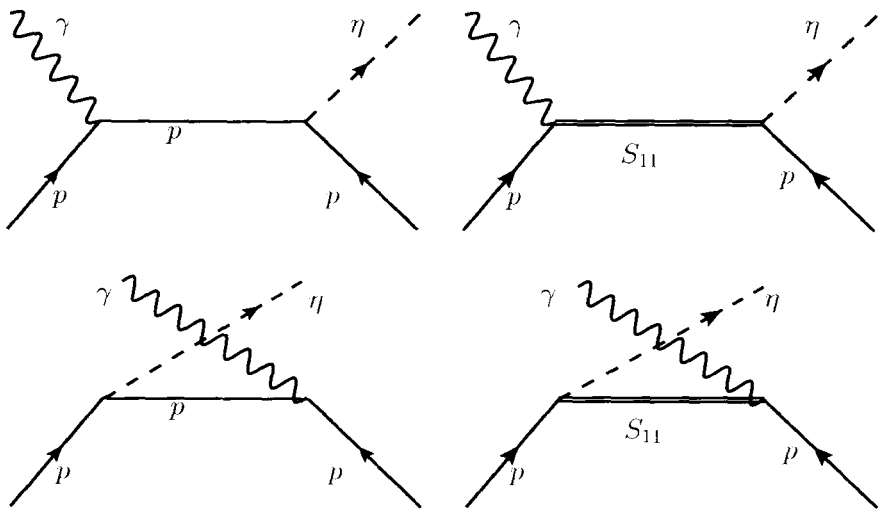

Figure 4.1: Feynman diagrams for the processes $\gamma(q) + p(p) \rightarrow \eta(p_\eta) + p(p')$

Furthermore, if the polarization states of hadrons remain undetected, the averaging(summation) over the initial(final) spins reduces to:

$$\overline{\sum}|\mathcal{M}_r^{(s)}|^2 = -\frac{1}{4}e^2 g_{\mu\nu} H^{\mu\nu} \tag{4.5}$$

The hadronic tensor $H^{\mu\nu}$ in Eq. 4.3 may be written in terms of hadronic current J^μ as

$$H^{\mu\nu} = \mathrm{Tr}\left[(\not{p} + \mathrm{M})\tilde{\mathrm{J}}^\mu(\not{p}' + \mathrm{M})\mathrm{J}^\nu\right], \qquad \tilde{\mathrm{J}}^\mu = \gamma_0(\mathrm{J}^\mu)^\dagger\gamma_0 \tag{4.6}$$

To get the hadronic current J^μ we used the Feynman diagrams which have been depicted in Fig. 4.1.

For the nonresonant terms we have used the Lagrangian obtained from the chiral perturbation theory(χPT) as discussed in Eqs. 2.15 and 2.19 of Sec.2.1.1. The left(l_μ) and right(l_μ) handed currents for photoproduction process are taken from Eq. 2.17, which are given by

$$l_\mu = r_\mu = -e\hat{Q}\mathcal{A}_\mu \ , \tag{4.7}$$

where $\mathcal{A}_\mu$ is the electromagnetic four-vector potential with '$\hat{Q}$' as the $SU(3)$ quark

charge given by

$$\hat{Q} = \begin{pmatrix} \frac{2}{3} & 0 & 0 \\ 0 & -\frac{1}{3} & 0 \\ 0 & 0 & -\frac{1}{3} \end{pmatrix}. \tag{4.8}$$

Currents corresponding to the nucleon Born terms are obtained using χPT approach as:

$$\begin{aligned} J^{\mu}_{N(s)} &= \frac{D-3F}{2\sqrt{3}f_{\pi}} \bar{u}_N(p') \not{p}_{\eta} \gamma^5 \frac{\not{p} + \not{q} + M}{(p+q)^2 - M^2} \mathcal{O}^{\mu}_N u_N(p) \\ J^{\mu}_{N(u)} &= \frac{D-3F}{2\sqrt{3}f_{\pi}} \bar{u}_N(p') \mathcal{O}^{\mu}_N \frac{\not{p} - \not{p}_{\eta} + M}{(p-p_{\eta})^2 - M^2} \not{p}_{\eta} \gamma^5 u_N(p), \end{aligned} \tag{4.9}$$

where

$$\mathcal{O}^{\mu}_N \equiv f_1^N(q^2)\gamma^{\mu} + f_2^N(q^2) i\sigma^{\mu\rho}\frac{q_{\rho}}{2M} \tag{4.10}$$

For real photons $q^2 = 0$, therefore, one may write the above expression as.

$$\mathcal{O}^{\mu}_N \equiv f_1^N(0)\gamma^{\mu} + f_2^N(0) i\sigma^{\mu\rho}\frac{q_{\rho}}{2M}. \tag{4.11}$$

While in the case of hadronic current corresponding to the S_{11} resonance, $N^*(1535)$ and $N^*(1650)$ the currents are written keeping their odd parities in mind. Therefore, for the resonant terms, we write the s-channel $J^{\mu}_{R(s)}$ and the u-channel $J^{\mu}_{R(u)}$ currents as:

$$\begin{aligned} J^{\mu}_{R(s)} &= i g_{\eta N S_{11}} \bar{u}_{N^*}(p') \not{p}_{\eta} \frac{\not{p} + \not{q} + M_R}{(p+q)^2 - M_R^2 + i\Gamma_R M_R} \mathcal{O}^{\mu}_R u_N(p) \\ J^{\mu}_{R(u)} &= i g_{\eta N S_{11}} \bar{u}_{N^*}(p') \mathcal{O}^{\mu}_R \frac{\not{p} - \not{p}_2 + M_R}{(p-p_{\eta})^2 - M_R^2 + i\Gamma_R M_R} \not{p}_{\eta} u_N(p), \end{aligned} \tag{4.12}$$

where

$$\mathcal{O}^{\mu}_R \equiv \pm \frac{F_2^N(q^2=0)}{2M} i\sigma^{\mu\rho} q_{\rho}\gamma_5 \tag{4.13}$$

The plus sign in $\mathcal{O}^{\mu}_R$ is with s-channel and minus sign is with u-channel diagrams. For the real photons no contribution comes from $F_1^N(0)$ and therefore not mentioned in Eq. 4.13. Here we must point out that the currents in Eqs. 4.12 and 4.13 are written for both the resonances viz. $S_{11}(1535)$ and $S_{11}(1650)$. However, the parameters like the coupling constants $g_{\eta N S_{11}}$, mass of resonance M_R, decay width Γ_R and the form factors $F^N_{1,2}$ are different for both the resonances.

To fix the coupling we follow the same procedure as described in Chapter- 2 for Σ^* resonance in antineutrino induced $K^-/\bar{K}^0$ production. The primary decay channels with their decay fraction for the $N^*(1535)$ resonance are

$$\begin{array}{lll} N^* \to & N\pi & 35-50\% \\ N^* \to & N\eta & (42 \pm 10)\% \\ N^* \to & N\pi\pi & 1-10\%, \end{array} \tag{4.14}$$

and for $N^*(1650)$ are,

$$\begin{array}{lll} N^* \to & N\pi & 50-90\% \\ N^* \to & N\eta & 5-15\% \\ N^* \to & \Lambda K & 3-11\% \\ N^* \to & N\pi\pi & 10-20\% . \end{array} \tag{4.15}$$

By looking at the above branching ratios, we must realize that the decay channels also have large uncertainties.

The couplings for the vertices $\eta NN^*(1535)$ and $\eta NN^*(1650)$ are fixed using the partial decay widths at their on-mass shell. To obtain the partial decay width we start from the Lagrangian

$$\mathcal{L}_{N^*N\pi} = -\frac{g_\pi}{f_\pi}\bar{u}_{N^*}\gamma^\mu(\tau_3\partial_\mu\pi^0 + \sqrt{2}\tau_0\partial_\mu\pi^+ + \sqrt{2}\tau_-\partial_\mu\pi^-)u_N + \text{h.c.} \tag{4.16}$$

where for convenience we have redefined $g_{\phi NS_{11}}$ as $\frac{g_\phi}{f_\pi}$, with $\phi \equiv \pi, \eta$. $\tau_{3,\pm}$ are the Pauli matrices in spherical basis which act on the nucleon states

$$\begin{aligned} \tau_+ |n\rangle &= |p\rangle , & \tau_3 |p\rangle &= |p\rangle , \\ \tau_- |p\rangle &= |n\rangle , & \tau_3 |n\rangle &= -|n\rangle . \end{aligned}$$

For the case of $N^* \to N\eta$ the interaction Lagrangian is given by

$$\mathcal{L}_{N^*N\eta} = -\frac{g_\eta}{f_\pi}\bar{u}_{N^*}\,\gamma^\mu\,\partial_\mu\eta\,u_N + \text{h.c.} \tag{4.17}$$

Now using the general expression for partial decay width

$$d\Gamma_{N^*\to N\Phi} = \frac{1}{2W}\frac{d^3p_N}{2E_N}\frac{d^3p_\Phi}{2E_\Phi}\delta^4(p_{N^*} - p_N - p_\Phi)\overline{\sum}\sum|\mathcal{M}|^2(2\pi)^4 \tag{4.18}$$

along with Eq. 4.17 we obtain the expression for $\Gamma(N^* \to N\phi)$ decay width as

$$\Gamma_{N^*\to N\Phi} = C_\Phi\left(\frac{g_\Phi}{f_\pi}\right)^2\frac{|\vec{p}_{CM}|}{8\pi}\frac{(W^2-M^2)^2 - m_\Phi^2(W^2+M^2-2MM_R)}{W^2} \tag{4.19}$$

where $C_\Phi = 3$ for pion and $C_\Phi = 1$ for eta meson and

$$|\vec{p}_{CM}| = \frac{1}{2W}\sqrt{[W^2-(M+m_\Phi)^2]\ \ [W^2-(M-m_\Phi)^2]}. \tag{4.20}$$

W is the energy at resonance rest frame, which for on-mass shell reduces to the mass of resonance i.e. $W_{\text{on-mass}} = M_R$. Using the expression of partial decay width, we obtain the following values for the different couplings:

S_{11} resonance with positive charge:

$$\begin{aligned} g_\pi^{1650} &= -0.105 \\ g_\eta^{1650} &= -0.088 \\ g_\eta^{1535} &= 0.284 \\ g_\pi^{1535} &= 0.092 \end{aligned}$$

S_{11} resonance with neutral charge:

$$\begin{aligned} g_\pi^{1650} &= 0.131 \\ g_\eta^{1650} &= 0.0868 \\ g_\eta^{1535} &= 0.286 \\ g_\pi^{1535} &= 0.106 \end{aligned} \tag{4.21}$$

The nucleon form factors $f_{1,2}^{N=n,p}$ are determined in terms of the Sachs electric $G_E^{p,n}(q^2)$ and magnetic $G_M^{p,n}(q^2)$ form factors, which for the case of real photon becomes:

$$\begin{aligned} f_1^{p,n}(0) &= G_E^{p,n}(0) \\ f_2^{p,n}(0) &= G_M^{p,n}(0) - G_E^{p,n}(0) \end{aligned} \tag{4.22}$$

with,

$$G_E^p(0) = 1, \qquad G_M^p(0) = (1+\mu_p) \text{ and } \qquad \mathrm{G_M^n}(0) = \mu_\mathrm{n}.$$

We fix the form factors associated with the N^* resonances using the helicity amplitudes, which are given by [141];

$$\begin{aligned} A_{\frac{1}{2}} &= \sqrt{\frac{2\pi\alpha_e}{K_R}}\left\langle N^*, J_Z = \frac{1}{2}\middle|\, \epsilon_\mu^+ J_i^\mu \,\middle| N, J_Z = \frac{-1}{2}\right\rangle \zeta \\ S_{\frac{1}{2}} &= -\sqrt{\frac{2\pi\alpha_e}{K_R}}\frac{|\vec{q}|}{\sqrt{Q^2}}\left\langle N^*, J_Z = \frac{1}{2}\middle|\, \epsilon_\mu^0 J_i^\mu \,\middle| N, J_Z = \frac{-1}{2}\right\rangle \zeta \end{aligned} \tag{4.23}$$

Table 4.1: Parameters fitted using the data from the MAMI Crystal Ball [136] experiment

Resonance→	S11(1535)	S11(1650)
Helicity Amplitude↓	$A_\lambda(0)$ 10^{-3}	$A_\lambda(0)$ 10^{-3}
$A^p_{1/2}(0)$	89.38	53.0
$S^p_{1/2}(0)$	-16.5	−3.5

In the resonance rest frame $K_R = \frac{M_R^2 - M^2}{2M_R}$ and $\epsilon_+^\mu = -\frac{1}{\sqrt{2}}(0, 1, i, 0)$. The parameter ζ is model dependent which is related to the sign of $N^* \to N\pi$, and for the present calculation we have taken $\zeta = 1$. $A_{\frac{1}{2}}$ is generally parameterized as [142]:

$$A^{p,n}_{\frac{1}{2}} = \sqrt{\frac{2\pi\alpha_e}{M}\frac{(M_R + M)^2}{M_R^2 - M^2}}\frac{M_R - M}{2M}F_2^N(0) \tag{4.24}$$

We must point out that as $S_{\frac{1}{2}}$ amplitude comes from the longitudinal component, therefore, it is not relevant for the case of real photons. To fix the helicity amplitude on proton target we used the data from the MAMI Crystal Ball [136].

Once we have fixed the parameters mentioned in Eq. 4.21, the results for the total scattering cross section using Eq. 4.2 for the photon induced processes are obtained. We find that the present results describe qualitatively well the experimental data represented by the MAMI Crystal Ball experiment [136] except at high photon energies as shown in Fig. 4.2. Once we have fixed the electromagnetic form factors and the coupling constant as mentioned in Eq. 4.21, we now proceed to develop the formalism for $\nu/\bar{\nu}$ induced η production off the nucleon and obtain the results for the differential and total scattering cross sections.

4.2.2 Weak Production of η

$\nu/\bar{\nu}-$induced charged current η production processes are,

$$\begin{aligned} \nu_\mu(k) + n(p) &\to \mu^-(k') + \eta(p_\eta) + p(p') \\ \bar{\nu}_\mu(k) + p(p) &\to \mu^+(k') + \eta(p_\eta) + n(p') \end{aligned} \tag{4.25}$$

The quantities in the parenthesis are the four momenta of the particles. The general expression of the differential scattering cross section for the reaction shown in

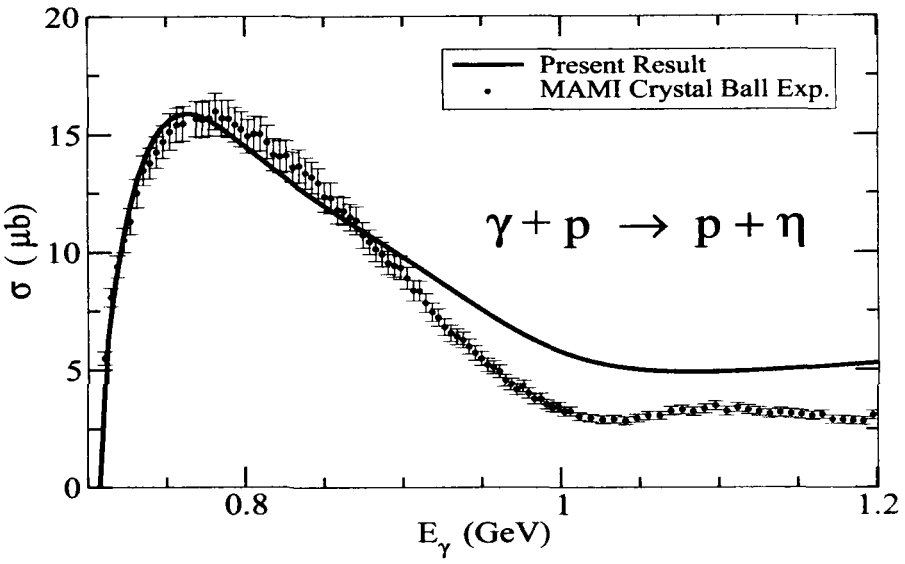

Figure 4.2: Cross section for $\gamma p \to \eta p$ process. The experimental points are obtained from MAMI crystal ball [136] and the results are shown upto the ΛK threshold.

Eq. 4.25 in the laboratory frame is given by,

$$d^9\sigma = \frac{1}{4ME(2\pi)^5}\frac{d\vec{k}'}{(2E_l)}\frac{d\vec{p}'}{(2E'_p)}\frac{d\vec{p}_\eta}{(2E_\eta)}\delta^4(k+p-k'-p'-p_\eta)\bar{\Sigma}\Sigma|\mathcal{M}|^2. \quad (4.26)$$

where the symbols have usual meaning and $|\mathcal{M}|^2$ is square of the transition amplitude written in terms of the leptonic ($L^{\mu\nu}$) and hadronic tensors ($H^{\mu\nu}$) as,

$$\bar{\Sigma}\Sigma|\mathcal{M}|^2 = \frac{1}{2}\frac{G_F^2}{2}L^{\mu\nu} \times H_{\mu\nu}, \quad (4.27)$$

where the factor $\frac{1}{2}$ comes from the spin averaging and G_F is the Fermi coupling constant. The hadronic tensor may be expressed in terms of the amplitudes corresponding to the Feynman diagrams shown in Fig. 4.3.

The standard $V-A$ current is taken for the leptonic part and the hadronic currents are obtained for the Born diagrams (s- and u-channels) with nucleon poles and for the resonant diagrams corresponding to the $S_{11}(1535)$ and $S_{11}(1650)$ resonances. The Feynman diagrams corresponding to the above processes are depicted in Fig. 4.3

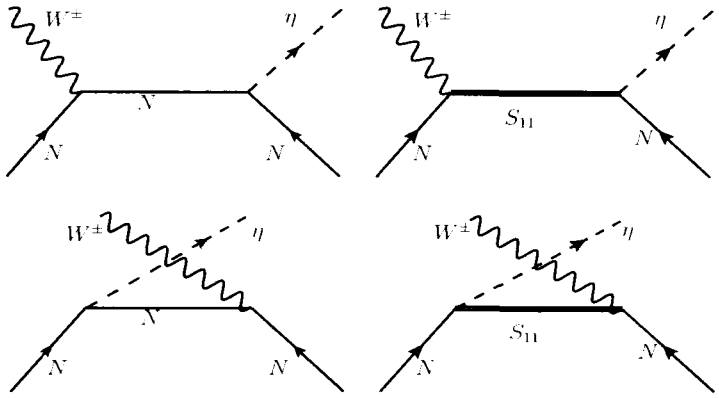

Figure 4.3: Feynman diagrams for the processes $\nu/\bar{\nu}(k)+N(p) \to \mu^{\mp}(k')+\eta(p_\eta)+N'(p')$. First row from left to right: s-channel nucleon pole(SC) and S_{11} resonance(SC N^*); second row: u-channel nucleon pole(UC) and S_{11} resonance (UC N^*).

and the hadronic currents for nonresonant terms using χPT is obtained as,

$$
\begin{aligned}
J^{\mu}_{N(s)} &= \frac{gV_{ud}}{2\sqrt{2}}\frac{D-3F}{2\sqrt{3}f_\pi}\bar{u}_N(p')\not{p}_\eta\gamma^5\frac{\not{p}+\not{q}+M}{(p+q)^2-M^2}\mathcal{O}^{\mu}_N u_N(p) \\
J^{\mu}_{N(u)} &= \frac{gV_{ud}}{2\sqrt{2}}\frac{D-3F}{2\sqrt{3}f_\pi}\bar{u}_N(p')\mathcal{O}^{\mu}_N\frac{\not{p}-\not{p}_\eta+M}{(p-p_\eta)^2-M^2}\not{p}_\eta\gamma^5 u_N(p), \\
&\text{where} \\
\mathcal{O}^{\mu}_N &\equiv f_1^V(q^2)\gamma^\mu + f_2^V(q^2)i\sigma^{\mu\rho}\frac{q_\rho}{2M_N} - f_A(q^2)\gamma^\mu\gamma^5 - f_P(q^2)q^\mu\gamma^5 \qquad (4.28)
\end{aligned}
$$

For the resonant $S_{11}(1535)$ and $S_{11}(1650)$ channels the hadronic currents are given by,

$$
\begin{aligned}
J^{\mu}_{R(s)} &= \frac{gV_{ud}}{2\sqrt{2}}ig_\eta\bar{u}_N(p')\not{p}_\eta\frac{\not{p}+\not{q}+M_R}{(p+q)^2-M_R^2+i\Gamma_R M_R}\mathcal{O}^{\mu}_R u_N(p) \\
J^{\mu}_{R(u)} &= \frac{gV_{ud}}{2\sqrt{2}}ig_\eta\bar{u}_N(p')\mathcal{O}^{\mu}_R\frac{\not{p}-\not{p}_2+M_R}{(p-p_\eta)^2-M_R^2+i\Gamma_R M_R}\not{p}_\eta u_N(p), \\
&\text{where} \\
\mathcal{O}^{\mu}_R &\equiv \frac{F_1^V(q^2)}{(2M)^2}(\not{q}q^\mu - q^2\gamma^\mu)\gamma_5 \pm \frac{F_2^V(q^2)}{2M}i\sigma^{\mu\rho}q_\rho\gamma_5 \\
&\quad -F_A(q^2)\gamma^\mu \mp \frac{F_P(q^2)}{M}q^\mu \qquad (4.29)
\end{aligned}
$$

where, $f_{1,2}^V(q^2)$ are the isovector form factors and $f_A(q^2)$, $f_P(q^2)$ are the axial vector and pseudoscalar form factors, respectively for nucleons. The two isovector form factors $f_{1,2}^V(q^2)$ are expressed in terms of Dirac($f_1^{p,n}(q^2)$) and Pauli($f_2^{p,n}(q^2)$) form factors for protons and neutrons and are given by

$$f_{1,2}^V(q^2) = f_{1,2}^p(q^2) - f_{1,2}^n(q^2) \tag{4.30}$$

where,

$$\begin{aligned} f_1^{p,n}(q^2) &= \left(1 - \frac{q^2}{4M^2}\right)^{-1} \left[G_E^{p,n}(q^2) - \frac{q^2}{4M^2} G_M^{p,n}(q^2)\right] \\ f_2^{p,n}(q^2) &= \left(1 - \frac{q^2}{4M^2}\right)^{-1} \left[G_M^{p,n}(q^2) - G_E^{p,n}(q^2)\right]. \end{aligned} \tag{4.31}$$

Here, $G_E^{p,n}(Q^2)$ and $G_M^{p,n}(Q^2)$ are Sach's electric and magnetic form factors. They are obtained using electron scattering experiments. There are various parameterization for $G_{E,M}^{p,n}(Q^2)$ those are available in literature. For the present work we have taken parameterization from Bradford et al. [143] also known as BBBA-05 parameterization. The functional form of the BBBA-05 parameterization is given by,

$$G_{E,M}^N(Q^2) = \frac{\sum_{k=0}^{n=3} a_k \tau^k}{1 + \sum_{k=1}^{n=4} b_k \tau^k}, \qquad \tau = \frac{Q^2}{4M^2}; \quad Q^2 = -q^2 \tag{4.32}$$

The coefficients for the fit of the functional form is summarized in Table 4.2

The axial form factor is parameterized as

$$f_A(q^2) = f_A(0) \left[1 - \frac{q^2}{M_A^2}\right]^{-2}, \tag{4.33}$$

where $f_A(0)$ is the axial charge and M_A is the axial dipole mass. For the numerical calculations we have taken $f_A(0)$ = - 1.267 and M_A = 1.05 GeV. The pseudoscalar form factor $f_p^V(q^2)$ is given in terms of $f_A(q^2)$ using the Goldberger-Treiman relation defined as

$$f_p^V(q^2) = \frac{2M f_A(q^2)}{m_\pi^2 - q^2}, \tag{4.34}$$

where m_π is the mass of pion.

Table 4.2: The coefficients of the functional form fit for the $G_E^p(Q^2)$, $G_E^n(Q^2)$, $G_M^p(Q^2)$ and $G_M^n(Q^2)$ in BBBA-05 parameterization.

Form Factors	a_0	a_1	a_2	b_1	b_2	b_3	b_4
$G_E^p(Q^2)$	1	-0.0578±0.166	-	11.1±0.217	13.6±1.39	33.0±8.95	-
$G_M^p(Q^2)$	1	0.150±0.0312	-	11.1±0.103	19.6±0.281	7.54±0.967	-
$G_E^n(Q^2)$	0	1.25±0.368	1.30 ±1.99	-9.86±6.46	305±28.6	-758±77.5	802 ±156
$G_M^n(Q^2)$	1	1.81±0.402	-	14.1±0.597	20.7±2.55	68.7±14.1	-

In the case of S_{11} resonance, isovector form factors $F_{1,2}^V$ are given in terms of the electromagnetic transition form factors of charged(P^*) $F_{1,2}^p$ and neutral(N^*) $F_{1,2}^n$ form factors and are given by,

$$\begin{aligned} F_1^V(q^2) &= F_1^p(q^2) - F_1^n(q^2) \\ F_2^V(q^2) &= F_2^p(q^2) - F_2^n(q^2). \end{aligned} \tag{4.35}$$

These form factors are related to the helicity amplitudes as we have already mentioned earlier for the case of the N^* resonance. However, in the case of weak production their q^2 dependence is also important, and therefore we rewrite them as [141]:

$$\begin{aligned} A_{\frac{1}{2}} &= \sqrt{\frac{2\pi\alpha_e}{K_R}} \left\langle N^*, J_Z = \frac{1}{2} \middle| \epsilon_\mu^+ J_i^\mu \middle| N, J_Z = \frac{-1}{2} \right\rangle \zeta \\ S_{\frac{1}{2}} &= -\sqrt{\frac{2\pi\alpha_e}{K_R}} \frac{|\vec{q}|}{\sqrt{Q^2}} \left\langle N^*, J_Z = \frac{1}{2} \middle| \epsilon_\mu^0 J_i^\mu \middle| N, J_Z = \frac{-1}{2} \right\rangle \zeta \end{aligned} \tag{4.36}$$

where in the resonance rest frame.

$$\begin{aligned} K_R &= \frac{M_R^2 - M^2}{2M_R}, \quad |\vec{q}|^2 = \frac{(M_R^2 - M^2 + q^2)^2}{4M_R^2} - q^2 \\ \epsilon_\pm^\mu &= \mp\frac{1}{\sqrt{2}}(0, 1, \pm i, 0) \\ \epsilon_0^\mu &= \frac{1}{\sqrt{Q^2}}(|\vec{q}|, 1, 0, q^0), \qquad \text{and } \mathrm{Q}^2 = -\mathrm{q}^2. \end{aligned} \tag{4.37}$$

The parameter ζ is model dependent which is related to the sign of $N^* \to N\pi$, and for the present calculation is taken as $\zeta = 1$. The parameters $A_{\frac{1}{2}}$ and $S_{\frac{1}{2}}$ are generally parameterized as [142]:

$$\begin{aligned} A_{\frac{1}{2}}(Q^2) &= A_{\frac{1}{2}}(0)\left(1+\alpha\, Q^2\right)\, e^{-\beta Q^2} \\ S_{\frac{1}{2}}(Q^2) &= S_{\frac{1}{2}}(0)\left(1+\alpha\, Q^2\right)\, e^{-\beta Q^2}\,, \end{aligned} \tag{4.38}$$

The amplitudes $A_{\frac{1}{2}}(Q^2)$ and $S_{\frac{1}{2}}(Q^2)$ are related to the form factors $F_1^{p,n}$ and $F_2^{p,n}$ as [120]:

$$\begin{aligned} A_{\frac{1}{2}}^{p,n} &= \sqrt{\frac{2\pi\alpha_e}{M}\frac{(M_R+M)^2+Q^2}{M_R^2-M^2}}\left(\frac{Q^2}{4M^2}F_1^{p,n}(Q^2)+\frac{M_R-M}{2M}F_2^{p,n}(Q^2)\right) \\ S_{\frac{1}{2}}^{p,n} &= \sqrt{\frac{\pi\alpha_e}{M}\frac{(M_R-M)^2+Q^2}{M_R^2-M^2}\frac{(M_R+M)^2+Q^2}{4M_RM}} \\ &\quad\times\left(\frac{M_R-M}{2M}F_1^{p,n}(Q^2)-F_2^{p,n}(Q^2)\right). \end{aligned} \tag{4.39}$$

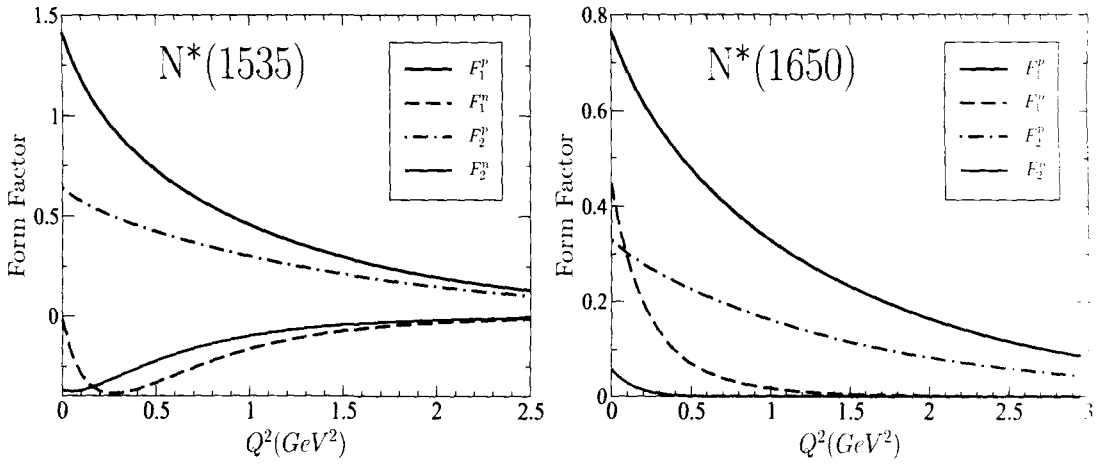

Figure 4.4: Form factors for S_{11} resonances. The fittings are obtained using data from the MAMI Crystal Ball experiment [136].

Thus after getting a proper fitting for the amplitudes $A_{\frac{1}{2}}(Q^2)$ and $S_{\frac{1}{2}}(Q^2)$, the form factors $F_1^{p,n}$ and $F_2^{p,n}$ have been obtained. The parameters used to fit the

Table 4.3: Parameters used for the helicity amplitude

Resonance→	S11(1535)			S11(1650)		
Helicity Amplitude↓	$A_\lambda(0)$ 10^{-3}	α	β	$A_\lambda(0)$ 10^{-3}	α	β
$A^p_{1/2}(Q^2)$	89.38	1.61364	0.75879	53	1.45	0.62
$S^p_{1/2}(Q^2)$	-16.5	2.8261	0.73735	-3.5	2.88	0.76
$A^n_{1/2}(Q^2)$	-52.79	2.86297	1.68723	9.3	0.13	1.55
$S^n_{1/2}(Q^2)$	29.66	0.35874	1.55	10.0	-0.5	1.55

amplitudes for N^* resonances are tabulated in Table 4.3. We used the MAMI Crystal Ball data to parameterize $A_{\frac{1}{2}}(0)$ and $S_{\frac{1}{2}}(0)$, however, for the Q^2 dependence we used MAID parameterization [142]. At this point we would like to emphasize that none of the parameterization is able to define η photoproduction data completely. The Q^2 dependence of $F_i^{p,n}(Q^2)$(i=1,2) form factors are shown in Fig. 4.4.

The Q^2-dependence of isovector form factors F_1^V and F_2^V, obtained using Eq. 4.35, shown in Fig. 4.5. We must point out that the form factors $F_{1,2}^{p,n}$ which are used to obtain $F_{1,2}^V$ are parameterized with the help of helicity amplitudes as discussed earlier which in turn is the direct consequence of CVC(Conserved Vector Current) hypothesis. The weak form factors $F_A(Q^2)$ and $F_P(Q^2)$ are fixed using PCAC(Partial Conservation of Axial Current) and pion pole dominance. For this we start with the pion pole contribution to the axial current as shown in Fig. 4.6. The Lagrangian for the $W^+\pi^+$ vertex is

$$\mathcal{L} = \frac{-g}{2\sqrt{2}} V_{ud} \sqrt{2} f_\pi \partial^\mu \pi^- W^\mu_+ \tag{4.40}$$

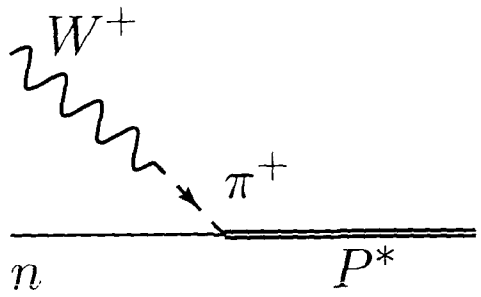

Figure 4.6: Pion pole contribution to the axial current.

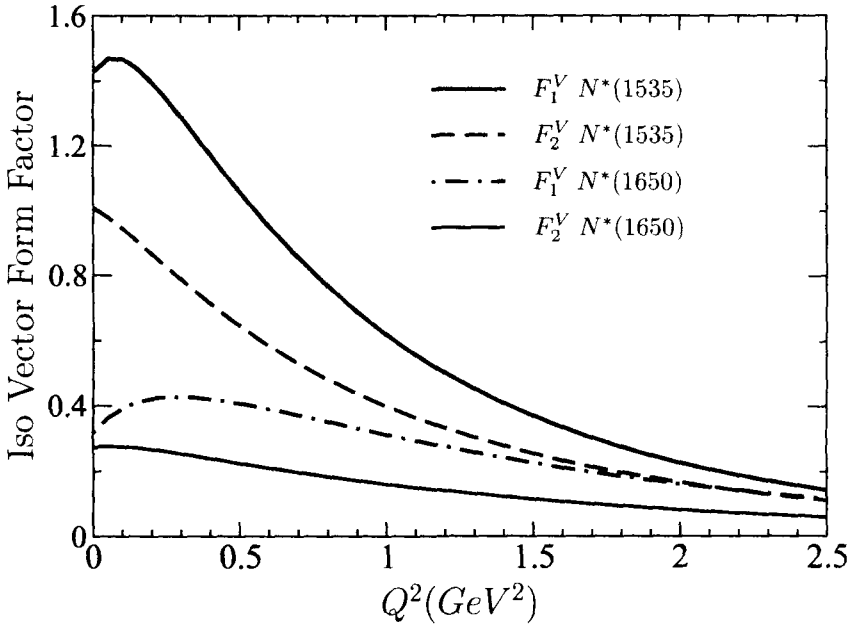

Figure 4.5: The isovector F_1^V and F_2^V form factors for the S_{11} resonances.

Using the above Lagrangian along with $N^*N\pi$ vertex given by Eq.4.16, one may write

$$\begin{aligned} & -i\frac{-g}{2\sqrt{2}}V_{ud}\bar{u}_{P^*}(-F_p q^\mu)u_n \\ = \; & i\sqrt{2}f_\pi iq^\mu \frac{i}{q^2-m_\pi^2} i\frac{-g_\pi}{f_\pi}\sqrt{2}(-iq_\alpha)\bar{u}_{P^*}\gamma^\alpha u_N \frac{-g}{2\sqrt{2}}V_{ud}F_{N^*N\pi}(q^2). \end{aligned} \tag{4.41}$$

We introduced here a new form factor $F_{N^*N\pi}$ which accounts for off-shell dependence for the vertex shown in Fig. 4.6. Using Dirac equation and comparing both the sides of Eq. 4.41, we get

$$F_P = -2g_\pi \, F_{N^*N\pi}(q^2)\frac{M_R - M}{q^2 - m_\pi^2}, \tag{4.42}$$

which in the chiral limit i.e. $m_\pi \to 0$ and assuming PCAC, may be written as

$$\begin{aligned} \partial_\mu A^\mu = \; 0 \; &= F_A \not{q} + F_P q^2 \\ &= F_A(M_R - M) - 2\, g_\pi \, F_{N^*N\pi}(q^2)(M_R - M) \end{aligned} \tag{4.43}$$

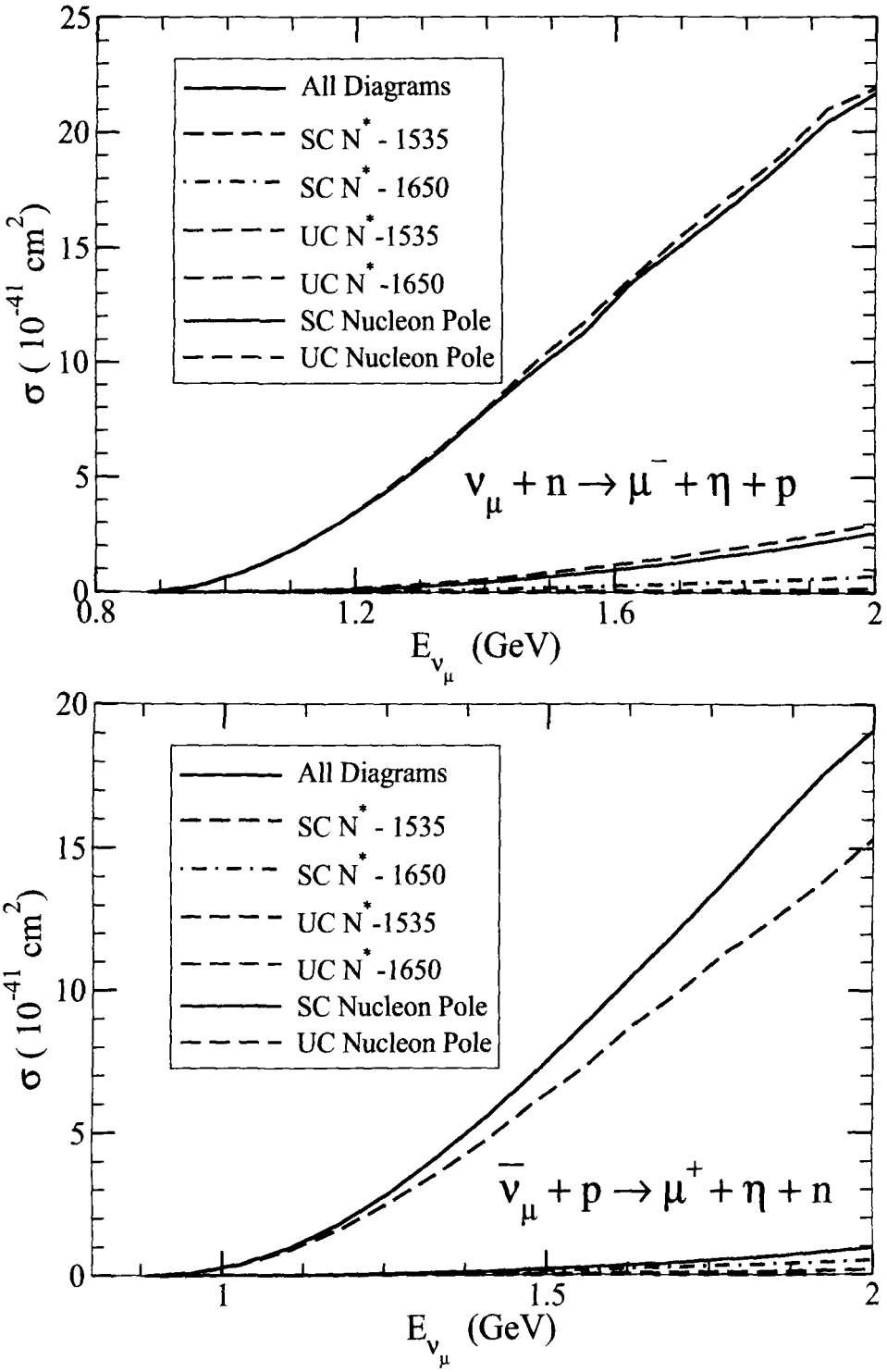

Figure 4.7: Cross section corresponding to Feynman diagrams as shown in Fig. 4.3

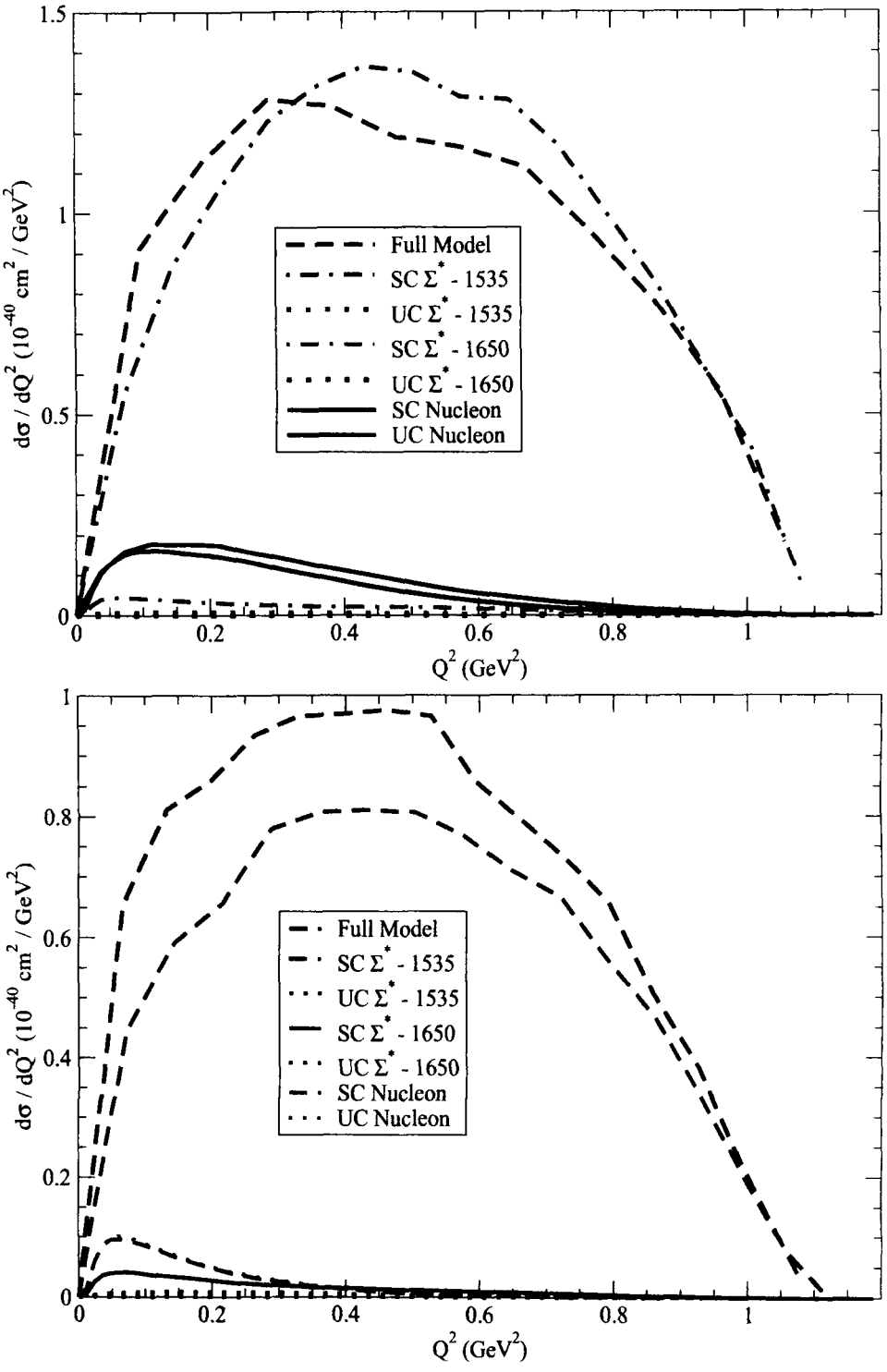

Figure 4.8: Q^2 distribution corresponding to Feynman diagrams as shown in Fig. 1.3

This leads to,

$$F_A(q^2) = 2\, g_\pi F_{N^*N\pi}(q^2) \tag{4.44}$$

Furthermore, by using Goldberger-Treiman relation $F_A(0)$ is related to g_π as, $F_A(0) = 2g_\pi$. We take the form factor $F_{N^*N\pi}(q^2)$ to be of dipole form. Therefore, form of the weak form factors of N^* resonance are taken as,

$$\begin{aligned} F_A(q^2) &= g_\pi \left(1 - \frac{q^2}{M_A^2}\right)^{-2} \\ F_P(q^2) &= -F_A(q^2)\frac{M_R - M}{q^2 - m_\pi^2}. \end{aligned} \tag{4.45}$$

We have used the same coupling strength for S_{11} resonance which has been earlier used to describe the photoproduction results and are given in Eq. 4.21. In the next section we are going to present the results of our numerical calculations obtained for the $\nu/\bar{\nu}$ induced η production off the nucleon.

4.3 Results and Discussion

To get the numerical results for the differential and total scattering cross section we integrate Eq. 4.26 and used Eqs. 4.27-4.29. In Fig. 4.7, the results for neutrino and antineutrino induced η production cross sections are presented both for the total(taking all the diagrams shown in Fig. 4.3) as well as individual contributions of each diagram. We find that $S_{11}(1535)$ resonance is dominant while the contribution of $S_{11}(1650)$ to the total cross section is small. This can be understood easily because $S_{11}(1535)$ is lighter in mass and has a relatively larger branching ratio for $S_{11} \to N\eta$. We also find that the contribution of the nonresonant diagrams in the case of neutrino induced process is higher than the corresponding antineutrino induced processes. Also in neutrino mode the contribution of u-channel diagram is slightly larger than the corresponding s-channel diagram. We find that around 1-2 GeV the contribution of $S_{11}(1535)$ is very dominant for the neutrino induced process. In the case of antineutrino induced reaction up to 1 GeV, $S_{11}(1535)$ is dominant, however at $E_{\bar{\nu}} = 1.5$ GeV its contribution is around 80% of the total η production cross section. The contribution of $S_{11}(1650)$ resonance is not more than 5% in the entire neutrino energy spectrum. Contributions from the s- and u- channel diagrams of nucleon pole are around $10 - 15\%$ to the total cross section. In Figs. 4.8, 4.9 and 4.10, we have presented separately the results for the Q^2 distribution ($d\sigma/dQ^2$), η energy distribution ($d\sigma/dE_\eta$) and muon energy distribution ($d\sigma/dE_\mu$), respectively.

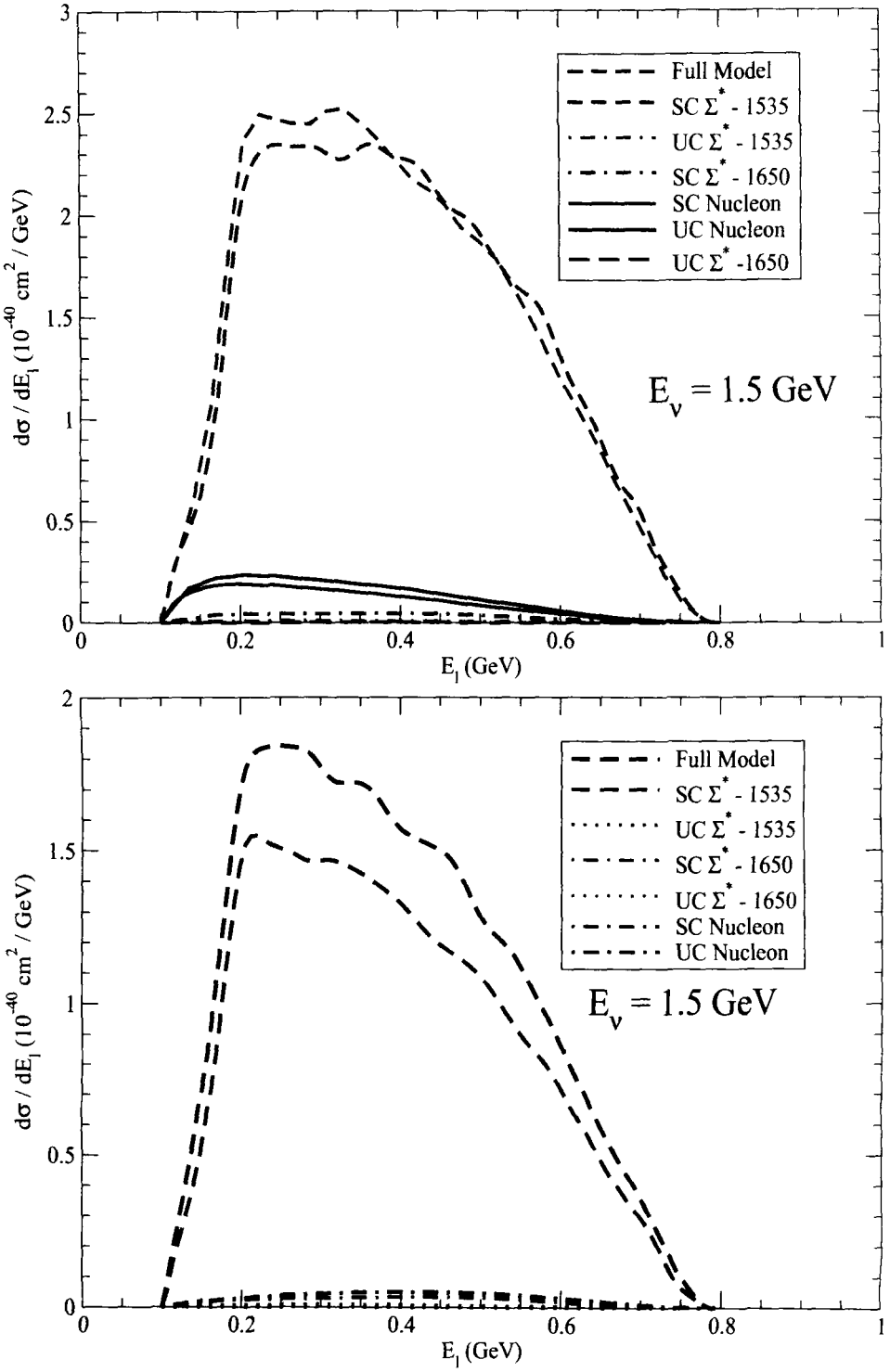

Figure 4.9: Lepton Energy distribution corresponding to Feynman diagrams as shown in Fig. 4.3

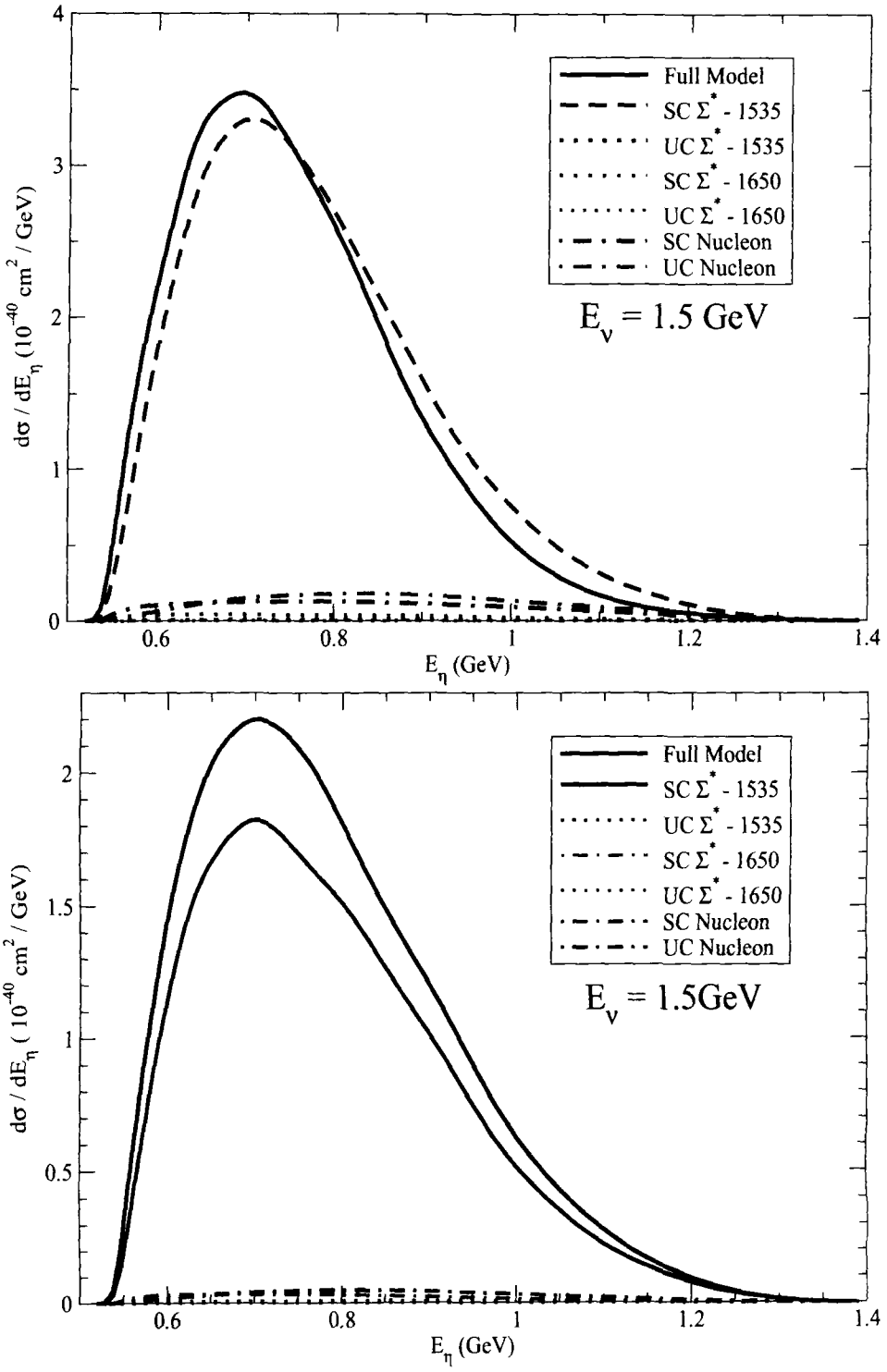

Figure 4.10: Eta Energy distribution corresponding to Feynman diagrams as shown in Fig. 4.3

In Fig. 4.8, we have shown the Q^2 dependence for neutrino and antineutrino induced processes at the incident energy of 1.5 GeV. We find that the distribution is almost flat. Although the background terms(nucleon pole) are more sharply peaked but the dominance of $S_{11}(1535)$ resonance gets reflected even in the Q^2 distribution. $S_{11}(1650)$ does not contribute significantly at these energies. Moreover, the contribution of u-channel diagram is almost nonsignificant in the present kinematical range.

In Fig. 4.9, we present the results for the lepton energy distribution at neutrino energy of 1.5 GeV. Here also we can see the dominance of the $S_{11}(1535)$ resonance. Unlike the Q^2 distribution here the nucleon pole term has flat distribution, however, the low energy peaking comes from $S_{11}(1535)$. Again the contribution of $S_{11}(1650)$ and the u-channel resonant diagrams are not significant. However, their contributions lead to modified nature of lepton energy distribution as can be seen in Fig. 4.9, where the peaking tends to shift towards the lower lepton energies. For example in the case of neutrino induced η production processes the contribution from the full term is slightly lower than the contribution coming from $S_{11}(1535)$ resonance, the opposite interference effect is observed in the case of antineutrino where enhancement in the lepton energy distribution is observed. This can be understood by looking at the different signs in the antisymmetric term of the leptonic tensor for neutrino and antineutrino cases.

In the case of eta energy distribution, shown in Fig. 4.10, we find that the trend is almost of similar nature as in the case of lepton energy distribution. Here also the distribution due to nucleon pole is flat but the overall peaking is dominated by the $S_{11}(1535)$ resonance.

To conclude, in this work we have studied charged current neutrino and antineutrino induced η production off free nucleons. We find that the cross sections are large enough to be measured in experiments like T2K, NOνA and MINERνA. We must point out that this is perhaps the first study to best of our knowledge where the total scattering cross section as well as differential cross sections have been obtained for the neutrino/antineutrino induced processes. This study may be used in the analysis of neutrino oscillation results.

In the next chapter, we present the formalism for the associated particle production and present the results for the total scattering cross section as well as differential scattering cross section.

Chapter 5

Associated Kaon Production

5.1 Introduction

The study of weak neutrino-nucleus interactions involving associated particle production in the energy region of a few GeV has become one of the major theoretical and experimental area of interest due to its importance in the fields of astrophysics, cosmology, particle as well as nuclear physics. First of all a good understanding of these interactions would lead to a better insight into nucleon and nuclear structures. This will be an additional tool to complement the theories of particle and nuclear physics, the knowledge of which one obtains from electromagnetic reactions with real and virtual photons. Moreover, the study of neutrino induced ΔS=0 associated particle production processes provide an improved understanding of basic symmetries of the standard model, structure of the weak hadronic form factors, strange-quark content of the nucleon, coupling constants, etc. One may also get information on the medium modification of the elementary amplitudes. Furthermore, the efforts of proton decay searches at various laboratories like SuperK [35], HyperK [38], UNO [37], LAGUNA [144], etc., are going on where the atmospheric neutrinos while interacting with a nucleon target also produce kaons, either through $\Delta S = 0$ or $\Delta S = 1$ processes. This poses a background in the proton decay searches as the main source of proton decay in supersymmetric grand unified models has been proposed through $p \to K\bar{\nu}$. Therefore, the importance of thorough understanding and reliable estimate of the cross sections for neutrino induced kaon production contributing as background event has been emphasized as the proton decay experiments will be limited in statistics also [44, 96].

The experimental observations of the neutrino induced associated particle pro-

duction processes are quite limited. These are limited both by statistics as well as by the large systematic errors. Earlier the experiments were performed at BNL[41], ANL [42] and CERN[145, 146, 147], however, to have neutrino oscillation parameters with high precision, many experiments are coming up in the energy range of a few GeV, where nuclear targets are being used or have been planned with. The aim of these experiments is to understand the nucleon dynamics in the nuclear medium. For example the MINERνA experiment at Fermi Lab [44], which is a dedicated experiment to measure the cross sections, and their aim is also to study many associated particle production processes using several nuclear targets like ^4He, ^{12}C, ^{16}O, ^{56}Fe and ^{208}Pb. This will allow physicists to gain considerable insight into the structure of the nucleon and the hadronic weak current via the (anti)neutrino induced weak production of strange particles. There are other planned experiment like LBNE [148] which would also be sensitive to the measurement of strange particles.

Theoretically, the early attempts were made by Shrock et al. [45], Mecklenburg et al. [46], Dewan et al. [47] and Amer et al.[48]. Shrock et al. [45] considered both charged and neutral current processes in the region of the ANL [42] neutrino spectrum which is concentrated in the low-energy region. The processes considered by this group may be written as $\nu + N \rightarrow l + K + Y$ and $\nu + N \rightarrow \nu + K + Y$, where Y refers to a Λ or a Σ hyperon. The calculations were performed using nonresonant Born approximation and only s, t and u channels were considered. However, the results do not fit into the experimental data very well and do not level off at high energies. Amer et al. [48] used a model of neutrino production based on harmonic oscillator quark model. They estimated cross section to be between 1.35 and 2.65 $\times 10^{-41}$ cm^2 for $K^+\Lambda$ production, however, this has also been found out to be an order of magnitude smaller than the experimental results [149]. Dewan et al. [47] extended the calculation of Shrock et al. [45] to high energies, where the form factors at the hadron vertices were used. Recently Adera et al. [150, 151], have studied associated particle production using the Born approximation in the framework of the Cabibbo theory and SU(3) symmetry and presented the results at the level of differential cross section $\frac{d^3\sigma}{dE_k d(\cos\theta_k) d\Omega_{\nu l}}$. In their calculation no resonance was considered. On the other hand the associated particle production cross sections used for example in the NUANCE Monte Carlo generator [55] considers only the resonant kaon production based on the Rein and Sehgal model for pion production [61]. Moreover, these cross sections misses the experimental data points by almost a factor of four and has an overall χ^2 of $^{11}/_6$ [152]. Therefore, there is an urgent need for estimating the weak interaction induced associated particle production cross section were the efforts are being made to get the neutrino oscillation parameters with high precision.

In this chapter, we have studied associated particle production off the nucleon

induced by neutrino and antineutrino. The formalism for writing the hadronic current is the same as was adopted in the case of single kaon and eta meson production processes discussed in Chapter- 2 and Chapter- 4 respectively. Specifically, we have studied charged current(CC) induced $\Delta S = 0$ process like

$$\left.\begin{array}{l} \nu_l + N \to l^- + Y + K \\ \bar{\nu}_l + N \to l^+ + Y + K \end{array}\right\} \quad \text{CC} \quad (\Delta \text{S} = 0), \tag{5.1}$$

where $l = e, \mu$ and N is nucleon, K stands for a kaon and Y is a hyperon(Λ or Σ). For the energies above 1.5 GeV it is $\Delta S = 0$ kaon production which is more dominant in comparison to the corresponding $\Delta S = 1$ processes as the later is suppressed by a factor of $\tan^2\theta_C$. However, in the case of antikaon the $\Delta S = 0$ mode is not possible in three body final state due to the change in the total strangeness quantum number by 2 units ($|\Delta S| = 2$). This can be understood with a simple argument, like

$$\begin{array}{cccccccc} & \nu_l & N & \to & l^- & \bar{K} & Y & \\ S & & 0 & & & -1 & -1 & |\Delta S| = 2 \end{array} \tag{5.2}$$

The only possible strangeness conserving process for $K^-, \bar{K}^0$ is through the channels like,

$$\nu_l + N \to l^- + K + \bar{K} + N', \qquad (\Delta S = 0), \tag{5.3}$$

however, threshold for such type of process is around 2 GeV and we are focused here upto an energy region of 2 GeV.

In this chapter we present the results of our calculations for (anti)neutrino induced associated production ($|\Delta S| = 0$) of kaon along with a hyperon. Our microscopic model is based on the SU(3) chiral Lagrangian which has been briefly discussed in Chapter-2. The basic parameters of the model are f_π, the pion decay constant, Cabibbo angle, the proton and neutron magnetic moments and the axial vector coupling constants for the baryon octet, D and F, that are obtained from the analysis of the semileptonic decays of neutron and hyperon. We have considered only non-resonant diagrams. In Sec. 5.2, we describe the formalism in brief and in Sec. 5.3, the results and discussions are presented.

5.2 Formalism

The basic reactions for $\nu(\bar{\nu})$ charged current induced associated particle production accompanied by a kaon from a nucleon(p or n) target are,

$$\begin{array}{ll} \nu_\mu n \to \mu^- K^+ \Lambda & \bar{\nu}_\mu p \to \mu^+ K^0 \Lambda \\ \nu_\mu p \to \mu^- K^+ \Sigma^+ & \bar{\nu}_\mu p \to \mu^+ K^0 \Sigma^0 \\ \nu_\mu n \to \mu^- K^+ \Sigma^0 & \bar{\nu}_\mu p \to \mu^+ K^+ \Sigma^- \\ \nu_\mu n \to \mu^- K^0 \Sigma^+ & \bar{\nu}_\mu n \to \mu^+ K^0 \Sigma^- \end{array}$$

for which the differential cross section is generally written as,

$$d^9\sigma = \frac{1}{4ME(2\pi)^5} \frac{d\vec{k}'}{(2E_l)} \frac{d\vec{p}'}{(2E'_Y)} \frac{d\vec{p}_k}{(2E_K)} \delta^4(k + p - k' - p' - p_k) \bar{\Sigma}\Sigma |\mathcal{M}|^2, \quad (5.4)$$

where $\vec{k}$ and $\vec{k}'$ are the 3-momenta of the incoming and outgoing leptons in the lab frame with energies E and E' respectively. $\vec{p}_k$ and E_K are the 3-momentum and energy of the final state kaon. The hyperon energy and 3-momentum are denoted by $\vec{p}'$ and E_Y respectively. M is the nucleon mass, $\bar{\Sigma}\Sigma|\mathcal{M}|^2$ is the square of the transition amplitude averaged(summed) over the spins of the initial(final) state and is generally written as

$$|\mathcal{M}|^2 = \frac{G_F^2}{2} L_{\mu\nu} H^{\mu\nu} \quad (5.5)$$

where, G_F is the Fermi coupling constant. The leptonic tensor $L_{\mu\nu}$ is given by

$$L_{\mu\nu} = 8 \left(k_\mu k'_\nu + k_\nu k'_\mu - g_{\mu\nu} k.k' \pm \epsilon_{\mu\nu\alpha\beta} k^\alpha k'^\beta \right) \quad (5.6)$$

where, plus sign is for neutrino and minus sign is for antineutrino. The hadronic tensor $H^{\mu\nu}$ occurring in Eq. 5.5 is written in terms of the hadronic current J^μ as,

$$H^{\mu\nu} = \bar{\sum} \sum J^{\mu\dagger} J^\nu \quad (5.7)$$

The contribution to the hadronic current J^μ comes from the different pieces of the Lagrangian corresponding to the Feynman diagrams shown in Fig. 5.1.

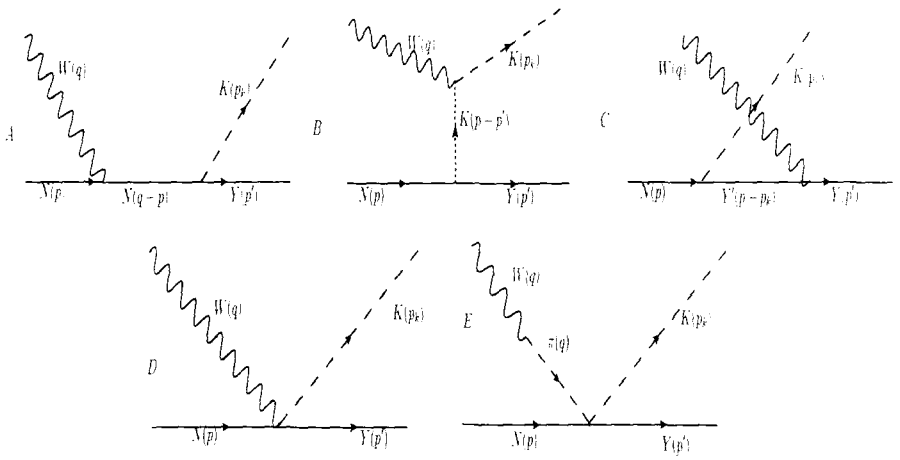

Figure 5.1: Feynman diagrams corresponding to the neutrino/antineutrino induced $\Delta S = 0$ kaon production process.

We generalize the nucleon and hyperon pole diagrams to incorporate form factors at the weak vertices where the relevant diagrams are labeled by 'A' and 'C' respectively in Fig. 5.1. To understand the introduction of the form factors in our formalism we proceed by taking a simple example as shown in Fig. 5.2. Here a hyperon(or a nucleon) with momentum k is changing its identity after interacting with the weak field to another nucleon(or hyperon) with momentum k'. However, this formalism may be extended for any allowed process like $N \leftrightarrow N'$, $N \leftrightarrow Y$ and $Y \leftrightarrow Y'$. where $N, N' = n, p$ and Y, Y' =hyperon. The matrix element corresponding to the

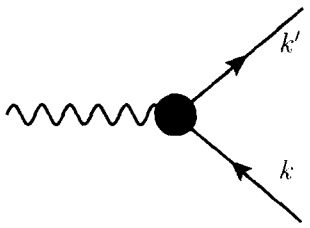

Figure 5.2: Weak transition vertex.

hyperon nucleon transition may be written as,

$$J^\mu = \langle Y(k')|V^\mu - A^\mu|N(k)\rangle \tag{5.8}$$

The currents V^μ and A^μ are expressed in terms of the vector $f_i(q^2)$ and axial-vector $g_i(q^2)$ transition form factors as,

$$\begin{aligned} V^\mu &= \gamma^\mu f_1(q^2) + i\sigma^{\mu\nu}\frac{q^\nu}{M+M_Y} f_2(q^2) + f_3(q^2)\frac{q^\mu}{M_Y} \\ A^\mu &= \left[\gamma^\mu g_1(q^2) + i\sigma^{\mu\nu}\frac{q^\nu}{M+M_Y} g_2(q^2) + g_3(q^2)\frac{q^\mu}{M_Y}\right].\gamma^5 \end{aligned} \tag{5.9}$$

The various form factors those appear in the vector and axial vector currents may be determined using the prescription given in Refs. [49, 93]. In the Standard Model these currents are written as:

$$\begin{aligned} V^i_\mu &= \bar{q}\frac{\lambda^i}{2}\gamma_\mu q \\ A^i_\mu &= \bar{q}\frac{\lambda^i}{2}\gamma_\mu\gamma_5 q\,, \end{aligned} \tag{5.10}$$

where q is quark field and $\frac{\lambda^i}{2}$ are the generators of flavor $SU(3)$. The form of λ_i are given in Eq. 2.3. For light quarks u, d and s, we may neglect their mass differences leading to the non-breaking effects of flavor $SU(3)$, which may be taken as a reasonable approximation at low energies. Now we define a $SU(3)$ octet operator $\mathcal{O}_i$ which connects two octet states through the reduced matrix elements F and D as:

$$\langle B_n|\mathcal{O}_i|B_m\rangle = F\; d_{inm} + D\; f_{inm} \tag{5.11}$$

where f_{inm} are the structure constants of $SU(3)$ and d_{inm} comes from the anticommutation relations of the generators: $\{\lambda_i, \lambda_n\} = 2\delta_{in} + 2\mathrm{d}_{inm}$. The above definition also suggests that F and D are related to the antisymmetric and symmetric couplings of baryon octet(B_n and B_m) in the initial and final states. Therefore, the vector and axial vector form factors $f_i(q^2)$ and $g_i(q^2)$ may also be expressed in terms of the two reduced matrix elements, say $F_i^V(q^2)$ and $D_i^V(q^2)$ for vector and $F_i^A(q^2)$ and $D_i^A(q^2)$ for axial vector currents as:

$$\begin{aligned} f_i(q^2) &= \alpha F_i^V(q^2) + \beta D_i^V(q^2), \\ g_i(q^2) &= \alpha F_i^A(q^2) + \beta D_i^A(q^2), \qquad \text{where,} \quad (\mathrm{i} = 1, \cdots, 3) \end{aligned} \tag{5.12}$$

The constants α, β appearing in Eq. 5.12 may be understood as the $SU(3)$ Clebsch-Gordon coefficient. In the next section we discuss in brief the vector form factors appearing in Eq. 5.9.

5.2.1 Vector Form Factor

In this section we discuss the vector form factors, $f_i(q^2), i = 1,2,3$, those appeared in Eq. 5.9. Following the Conserved Vector Current(CVC) hypothesis the vector part of the weak and electromagnetic currents belong to the same octet. Therefore, the form factor $f_3(q^2) = 0$ and the other two vector transition form factors($f_{1,2}^N(q^2)$) are determined in terms of the electromagnetic form factors of protons and neutrons. The electromagnetic form factors $f_{1,2}^N(q^2)$ are defined by the expectation values of electromagnetic current V_μ^{em} of the quark fields as:

$$\langle B'_N|V_\mu^{em}|B_N\rangle = \bar{u}(k')\left[\gamma^\mu f_1^N(q^2) + i\sigma^{\mu\nu}\frac{q^\nu}{2M}f_2^N(q^2)\right]u(k), \qquad N = p, n \tag{5.13}$$

with

$$V_\mu^{em} = \bar{q}\gamma^\mu\hat{Q}q \tag{5.14}$$

where $\hat{Q}$ is the charge operator of quark field which is expressed in terms of the third component of the isospin(I_3) and the hypercharge(Y) using the Gell-Mann-Nishjima formula as,

$$\hat{Q} = I_3 + \frac{Y}{2} \tag{5.15}$$

Therefore, the electromagnetic current V_μ^{em} is decomposed into SU(3) octet currents as

$$V_\mu^{em} = V_\mu^{(3)} + \frac{1}{\sqrt{3}}V_\mu^{(8)} \tag{5.16}$$

with

$$\begin{aligned} V_\mu^{(3)} &= \bar{q}\gamma^\mu\frac{\lambda^3}{2}q \\ V_\mu^{(8)} &= \bar{q}\gamma^\mu\frac{\lambda^8}{2}q \end{aligned} \tag{5.17}$$

where the superscripts in Eqs. 5.16,5.17 are the $SU(3)$ indices. Using Eqs. 5.13-5.17, the nucleon form factors may be expressed in terms of the functions $F_i^V(q^2)$ and $D_i^V(q^2)$ as:

$$\begin{aligned} f_i^n(q^2) &= \frac{2}{3}D_i^V(q^2) \\ f_i^p(q^2) &= F_i^V(q^2) + \frac{1}{3}D_i^V(q^2), \qquad i = 1,2 \end{aligned} \tag{5.18}$$

Since the nucleon form factors $f_i^{n,p}$ are well known, we may express $F_i^V(q^2)$ and $D_i^V(q^2)$ in terms of $f_i^{n,p}(q^2)$ as

$$\begin{aligned} F_i^V(q^2) &= f_i^p(q^2) + \frac{1}{2} f_i^n(q^2) \\ D_i^V(q^2) &= -\frac{3}{2} f_i^n(q^2) \end{aligned} \tag{5.19}$$

Once the values for $F_i^V(q^2)$ and $D_i^V(q^2)$ are determined, all the vector transition form factors may be expressed in terms of the nucleon form factors $f_i^{n,p}(q^2)$. The electromagnetic form factors $f_i^{n,p}(q^2)$ are written in terms of the experimentally determined Sachs electric $G_E^{p,n}(q^2)$ and magnetic $G_M^{p,n}(q^2)$ form factors as [153].

$$\begin{aligned} f_1^{p,n}(q^2) &= \left[1 - \frac{q^2}{4M^2}\right]^{-1} \left[G_E^{p,n}(q^2) - \frac{q^2}{4M^2} G_M^{p,n}(q^2)\right] \\ f_2^{p,n}(q^2) &= \left[1 - \frac{q^2}{4M^2}\right]^{-1} \left[G_M^{p,n}(q^2) - G_E^{p,n}(q^2)\right], \end{aligned} \tag{5.20}$$

where we have taken the following parameterization [49, 153] for the electric and magnetic Sachs form factors:

$$\begin{aligned} G_E^p(q^2) &= \frac{1}{(1 - \frac{q^2}{M_V^2})^2} \\ G_E^n(q^2) &= \mu_n \left(\frac{q^2}{4M^2}\right) G_E^p(q^2) \xi_n \\ G_M^p(q^2) &= (1 + \mu_p) G_E^p(q^2) \\ G_M^n(q^2) &= \mu_n G_E^p(q^2) \\ \xi_n &= \frac{1}{1 - \lambda_n \frac{q^2}{4M^2}} \\ \text{with} \quad \lambda_n &= 5.6 \\ \mu_p &= 1.792847 \\ \mu_n &= -1.913043 \\ M_V &= 0.84 GeV \end{aligned} \tag{5.21}$$

Now we shall present in brief the parameterization for the axial vector form factors.

5.2.2 Axial Form Factor

The form factors, in the axial vector current $g_i(q^2)$ in Eq. 5.9 are obtained in terms of the $F_i^A(q^2)$ and $D_i^A(q^2)$ defined in Eq.5.12. However, before going into the details of it we shall point out the constraints which comes from various symmetries, like

(i) In the case of exact flavor $SU(3)$ symmetry the weak - electric form factor g_2 will not contribute i.e. $g_2(q^2) = 0$.

(ii) Applying Partial Conservation of Axial Current(PCAC) the pseudo-vector transition form factor $(g_3(q^2))$ is related to the axial vector transition form factor $(g_1(q^2))$ as

$$g_3(q^2) = \frac{2M^2}{m_\pi^2 - q^2} g_1(q^2) \tag{5.22}$$

The major source of information on the weak axial vector transition form factor $g_i(q^2)$ comes from the semileptonic hyperon decays and $\Delta S = 0$ neutrino-nucleon scattering. In such processes the contribution of $g_3(q^2)$ is proportional to the lepton masses and may be neglected. This implies that in the case of axial vector current we are left with only one form factor i.e. $g_1(q^2)$.

From the beta decay experiments and the reactions of the kind $\nu_\mu + p \to \mu^- + p$ the form of $g_1^N(q^2)$ is determined and is generally taken to be of dipole form

$$g_1^N(q^2) = g_A(0)\left(1 - \frac{q^2}{M_A^2}\right)^{-2}, \tag{5.23}$$

with axial dipole mass M_A taken as 1.03 ± 0.5GeV. As for the transition of $N \to N'$ the $SU(3)$ Clebsch Gordon coefficient in Eq. 5.12 turns out to be 1 for both α and β, and the form factor may be expressed as

$$g_1^N(q^2) = F_1^A(q^2) + D_1^A(q^2). \tag{5.24}$$

Assuming, the same q^2 dependence as for $g_1^N(q^2)$ in Eq. 5.23 we may write the separate q^2 dependence for both $F_1^A(q^2)$ and $D_1^A(q^2)$ as

$$\begin{aligned} F_1^A(q^2) &= F_1(0)\left(1 - \frac{q^2}{M_A^2}\right)^{-2} \\ D_1^A(q^2) &= D_1(0)\left(1 - \frac{q^2}{M_A^2}\right)^{-2}, \end{aligned} \tag{5.25}$$

where $F_1(0)$ and $D_1(0)$[1] are extracted from semileptonic decays of nucleons and hyperons [93]. Once $F_1^A(q^2)$ and $D_1^A(q^2)$ are fixed following the same procedure as we did for vector current we obtain the other transition form factors. The form factors $f_{1,2}$ and g_1 in terms of the known quantities are listed in Tab. 5.1. Also we write the amplitudes corresponding to the Feynman diagrams as shown in Fig. 5.1 in Eq. 5.26. The various constants/parameters appearing in Eq. 5.26 are tabulated in Table 5.2. The hadronic currents corresponding to the diagrams shown in Fig. 5.1 now read as

$$\begin{aligned}
j^\mu|_s &= iA_{SY}V_{ud}\frac{\sqrt{2}}{2f_\pi}\,\bar{u}_Y(p')\not{p}_k\gamma^5\frac{\not{p}+\not{q}+M}{(p+q)^2-M^2}\mathcal{H}^\mu u_N(p)\\
j^\mu|_u &= iA_{UY}V_{ud}\frac{\sqrt{2}}{2f_\pi}\,\bar{u}_Y(p')\mathcal{H}^\mu\frac{\not{p}-\not{p}_k+M_{Y'}}{(p-p_k)^2-M_{Y'}^2}\not{p}_k\gamma^5 u_N(p)\\
j^\mu|_t &= iA_{TY}V_{ud}\frac{\sqrt{2}}{2f_\pi}(M+M_Y)\,\bar{u}_Y(p')\gamma_5\,u_N(p)\;\frac{q^\mu-2p_k^\mu}{(p-p')^2-m_k^2}\\
j^\mu|_{CT} &= iA_{CT}V_{ud}\frac{\sqrt{2}}{2f_\pi}\,\bar{u}_Y(p')\left(\gamma^\mu+B_{CT}\,\gamma^\mu\gamma^5\right)u_N(p)\\
j^\mu|_{\pi F} &= iA_\pi V_{ud}\frac{\sqrt{2}}{4f_\pi}\,\bar{u}_Y(p')(\not{q}+\not{p}_k)u_N(p)\frac{q^\mu}{q^2-m_\pi^2}
\end{aligned}\tag{5.26}$$

where,

$$\mathcal{H}^\mu = f_1^V\gamma^\mu + i\frac{f_2^V}{2M}\sigma^{\mu\nu}q_\nu - g_A\left(\gamma^\mu-\frac{\not{q}q^\mu}{q^2-m_\pi^2}\right)\gamma^5 \tag{5.27}$$

is the transition current for $Y \leftrightarrows Y'$ with $Y = Y' \equiv$ Nucleon and/or Hyperon. Using the expression for hadronic current given in Eq. 5.26 we obtain the hadronic tensor $H^{\mu\nu}$ which contract with the leptonic tensor $L^{\mu\nu}$, and we get the expression for matrix element square which is used in Eq. 5.4 to obtain the results for the differential and total scattering cross sections. In the next section we present and discuss the results of our findings.

[1]For convenience we will now refer $F_1(0)$ and $D_1(0)$ as F and D.

Table 5.1: The standard form factors for weak CC transitions of the SU(3) baryon octet.

Weak transition	$f_1^V(Q^2)$	$f_2^V(Q^2)$	$g_A(Q^2)$
$p \to n$	$f_1^p(Q^2) - f_1^n(Q^2)$	$f_2^p(Q^2) - f_2^n(Q^2)$	$g_A(Q^2)$
$\Sigma^\pm \to \Lambda$	$-\sqrt{\frac{3}{2}} f_1^n(Q^2)$	$-\sqrt{\frac{3}{2}} f_2^n(Q^2)$	$\sqrt{\frac{2}{3}} \frac{D}{F+D} g_A(Q^2)$
$\Sigma^\pm \to \Sigma^0$	$\mp \frac{1}{\sqrt{2}} [2 f_1^p(Q^2) + f_1^n(Q^2)]$	$\mp \frac{1}{\sqrt{2}} [2 f_2^p(Q^2) + f_2^n(Q^2)]$	$\mp \sqrt{2} \frac{F}{F+D} g_A(Q^2)$

Process	A_{CT}	B_{CT}	A_{SY}	A_{UY}		A_{TY}	A_π
				$Y' = \Sigma$	$Y' = \Lambda$		
$\bar{\nu}_l p \to l^+ \Sigma^- K^+$ $\nu_l n \to l^- \Sigma^+ K^0$	0	0	$D - F$	$D - F$	$\frac{1}{3}(D + 3F)$	0	0
$\bar{\nu}_l p \to l^+ \Lambda K^0$ $\nu_l n \to l^- \Lambda K^+$	$-\sqrt{\frac{3}{2}}$	$\frac{-1}{3}(D + 3F)$	$\frac{-1}{\sqrt{6}}(D + 3F)$	$-\sqrt{\frac{2}{3}}(D - F)$	0	$\frac{-1}{\sqrt{6}}(D + 3F)$	$\sqrt{\frac{3}{2}}$
$\bar{\nu}_l p \to l^+ \Sigma^0 K^0$ $\nu_l n \to l^- \Sigma^0 K^+$	$\mp \frac{1}{\sqrt{2}}$	$D - F$	$\mp \frac{1}{\sqrt{2}}(D - F)$	$\mp \sqrt{2}(D - F)$	0	$\pm \frac{1}{\sqrt{2}}(D - F)$	$\pm \frac{1}{\sqrt{2}}$
$\bar{\nu}_l n \to l^+ \Sigma^- K^0$ $\nu_l p \to l^- \Sigma^+ K^+$	-1	$D - F$	0	$F - D$	$\frac{1}{3}(D + 3F)$	$D - F$	1

Table 5.2: Constant factors appearing in the hadronic current. The upper sign corresponds to the processes with antineutrino and lower with neutrino.

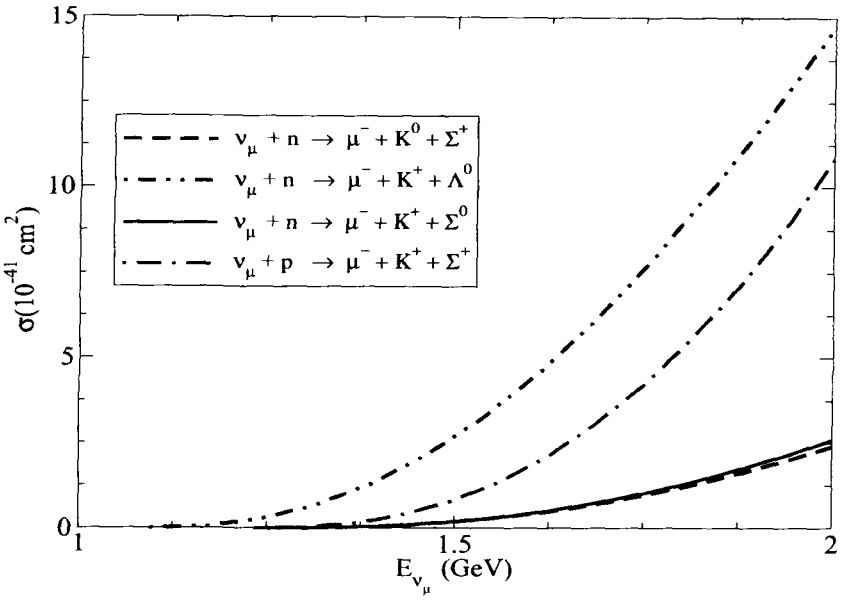

Figure 5.3: Cross section for neutrino induced $|\Delta S| = 0$ associated kaon production process.

5.3 Results and Discussion

The total scattering cross section σ has been obtained after integrating Eq. 5.4 over the kinematical variables and using Eqs.5.5-5.7 and 5.26. The cross sections for the $\nu_\mu N \to \mu^- Y K$ and $\bar{\nu}_\mu N \to \mu^+ Y \bar{K}$ processes are shown in Figs. 5.3 and 5.4, respectively. We find that the cross section for the reaction channel with a Λ in the final state are in general larger than that for the reactions where Σ is in the final state. This can be understood by looking at the relative strength of the coupling, for example the ratio of square of the couplings for the vertices $nK^0\Lambda$ to $nK^0\Sigma^0$ is $g^2_{NK\Lambda}/g^2_{NK\Sigma} \simeq 14$. Furthermore, the cross section for the Λ production is favored by the available phase space due to its small mass relative to Σ baryons.

When we compare the results of the cross sections in Fig. 5.3 for the processes $\nu_\mu p \to \mu^- \Sigma^+ K^+$ and $\nu_\mu n \to \mu^- \Lambda K^+$, we find that the cross section for the $K^+\Sigma^+$ channel is around 70% smaller at $E_\nu = 1.5$ GeV and around 25% smaller at $E_\nu = 2$ GeV in comparison to the cross section for the $K^+\Lambda$ channel. While the cross sections for the other two channels namely $\nu_\mu n \to \mu^- \Sigma^+ K^0$ and $\mu^- \Sigma^0 K^+$ are much smaller than the $K^+\Lambda$ cross section.

In Fig. 5.4 we have shown the cross section for antineutrino induced production processes where one may notice that unlike the neutrino induced processes the chan-

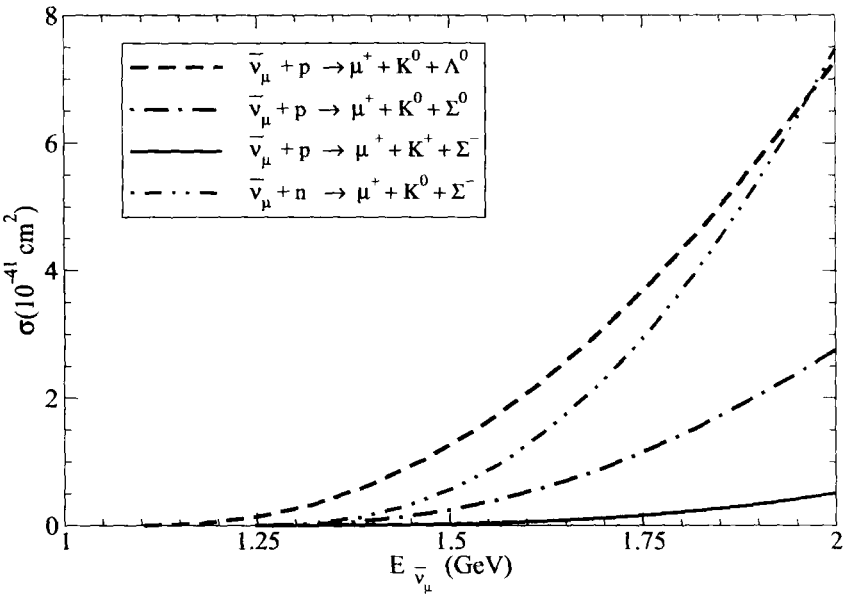

Figure 5.4: Cross section for antineutrino induced $|\Delta S| = 0$ associated kaon production process.

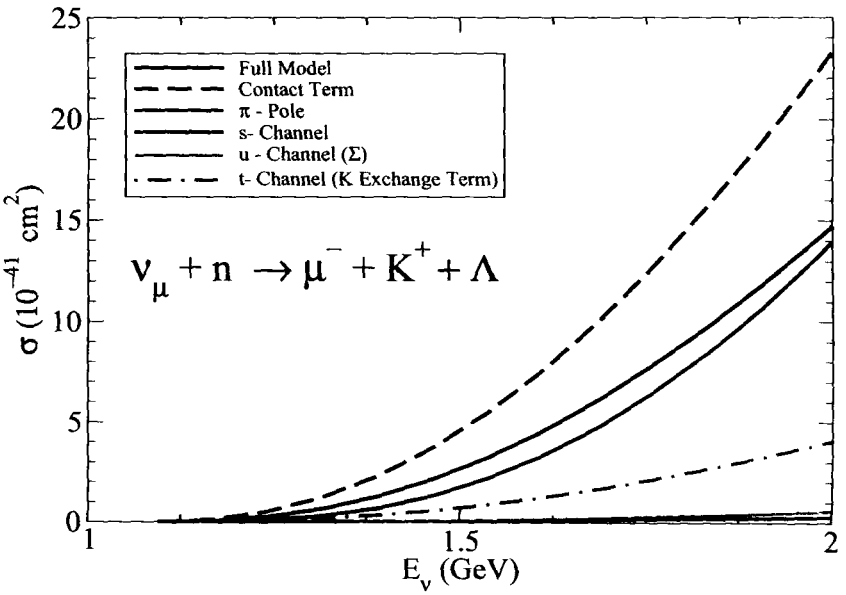

Figure 5.5: Cross section for the $\nu_\mu + n \rightarrow \mu^- + K^+ + \Lambda$ process explicitly showing the Feynman diagrams involved.

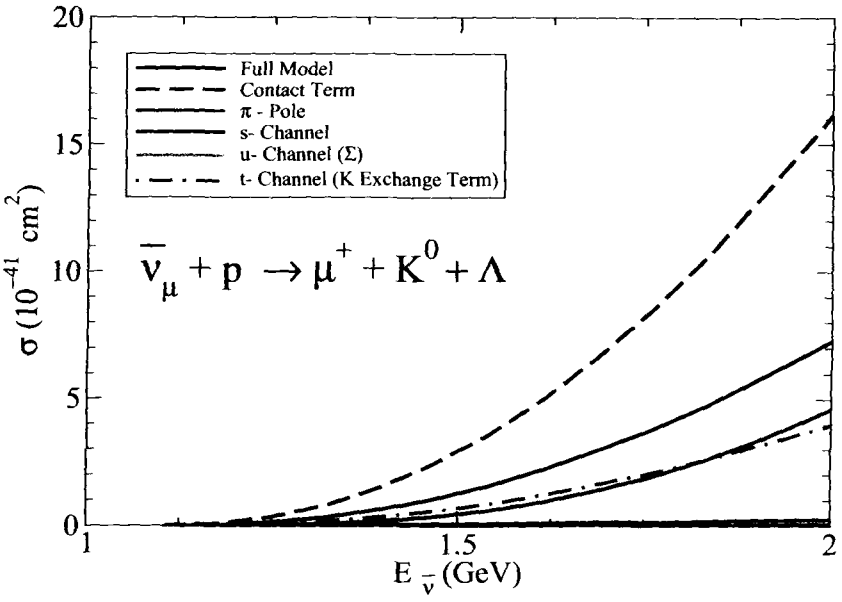

Figure 5.6: Cross section for the $\bar{\nu}_\mu + p \rightarrow \mu^+ + K^0 + \Lambda$ process explicitly showing the Feynman diagrams involved.

nel with Λ in the final state is not very dominating. For example, we find that at low energies say $E_{\bar{\nu}_\mu} \sim 1.5$ GeV the cross section for $\bar{\nu}_\mu p \rightarrow \mu^+ K^0 \Lambda$ is around 55% larger than the cross section for $\bar{\nu}_\mu n \rightarrow \mu^+ K^0 \Sigma^-$, while around 2 GeV the production cross section for $\bar{\nu}_\mu p \rightarrow \mu^+ K^0 \Lambda$ is comparable with that of $\bar{\nu}_\mu n \rightarrow \mu^+ K^0 \Sigma^-$. The cross section for the reaction $\bar{\nu}_\mu p \rightarrow \mu^+ K^0 \Sigma^0$ is around 40% smaller than the cross section for $K^0 \Lambda$ channel at $E_{\bar{\nu}_\mu} = 2$ GeV, whereas $\bar{\nu}_\mu p \rightarrow \mu^+ K^+ \Sigma^-$ cross section is about 10% to the cross section of $K^0 \Lambda$ channel. We have also compared our results of the cross section with the results of Shrock et al. [45]. The results are tabulated in Table 5.3. We find that our results are about 2 times larger than the results of Shrock et al. [45].

From Figs. 5.3 and 5.4 we notice that the neutrino induced reactions are dominant source of K^+ production where as antineutrino induced reactions favors the K^0 production. For example at $E_\nu = 1.5$ GeV, $\sigma(K^+) \equiv \sigma(\Lambda K^+) + \sigma(\Sigma^0 K^+) + \sigma(\Sigma^+ K^+)$, is around $3.7 \times 10^{-41} cm^2$, while $\sigma(K^0) = \sigma(\Sigma^+ K^0)$ is around 0.18×10^{-41} cm^2. At $E_\nu = 2$ GeV, $\sigma(K^+)$ is $\sim 29 \times 10^{-41}$ cm^2 while $\sigma(K^0)$ is about 2×10^{-41} cm^2. Similarly, for the antineutrino induced reactions at $E_\nu = 2$ GeV, $\sigma(K^0) \equiv \sigma(\Lambda K^0) + \sigma(\Sigma^0 K^0) + \sigma(\Sigma^- K^0)$, is around 11×10^{-41} cm^2 whereas $\sigma(K^+) = \sigma(\Sigma^- K^+)$ is about 0.5×10^{-41} cm^2.

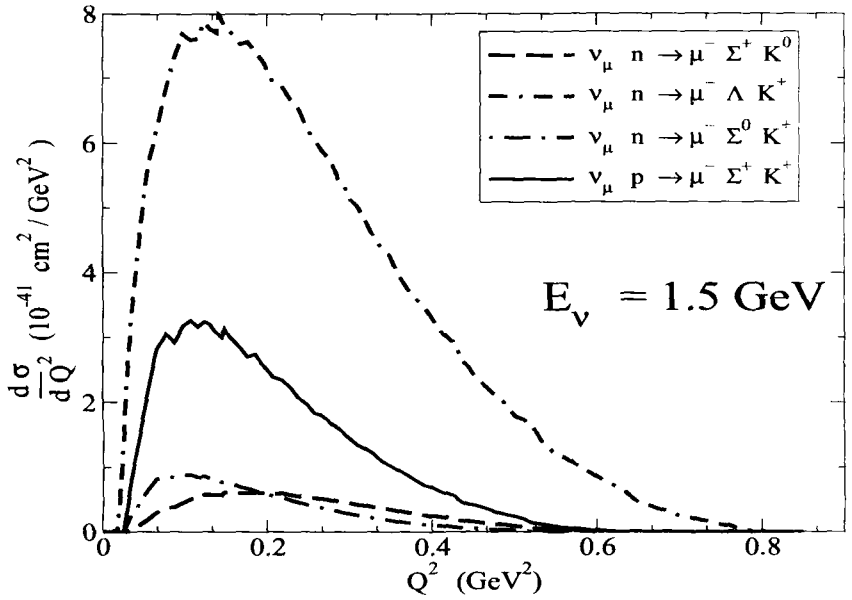

Figure 5.7: Q^2- distribution for the ν_μ induced $|\Delta S| = 0$ associated kaon production process.

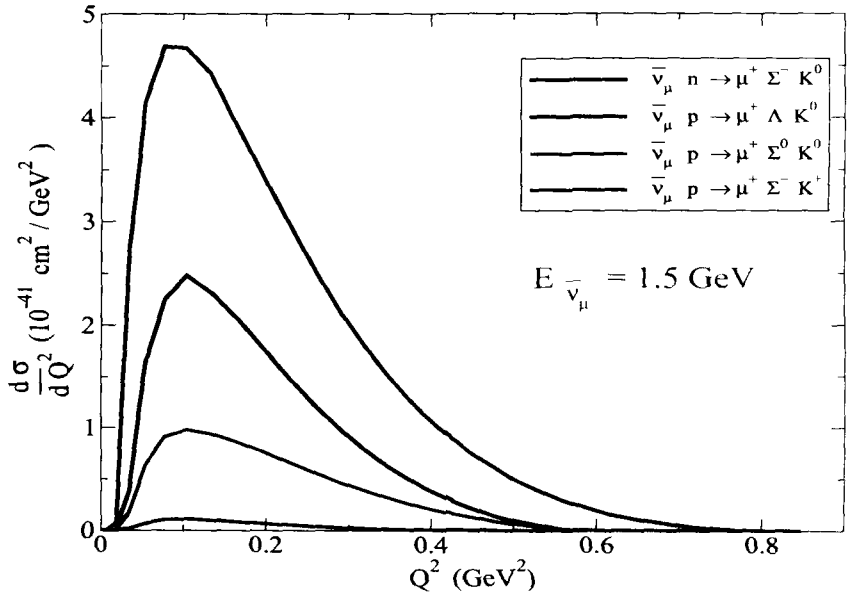

Figure 5.8: Q^2-distribution for the $\bar{\nu}_\mu$ induced $|\Delta S| = 0$ associated kaon production process.

Process		$\sigma \times 10^{-41} cm^2$		
		E_{ν_μ} =1.2 GeV	E_{ν_μ} =1.6 GeV	E_{ν_μ} =2 GeV
$\nu_\mu n \to \mu^- \Lambda K^+$	Present Work	0.2	4.0	15.0
	Shrock et al. [45]	0.14	1.8	5.4
$\bar{\nu}_\mu p \to \mu^+ \Lambda K^0$	Present Work	0.1	2.0	8.0
	Shrock et al. [45]	0.12	1.4	4.1

Table 5.3: Comparison of total cross section for the CC ν_μ/ν_μ induced $K\Lambda$ channel with the results of Shrock et al. [45].

One may notice from Table 5.3 that our results for the cross sections are quite different from the results of Ref. [45]. This difference may be due to the additional Feynman diagrams like contact term and π in flight term taken in our approach which is absent in their work besides some minor differences like choosing the value of axial dipole mass M_A=1.05GeV vs 0.95GeV, etc. In Fig. 5.5 we have presented the results for the total cross section σ for $\nu_\mu + n \to \mu^- + K^+ + p$ process, and in and in Fig.5.6 the results are presented for $\bar{\nu}_\mu + p \to \mu^+ + K^0 + n$ process. In these figures the contribution of individual channel(like s-channel, u-channel, contact term, etc.) as well as the results of "Full Model" (when all the diagrams are taken together) are shown. We find that the contribution to the total cross section from the contact term is the largest followed by s-channel and t-channel(K-exchange) terms and the results from the "Full Model" is smaller than the results obtained only with the contact term. This may be due to the destructive interference of the different amplitudes contributing to the cross section.

In Figs. 5.7 and 5.8, we have presented the results for Q^2 distribution at $E_{\nu_\mu,\bar{\nu}_\mu}$ =1.5 GeV. In the case of Q^2 distribution for ν_μ induced process shown in Fig. 5.7, we find that except for $\nu_\mu n \to \mu^- \Sigma^+ K^0$ channel the other channels producing K^+ in the final state peak at low Q^2. The Q^2 distribution for antineutrino induced reaction as shown in Fig. 5.8 is more forward peaked than corresponding to those of neutrino induced reactions.

In Figs. 5.9 and 5.10, we present the results for the kaon energy distribution $(d\sigma/dE_k)$ at the neutrino and antineutrino energies of 1.5 GeV. Here also we find that, kaon energy distribution for antineutrino induced reactions is more forward peaked than the kaon energy distribution in the case of neutrino induced processes. In Figs. 5.11 and 5.12 we present the results for the muon energy distribution $(d\sigma/dE_\mu)$ for neutrino and antineutrino induced processes. We find that the muon energy distributions are more forward peaked in neutrino induced reactions as compared to

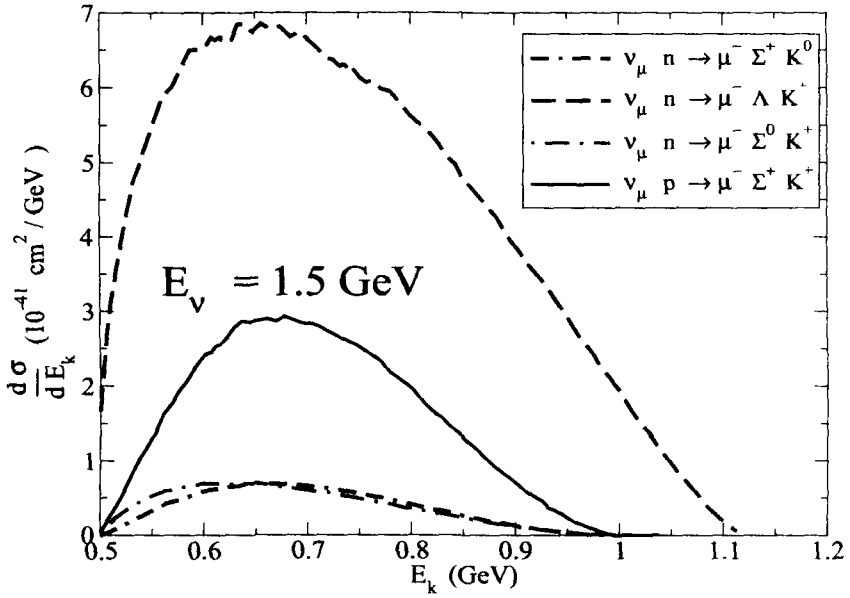

Figure 5.9: E_k- distribution for the ν_μ induced $|\Delta S| = 0$ associated kaon production process.

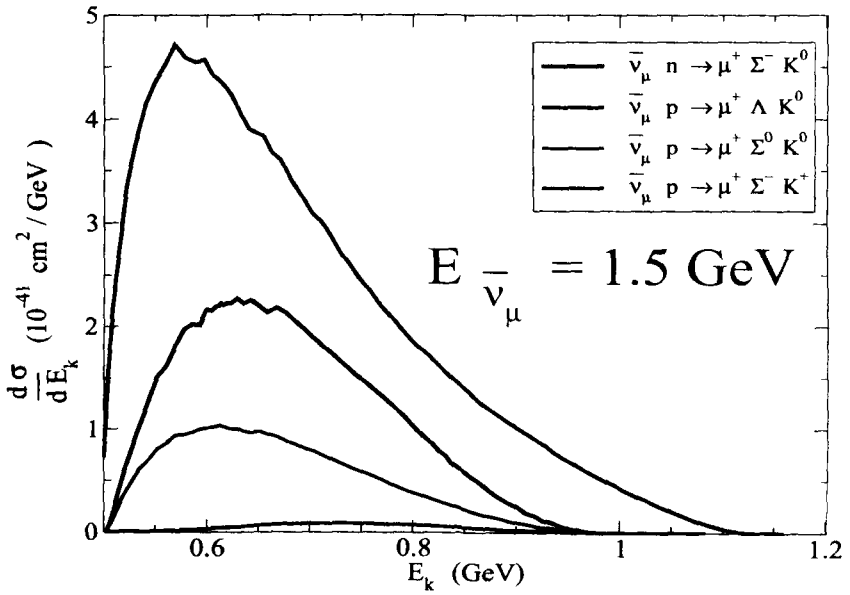

Figure 5.10: E_k- distribution for the $\bar{\nu}_\mu$ induced $|\Delta S| = 0$ associated kaon production process.

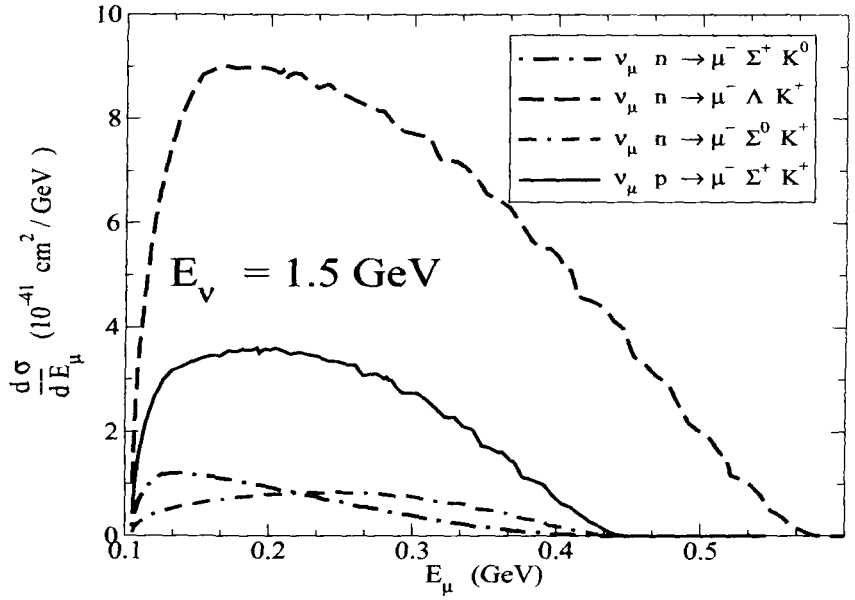

Figure 5.11: Lepton energy distribution for the ν_μ induced $|\Delta S| = 0$ associated kaon production process.

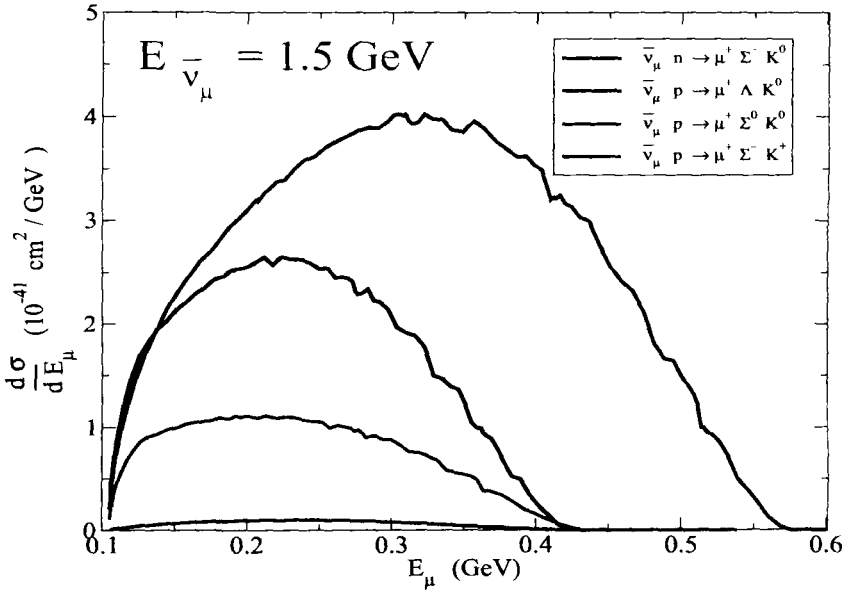

Figure 5.12: Lepton energy distribution for the $\bar{\nu}_\mu$ induced associated kaon production process.

the antineutrino induced reactions.

We must point out that in the present work, resonances contributing to the associated particle production processes have not been considered. This we plan to include in our future studies. In the next chapter we present the summary of our results and conclude our findings.

Chapter 6

Conclusions

Neutrino oscillation physics has entered into an era of precision physics in which both theoretically and experimentally enormous efforts are going on for better understanding of the oscillation physics as well as for understanding the hadron physics as these neutrino oscillation experiments are also providing cross section measurements for many quasielastic and inelastic processes induced by the neutrino and antineutrino on nuclear targets. These recent cross section measurements are available mostly for $\Delta S = 0$ processes in nonstrange sector. In strange sector neutrino Monte-Carlo generators use the results of older work available in literature for $\Delta S = 0$ and $\Delta S = 1$ processes. However, with the availability of high intensity neutrino and antineutrino beams in present generation neutrino oscillation experiments the possibility of experimentally studying, with better statistics, the weak production of strange particles through $\Delta S = 0$ and $\Delta S = 1$ processes induced by neutrinos and antineutrinos from nuclear targets are being made. On the theoretical side there are very few works available in literature. However, specific and precise knowledge about these processes would be very important for the analysis of future and ongoing neutrino oscillation experiments and these processes as well would facilitate in understanding of hadron structure and their properties. In the present thesis we performed theoretical calculations for some of the channels which are not well studied like single kaon production, eta production and associated particle production processes. These studies are performed for neutrino/antineutrino induced reaction off free nucleon targets.

In Chapter-1, we briefly introduced neutrinos and their fundamental properties and outlined the importance of strange quarks in the sector of inelastic processes. The study of these processes have been made by developing a microscopic model

which is based on the $SU(3)$ chiral perturbation theory(for nonresonant terms) which provides us model independent prediction for the cross sections. The basic parameters of the model are the pion decay constant f_π, Cabibbo angle, the proton and neutron magnetic moments, and the axial vector coupling constants for the baryons octet, D and F, obtained from the analysis of the hyperon semileptonic decays.

In Chapter-2, we briefly introduced Chiral Perturbation Theory, the basic ingredients of the model and the various coupling constants. Using this microscopic model we have studied single kaon/antikaon production off nucleons induced by neutrinos/antineutrinos. For the neutrino induced single kaon production processes this model would be quite reliable at low and intermediate energies given the absence of $S = 1$ baryonic resonances in the s-channel. We presented the results for the total scattering cross section σ, kaon energy distribution and Q^2 distribution. We also discussed the results of the contributions from the different Feynman diagrams like contact, kaon pole, u-channel $Cr\Sigma$, $Cr\Lambda$, pion and eta in flight terms to the total cross section. We found the contribution of kaon pole term to be almost negligible at the studied energies. We observed the relevance of the contact term, not included in earlier calculations by Dewan et al. [47]. In fact this term has been found to be very dominant followed by the u-channel diagram with a Λ intermediate state and the π exchange term. We have found that although the total scattering cross section obtained for the neutrino induced processes are around two orders of magnitude smaller than that of cross section for pion production for neutrino spectra such as those of ANL or MiniBooNE, nevertheless, the cross sections are large enough to be measured, for instance, with the expected MINERνA and T2K fluxes and could have been well measured at MiniBooNE. Furthermore, we found that due to higher threshold of the associated kaon production, the reactions we have studied are the dominant source of kaons for a wide range of energies, and thus their study is important for some low energy experiments and for the atmospheric neutrino flux. For the antineutrino induced single antikaon production we extended our model to include the lowest lying decuplet baryon e.g. in the case of inelastic production of pions the cross section is dominated by the decuplet resonance $\Delta(1232)$. Our model is inspired by the model that predict pion production in the resonance region. The background terms were obtained from the chiral Lagrangian and the resonant mechanism that include the $\Sigma^*(1385)$ have been included in the model. We understand that the presently studied process is the dominant source of antikaons for a wide range of energies. We found that the cross sections are clearly dominated by the nonresonant terms, and in this case also the largest contribution comes from the contact term. More specifically, we observed destructive interference that leads to a total cross section smaller than obtained from the contact term alone. There

is almost negligible contribution from $\Sigma^*(1385)$ channel. For antikaon production we found that the cross sections are around two orders of magnitude smaller than that for pion production for antineutrino fluxes used in the MiniBooNE experiment. Nonetheless, the study may be useful in the analysis of antineutrino experiments at MINERνA, NOνA, T2K and others with high statistics and/or higher antineutrino energies.

In Chapter-3, we have used the model discussed in Chapter-2 to study the single kaon production off nucleons induced by electrons/positrons. This study is quite important as the strangeness conserving electromagnetic reactions have a higher energy threshold for $\bar{K}(K)$ production and with the availability of high luminosity beams at TJNAF and Mainz there exists a chance of observing single kaon production. For the electron induced process, we have also considered the contribution from the $\Sigma^*(1385)$ resonance term, the weak couplings for which has been obtained using SU(3) symmetry from those of the well established $\Delta(1232)$ resonance. We observed that the cross sections, although small, could be measured at current experimental facilities. Furthermore, our results could facilitate the study of Q^2 dependence of the hyperon/nucleon weak form factors.

In Chapter-4, we have studied charged current neutrino/antineutrino induced η production off free nucleons. We considered s- and u-channel Born diagrams and used the prescription discussed in Chapter-2. In addition to that, we considered $S_{11}(1535)$ and $S_{11}(1650)$ resonances as it is well known from electro- and photo-induced processes that eta production is dominated by $S_{11}(1535)$ resonance. To obtain precise value for the vector part of the N-S_{11} transition form factor, we studied photon induced eta production to fix the electromagnetic form factors by comparing it with the available results for the scattering cross section from Crystal Ball experiment [136]. The vector form factors of the N-S_{11} transition have been obtained from the helicity amplitudes extracted in the analysis of world pion photo- and electro-production data using the unitary isobar model [140]. The properties of the axial N-S_{11} transition current are basically unknown but assuming the pion-pole dominance of the pseudoscalar form factor, together with PCAC and fixed the axial coupling using the empirical $N^* \to N\pi$ partial decay width. We have found that $N^*(1535)$ resonance is dominant while the contribution of $N^*(1650)$ to the total cross section is small. Furthermore, we have observed that the contribution from nonresonant diagrams are also non-negligible. Moreover, the contribution from nonresonant diagrams in the case of neutrino induced process is higher than in the corresponding antineutrino induced processes. We observed that the cross sections are large enough to be measured in experiments like T2K, NOνA and MINERνA. This study may be quite useful in the analysis of neutrino oscillation physics.

In Chapter-5, we have studied associated strange particle production processes from nucleons induced by neutrino and antineutrino. In the present work we have only considered Born-diagrams based on the $SU(3)$ chiral Lagrangian discussed in Chapter-2. In this case also we found that the contribution from the contact term is largest followed by s-channel nucleon pole and meson exchange term. The cross section for the reaction $\nu_\mu n \to \mu^- \Lambda K^+$ is largest in comparison to the cross section where we have Σ in the final state, and this is understood because of the coupling as well as the available phase space. We presented the results for Q^2 distribution and kaon energy distribution. Furthermore, we also discussed total K^+ vs K^0 production, i.e. by taking into account all the reaction channels studied in Chapter-5 those have K^+ or K^0 in the final state, and we found that the neutrino induced reactions are dominant source of K^+ production while the antineutrino favors K^0 production.

Our future plan is to include resonances in the associated particle production processes. We also plan to study these processes for nucleons bound inside the nuclear targets as all the neutrino/antineutrino experiments are using heavy nuclear targets to get significant number of events.

Appendices

Appendix A

$\Delta(1232)$ Decay Width

A.1 The Lagrangian N$\Delta\pi$

We start with the following interaction Lagrangian for the diagram shown in Fig. A.1

$$\mathcal{L}_{N\Delta\pi} = \frac{f^*}{m_\pi}\bar{\Psi}_\mu(\tilde{\mathbf{T}}^\dagger \cdot \partial^\mu\vec{\phi})\,\Psi \tag{A.1}$$

where $\bar{\Psi}_\mu$ is 4-plet of of Rarita-Schwinger field for Δs and

$$\bar{\Psi}_\mu \equiv \left(\begin{array}{cccc} \bar{\Delta}^{++} & \bar{\Delta}^{+} & \bar{\Delta}^{0} & \bar{\Delta}^{-} \end{array} \right)_\mu \tag{A.2}$$

Ψ is the nucleon doublet,

$$\Psi \equiv \left(\begin{array}{c} p \\ n \end{array} \right). \tag{A.3}$$

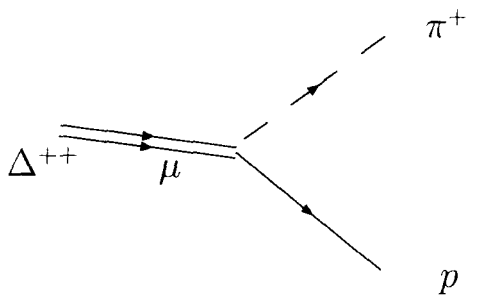

Figure A.1: Feynman diagram for the Δ^{++} decay

$\vec{\phi}$ is the triplet of pion fields and $\tilde{\mathbf{T}}^\dagger$ is a collection of three 4×2 matrices (one matrix for each pion field) that connects the correct nucleon field with the right Rarita-Schwinger field of the Δs; each 4×2 matrix is basically a Clebsch-Gordan array. Expanding the dot product in the spherical basis, we may write

$$\mathcal{L}_{N\Delta\pi} = \frac{f^*}{m_\pi}\bar{\Psi}_\mu(T_0^\dagger\partial^\mu\phi_0 - T_{+1}^\dagger\partial^\mu\phi_{-1} - T_{-1}^\dagger\partial^\mu\phi_{+1})\Psi + \text{h.c.} \tag{A.4}$$

The spherical components are related to the cartesian ones as:

$$\phi_0 \equiv \phi_z \tag{A.5}$$

$$\phi_{-1} \equiv \frac{1}{\sqrt{2}}(\phi_x - i\phi_y) \tag{A.6}$$

$$\phi_{+1} \equiv -\frac{1}{\sqrt{2}}(\phi_x + i\phi_y) = -\phi_{-1}^\dagger \tag{A.7}$$

The field ϕ_0 annihilates and creates a neutral pion π^0. $\phi_{-1}/\phi_{+1}^\dagger$ creates a π^- and annihilates a π^+. And finally, $\phi_{-1}^\dagger/\phi_{+1}$ creates a π^+ and annihilates a π^-.

We have taken the following normalization for the isospin transition operator $T_\lambda^\dagger$

$$\left\langle \frac{3}{2}, M|T_\lambda^\dagger|\frac{1}{2}, m\right\rangle = (1, \frac{1}{2}, \frac{3}{2}|\lambda, m, M) \tag{A.8}$$

with λ a spherical basis index. For $\Delta^{++} \longrightarrow p + \pi^+$, the Lagrangian may be written as

$$\begin{aligned}
\mathcal{L} &= -\frac{f^*}{m_\pi}\bar{\Psi}_\mu T_{+1}^\dagger \Psi\ \partial^\mu\phi_{-1} + \text{h.c} \\
&= -\frac{f^*}{m_\pi}\bar{\Psi}_\mu \begin{pmatrix} (1,\frac{1}{2},\frac{3}{2}|1,\frac{1}{2},\frac{3}{2}) & (1,\frac{1}{2},\frac{3}{2}|1,\frac{-1}{2},\frac{3}{2}) \\ (1,\frac{1}{2},\frac{3}{2}|1,\frac{1}{2},\frac{1}{2}) & (1,\frac{1}{2},\frac{3}{2}|1,\frac{-1}{2},\frac{1}{2}) \\ (1,\frac{1}{2},\frac{3}{2}|1,\frac{1}{2},\frac{-1}{2}) & (1,\frac{1}{2},\frac{3}{2}|1,\frac{-1}{2},\frac{-1}{2}) \\ (1,\frac{1}{2},\frac{3}{2}|1,\frac{1}{2},\frac{-3}{2}) & (1,\frac{1}{2},\frac{3}{2}|1,\frac{-1}{2},\frac{-3}{2}) \end{pmatrix} \Psi\ \partial^\mu\phi_{-1} + \text{h.c} \\
&= -\frac{f^*}{m_\pi}\bar{\Psi}_\mu \begin{pmatrix} 1 & 0 \\ 0 & \frac{1}{\sqrt{3}} \\ 0 & 0 \\ 0 & 0 \end{pmatrix} \begin{pmatrix} p \\ n \end{pmatrix} .\ \partial^\mu\phi_{-1} + \text{h.c} \\
&= -\frac{f^*}{m_\pi}\partial^\mu\phi_{-1}\left(\bar{\Delta}_\mu^{++}p + \frac{1}{\sqrt{3}}\bar{\Delta}_\mu^{+}n\right) + \text{h.c}
\end{aligned} \tag{A.9}$$

For the decay of the Δ^{++}, we need the Hermitian conjugate vertex of Eq. A.9, i.e:

$$\mathcal{L}_{\text{h.c.}} = -\frac{f^*}{m_\pi}\partial^\mu \phi^\dagger_{-1}\left(\bar{p}\,\Delta^{++}_\mu + \frac{1}{\sqrt{3}}\bar{n}\,\Delta^{+}_\mu\right) \tag{A.10}$$

Applying the Feynman rules, we obtain the transition matrix element, as corresponding to Fig. A.1

$$\mathcal{M} = \frac{if^*}{m_\pi} k^\mu_\pi\, \bar{u}(\vec{p}')u_\mu(\vec{p}_\Delta) \tag{A.11}$$

and the square of the transition matrix element is

$$|\mathcal{M}|^2 = \left(\frac{f^*}{m_\pi}\right)^2 k^\mu_\pi k^\nu_\pi\, \bar{u}(\vec{p}')u_\mu(\vec{p}_\Delta)\bar{u}_\nu(\vec{p}_\Delta)u(\vec{p}') \tag{A.12}$$

If now we sum over the final spin of the proton and average over the initial spin of the Δ^{++}, we get

$$\begin{aligned}\bar{\Sigma}\Sigma|\mathcal{M}|^2 &= \frac{1}{2J_\Delta+1}\sum_{spins}\left(\frac{f^*}{m_\pi}\right)^2 k^\mu_\pi k^\nu_\pi\, \bar{u}(\vec{p}')u_\mu(\vec{p}_\Delta)\bar{u}_\nu(\vec{p}_\Delta)u(\vec{p}') \\ &= \frac{1}{4}\left(\frac{f^*}{m_\pi}\right)^2 k^\mu_\pi k^\nu_\pi\, \mathtt{Tr}\left[\mathcal{P}_{\mu\nu}(p_\Delta)\,(\not{p}' + M)\right]\end{aligned} \tag{A.13}$$

where $\mathcal{P}^{\mu\nu}(p_\Delta)$ is the spin $\frac{3}{2}$ projection operator, given by:

$$\mathcal{P}^{\mu\nu}(p_\Delta) = -\,(\not{p}_\Delta + M_\Delta)\left[g^{\mu\nu} - \frac{1}{3}\gamma^\mu\gamma^\nu - \frac{2}{3}\frac{p^\mu_\Delta p^\nu_\Delta}{M^2_\Delta} + \frac{1}{3}\frac{p^\mu_\Delta\gamma^\nu - p^\nu_\Delta\gamma^\mu}{M_\Delta}\right] \tag{A.14}$$

Using Eqs. A.13 and A.14, we have:

$$\begin{aligned}\bar{\Sigma}\Sigma|\mathcal{M}|^2 &= \left(\frac{f^*}{m_\pi}\right)^2\left(\frac{2}{3M^2_\Delta}(p^2_\Delta - p_\Delta\cdot k_\pi)(p_\Delta\cdot k_\pi)^2\right. \\ &+ \left.\frac{2M}{3M_\Delta}(p_\Delta\cdot k_\pi)^2 - \frac{2}{3}MM_\Delta m^2_\pi - \frac{2}{3}m^2_\pi(p^2_\Delta - p_\Delta\cdot k_\pi)\right)\end{aligned} \tag{A.15}$$

where $|\mathcal{M}|^2$ is evaluated in the Δ rest frame and it does not contain any angular dependence. Now using the general expression for partial decay width

$$d\Gamma_{\Delta\to p\pi} = \frac{1}{2M_\Delta}\frac{d^3k_p}{2E_p}\frac{d^3k_\pi}{2E_\pi}\,(2\pi)^4\,\delta^4(p_\Delta - k_p - k_\pi)\bar{\sum}\sum|\mathcal{M}|^2 \tag{A.16}$$

along with Eq. 4.17 we obtain the expression for $\Gamma(\Delta \to p\pi)$ decay width as

$$\begin{aligned}\Gamma &= \frac{1}{32\pi^2 M_\Delta^2} \cdot 4\pi \cdot |\vec{k}_\pi| \left(\frac{f^*}{m_\pi}\right)^2 \cdot \left(\frac{2}{3}(M_\Delta^2 - M_\Delta E_\pi)E_\pi^2 \right. \\ &+ \left. \frac{2}{3}MM_\Delta E_\pi^2 - \frac{2}{3}MM_\Delta m_\pi^2 - \frac{2}{3}m_\pi^2(M_\Delta^2 - M_\Delta E_\pi)\right) \end{aligned} \tag{A.17}$$

where E_π is

$$E_\pi = \frac{M_\Delta^2 + m_\pi^2 - M^2}{2M_\Delta} \tag{A.18}$$

and

$$|\vec{k}_\pi| = \frac{\lambda^{1/2}(M_\Delta^2, M^2, m_\pi^2)}{2M_\Delta} \tag{A.19}$$

where $\lambda(x, y, z)$ is the Callen lambda function. Putting the values for the rest mass of the particles we obtain $\Gamma \sim 112$ MeV.

A.2 Width from Chiral Lagrangian

Let us again take the example of $\Delta^{++} \to p + \pi^+$. The vertex for such transition is given by following Eq. 2.25:

$$\mathcal{L} = -\sqrt{2}\,\frac{\mathcal{C}}{f_\pi}\,\bar{\Delta}_\mu^{++}\, p\, \partial^\mu \pi_+ + \text{h.c.} \tag{A.20}$$

Comparing Eq. A.10 with Eq. A.20, we get a relation between the two parameters as:

$$\frac{f^*}{m_\pi} \to \sqrt{2}\frac{\mathcal{C}}{f_\pi} \tag{A.21}$$

Using the above relation together with the value of width ($\Gamma \sim 112$ MeV) as obtained from the Eq. A.17, we get $\mathcal{C} \sim 1.0$.

A.3 Relation between $\mathcal{C}$ and $C_5^A(0)$

In the previous section we have obtained the relation between $\mathcal{C}$ and f^*, namely:

$$\mathcal{C} = \frac{f^* f_\pi}{m_\pi \sqrt{2}} = \frac{2.14 \times 93}{\sqrt{2} \times 139} = 1.012 \tag{A.22}$$

Now we are going to obtain the relation between $\mathcal{C}$ and $C_5^A(0)$. For the weak transition $n - \Delta^+$ we have the following vertex from the Lagrangian:

$$\mathcal{L}_{weak} = \frac{\mathcal{C} g V_{ud}}{\sqrt{6}} \bar{\Delta}_+^\beta \, n \, W_\beta^+ \tag{A.23}$$

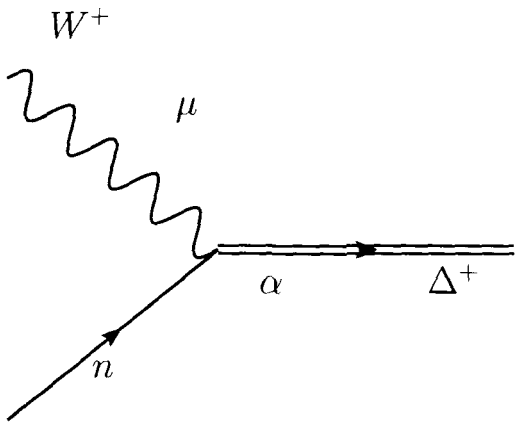

Figure A.2: Weak $n - \Delta^+$ transition vertex

The current for the vertex shown in Fig. A.2 may be written as:

$$\begin{aligned} \langle \Delta^+; p_\Delta = p + q | j_{cc+}^\mu(0) | n; p \rangle &= \bar{u}_\alpha(\vec{p}_\Delta) \frac{i\mathcal{C} g V_{ud}}{\sqrt{6}} u(\vec{p}) g^{\alpha\mu} \\ &= \frac{ig}{2\sqrt{2}} \frac{2\mathcal{C} V_{ud}}{\sqrt{3}} \bar{u}^\mu(\vec{p}_\Delta) u(\vec{p}) \end{aligned} \tag{A.24}$$

Taking out $\frac{ig}{2\sqrt{2}}$ as it has been used explicitly in the definition of hadronic current (in order to write $\mathcal{M} = \frac{G_F}{\sqrt{2}} j_{leptonic}^\mu j_\mu^{hadronic}$), we may write:

$$\langle \Delta^+; p_\Delta = p + q | j_{cc+}^\mu(0) | n; p \rangle = \frac{2\mathcal{C} V_{ud}}{\sqrt{3}} \bar{u}^\mu(\vec{p}_\Delta) u(\vec{p}) \tag{A.25}$$

We compare our parameterizations with the available parameterization like in Ref. [95]. According to this parameterization, the matrix element reads, when one takes for $\Gamma^{\alpha\mu}(p,q)$ only the leading contribution $C_5^A g^{\alpha\mu}$:

$$\begin{aligned} \langle \Delta^+; p_\Delta = p + q | j_{cc+}^\mu(0) | n; p \rangle &= V_{ud} \bar{u}_\alpha(\vec{p}_\Delta) C_5^A(0) g^{\alpha\mu} u(\vec{p}) \\ &= V_{ud} C_5^A(0) \bar{u}^\mu(\vec{p}_\Delta) u(\vec{p}) \end{aligned} \tag{A.26}$$

Comparing Eqs. A.24 and A.25, we get the following result:

$$\frac{2\mathcal{C}}{\sqrt{3}} = C_5^A(0) \Longrightarrow \mathcal{C} = \frac{\sqrt{3}}{2} C_5^A(0) = \frac{\sqrt{3}}{2} \times 1.15 = 0.996 \sim 1.0 \tag{A.27}$$

Appendix B

Weak Magnetism in Hadronic Current

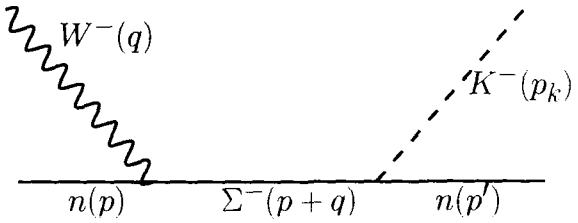

Figure B.1: s-channel diagram for $\bar{\nu}n \to l^+K^-n$ process.

We start with a specific case of $\bar{\nu}n \to l^+K^-n$, the Lagrangian for the vertices $n\Sigma^-W^-$ and $n\Sigma^-K^-$ which are obtained from the chiral Lagrangian

$$\begin{aligned}
\mathcal{L}_{n\Sigma^-K^-} &= \frac{-i}{\sqrt{2}f_\pi}\bar{u}_n(p')\gamma_\nu\gamma_5(D-F)\partial^\nu K_+\, u_{\Sigma^-}(p) + \text{h.c.} \\
\mathcal{L}_{n\Sigma^-W^-} &= \frac{ig}{2\sqrt{2}}V_{us}\bar{u}_\Sigma(p)\,(\gamma^\mu\gamma^5(D-F)+\gamma^\mu)u_n(p)\,W_\mu^- + \text{h.c.} \qquad \text{(B.1)}
\end{aligned}$$

Using the above Lagrangian the hadronic current may be written as,

$$\begin{aligned}
&\frac{-i}{\sqrt{2}f_\pi}\bar{u}_n(p')\gamma_\nu\gamma_5(D-F)\partial^\nu K_+\frac{i}{\not p+\not q-M_\Sigma}\frac{ig}{2\sqrt{2}}V_{us}(\gamma^\mu\gamma^5(D-F)+\gamma^\mu)u_n(p) \\
= \; &-V_{us}\frac{g}{4f_\pi}(D-F)\bar{u}_n(p')\not p_k\gamma_5\frac{\not p+\not q+M_\Sigma}{(p+q)^2-M_\Sigma^2}(\gamma^\mu+\gamma^\mu\gamma^5(D-F))u_n(p) \qquad \text{(B.2)}
\end{aligned}$$

Now we try to incorporate the kaon pole at weak vertex,

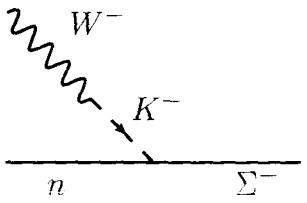

Figure B.2: Kaon pole dominance at weak vertex

The Lagrangian for the additional piece is,

$$\mathcal{L}_{W^-K^-} = \frac{-i}{2}\partial^\alpha K_+ f_\pi g V_{us} W_-^\alpha \tag{B.3}$$

With the insertion of the pole term we get,

$$\frac{-i(D-F)}{\sqrt{2}f_\pi}\bar{u}_n(p')\gamma_\nu\gamma_5\partial^\nu K_+ \frac{i}{\not p + \not q - M_\Sigma}\frac{ig}{2\sqrt{2}}V_{us}\left(\gamma^\mu + (D-F)\gamma^\mu\gamma^5\right.$$
$$\left.-(D-F)\frac{q^\mu}{q^2 - {M_k}^2}\not q\gamma^5\right) u_n(p) \tag{B.4}$$

We next try to incorporate the weak magnetism in the above current as we did for the $\Delta S = 1$ production of K-production. For this we took the prescription given in the works of Cabbibo et al. [93] and has been depicted in Fig. B.3,

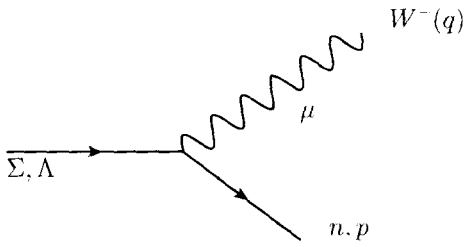

Figure B.3: Semileptonic decays of hyperons

The weak part of hadronic current following Cabibbo et al. [93] is written as

$$\bar{u}_N(\vec{p}_N)\left(O_\mu^V + O_\mu^A\right) u_\Sigma(\vec{p}_\Sigma).$$

for the semileptonic decays of hyperon Σ, Λ. O_μ^V and O_μ^A are vector and axial-vector currents. Here we must point out that we have used a different convention from

Cabbibo model [93] and to distinguish it with our model we put a (sub)superscript c where it differs from our conventions

$$\begin{aligned} O_\mu^{V(c)} &= f_1\gamma_\mu + \frac{f_2}{M}\sigma^c_{\mu\nu}q^\nu + \frac{f_3}{M}q_\mu \\ O_\mu^{V(c)} &= g_1\gamma_\mu\gamma_5^c + \frac{g_2}{M}\sigma^c_{\mu\nu}\gamma_5^c q^\nu + \frac{g_3}{M}\gamma_5^c q_\mu. \end{aligned} \tag{B.5}$$

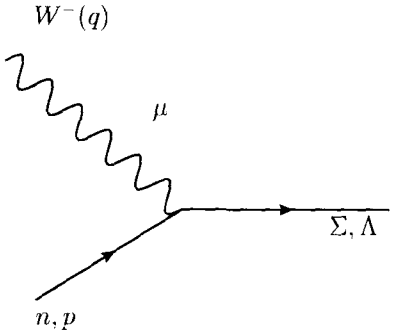

Figure B.4: Weak hyperon production. The conjugate diagram of Fig. B.3

To match the expressions with our conventions the relationships among the different terms are, $\gamma_c^5 = -\gamma^5$, $\sigma_c^{\mu\nu} = -i\sigma^{\mu\nu}$ and $M_p \sim M$. Therefore, with these changes Eq. B.5 may be written as,

$$\begin{aligned} O_\mu^V &= f_1\gamma_\mu - i\frac{f_2}{M}\sigma_{\mu\nu}q^\nu + \frac{f_3}{M}q_\mu \\ O_\mu^A &= -g_1\gamma_\mu\gamma_5 + i\frac{g_2}{M}\sigma_{\mu\nu}\gamma_5 q^\nu - \frac{g_3}{M}\gamma_5 q_\mu \end{aligned} \tag{B.6}$$

The Hermitian conjugate of it will give us the current which is of our interest i.e. current for weak hyperon production,

$$\bar{u}_\Sigma(\vec{p}_\Sigma)\gamma^0\left(O_\mu^V + O_\mu^A\right)^\dagger\gamma^0 u_N(\vec{p}_N) \tag{B.7}$$

Using the properties of Dirac gamma matrixes,

$$\begin{aligned} \gamma_\mu^\dagger &= \gamma^0\gamma_\mu\gamma^0 \\ \sigma_{\mu\nu}^\dagger &= \gamma^0\sigma_{\mu\nu}\gamma^0 \\ \gamma_5^\dagger &= \gamma_5 \\ [\sigma_{\mu\nu}, \gamma_5] &= 0 \end{aligned} \tag{B.8}$$

one can easily obtain the following expressions:

$$\gamma^0 O_\mu^{V\dagger}\gamma^0 = f_1\gamma_\mu + i\frac{f_2}{M}\sigma_{\mu\nu}q^\nu + \frac{f_3}{M}q_\mu \tag{B.9}$$

$$\gamma^0 O_\mu^{A\dagger}\gamma^0 = -g_1\gamma_\mu\gamma_5 + i\frac{g_2}{M}\sigma_{\mu\nu}\gamma_5 q^\nu + \frac{g_3}{M}\gamma_5 q_\mu \tag{B.10}$$

In the above expression we neglect the contribution of f_3, as it comes from higher orders in the chiral expansion and set $g_2 = 0$ which is exact in the SU(3) flavor symmetry limit. In the limit of chiral symmetry the masses of all octet baryons are same. Using Table-I of Cabibbo [93] for the weak vertex $NW\Sigma$, we have $\frac{f_2}{f_1} = \frac{(\mu_p+2\mu_n)}{2}$. Therefore, after inserting the weak magnetism part i.e. f_2, the hadronic current may be written in terms of the magnetic moments for neutron μ_n and proton μ_n as.

$$\begin{aligned}
&\frac{-i(D-F)}{\sqrt{2}f_\pi}\bar{u}_n(p')\gamma_\nu\gamma_5 ip_k^\nu \frac{i}{\not p + \not q - M_\Sigma}\frac{ig}{2\sqrt{2}}V_{us}\times\left(\gamma^\mu + \frac{f_2}{f_1 M}i\sigma^{\mu\nu}q_\nu\right.\\
&\left.-\frac{g_1}{f_1}\gamma^\mu\gamma^5 - \frac{(D-F)q^\mu}{q^2 - {M_k}^2}\not q\,\gamma^5\right)u_n(p)\\
=\ &-V_{us}(D-F)\frac{g}{4f_\pi}\bar{u}_n(p')\not p_k\gamma_5\frac{\not p + \not q + M_\Sigma}{(p+q)^2 - M_\Sigma^2}\left(\gamma^\mu + i\frac{(\mu_p+2\mu_n)}{2M}\sigma^{\mu\nu}q_\nu\right.\\
&\left.+(D-F)\left\{\gamma^\mu - \frac{q^\mu}{q^2-{M_k}^2}\not q\right\}\gamma^5\right)u_n(p)
\end{aligned} \tag{B.11}$$

Appendix C

Kinematics

C.1 Total Cross Section in Lab Frame

For the process

$$\nu_l(k) + N(p) \rightarrow l^-(k') + K(p_1) + Y(p_2); \text{where } l = e, \mu, \tau \tag{C.1}$$

the expression for differential cross section is given by

$$\begin{aligned} d^9\sigma &= (2\pi)^4\delta^4\left(\sum_i p_i - \sum_f p_f\right)\frac{1}{2E(\vec{k})}\frac{1}{2E(\vec{p})}\frac{d^3\vec{k}'}{(2\pi)^3}\frac{1}{2E_l(\vec{k}')}\frac{d^3\vec{p}_2}{(2\pi)^3} \\ &\times\frac{1}{2E_2(\vec{p}_2)}\frac{d^3\vec{p}_1}{(2\pi)^3}\frac{1}{2E_1(\vec{p}_1)}\bar{\Sigma}\Sigma|\mathcal{M}|^2 \end{aligned} \tag{C.2}$$

where $2E(k)\cdot 2E(p) = 4ME$ and in lab frame $E(p) = M$ the rest mass of nucleon. v_{rel}=1(in natural units) for neutrino[1].

From momentum conservation $k + p = k' + p_1 + p_2$ The above expression will be

$$d^9\sigma = \frac{(2\pi)^4}{4ME}\frac{d^3k'}{(2\pi)^3(2E_l)}\frac{d^3p_1}{(2\pi)^3(2E_1)}\frac{d^3p_2}{(2\pi)^3(2E_2)}\delta^4(k+p-k'-p_1-p_2)\Sigma\Sigma|\mathcal{M}|^2 \tag{C.3}$$

Since $\vec{p}_2 = \vec{k} + \vec{p} - \vec{k}' - \vec{p}_1$

$$\int \delta^3(\vec{k} + \vec{p} - \vec{k}' - \vec{p}_1 - \vec{p}_2)d^3p_2 = 1 \tag{C.4}$$

[1]For convenience we dropped the vector sign.

and

$$d^3k' = |\vec{k'}|^2 d|\vec{k'}| d\Omega_{\nu l} = E_l |\vec{k'}| dE_l d\Omega_{\nu l}$$

$$d^3p_1 = |\vec{p_1}|^2 d|\vec{p_1}| d\Omega_{p_1} = E_1 |\vec{p_1}| dE_1 d\Omega_{p_1}$$

This would result

$$\begin{aligned} d^6\sigma &= \frac{1}{4ME}\frac{1}{(2\pi)^5}\delta^0(q_0 + M - E_2 - E_1)\frac{1}{8E_l E_2 E_1} dE_l d\Omega_{\nu l}\, dE_1 d\Omega_{p_1} \\ &\quad \times E_l\, |\vec{k'}|\, E_1\, |\vec{p_1}|\, \bar{\Sigma}\Sigma |\mathcal{M}|^2 \\ \Rightarrow \frac{d^6\sigma}{dE_l d\Omega_{\nu l}\, dE_1 d\Omega_{p_1}} &= \frac{1}{32}\frac{1}{(2\pi)^5}\delta^0(q_0 + M - E_2 - E_1)\frac{|\vec{k'}||\vec{p_1}|}{MEE_2}\bar{\Sigma}\Sigma |\mathcal{M}|^2 \end{aligned} \tag{C.5}$$

C.2 Recoil Factor

C.2.1 Kaon Momentum Distribution p_1

Using Eq.(C.3) with substitution

$$\int \delta^3(\vec{k} + \vec{p} - \vec{k'} - \vec{p_1} - \vec{p_2}) d^3p_2 = 1 \tag{C.6}$$

and using the relations

$$d^3k' = |\vec{k'}|^2 d|\vec{k'}| d\Omega_{\nu l}$$

and

$$d^3p_1 = |\vec{p_1}|^2 d|\vec{p_1}| d\cos\theta_{p_1} d\phi_{p_1}$$

the differential scattering cross section is given by

$$\begin{aligned} \Rightarrow \frac{d^6\sigma}{d|\vec{k'}| d\Omega_{\nu l} d|\vec{p_1}| d\phi_{p_1}} &= \frac{1}{32}\frac{1}{(2\pi)^5} d\cos\theta_{p_1}\delta^0(q_0 + M - E_2 - E_1) \\ &\quad \times \frac{|\vec{k'}|^2 |\vec{p_1}|^2}{MEE_l E_2 E_1}\bar{\Sigma}\Sigma |\mathcal{M}|^2 \end{aligned} \tag{C.7}$$

For observing kaon momentum distribution we have to calculate recoil factor by performing integration $\int \delta^0(q_0 + M - E_1 - E_2) dcos\theta_{p_1}$ and using property of delta function

$$\int dx \delta[f(x)] = \left|\frac{\partial f}{\partial x}\right|^{-1}_{x=x_0} \tag{C.8}$$

And the $\delta-$function appeared in Eq. C.7 goes with the integration of

$$\int \delta^0(q_0 + M - E_1 - E_2) dcos\theta_{p_1} \tag{C.9}$$

The above integration can be evaluate using Eq. C.8.

$$\begin{aligned} \frac{\partial f}{\partial cos\theta_{p_1}} &= \frac{\partial(q_0 + M - \sqrt{|\vec{q}|^2 + |\vec{p}_1|^2 - 2|\vec{q}||\vec{p}_1|cos\theta_{p_1} + m_2^2} - E_1)}{\partial cos\theta_{p_1}} \\ \Rightarrow \frac{\partial f}{\partial cos\theta_{p_1}} &= \frac{|\vec{q}||\vec{p}_1|}{\sqrt{|\vec{q}|^2 + |\vec{p}_1|^2 - 2|\vec{q}||\vec{p}_1|cos\theta_{p_1} + m_2^2}} \end{aligned} \tag{C.10}$$

The recoil factor($\mathcal{R}$) thus obtained from the Eq. C.10 [2] may be written as

$$\mathcal{R} = \left|\frac{\partial f}{\partial cos\theta_{p_1}}\right|^{-1} = \left|\frac{\sqrt{|\vec{q}|^2 + |\vec{p}_1|^2 - 2|\vec{q}||\vec{p}_1|cos\theta_{p_1} + m_2^2}}{|\vec{q}||\vec{p}_1|}\right| = \frac{E_2}{|\vec{q}||\vec{p}_1|} \tag{C.11}$$

Using the $\delta-$function we can find the $cos\theta_{p_1}$ and it comes out to be

$$\cos\theta_{p_1} = \frac{|\vec{q}|^2 + |\vec{p}_1|^2 + m_2^2 - (q_0 + M - E_1)^2}{2|\vec{q}||\vec{p}_1|} \tag{C.12}$$

Using this form of recoil factor the expression of differential scattering cross section given by Eq.(C.7) modifies to

$$\Rightarrow \frac{d^5\sigma}{d|\vec{k}'|d\Omega_{\nu l}d|\vec{p}_1|d\phi_{p_1}} = \frac{1}{32}\frac{1}{(2\pi)^5}\frac{|\vec{k}'|^2|\vec{p}_1|^2}{MEE_lE_2E_1}\frac{E_2}{|\vec{q}||\vec{p}_1|}\bar{\Sigma}\Sigma|\mathcal{M}|^2 \tag{C.13}$$

To get the cross section we have to integrate over all the kinematical variables

$$\frac{d\sigma}{|\vec{dp}_1|} = \int_{k^l_{min}}^{k^l_{max}} dk_l \int_0^{2\pi} d\phi_{p_1} 2\pi \int_{-1}^{1} dcos\theta_{\nu l} \frac{d^5\sigma}{d|\vec{k}'|d\Omega_{\nu l}dp_1 d\phi_{p_1}}, \tag{C.14}$$

here we used,

$$E_1^2 = \vec{p}_1^2 + M_1^2, \qquad E_1\, dE_1 = |\vec{p}_1|d|\vec{p}_1|$$

$$T_1 = E_1 - m_1, \quad dE_1 = dT_1$$

where T_1 is the kinetic energy of kaon.

[2] This has to be positive as it is absolute.

Bibliography

Bibliography

[1] J. Chadwick, "The intensity distribution in the magnetic spectrum of beta particles from radium (B + C)," **Verh.Phys.Gesell.**, **16**, pp. 383–391, 1914.

[2] L. Meitner and W. Orthmann, "Über eine absolute Bestimmung der Energie der primären β-Strahlen von Radium E," **Z. Phys.**, **60**, p. 143, 1930.

[3] C. D. Ellis and W. A. Wooster, "Average Energy of Disintegration of Radium E," **Proc. Roy. Soc.**, **A 117**, p. 109, 1927.

[4] W. Pauli, "Dear radioactive ladies and gentlemen," **Phys. Today**, **31N9**, p. 27, 1978.

[5] E. Fermi, "An attempt of a theory of beta radiation. 1.," **Z. Phys.**, **88**, p. 161, 1934.

[6] G. Gamow and E. Teller, "Selection rules for the beta-disintegration," **Phys.Rev.**, **49**, pp. 895–899, 1936.

[7] E. Sudarshan and R. Marshak, "Chirality invariance and the universal Fermi interaction," **Phys.Rev.**, **109**, pp. 1860–1860, 1958.

[8] R. Feynman and M. Gell-Mann, "Theory of Fermi interaction," **Phys.Rev.**, **109**, pp. 193–198, 1958.

[9] C. Wu, E. Ambler, R. Hayward, D. Hoppes, and R. Hudson, "Experimental Test of Parity Conservation in Beta Decay," **Phys.Rev.**, **105**, pp. 1413–1414, 1957.

[10] T. Lee and C.-N. Yang, "Question of Parity Conservation in Weak Interactions," **Phys.Rev.**, **104**, pp. 254–258, 1956.

[11] M. Goldhaber, L. Grodzins, and A. Sunyar, "Helicity of Neutrinos," **Phys.Rev.**, **109**, pp. 1015–1017, 1958.

[12] F. Reines and C. L. Cowan, "The neutrino," **Nature**, **178**, p. 446, sep 1956.

[13] G. Danby, J. Gaillard, K. A. Goulianos, L. Lederman, N. B. Mistry, *et al.*, "Observation of High-Energy Neutrino Reactions and the Existence of Two Kinds of Neutrinos," **Phys.Rev.Lett.**, **9**, pp. 36–44, 1962.

[14] K. Kodama *et al.*, "Observation of tau neutrino interactions," **Phys. Lett.**, **B504**, p. 218, 2001.

[15] B. Pontecorvo, "Mesonium and anti-mesonium," **Sov.Phys.JETP**, **6**, p. 429, 1957.

[16] V. Gribov and B. Pontecorvo, "Neutrino astronomy and lepton charge," **Phys.Lett.**, **B28**, p. 493, 1969.

[17] J. Davis, Raymond, D. S. Harmer, and K. C. Hoffman, "Search for neutrinos from the sun," **Phys.Rev.Lett.**, **20**, pp. 1205–1209, 1968.

[18] J. Bahcall, **Neutrino Astrophysics**. Cambridge University Press, 1989.

[19] T. Haines, R. Bionta, G. Blewitt, C. Bratton, D. Casper, *et al.*, "Calculation of Atmospheric Neutrino Induced Backgrounds in a Nucleon Decay Search," **Phys.Rev.Lett.**, **57**, pp. 1986–1989, 1986.

[20] K. Hirata *et al.*, "Experimental Study of the Atmospheric Neutrino Flux," **Phys.Lett.**, **B205**, p. 416, 1988.

[21] S. Mikheyev and A. Smirnov, "Resonant amplification of oscillations in matter and solar-neutrino spectroscopy," **Il Nuovo Cimento C**, **9**, no. 1, pp. 17–26, 1986.

[22] B. Pontecorvo, "Electron and Muon Neutrinos," **Sov.Phys.JETP**, **10**, pp. 1236–1240, 1960.

[23] Z. Maki, M. Nakagawa, and S. Sakata, "Remarks on the unified model of elementary particles," **Prog.Theor.Phys.**, **28**, pp. 870–880, 1962.

[24] D. Forero, M. Tortola, and J. Valle, "Global status of neutrino oscillation parameters after Neutrino-2012," **Phys.Rev.**, **D86**, p. 073012, 2012.

[25] Y. Abe *et al.*, "First Measurement of θ_{13} from Delayed Neutron Capture on Hydrogen in the Double Chooz Experiment," **Phys.Lett.**, **B723**, pp. 66–70, 2013.

[26] A. Aguilar-Arevalo *et al.*, "First Measurement of the Muon Anti-Neutrino Double-Differential Charged Current Quasi-Elastic Cross Section," **Phys.Rev.**, **D88**, p. 032001, 2013.

[27] S. Ahn *et al.*, "Detection of accelerator produced neutrinos at a distance of 250-km," **Phys.Lett.**, **B511**, pp. 178–184, 2001.

[28] K. Abe *et al.*, "The T2K Experiment," **Nucl.Instrum.Meth.**, **A659**, pp. 106–135, 2011.

[29] M. Muether, "NOvA: Current Status and Future Reach," **Nucl. Phys. Proc. Suppl.**, **237-238**, p. 135, 2013.

[30] P. Lipari, "Neutrino oscillation studies and the neutrino cross-section," **Nucl.Phys.Proc.Suppl.**, **112**, pp. 274–287, 2002.

[31] J. G. Morfin, J. Nieves, and J. T. Sobczyk, "Recent Developments in Neutrino/Antineutrino - Nucleus Interactions," **Adv.High Energy Phys.**, **2012**, p. 934597, 2012.

[32] NUINT, "8th International Workshop on Neutrino Nucleus Interactions in Few-GeV Region." `https://indico.fnal.gov/conferenceDisplay.py?confId=5361`, 2012.

[33] NuFact, "Superbeams,Neutrino Factories, and Beta Beams," in **International Workshop on Superbeams, Neutrino Factories, and Beta Beams**.

[34] Y. Hayato *et al.*, "Search for proton decay through $p \to \bar{\nu} K^+$ in a large water Cherenkov detector," **Phys.Rev.Lett.**, **83**, pp. 1529–1533, 1999.

[35] C. Regis *et al.*, "Search for Proton Decay via $p \to \mu^+ K^0$ in Super-Kamiokande I, II, and III," **Phys.Rev.**, **D86**, p. 012006, 2012.

[36] G. Ross, **Grand Unified Theories**. Frontiers in physics, Westview Press, 1984.

[37] C. K. Jung, "Feasibility of a next generation underground water Cherenkov detector: UNO," **AIP Conf.Proc.**, **533**, pp. 29–34, 2000.

[38] K. Abe, T. Abe, H. Aihara, Y. Fukuda, Y. Hayato, *et al.*, "Letter of Intent: The Hyper-Kamiokande Experiment — Detector Design and Physics Potential —," **arXiv:1109.3262**, 2011.

[39] A. Bueno, "The ICARUS project," **Nucl.Phys.Proc.Suppl.**, **143**, pp. 262–265, 2005.

[40] S. Barish, M. Derrick, T. Dombeck, L. Hyman, K. Jaeger, *et al.*, "Study of Neutrino Interactions in Hydrogen and Deuterium: Inelastic Charged Current Reactions," **Phys.Rev.**, **D19**, p. 2521, 1979.

[41] N. Baker, P. Connolly, S. Kahn, H. Kirk, M. Murtagh, *et al.*, "Strange Particle Production from Neutrino Interactions in the BNL 7-Ft Bubble Chamber," **Phys.Rev., D24**, pp. 2779–2786, 1981.

[42] S. Barish, M. Derrick, L. Hyman, P. Schreiner, R. Singer, *et al.*, "Strange-Particle Production in Neutrino Interactions," **Phys.Rev.Lett., 33**, p. 1446, 1974.

[43] D. W. Schmitz, "The MINERvA neutrino scattering experiment at Fermilab," **AIP Conf.Proc., 1405**, pp. 243–249, 2011.

[44] N. Solomey, "A proposed study of neutrino-induced strange-particle production reactions at Minerva," **Nucl.Phys.Proc.Suppl., 142**, pp. 74–78, 2005.

[45] R. E. Shrock, "Associated Production by Weak Charged and Neutral Currents," **Phys.Rev., D12**, p. 2049, 1975.

[46] W. Mecklenburg, "Neutrino-Induced Associated Production," **Acta Phys.Austriaca, 48**, p. 293, 1978.

[47] H. Dewan, "Strange Particle Production In Neutrino Scattering," **Phys.Rev., D24**, pp. 2369–2378, 1981.

[48] A. Amer, "Production of Strange Particles by Neutrinos and anti-neutrinos," **Phys.Rev., D18**, p. 2290, 1978.

[49] S. Singh and M. Vicente Vacas, "Weak quasi-elastic production of hyperons," **Phys.Rev., D74**, p. 053009, 2006.

[50] S. Mintz and L. Wen, "New results for the production of Lambda and Sigma0 hyperons in antineutrino scattering from protons," **Eur.Phys.J., A33**, pp. 299–301, 2007.

[51] Y. Hayato, "A neutrino interaction simulation program library NEUT," **Acta Phys.Polon., B40**, pp. 2477–2489, 2009.

[52] Y. Fukuda *et al.*, "Evidence for oscillation of atmospheric neutrinos," **Phys.Rev.Lett., 81**, pp. 1562–1567, 1998.

[53] Y. Kurimoto *et al.*, "Improved measurement of neutral current coherent π^0 production on carbon in a few-GeV neutrino beam," **Phys.Rev., D81**, p. 111102, 2010.

[54] H. Gallagher, "The NEUGEN neutrino event generator," **Nucl.Phys.Proc.Suppl., 112**, pp. 188–194, 2002.

[55] D. Casper, "The Nuance neutrino physics simulation, and the future," **Nucl.Phys.Proc.Suppl., 112**, pp. 161–170, 2002.

[56] G. Zeller, "Low-energy neutrino cross-sections: Comparison of various Monte Carlo predictions to experimental data," **arXiv:hep-ex/0312061**, 2003.

[57] C. Andreopoulos, A. Bell, D. Bhattacharya, F. Cavanna, J. Dobson, *et al.*, "The GENIE Neutrino Monte Carlo Generator," **Nucl.Instrum.Meth.**, **A614**, pp. 87–104, 2010.

[58] C. B. Dover and P. M. Fishbane, "Eta and eta-prime scattering: a probe of the strange quark (s anti-s) content of the nucleon," **Phys.Rev.Lett.**, **64**, pp. 3115–3118, 1990.

[59] D. Wall *et al.*, "Search for nucleon decay with final states $l^+\eta^0$, $\bar{\nu}\eta^0$, and $\bar{\nu}\pi^{+,0}$ using Soudan-2," **Phys.Rev.**, **D62**, p. 092003, 2000.

[60] N. Dombey, "Weak Eta production and the existence of second-class currents," **Phys.Rev.**, **174**, pp. 2127–2129, 1968.

[61] D. Rein and L. M. Sehgal, "Neutrino Excitation of Baryon Resonances and Single Pion Production," **Annals Phys.**, **133**, pp. 79–153, 1981.

[62] P. Achenbach, "Strangeness physics with Kaos at MAMI," **arXiv:1101.4394**, 2011.

[63] P. Achenbach *et al.*, "Strange hadrons - strangeness in strongly interacting particles," **Eur.Phys.J.ST**, **198**, pp. 307–327, 2011.

[64] P. Achenbach, A. Esser, C. Ayerbe Gayoso, R. Bohm, O. Borodina, *et al.*, "Strange hadronic physics in electroproduction experiments at the Mainz Microtron," **Nucl.Phys.**, **A881**, pp. 187–198, 2012.

[65] B. Beckford, A. Chiba, D. Doi, J. Fujibayashi, T. Fujii, *et al.*, "Report on strangeness photoproduction experiments performed with the Neutral Kaon Spectrometer 2," 2012.

[66] R. Zegers *et al.*, "Beam polarization asymmetries for the $p(\vec{\gamma}, K^+)\Lambda$ and $p(\vec{\gamma}, K^+)\Sigma^0$ reactions at E_γ =1.5–2.4 GeV," **Phys.Rev.Lett.**, **91**, p. 092001, 2003.

[67] M. Sumihama, "Experimental results of K^+ photoproduction at SPring-8/LEPS," **Nucl.Phys.**, **A754**, pp. 303–309, 2005.

[68] A. Lleres, O. Bartalini, V. Bellini, J. Bocquet, P. Calvat, *et al.*, "Polarization observable measurements for $\gamma p \to K^+\Lambda$ and $\gamma p \to K^+\Sigma^0$ for energies up to 1.5-GeV," **Eur.Phys.J.**, **A31**, pp. 79–93, 2007.

[69] R. Lawall, J. Barth, C. Bennhold, K.-H. Glander, S. Goers, *et al.*, "Measurement of the reaction $\gamma p \to K^0\Sigma^+$ at photon energies up to 2.6-GeV," **Eur.Phys.J.**, **A24**, pp. 275–286, 2005.

[70] K. Glander, J. Barth, W. Braun, J. Hannappel, N. Jopen, *et al.*, "Measurement of $\gamma p \to K^+\Lambda$ and $\gamma p \to K^+\Sigma^0$ at photon energies up to 2.6-GeV," **Eur.Phys.J.**, **A19**, pp. 251–273, 2004.

[71] D. Carman *et al.*, "First measurement of transferred polarization in the exclusive $\vec{e}p \to e'K^+\vec{\Lambda}$ reaction," **Phys.Rev.Lett.**, **90**, p. 131804, 2003.

[72] P. Ambrozewicz *et al.*, "Separated structure functions for the exclusive electroproduction of $K^+\Lambda$ and $K^+\Sigma^0$ final states," **Phys.Rev.**, **C75**, p. 045203, 2007.

[73] T. Mart, C. Bennhold, and C. E. Hyde, "Constraints on coupling constants through charged sigma photoproduction," **Phys.Rev.**, **C51**, pp. 1074–1077, 1995.

[74] T. Mart, "Role of Resonances in the Electromagnetic Production of Kaon Near Threshold," **EPJ Web Conf.**, **20**, p. 02007, 2012.

[75] Z.-P. Li, "The Kaon photoproduction of nucleons in the chiral quark model," **Phys.Rev.**, **C52**, pp. 1648–1661, 1995.

[76] S. Steininger and U.-G. Meißner, "Threshold kaon photoproduction and electroproduction in SU(3) baryon chiral perturbation theory," **Phys.Lett.**, **B391**, pp. 446–450, 1997.

[77] B. Borasoy, P. Bruns, U.-G. Meißner, and R. Nißler, "A Gauge invariant chiral unitary framework for kaon photo- and electroproduction on the proton," **Eur.Phys.J.**, **A34**, pp. 161–183, 2007.

[78] N. Kaiser, T. Waas, and W. Weise, "SU(3) chiral dynamics with coupled channels: Eta and kaon photoproduction," **Nucl.Phys.**, **A612**, pp. 297–320, 1997.

[79] T. Feuster and U. Mosel, "Photon and meson induced reactions on the nucleon," **Phys.Rev.**, **C59**, pp. 460–491, 1999.

[80] T. Corthals, J. Ryckebusch, and T. Van Cauteren, "Forward-angle K+ Lambda photoproduction in a Regge-plus-resonance approach," **Phys.Rev.**, **C73**, p. 045207, 2006.

[81] A. Anisovich, A. Sarantsev, O. Bartholomy, E. Klempt, V. Nikonov, *et al.*, "Photoproduction of baryons decaying into N pi and N eta," **Eur.Phys.J.**, **A25**, pp. 427–439, 2005.

[82] B. Julia-Diaz, B. Saghai, T.-S. Lee, and F. Tabakin, "Dynamical coupled-channel approach to hadronic and electromagnetic production of kaon-hyperon on the proton," **Phys.Rev.**, **C73**, p. 055204, 2006.

[83] M. Guidal, J. Laget, and M. Vanderhaeghen, "Pion and kaon photoproduction at high-energies: Forward and intermediate angles," **Nucl.Phys., A627**, pp. 645–678, 1997.

[84] J. Gasser and H. Leutwyler, "Chiral Perturbation Theory to One Loop," **Annals Phys., 158**, p. 142, 1984.

[85] J. Gasser and H. Leutwyler, "Chiral Perturbation Theory: Expansions in the Mass of the Strange Quark," **Nucl.Phys., B250**, p. 465, 1985.

[86] S. Scherer, "Introduction to chiral perturbation theory," **Adv.Nucl.Phys., 27**, p. 277, 2003.

[87] S. Scherer and M. R. Schindler, "A Primer for Chiral Perturbation Theory," **Lect.Notes Phys., 830**, pp. 1–338, 2012.

[88] T. Mannel, "Effective Field Theories in Flavour Physics," **Springer Tracts in Modern Phys., 203**, pp. 1–176.

[89] G. Ecker, "Chiral perturbation theory," **Prog.Part.Nucl.Phys., 35**, pp. 1–80, 1995.

[90] B. Kubis, "An Introduction to chiral perturbation theory," **arXiv:hep-ph/0703274**, 2007.

[91] A. Pich, "Effective field theory: Course," **arXiv:hep-ph/9806303**, 1998.

[92] J. Beringer *et al.*, "Review of Particle Physics (RPP)," **Phys.Rev., D86**, p. 010001, 2012.

[93] N. Cabibbo, E. C. Swallow, and R. Winston, "Semileptonic hyperon decays," **Ann.Rev.Nucl.Part.Sci., 53**, pp. 39–75, 2003.

[94] J. A. Oller, M. Verbeni, and J. Prades, "Meson-baryon effective chiral lagrangians to O(q**3)," **JHEP, 0609**, p. 079, 2006.

[95] E. Hernandez, J. Nieves, and M. Valverde, "Weak Pion Production off the Nucleon," **Phys.Rev., D76**, p. 033005, 2007.

[96] W. Mann, T. Kafka, M. Derrick, B. Musgrave, R. Ammar, *et al.*, "K Meson Production By Muon-Neutrino - Deuterium Reactions Near Threshold: Implications For Nucleon Decay Searches," **Phys.Rev., D34**, pp. 2545–2553, 1986.

[97] T. Marrodan Undagoitia, F. von Feilitzsch, M. Goger-Neff, C. Grieb, K. Hochmuth, *et al.*, "Proton decay in the large liquid scintillator detector LENA: Study of the background," **J.Phys.Conf.Ser., 39**, pp. 269–271, 2006.

[98] K. Kobayashi *et al.*, "Search for nucleon decay via modes favored by supersymmetric grand unification models in Super-Kamiokande-I," **Phys.Rev., D72**, p. 052007, 2005.

[99] R. Flores-Mendieta, "V(us) from hyperon semileptonic decays," **Phys.Rev., D70**, p. 114036, 2004.

[100] L. Geng, J. Martin Camalich, and M. Vicente Vacas, "SU(3)-breaking corrections to the hyperon vector coupling f(1)(0) in covariant baryon chiral perturbation theory," **Phys.Rev., D79**, p. 094022, 2009.

[101] O. Benhar, N. Farina, H. Nakamura, M. Sakuda, and R. Seki, "Electron- and neutrino-nucleus scattering in the impulse approximation regime," **Phys.Rev., D72**, p. 053005, 2005.

[102] T. Leitner, O. Buss, U. Mosel, and L. Alvarez-Ruso, "Neutrino induced pion production at MiniBooNE and K2K," **Phys.Rev., C79**, p. 038501, 2009.

[103] V. Bernard, L. Elouadrhiri, and U. Meißner, "Axial structure of the nucleon: Topical Review," **J.Phys., G28**, pp. R1–R35, 2002.

[104] K. S. Kuzmin, V. V. Lyubushkin, and V. A. Naumov, "Quasielastic axial-vector mass from experiments on neutrino-nucleus scattering," **Eur.Phys.J., C54**, pp. 517–538, 2008.

[105] R. Gran *et al.*, "Measurement of the quasi-elastic axial vector mass in neutrino-oxygen interactions," **Phys.Rev., D74**, p. 052002, 2006.

[106] A. Aguilar-Arevalo *et al.*, "Measurement of muon neutrino quasi-elastic scattering on carbon," **Phys.Rev.Lett., 100**, p. 032301, 2008.

[107] S. Barish, J. Campbell, G. Charlton, Y. Cho, M. Derrick, *et al.*, "Study of Neutrino Interactions in Hydrogen and Deuterium. 1. Description of the Experiment and Study of the Reaction $\nu d \to \mu^- pp_s$," **Phys.Rev., D16**, p. 3103, 1977.

[108] A. Aguilar-Arevalo *et al.*, "First Measurement of the Muon Neutrino Charged Current Quasielastic Double Differential Cross Section," **Phys.Rev., D81**, p. 092005, 2010.

[109] A. Ichikawa, "The T2K long-baseline neutrino experiment," **Lect.Notes Phys., 781**, pp. 17–43, 2009.

[110] A. A. Aguilar-Arevalo *et al.*, "Measurement of ν_μ and $\bar{\nu}_\mu$ induced neutral current single π^0 production cross sections on mineral oil at $E_\nu \sim O(1-GeV)$," **Phys.Rev., D81**, p. 013005, 2010.

[111] M. Honda, T. Kajita, K. Kasahara, S. Midorikawa, and T. Sanuki, "Calculation of atmospheric neutrino flux using the interaction model calibrated with atmospheric muon data," **Phys.Rev., D75**, p. 043006, 2007.

[112] Y. Ashie *et al.*, "A Measurement of atmospheric neutrino oscillation parameters by SUPER-KAMIOKANDE I," **Phys.Rev., D71**, p. 112005, 2005.

[113] D. Rein, "Angular Distribution In Neutrino Induced Single Pion Production Processes," **Z.Phys., C35**, pp. 43–64, 1987.

[114] L. Alvarez-Ruso, S. Singh, and M. Vicente Vacas, "Neutrino $d \to \mu^- \Delta^{++} n$ reaction and axial vector N - Delta coupling," **Phys.Rev., C59**, pp. 3386–3392, 1999.

[115] T. Leitner, L. Alvarez-Ruso, and U. Mosel, "Charged current neutrino nucleus interactions at intermediate energies," **Phys.Rev., C73**, p. 065502, 2006.

[116] J. Amaro, E. Hernandez, J. Nieves, and M. Valverde, "Theoretical study of neutrino-induced coherent pion production off nuclei at T2K and MiniBooNE energies," **Phys.Rev., D79**, p. 013002, 2009.

[117] T. Kobayashi, "Super beams," **Nucl.Phys.Proc.Suppl., 143**, pp. 303–308, 2005.

[118] M. Lindroos and M. Mezzetto, **Beta Beams: Neutrino Beam**. Imperial College, London, 2009.

[119] O. Lalakulich and E. A. Paschos, "Resonance production by neutrinos. I. J = 3/2 resonances," **Phys.Rev., D71**, p. 074003, 2005.

[120] T. Leitner, O. Buss, L. Alvarez-Ruso, and U. Mosel, "Electron- and neutrino-nucleus scattering from the quasielastic to the resonance region," **Phys.Rev., C79**, p. 034601, 2009.

[121] E. Hernandez, J. Nieves, M. Valverde, and M. Vicente Vacas, "N-Delta(1232) axial form factors from weak pion production," **Phys.Rev., D81**, p. 085046, 2010.

[122] M. Doring, E. Oset, and S. Sarkar, "Radiative decay of the Lambda(1520)," **Phys.Rev., C74**, p. 065204, 2006.

[123] S. Taylor *et al.*, "Radiative decays of the Sigma0(1385) and Lambda(1520) hyperons," **Phys.Rev., C71**, p. 054609, 2005.

[124] M. Rafi Alam, I. Ruiz Simo, M. Sajjad Athar, and M. Vicente Vacas, "Weak Kaon Production off the Nucleon," **Phys.Rev., D82**, p. 033001, 2010.

[125] A. Aguilar-Arevalo *et al.*, "Measurement of the neutrino component of an anti-neutrino beam observed by a non-magnetized detector," **Phys.Rev., D84**, p. 072005, 2011.

[126] S. A. Adjei, D. A. Dicus, and V. L. Teplitz, "Charged Current Two Pion Production From Nucleons," **Phys.Rev., D24**, p. 623, 1981.

[127] T. Kitagaki, H. Yuta, S. Tanaka, A. Yamaguchi, K. Abe, *et al.*, "Charged Current Exclusive Pion Production In Neutrino Deuterium Interactions," **Phys.Rev., D34**, pp. 2554–2565, 1986.

[128] M. R. Alam, I. R. Simo, M. S. Athar, and M. Vicente Vacas, "$\bar{\nu}$ induced $\bar{K}$ production off the nucleon," **Phys.Rev., D85**, p. 013014, 2012.

[129] I. Altarev, E. Schilling, S. Baunack, L. Capozza, J. Diefenbach, *et al.*, "A High power liquid hydrogen target for the Mainz A4 parity violation experiment," **Nucl.Instrum.Meth., A564**, pp. 13–25, 2006.

[130] K. Aniol *et al.*, "Parity violating electroweak asymmetry in polarized-e p scattering," **Phys.Rev., C69**, p. 065501, 2004.

[131] D. Ruic, M. Mai, and U.-G. Meißner, "η-photoproduction in a gauge-invariant chiral unitary framework," **Phys.Lett., B704**, pp. 659–662, 2011.

[132] A. Fix and H. Arenhovel, "Do We Understand the Eta N Interaction from the Near Threshold Eta Photoproduction on the Deuteron?," **Eur.Phys.J., A19**, pp. 275–282, 2004.

[133] B. Krusche, J. Ahrens, G. Anton, R. Beck, M. Fuchs, *et al.*, "New threshold photoproduction of eta mesons off the proton," **Phys.Rev.Lett., 74**, pp. 3736–3739, 1995.

[134] O. Bartholomy *et al.*, "Photoproduction of eta-mesons off protons," **Eur.Phys.J., A33**, pp. 133–146, 2007.

[135] V. Crede *et al.*, "Photoproduction of eta and eta-prime mesons off protons," **Phys.Rev., C80**, p. 055202, 2009.

[136] E. McNicoll *et al.*, "Study of the $\gamma p \to \eta p$ reaction with the Crystal Ball detector at the Mainz Microtron(MAMI-C)," **Phys.Rev., C82**, p. 035208, 2010.

[137] V. Kuznetsov, M. Polyakov, T. Boiko, J. Jang, A. Kim, *et al.*, "Evidence for a narrow N*(1685) resonance in eta photoproduction off the nucleon," **Acta Phys.Polon., B39**, pp. 1949–1967, 2008.

[138] E. Breitmoser and H. Arenhovel, "Coherent eta photoproduction on the deuteron in the S11 resonance region," **Nucl.Phys.**, **A612**, pp. 321–345, 1997.

[139] M. Kirchbach and L. Tiator, "On the coupling of the eta meson to the nucleon," **Nucl.Phys.**, **A604**, pp. 385–394, 1996.

[140] D. Drechsel, S. Kamalov, and L. Tiator, "Unitary Isobar Model - MAID2007," **Eur.Phys.J.**, **A34**, pp. 69–97, 2007.

[141] T. J. Leitner, "Ph.D. Thesis: Neutrino-nucleus interactions in a coupled-channel hadronic transport model," **Universitat Gießen**, 2009.

[142] L. Tiator, D. Drechsel, S. Kamalov, and M. Vanderhaeghen, "Electromagnetic Excitation of Nucleon Resonances," **Eur.Phys.J.ST**, **198**, pp. 141–170, 2011.

[143] R. Bradford, A. Bodek, H. S. Budd, and J. Arrington, "A New parameterization of the nucleon elastic form-factors," **Nucl.Phys.Proc.Suppl.**, **159**, pp. 127–132, 2006.

[144] J. Kisiel *et al.*, "The LAGUNA project: Towards the giant liquid based detectors for proton decay searches and for low energy neutrino astrophysics," **PoS. EPS-HEP2009**, p. 283, 2009.

[145] H. Deden, F. Hasert, W. Krenz, J. Von Krogh, D. Lanske, *et al.*, "Strange Particle Production and Charmed Particle Search in the Gargamelle Neutrino Experiment," **Phys.Lett.**, **B58**, pp. 361–366, 1975.

[146] O. Erriquez, M. Fogli Muciaccia, S. Natali, S. Nuzzo, A. Halsteinslid, *et al.*, "Strange Particle Production by anti-neutrinos," **Phys.Lett.**, **B70**, pp. 383–386, 1977.

[147] O. Erriquez, M. Fogli-Muciaccia, S. Natali, S. Nuzzo, A. Halsteinslid, *et al.*, "Production of Strange Particles in anti-neutrino Interactions at the CERN PS," **Nucl.Phys.**, **B140**, pp. 123–140, 1978.

[148] B. Choudhary *et al.*, "Proposal of Indian Institutions and Fermilab Collaboration for Participation in the Long-Baseline Neutrino Experiment at Fermilab," **LBNE**, **6704-v1**, 2013.

[149] D. Son, G. Snow, S. Chang, S. Kunori, P. Steinberg, *et al.*, "Quasielastic Charmed Baryon Production and Exclusive Strange Particle Production by High-energy Neutrinos," **Phys.Rev.**, **D28**, p. 2129, 1983.

[150] G. Adera, B. Van Der Ventel, D. van Niekerk, and T. Mart, "Strange-particle production via the weak interaction," **Phys.Rev.**, **C82**, p. 025501, 2010.

[151] G. Adera and B. Van der Ventel, "Associated hyperon-kaon production via neutrino-nucleus scattering," **Int.J.Mod.Phys., E20**, p. 2475, 2011.

[152] K. Datchev, "Kaon Production at MiniBooNE," in **APS Meeting Abstracts**, p. 1037P, Oct. 2002.

[153] S. Galster, H. Klein, J. Moritz, K. Schmidt, D. Wegener, *et al.*, "Elastic electron - deuteron scattering and the electric neutron form-factor at four momentum transfers $5 - fm^{-2} < q^2 < 14 - fm^{-2}$," **Nucl.Phys., B32**, pp. 221–237, 1971.